HYBRID CARBON-GLASS FIBER/TOUGHENED EPOXY THICK COMPOSITES SUBJECT TO DROP-WEIGHT AND BALLISTIC IMPACTS

by

ERCAN SEVKAT

A dissertation submitted to the Graduate Faculty in Mechanical Engineering in partial fulfillment of the requirements for the degree of Doctor of Philosophy, The City University of New York

2009

This manuscript has been read and accepted for the
Graduate Faculty in Engineering in satisfaction of the
dissertation requirement for the degree of Doctor of Philosophy.

01/14/2009	Prof. Feridun Delale
Date	Chair of Examining Committee
01/15/2009	Prof. Mumtaz K. Kassir
Date	Executive Officer

Prof. Feridun Delale, Dept. of Mechanical Engineering, The City College of New York

Prof. Benjamin Liaw, Dept. of Mechanical Engineering, The City College of New York

Prof. Jackie Li, Dept. of Mechanical Engineering, The City College of New York

Prof. Kolluru V. Subramaniam, Dept. of Civil Engineering, The City College of New York

Prof. Alan Lau, Dept. of Mechanical Engineering and Mechanics, Drexel University
Supervision Committee

THE CITY UNIVERSITY OF NEW YORK

Abstract

HYBRID CARBON-GLASS FIBER/TOUGHENED EPOXY THICK COMPOSITES SUBJECT TODROP-WEIGHT AND BALLISTIC IMPACTS

by

Ercan Sevkat

Adviser: Professor Feridun Delale

ABSTRACT

The goals of this study are to investigate the low velocity and ballistic impact response of thick-section hybrid fiber composites at room temperature. Plain-woven S2-Glass and IM7 Graphite fabrics are chosen as fiber materials reinforcing the SC-79 epoxy. Four different types of composites consisting of alternating layers of glass and graphite woven fabric sheets are considered. Tensile tests are conducted using 98 KN (22 kip) MTS testing machine equipped with environmental chamber. Low-velocity impact tests are conducted using an Instron-Dynatup 8250 impact test machine equipped with an environmental chamber. Ballistic impact tests are performed using helium pressured high-speed gas-gun.

Tensile tests results were used to define the material behavior of the hybrid and non-hybrid composites in Finite Element modeling. The low velocity and ballistic impact tests showed that hybrid composites performance was somewhere between non-hybrid woven composites. Using woven glass fabrics as outer skin improved the impact performance of woven graphite composite. However hybrid composites are prone to delamination especially between dissimilar layers. The ballistic limit velocity V_{50} hybrid composites were higher that of woven graphite composite and lower than that of woven glass composite.

Both destructive cross-sectional micrographs and nondestructive ultrasonic techniques are used to evaluate the damage created by impact.

The Finite Element code LS-DYNA is chosen to perform numerical simulations of low velocity and ballistic impact on thick-section hybrid composites. The damage progression in these composites shows anisotropic nonlinearity. The material model to describe this behavior is not available in LS-DYNA material library. Initially, linear orthotropic material with damage (Chan-Chan Model) is employed to simulate some of the experimental results. Then, user-defined material subroutine is incorporated into LS-DYNA to simulate the nonlinear behavior. The experimentally obtained force-time histories, strain-time histories and damage patterns of impacted composites are compared with Finite element results. The results indicate that LS-DYNA could simulate the impact responses with sufficient accuracy once proper material models and boundary conditions are defined.

ACKNOWLEDGEMENTS

I would like thank my academic advisor, Professor Feridun Delale, for his guidance throughout this study. I also want to acknowledge my co-mentor Prof. Benjamin Liaw for his valuable advises.

I want to express my gratitude to those who has worked in the Material Processing and Solid Mechanics laboratory in The City College of New York during the period of my study. I am very thankful to undergraduate student Tania Brown for the great contribution she has made in Ultrasonic damage evaluation part.

I would also like to express my thanks for funding from City University of New York through CUNY Collaborative Incentive Research Grants Program (80209-06 10) and CUNY Research Equipment Grant Competition (80212-12 04) for procuring part of the materials and equipment used in this research. This work is supported by U.S. Army Research Office through Grant No. DAAD19-03-1-00086.

Finally very special thanks to my wife Asli. She has been very supportive and patient during the period of my study. I also appreciate her for being a great mother to our daughters, Ahsen and Reyyan.

Ercan Sevkat

December 2008 in New York

TABLE OF CONTENTS

LIST OF TABLES

LIST OF FIGURES

1. LITERATURE REVIEW

Metals have always been the first choice for engineering design since steel was invented in 1850. The need for improved materials with high specific mechanical properties, high stiffness to-weight ratio, high strength to-weight ratio, tailor ability and damage tolerance led to the rise of composites. Since the 1960's, advanced composites have been used in many different applications, many in the military field such as aircraft, tanks, bulletproof body armors, etc. Composites have also been used in civil aerospace applications, the automotive industry and transportation. With increased environmental awareness, the use of composites in cars may accelerate because of fuel economy. Commercial applications such as fishing roads, boats, tennis rackets, etc. should also be noted. Most of the composite structures and parts used in industry are fiber-reinforced composites [1]. Thus, tremendous research has been conducted to understand the mechanical and thermal behavior of fiber reinforced composites. Recently, fibers in textile forms are also being introduced for use in composites to exploit the advantages of textile structures such as better dimensional stability, subtle conformability, and deep draw moldability/shapeability [2]. Textile structural composite products are usually made from high modulus fibers or yarns such as glass, graphite, aramid etc. to qualify for primary and secondary load-bearing applications. Each material has a particular advantage and deficiency relative to the other. For example, graphite exhibits the highest modulus or stiffness but lacks in toughness. Aramid exhibits great tenacity but it is poor in compression. Glass has better toughness but is not as stiff as the others. Glass has been the standard material for a variety of textile composites structures. However, in recent years, graphite and aramid fibers have begun to invade a segment of the woven composites market. For aircraft and other applications where stiffness to weight is important, graphite has become the dominant fiber. In applications where tensile strength to –weight is the major consideration, aramid is preferred. However glass fiber is the most dependable material for many textile composites due to its lower cost [3]. Since each fiber type has a particular advantage, one may ask the following question: Why not develop hybrid composites? Recently, there have been extensive investigations of thin-laminate composites made of hybrid fiber composites, which incorporate different types of fibers in a single composite system. The mechanical properties of the hybrid composite will be somewhere between those for single fiber composites. Hybrid composites can be classified as one of four types [4]: Type A is made by intermingling different fibers in a common matrix (i.e., intermingled or intraply); Type B is formed by laminating layers with fibers of different types (i.e., interlaminated or interply); Type C is in a form of fiber skins with a fiber core; and Type D is constructed by fiber skins with a non-fiber core. In addition, if the reinforcements are fabric, each fabric may contain more than one-type of fiber and is called interwoven [5].

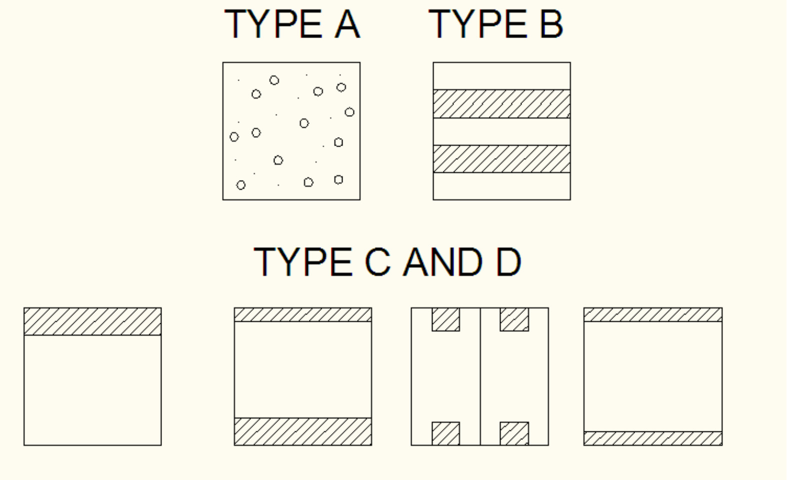

Figure 1.1. Schematic diagrams of hybrid types

1.1. STUDIES ON THE MECHANICAL PROPERTIES OF HYBRID AND WOVEN COMPOSITES.

a) Experimental studies

Fiber-reinforced composites are being used in applications that demand a high level of mechanical performance. Tensile, flexural or bending stresses develop in a structure under various loading situations. On the other hand, fatigue behavior is one of the main concerns in composite materials, especially when they are used in aerospace structures. Thus, the mechanical properties of composites should be clearly understood before using them in any design. There has been a lot of experimental research on the mechanical behaviour of hybrid and woven composites. Reyes [5] investigated the tensile and fatigue properties of thermoplastic fiber–metal laminates. The glass fiber-reinforced polypropylene hybrid systems exhibited higher fatigue strength. Lee [6] investigated the mechanical characteristics of hybrid composites with non-woven carbon tissue (NWCT) under static tensile and tension–tension fatigue loadings. Tsai [7] studied the fatigue behavior of 3D multi-layer angle interlock composite plates. Bellingardi and Cavatorta [8, 9] investigated the bending and fatigue behaviour of a hybrid glass–carbon non-woven fabric reinforced epoxy matrix composite, constituted by layers of biaxial carbon fabrics, biaxial glass fabrics and hybrid carbon–glass fabrics. Ni [10] studied titanium matrix hybrid composites and showed that the synergistic effect of TiBw and TiCp significantly affects the tensile properties of TMCs, and a proper volume ratio of TiBw to TiCp would provide the composite with better properties. Kang [11] studied the mechanical and thermal properties of interply hybrid carbon fiber (continuous and spun fabric)/phenolic composite materials. Through hybridization, tensile strength and modulus of spun type carbon fabric reinforced phenolic composites (spun CP) increased by approximately 28% and 20%, respectively. Hybrid CP also exhibited better interlaminar shear strength than continuous carbon fabric/phenolic composites (continuous CP). Khatri [12, 13] studied the tensile and flexural response of thick section hybrid composites with a polyphenylene sulfide matrix. The hybridization of the composite was achieved by using E-Glass and AS4-graphite fibers. Wan [14] studied the load–displacement behavior, flexural properties, impact property, and shear strength of 3D braided carbon/Kevlar hybrid composites. The new hybrid composite possessed advantages of both the carbon and Kevlar fibers. It was concluded that hybridization is an effective way of tailoring the properties of 3D braided composites for orthopedic applications. Park [15] studied the flexural properties, interlaminar shear strength, and impact properties of aramid/poly-ethylene intraply hybrid composites. Significant changes on the mechanical properties were observed due to hybridization. Muto and Arai [16] used the electrical resistance change method to detect damage in carbon-glass hybrid composites.

Hybrid fiber-reinforced composites may be exposed to high or low temperatures. Thus, it is necessary to perform laboratory tests to simulate the operational environment of the composite and further evaluate its structural integrity under practical service conditions. Unfortunately, available data on the influence of changing temperature on the mechanical properties and failure behavior of a given composite are somewhat limited. There are some studies on the high temperature effects on single species short fiber reinforced composites [68-70]. Bosze [17] investigated the effect of temperature on the tensile strength of the pultruded rods of unidirectional hybrid glass/carbon-epoxy composites core and proposed a convenient method to predict the temperature dependence of strength for similar unidirectional composites with the following formula:

$$\sigma_s(T) = \sigma_{To}[E^{'}(T)\frac{1}{E^{'}(T_o)}] \qquad (1.1)$$

where $\sigma_s(T)$ is the strength at temperature T, σ_{To} is the strength at the reference temperature (room temperature), $E^{'}(T)$ is the storage modulus at temperature T, and $E^{'}(T_o)$ is the storage modulus at the reference temperature. Dlouhy [18] studied the thermal aging of a glass matrix composite reinforced by short carbon fibers as well as by ZrO2 particles (hybrid composite) at temperatures in the range 500–700 ^{o}C for exposure durations of 24 hours in air. It was reported that the fracture toughness and flaw tolerance resistance decreased with increasing temperature. Schmitt-Thomas [19] investigated the effect of changing temperature on the strength performance and failure behavior of a hybrid short-fiber-reinforced thermoplastic composite. He concluded that the micro-failure behavior of the composite is closely related to temperature. Lipetzky [20] examined the mechanical behavior of a 2D woven, 0-90 SiC fiber-reinforced SiC matrix composite. Tensile experiments showed that the short-term behavior is largely independent of test temperature below 1000 °C. Microscopic examination revealed that the extent of fiber pull-out and the integrity of the remaining material are also independent of temperature in this range. Shan [21,22] studied the fatigue behaviour of Glass-Carbon Hybrid Composites immersed in water. It was found that the fatigue life of hybrid and all-glass composites in water is shorter than that found from tests done in air. However, hybrid samples showed better environmental fatigue resistance in water than all-glass samples.

Many researchers tried to improve the performance of hybrid composites by using different manufacturing techniques. Zhang [23] investigated the microstructure and mechanical properties of aluminum borate whisker (ABOw) and multi-wall carbon nanotubes (MWNT) hybrid composites. The results show that MWNTs decrease the compressive deformation of the hybrid preforms. Mader [24] investigated the effects of organic sizing, usually applied to the glass fiber surfaces, on the adhesive interaction with CBT resin. Li [25] proposed a new hybrid composite tube consisting of a tubular lattice of thick steel ribs and rings that are externally jacketed by a thin FRP skin. Gajiwala [26] used a novel approach to improve densification and mechanical properties of C/C composites by incorporating a lamina by lamina curing scheme using a new polyimide resin that exhibits much better thermal stability than conventional phenolic resins. Hussain [27] investigated the mechanical properties of carbon fiber reinforced composites. The Al_2O_2 particles dispersed into carbon fiber hybrid reinforced composites. It was shown that mechanical properties improved. Hitchen [28] developed a carbon-fiber/epoxy hybrid material which comprises ultra high-performance fibers in the principal load-bearing direction and standard carbon fibers in the secondary orientations. Another commonly used novel technique is adding different kinds of particles to the matrix. This technique enhances the wear and tribological behaviour of the composite. For instance, aluminum matrix composites reinforced with SiC and Gr particles are expected to have excellent wear resistance and friction properties due to the strengthening effect of SiC on the matrix and lubrication due to the smearing of Gr. Gupta and associates [29-31] investigated metal-matrix hybrid composites. They mixed different kinds of particles such as titanium, iron mesh, galvanized iron mesh and SiC into the matrix materials to enhance the properties of the composite. Aluminum, and magnesium alloys were used as matrix materials. Ko [32] investigated the mechanical properties of hybrid composites reinforced with both SiCw (whisker) and SiCp (particles) and their effect on aging.

In recent years there has been an increased environmental awareness, which has led to increased interest in the use natural fibers instead of man made fibers in composite materials. Natural fibers have proven to be suitable reinforcement materials for composites thanks to a combination of good mechanical properties and environmental advantages such as renewability and biodegradability. There has been a lot of research on natural fiber reinforced composites. Jute, sisal, coir, pineapple leaf, banana, sun hemp, broom and wood are some of the natural fibers used in composites [33]. Despite their attractiveness, such as low-cost, light-weight, enhanced mechanical properties, natural fiber reinforced polymer matrix composites suffer from low modulus, lower strength and relatively poor moisture resistance. Hybridization of natural fibers with stronger and more corrosion-resistant synthetic fibers such as glass fiber and carbon fiber can improve the properties of the composite. Velmurugan [34] investigated the properties of (randomly mixed) palmyra fiber, glass fiber hybrid composites. The results show that the mechanical properties of the composites improved due to the addition of glass fiber along with palmyra fiber in the matrix. The glass fiber skin - palmyra fiber core construction exhibits better mechanical properties than dispersed construction. Thwe [35] studied bamboo-glass fiber reinforced polypropylene composites. On the other hand, Jacob [36] studied the mechanical properties of sisal/oil palm hybrid fiber reinforced natural rubber composites. Paiva Júnior [37] investigated the tensile strength of plain weave hybrid ramie–cotton fabrics. Van de Velde [38] studied unidirectional (UD) and multidirectional (MD) flax/polypropylene composites. Arbelaiz [39] investigated the effect of fiber treatments and matrix modification on mechanical properties of flax fiber bundle/polypropylene composites. Some chemicals were used to improve the interfacial bonding between fibers and the polymeric matrix. The results suggest that matrix modification led to better mechanical performance than fiber surface modification. Meguid [40] studied the influence of the homogeneous dispersion of carbon nanotubes and alumina nanoparticles in epoxy adhesive for the purpose of enhancing its interface properties. Yao [41] studied concretes containing different types of hybrid fibers at the same volume fraction (0.5%) which were compared in terms of compressive, splitting tensile and flexural properties. Three types of hybrid composites were constructed using fiber combinations of polypropylene (PP) and carbon, carbon and steel, and steel and PP fibers. Test results showed that the fibers, when used in a hybrid form, could result in superior composite performance compared to individual fiber-reinforced concretes.

b) Analytical Models

Analytical models are being developed to predict the behavior of composites under various loading conditions, so that the best possible material is designed for a specific application. These models provide a cost effective tool to determine the effects of several parameters on the mechanical properties. These parameters include fabric weight\ constituent volume fraction\ yarn undulation\ weave style and properties of the constituent materials. Several micro mechanical models based on the classical thin laminate theory have been developed. Scida [42] developed a model called MESOTEX to predict the elastic behavior of composites reinforced with hybrid and non-hybrid weaves.

Naik and Ganish [43-45] considered strand continuity along both fill and warp directions and the presence of an inter-stand gap. In the Falzon and Herszberg [46-47] model the impregnated fill and warp yarns have undulated regions (assumed tone of a sinusoidal form) and non undulated regions (assumed to be of a constant form). Ishakawa and Chou [48-52] have presented three analytical models for the stiffness and strength investigation of woven composites (plain and satin weaves). In their mosaic model the fabric composite can be viewed as consisting of an asymmetric cross-ply laminate assemblage. The fiber undulation model takes into account fiber continuity and undulation only in the fill direction and not in the warp and fill directions. The bridging model breaks up the unit cell into interlaced regions, which are modeled as cross-ply laminates. The mosaic model is also applied to hybrid satin weaves. Peng and Cao [53] developed a non-orthogonal constitutive model to characterize the anisotropic material behavior of woven composite fabrics under large deformation. Huang [54, 55] developed a unified approach based on bridging micromechanics model to the simulation of inelastic and strength properties of textile (woven, braided, and knitted) fabric reinforced composite laminates. Yu [56] developed a new constitutive model based on a homogenization method by considering the microstructure of composites including both the mechanical and structural properties of fabric reinforcement.

c) Numerical Models

The finite element method can be used to study the overall behavior of composite structures at the macro level and the material behavior at the constituent level. Karakuzu and associates [57-59] numerically and experimentally investigated the bearing strength, failure load, failure modes and the effects of changing the geometric parameters in pin-loaded woven glass/vinylester and glass/epoxy laminated composites. Carvelli [60] developed a two- step 3-D finite element model using homogenization theory for periodic media both for the yarn and for the fabric to predict the strength and the stiffness of woven fabric laminates. Ge [61] presented a two-step finite element method (FEM) calculation to reveal the effects of reinforcement particles on the tensile properties and heat treatment behavior of silicon carbide (SiC) and graphite (Gr) particulate reinforced aluminum composites. Lin [62] studied the failure strength and failure mode of bolted connections of glass woven fabric composites numerically and experimentally. Zinoviev [63] performed numerical studies with the help of the UniCAD program, which is a computer program for the optimal design of unidirectional composites. Tabiei and associates [64-68] developed micromechanical models for woven composites using the method of cells and the four-cell method, to predict their properties. Most of the commercially available finite element software such as Abaqus, LS-Dyna do not have the material model to introduce nonlinear stress-strain behavior into the system. However these commercially available finite element software packages allow users to create user-defined interfaces to best simulate the real problem. Thus, Tabiei and associates successfully implemented nonlinearity into the finite element codes.

1.2. STUDIES ON THE IMPACT RESPONSE OF HYBRID AND WOVEN COMPOSITES

Composite structures may be subjected to various loading conditions during their service life. For the effective utilization of composites as protective structures, the critical requirement is the resistance to foreign object ballistic impact loading. In such applications, the condition of penetration of the projectile into the composite target and the associated damage mechanisms should be clearly understood. Post ballistic impact residual strength is also an important consideration. Impact loads can be classified into three categories: low velocity impact, high velocity impact and hyper velocity impact. The reason for this classification is that energy transfer between projectile and target, energy dissipation and damage propagation mechanisms undergo drastic changes as the velocity of the projectile changes. The kinetic energy of the projectile when it impacts the target is dissipated and absorbed in various ways by the target. The main energy absorbing mechanisms during ballistic impact are: kinetic energy absorbed by the moving cone formed on the back face of the target, shear plugging of the projectile into the target, energy absorbed due to tensile failure of the primary yarns, elastic deformation of the secondary yarns, matrix cracking and delamination and frictional energy absorbed during penetration. An impact event is considered to be a low velocity impact if the contact period of impactor is longer than the period of the lowest vibrational mode. In low velocity impact regime, the support conditions are crucial as the stress waves generated outward from the impact point have time to reach the edges of the structural element, causing its full-vibrational response. On the other hand, in high velocity or ballistic impact, the response of the structural element is governed by the ‘local’ behaviour of the material in the neighborhood of the impacted zone, the impact response of the element being generally independent of its support conditions. The contact period of the impactor is much smaller than the period of lowest vibrational mode of the structure. Hyper velocity impact involves projectiles moving at extremely high velocities such that the local target materials behave like fluids and the stress induced by the impact is many times the material strength [69]. Some researchers [70] have classified impact loads depending on the -velocity of the impact. Low velocity impact, in the order of 1 m/s, represents a tool dropped on a composite structure. Intermediate velocities, in the range of 10-100 m/s, represent runway debris striking an airplane. Ballistic impacts, in the velocity range of 100-1000 m/s, represent the impact of bullets, fragment and other low-mass projectiles on composite and textile protective armours or structures. Low velocity impact tests can easily be simulated using a drop-weight impact tester. Force-time histories and the impact velocity can then be easily obtained. Ballistic impact tests are performed using a gas-gun or a powder-gun, where compressed gas or gun-powder is used to propel the projectile. Projectile impact velocity and projectile residual velocity can be obtained easily. However, it is very difficult to obtain force-time and velocity-time histories. Some researchers tried to attach sensors to the projectile and record the desired data but it was not very successful due to progressing erosion of the projectile.

In this section, the literature concerning low-impact and ballistic impact responses of non-hybrid, hybrid and woven composites is reviewed. Because it is not the subject of our interest, hyper-velocity impact phenomenon is not covered here. First, studies on the low velocity impact response of composites are classified into three groups: experimental studies, analytical models and numerical models. Second, the same approach is used to classify studies on the ballistic impact response of composites. Finally, studies on some important concepts related to low and ballistic impact response of composites are discussed.

1.2.1. LOW-IMPACT RESPONSE OF HYBRID, AND WOVEN COMPOSITES

a) Experimental studies

Composites are exposed to low velocity impact such as tool drop during their service life. Their response to low velocity impact should be examined. There is a lot of research on impact response of glass [71-72] and carbon [73] fiber reinforced, laminated epoxy composites. Matrix material can be varied for different applications. For example, Alcock [74] studied the low impact response of all-PP composites and compared it to that of conventional commercial glass reinforced polypropylene composites. On the other hand, Sutherland [75] investigated the low impact response of glass-polyester. Due to their excellent impact resistance compared to FRPs, FMLs [76] are being used in many applications. A growing environmental awareness across the world has aroused interest in research and development of environmentally friendly and sustainable materials. Natural fiber [77] reinforced composites have great potential in engineering applications. Lin [78], investigated the low-velocity impact response of nanoparticle filled composites. Nanocomposites are a rather remarkable form of composite materials, which involve imbedding nano or molecular sized particles into organic polymer, or resin matrix materials. The nanoparticles can serve as matrix reinforcement as well as change the mechanical behavior of these materials. To date most of the research on low velocity impact in composites has mainly focused on impacting unstressed specimens. However this does not adequately reflect the real multidirectional complex loading states that the materials experience during their service life. Limited research [79-81] has been done to evaluate the low impact response of composites under pre-stress condition. For example Whittingham [81] studied the effect of an initial pre-stress on the response of carbon-fibre/epoxy laminated plates subjected to low velocity impact. Prior to being impacted, the samples were loaded either uniaxially or biaxially using a specially designed test rig. It was concluded that pre-stress does not significantly affect the response of the composite. Sandwich composites have become increasingly popular for applications including aerospace, marine industries, and ground transportation. They are favored for their high specific strength and stiffness, corrosion resistance, tailorability, and stability. Sandwich composites are very suitable for lightweight structures requiring high in-plane and flexural stiffness. Traditional sandwich structures consist of two face sheets and a core. The most common core materials are: balsa wood [82], polyurethane foam [83], honeycomb, pvc and others. Face sheets can be metal or fiber reinforced laminates [84]. To enhance the impact response of sandwich composites woven fiber reinforced laminated sheets [85-86] are being used as well. Ulven [82] studied the impact behavior of E-glass/vinyl ester (VE) balsa wood core sandwich panels exposed to fire for a certain period of time. Fire resistance is an important issue in marine grade sandwich structures because core materials tend to degrade rapidly following degradation of the face sheet(s) when exposed to fire. Perez [87] used autoclaved aerated concrete as a core material in a sandwich panel and conducted low impact tests. AAC/FRP sandwich panels exhibit a considerable reduction in bending stiffness after being subjected to a concentrated impact. The reduction of flexural strength was not found to be significant in low energy level impact. Jiang [88] formed a novel sandwich panel with additional sheets inserted into the core. The low impact response of this sandwich panel was then studied. However, it was concluded that the additional sheets had no significant effects on the deflection of the sandwich structures, regardless of the location of the internal sheets and the impact energy. Kim [89] studied the low impact response of an aluminum honeycomb woven fabric face composite body shell of a tilting railway vehicle. In order to enhance the impact performance of composite laminates various parameters related to composites have been studied extensively. Avila [90] dispersed nanoclay (Nanomer 130E) into the epoxy system in different ratios. The results have shown that delamination is reduced and the damping is increased during the rebounds. Influence of laminate thickness on the low impact resistivity of composites has been investigated in [91-93]. It was reported that thickness has significant effects on the performance of the composite. Effect of geometry on the performance of composites has also been studied in [94-95]. Because geometry affects the loading conditions, it also affected the response of the composite to low impact. Atas [96] studied the effect of the weaving angle on the low impact response of woven composites. No significant effect was reported. Imieliska [97] studied the effect of water immersion. Water immersion aging affected the microstructural integrity of the composites, causing numerous internal defects. Controlling fiber/matrix interfacial bond strength is very important especially when delamination is concerned. Kim [98] studied the effects of silane coupling agents on impact response of glass fabric reinforced vinylester matrix composites. Woven composites have tremendous potential for uses in applications where high strength, weight reduction, and damage tolerance are important design objectives, such as vehicle and body armor systems. Investigations of textile composites have been more extensive in recent years. This is mainly due to the ability of textile materials to accommodate complex shapes, and the flexibility. These materials offer flexibility for designing innovative and damage tolerant woven in systems subjected to extreme changes in pressure, temperature and strain rate. Fabrics can be weaved in 2-D and 3-D [99]. In 2-D weaving, there are different kinds of types such as plain, twill [100], crow-foot [101] etc. Qiu [102] invented a novel approach to reduce the density of 3-D composite materials by purposely introducing voids or a gaseous phase into the matrix through foaming. Improvement on the tensile strength was observed. Kinsey [103] described the results of an experimental study to determine the effect of resin (matrix) on the post-impact compressive behavior of carbon fiber woven laminates. Shim [104] carried out compression and four-point bending tests to examine the residual mechanical properties of crowfoot-weave carbon/ epoxy laminates subjected to velocity impact load. Hybridization technique is commonly used to combine the advantage of different types of fibers in the same composite. Different types of fibers [105-106] can be mixed together into the same matrix. There is limited work on the low impact response of hybrid composites [107, 108].

b) Analytical Models

There are many experimental studies on the low impact response of composites. However experimental testing can yield response data for a particular plate and load, but it is not generally practical, in terms of time and monetary expense to experimentally characterize the effects of a wide range of variables. For complete understanding of a class of composite materials, analytical studies are necessary. There are many models, such as the spring-mass, energy-balance, complete and semi-analytical models developed to predict low impact response of composites.

1. Spring-mass model

In this model impactor and plate are represented by two masses and they are connected to each other with a hertzian spring that represents the force-indentation relationship of contact. The plate is attached to the fixed boundary through other springs that represent the stiffness, shear and membrane stiffnesses. Khalili [109] developed a model for a sandwich panel and derived closed-form solutions for the contact force, displacements of the impactor and the panel in the transverse direction. This model uses discrete three-degrees-of-freedom dynamic system with equivalent masses and springs.

2. Energy balance model

Shivakumar [110] developed a simple energy-balance model, which is based on the principle of conservation of total energy of the plate-impactor system. Assuming the whole system behaves quasi-statically; all the initial kinetic energy of the impactor was used to deform the plate when the plate reaches its maximum deflection.

3. Complete models

The impact information predicted from simple models is limited and not accurate enough. Hence, complete models, in which the whole impact system is fully modeled, are developed and accurate solutions can be obtained [111-112].

4. Semi analytical models

Some models make use of experimental data to complement the analysis in predicting the response of the composite. Jimenez [113] proposed a model which has two systems set up in a serial arrangement. The first one is a spring-dashpot and the second is a hertzian spring-dashpot that simulates the indentation. Since the differential equation that describes this system does not have an analytical solution, a 4th order Runge–Kutta algorithm was used. The overall energy loss was calculated by means of the restitution coefficient, which was measured experimentally; these results were compared with those obtained solving the differential equation.

5. Others

Christoforou [114] provided a methodology to estimate the mass and velocity of a foreign object impacting a structure. The inverse model employs the direct model developed by the author and a least square optimization technique to reconstruct the impact force history. Davies [115] developed a procedure for the prediction of the threshold impact energy for the onset of delamination in fiber-reinforced quasi-isotropic laminates under low-velocity impact. It is primarily based on two models. One is the energy-balance model which equates the kinetic energy of the impactor with the static deformation energy of the laminate. The geometrical non-linearity of the deformation of the laminate is also taken into account. The other model is the force-driven model previously proposed by Davies and Zhang [116]. The combination of these two models forms a simplified and straightforward procedure for the prediction of the threshold impact energy for the onset of delamination without relying on a time-consuming dynamic analysis. Malekzadeh [117] proposed a new three-degrees-of-freedom (TDOF) springs–masses–damper (SMD) model to predict the contact force history of composite sandwich panels with transversely flexible core. Chun [118] in his study assumed the contact area between the striker and plate very small, and used the Hertzian contact law to evaluate the contact force. Choi [119] performed a parametric study on contact law by changing the value of the contact coefficient and exponent in the law. It was shown that accurate analytical results could be obtained using the linearized contact law. Guinarda [120] studied the 3D damage analysis of low-velocity impacts on laminated composites.

c) Numerical Models

Closed-form methods for predicting the response of composite plates to mechanical loads are limited to linear solutions (with many simplifying assumptions) of stress states, for specific geometries, lay-ups, loads, and boundary conditions. On the other hand, numerical techniques like the finite element method (FEM) calculations have been applied to plates and shells of different shapes, sizes, compositions, loadings and supports without the expense and lead time required for testing. The accuracy and practicality of FEM are dependent on the governing theories, model complexity, mesh refinement, user's skill (in the representation of the geometric structures, material properties, boundary conditions and loads), and a given computer's memory capacity, speed, and precision [121]. While some researchers developed finite element codes, some used commercially available software such as Abaqus [122-123], Ansys, LS-Dyna [124-127] etc. to simulate the low-impact behavior of different composites. Li [128-129] developed a numerical model, based on the Mindlin [130] plate element for directly and completely simulating the low-velocity impact-induced damages in laminated plates which can describe the various damages and their mutual effects. Besant [131] further modified the existing finite element code FE77 for analysis of impact of composites. The sandwich panels were modeled using 8 noded shell elements for skin and two layers of 20 noded brick elements for core. Duan [132] proposed a technique for searching the contact point pair in 3D finite element analysis. Based on the results of contact-impact analysis, damage in the composite laminate was predicted. Elder [133] reviewed the damage mechanics and fracture methods available in the literature for predicting delamination under impact. It was concluded that the linear elastic fracture mechanics method has been used extensively where the shape of the delamination front can be predicted and a suitably shaped mesh can be provided. However, as impact events produce irregular shaped delamination fronts, this method requires an adaptive mesh approach that is not yet available in any of the major analysis codes. The cohesive fracture model solves some of the limitation of the linear elastic fracture mechanics method, however a definitive study of its abilities has yet to be found in the literature. The delamination threshold load method is an extremely simple method and provides surprisingly good results. The review concludes that additional development of current techniques is required before a definitive predictive delamination method will be available. Hou [134] implemented an improved delamination criterion for laminated composite structures into LS-DYNA3D to take into consideration the out-of-plane stresses for damage initiation. The new delamination criterion was verified by experimental results for low-velocity impact. Mikkor [135] developed a finite element (FE) model, based on the explicit FE code ‘Pam-Crash’, to predict the impact damage tolerance of loaded composite panels. The model is designed to predict the extent of damage and the residual tensile and compressive strengths of laminates under static loads. Naik [136] developed a code using modified Hertz contact law and a 3D transient finite element analysis. The overall response of the plate was obtained based on the response of the plate due to a unit impulse of time duration. Eight-noded brick elements with three degrees of freedom per node were used for the analysis. Palazzatto [137] predicted the response of composite sandwich plates to low-velocity impact by a displacement-based, plate bending finite element algorithm. Fifth order Hermitian interpolation allows three-dimensional equilibrium integration for transverse stress calculations to be carried out symbolically on the interpolation functions so that transverse stresses within the elements are expressed directly in terms of nodal quantities. Tiberkak [138] implemented Mindlin's plate theory into the FE approach in which a 9-node Lagrangian element is considered to study low velocity impact response of fiber-reinforced composite plates. Naik [140], in another study, simulated the behavior of woven-fabric laminated composite plates under transverse central low-velocity point impact by using a modified Hertz law and a 3D transient finite-element analysis code. The in-plane failure behavior of the composites was evaluated by means of a failure function based on the Tsai-Hill quadratic failure criterion. Lee [141] predicted low velocity impact response of hybrid laminated composite plates (graphite/epoxy-glass/epoxy and graphite/epoxy-kevlar/epoxy) using the finite element method, and compared the results with those of a single laminated composite plate (graphite/epoxy) impacted at the center of the plate with velocity v. The modified contact law suggested by Yang and Sun [142] was used for calculating the contact force.

1.2.2. BALLISTIC -IMPACT RESPONSE OF HYBRID, WOVEN COMPOSITES

a) Experimental Studies

Most of the experimental works on ballistic impact found in the literature follow the same approach. Basically, the different kinds of plates are impacted at different velocities and post-impact data is evaluated using different techniques. Ballistic impact response of steel [143], aluminum foam sandwich [144], natural fiber composites [145], fiber reinforced plastics [146], ceramic/metal composite armours [147], aluminum [148-150], fiber-metal laminates [151-152] have been extensively investigated through the same procedure mentioned earlier. Due to energy absorption capability of fabrics, ballistic response of fabric-reinforced composites has also been studied by few researchers [153-156]. Cheeseman [157] has reviewed a number of studies on the ballistic performance of textiles. He concluded that material properties, projectile geometry, impact velocity and multiple plies have a profound influence on performance. However the effect of other factors such as fabric structure, far field boundary conditions and friction are not as apparent. Hosur [158] investigated the repair strategies for thick section woven S2-glass/vinyl ester composites subjected to ballistic impact loading. Three different approaches of repair were used. In the first approach, patch lay-up was used along with vacuum bag curing. In the second approach, chopped fibers in conjunction with micro-balloons were used to reinforce the resin system and applied to wet out the patches. In the third approach, in addition to the patches, a single ply was used as additional stiff repair member. Ballistic limit of repaired panels was about 25%, 112%, and 64% of that of virgin samples and the flexural strength of repaired sections was about 53%, 51% and 58.5% of that of undamaged sections respectively. Boccaccini [159] investigated the ballistic impact resistance of novel mullite fiber/mullet matrix composites. Iremonger [160] conducted ballistic impact tests on helmet material laminates manufactured with different pressing loads. Influence of the various parameters such as experimental design [161], through-thickness cracks [162], and preforming binder applied to the fibers [163] and glass-fiber sizings [164] on the ballistic impact has also been studied experimentally. Stratt [165] used a new method for continuous measurement of projectile motion in ballistic impact experiments. In this method, velocity is measured directly using a laser. On the other hand time histories of projectile velocity and acceleration, impact force and projectile energy loss during impact are obtained through simple mathematical operations. Czarnecki [166] developed a semi empirical method to estimate V_{50} of composite laminates.

b) Analytical models

Classification that was made for low-impact analytical models is still valid for ballistic impact models. Naik [167-169] has a number of publications especially on the analytical modeling of woven composites. His models are based on the various energy absorbing mechanisms. These are: cone formation on the back face of the target, tensile failure of primary yarns, deformation of secondary yarns, delamination, matrix cracking, shear plugging and friction during penetration. Ben-Dor et al. [170] also have various publications on the same subject. A model was derived for describing penetration of monolithic semi-infinite and finite FRP laminates struck transversely by a rigid projectile with an arbitrary 3-D shape. In [171] new “area rules” was proposed for penetrating impactors. Using Florence’s model an optimal design of a two-component ceramic-faced lightweight armor against normal ballistic impact was determined [172]. Some models were proposed for calculating force, displacement and velocity in ballistic impact of woven fabrics [173-176]. Jovicic [177] discussed two models for gradient of composite armors: (a) an approximate fiber/epoxy two-phase model for the backing and (b) a damage-based, rate-dependent model for the ceramic spheres embedded in the epoxy. Sun [178-179] used a penetration model based on a ring element to predict penetration, delamination and residual velocities of thick composites. Puente [180] developed an analytical model to study the impact process of a spherical projectile penetrating at high velocity into a carbon/ epoxy plain woven laminate. The model is based on energy balance, where the kinetic energy of the projectile is absorbed by the laminate by three different mechanisms: laminate crushing, linear momentum transfer and tensile fiber failure. Went [181] proposed a model for FRP composites. This model was based on the assumption that the deformations are localized and that the mean pressure offered by the FRP laminate targets to resist the missiles consists of two parts. One part is a cohesive quasi-static resistive pressure due to the elastic-plastic deformation of the laminate materials. The other is a dynamic resistive pressure arising from velocity effects. Another model for FMLs was proposed by Fatt [182]. Morye [183] developed a simple model for calculating the energy absorption of polymer composites upon ballistic impact.

c) Numerical Models

Literature review shows that commercially available LS-DYNA FEM software is commonly used to simulate ballistic impact of composite materials. Various parameters in ballistic impact are evaluated using aforementioned software package. Normal and oblique impact ballistic impact on ceramic composite armours [184], response of an integral armor under high-velocity impact [185], penetration performance of typical aircraft structural components [186], ballistic performance of woven Kevlar armor [187] where successfully simulated. In some cases, certain conditions or material models may not be available in the software package [188-192]. The solution to this problem is to introduce user-defined codes into the software package to best satisfy the real conditions. The ballistic impact with 6 to 7 km/s velocity [193],ballistic impact response of Kevlar 29 reinforced thin composite laminated plates [194], ballistic impact behavior of mixed armors consisting of ceramic tiles backed by a metallic plate[195] were simulated using Auto-Dyna. Self-designed FEM models are also employed for ballistic-impact problems [196-197].

1.2.3. COMMON STUDIES ON THE LOW VELOCITY AND BALLISTIC IMPACT RESPONSE OF COMPOSITES

a) Thru-thickness improvement methods

Most of the composite components used in the aerospace industry are made of fiber reinforced laminated composites. When such a composite impacted, small dent at the impacted side and significant delamination at the backside is observed. This kind of damage reduces the load bearing capacity of the composite by 40-60% especially under compressive loads. Damage can be detected using nondestructive testing such as visual detection, C-scan and X-ray and the composite can be replaced with an undamaged one. However, sometimes the composite might be used in such places that access to the back side can be very difficult and non-destructive testing techniques might not be applicable. Thus, to improve the damage tolerance and interlaminar fracture toughness of the composite, great efforts have been made. Toughening of thermosetting matrices can increase interlaminar fracture toughness of the composite. On the other hand, 3-D weaving or braiding, stitching, pinning and short fiber insertions are some of the methods used to increase translaminar reinforcement [198-212]. These methods can be effective for composites subjected to low impact and ballistic impact. Stitching is the most commonly used method to improve impact resistance of the composite. Zhang [198] investigated the effect of z-pinning on the initiation and propagation stages of delamination damage due to low velocity impact, and the subsequent compressive strength. It was reported that pinning reduces the damage area by up to 64%. For pinned laminate, the critical impact force is slightly lower whereas the maximum impact force is higher than that of unpinned samples under the same impact energy. Z-pinning also significantly improves the after-impact compression strength. The pinned specimens had an approximately 45% higher residual strength than that of their unpinned counterparts. Byun [199] fabricated a new type of 3D structure by combining the ATP process and through-thickness stitching. Impact performance of 2D and 3D composites was characterized for comparison. Lopresto [200] studied low impact response of stitched carbon fibre-reinforced plastic (CFRP) laminates of various thicknesses and compared the results with those obtained from unstitched composites. It was concluded that stitching is effective in hindering delamination propagation, and that the penetration energy is 30% lower than that for unstitched composites. Aymerich [201] examined and compared the behaviour of stitched and unstitched cross-ply graphite/epoxy laminates subjected to low-velocity impact. He found that the insertion of stitches produces a reduction of the delamination area starting from impact energies of approximately 3 J. Stitching does not modify significantly the total amount of fiber fracture or interlaminar matrix damage, but it affects their through-thickness distribution, by promoting fiber fracture in the distal plies of the laminate and delaying delamination formation on the interface closest to the impact side. Hosur [202] experimentally investigated damage resistance of stitched/unstitched S2-glass/epoxy composites subjected to high velocity impact loading. Caprino [203] studied the response of stitched graphite/epoxy subjected to high velocity impact. Laminates of different thickness were considered. In order to predict the perforation energy as a function of target thickness and bullet diameter, the Reid and Wen model and the modified Cantwell and Morton model were used. It was found that the Reid and Wen model is effective in predicting the influence of panel thickness on the perforation energy. However, that was not the case for bullet diameter.

The modified Cantwell and Morton model yielded a good estimate of both the perforation energy and the residual velocity as a function of the coupon thickness and impactor diameter. Mouritz [204] studied the effectiveness of stitching in increasing damage resistance of glass reinforced vinyl ester composites. The composites were stitched in the through-thickness direction with Kevlar and were subjected to ballistic impact and under water explosive shock wave moving at 1.5 km s^{-1}. He found that the amount of delamination caused by a ballistic projectile was reduced slightly with stitching. Stitching was also effective in increasing the damage resistance against explosive blast loading. Larsson [205] evaluated the effect of stitching on the low velocity impact and on the ballistic impact damage tolerance of carbon fiber reinforced brittle epoxy laminates. He concluded that stitching increased damage resistance of the composite subjected to low velocity impact and ballistic impact. Mines [206] experimentally measured the perforation for woven, z-stitched and through-thickness z-stitched glass polyester laminates for a number of laminate thicknesses.

b) Temperature effect

Since they are being used as load carrying components in marine and aerospace structures, composites are often subjected to thermal loading in addition to significant dynamic loads due to impact by foreign objects. The loading conditions and the environmental conditions that a composite is subjected play a key role in determining its impact failure process. Thus, heat resistance of composites to low and high temperatures has to be studied carefully. However, the fracture behavior and failure mechanisms of laminated composites at low and high temperature levels are complicated when compared with those at room temperature. In the aeronautics and aerospace industries the specific behavior of the composite material at very low temperatures is extremely important. CFRP structural components can suffer high velocity impact at cryogenic temperatures. Such is the case for high-flying aircrafts (-60 ^{o}C) and spacecraft orbiting around the Earth (-150 ^{o}C when not directly exposed to solar radiation). Combat aircraft may suffer ballistic impact; commercial aircraft may be subjected to ballistic impact due to terrorist attack inside the plane; spacecraft may be impacted by space debris. In addition to these examples, cryogenic tanks can suffer low velocity impact during maintenance operations.

Temperature effect on low velocity impact of hybrid composites exhibits more complexity due to the difference in thermal expansion coefficients of fibers and resin. Thermal mismatch is already a concern in thin hybrid composites. This problem, as well as other issues (e.g., fiber waviness) would be even more severe when thick-section composites are considered. Since the majority of applications of thick-section composites are for military use, temperature in armor-grade hybrid fiber composites during ballistic impact and projectile penetration should also be carefully accounted for. The literature available on this particular subject for thick-section hybrid composites is very limited. It is practically none for thick-section interwoven hybrid composites. Bibi et al. [213] studied the impact performance of a number of thermoplastic and thermosetting matrix carbon fiber composites at room temperature, 70 ^{o}C and 120 ^{o}C. Levin [214] reported a decrease in delamination area with increase in temperature for temperatures between -40 ^{o}C and 70 ^{o}C for a carbon-fiber composite laminate subjected to high energy impact. Kwang-Hee et al. [215] studied the effect of temperature variation (-30 to 120 ^{o}C) on damage of orthotropic CFRP laminates at non-penetrating impact velocities (up to 100 m/s). They observed a linear relationship between the impact energy and the delaminated area, as well as an increase in the damaged area as the temperature decreased. In a similar high velocity impact study on cross ply laminates of polyethylene fiber/epoxy matrix system [216], it was found that the damage initiation energy doubled when the temperature was increased from -50° to 100 °C. In contrast, laminates containing plain-weave fabrics showed very little influence of temperature on the total impact energy required for complete penetration of the specimen. Lo´pez-Puente et al. [217] extended this analysis down to -150°C. Both of them focused their work on high velocity perforating impacts (from 100 to 500 m/s), far away from the threshold impact energy. Dutta [218] analyzed the energy absorption of graphite/epoxy plates under low velocity impact using a Split Hopkinson pressure bar, and found a small dependence on temperature. Hirai [219] evaluated the effect of temperature on the low-velocity impact response of vinyl-ester-matrix composites reinforced with woven E-glass fabric. It was shown that the extent of damage and the residual properties of the laminates vary with fiber surface treatment and impact test temperature. The damage area increases with increasing temperature and impact energy. Levin [220] reported a decrease in delamination area with increase in temperature in the range between -40 °C and 70 °C for a carbon–fiber composite laminate subjected to high-energy impact. Salehi-Khojin [221] studied low velocity impact behaviour of fiberglass and Kevlar composite at different temperatures ranging from -50 to 120 °C in an attempt to better characterize the impact properties of laminated composites. The energy levels chosen result in non-penetration, intermediate penetration, and full penetration of the composite plates at room temperature, respectively. The focus of this study was to show the effect of temperature on these impacted composites. Compression tests were conducted to determine the remaining compressive strength after impact. It was found that at low impact energy, the amount of maximum absorbed energy is almost constant and independent of temperature. With increasing energy level absorbed energy becomes more and more dependent on temperature. At each of the impact energies, maximum deflection is a function of impact energy and temperature so that maximum deflection increases with a corresponding increase in impact energy or temperature. Gomez [222-223] summarizes the results of low velocity impact tests carried out at different temperatures ranging from 20 to-150 ^{o}C on CFRP laminates. It was shown that damage induced in CFRP laminates by low velocity impact loads (when no perforation occurs) increases with impact energy. The experimental results obtained in this work showed that cooling the laminate before impact has an effect on damage similar to that of increasing the impact energy. Gustin et al. [224] investigated different combinations of carbon/Kevlar fiber and carbon/hybrid fiber at room temperature and at different impact energies. They showed that the addition of one layer of Kevlar and hybrid to the impact side of the face sheet improved the maximum absorbed energy and average maximum impact force. Khojin [225] has studied the temperature effect on carbon fiber sandwich composite plates with three layers carbon and a layer Kevlar or hybrid layer on impacted at energy levels of 15, 25 and 45 J at different temperatures ranging from -50 ^{o}C to 120 ^{o}C. In this investigation, temperature was found to have significant effect on the impact behavior of graphite and combinations of graphite with hybrid and Kevlar. Schultz [226] studied the effect of temperature and strain rate on the strength of PET/glass fiber composites.

c) Repeated impact

Low impact loading condition mostly occurs when tools are dropped onto the surface of a composite structure or from the impact of debris, fragments, or projectiles. Most of the experimental work on the low velocity impact response of composites focuses on impacting the composite at different energy levels and evaluating the created damage. However, rupture does not occur with a single hit. In fact, it is actually more important to determine the evolution of the damage produced than, solely, the absorbed energy. Some investigators have used compression-after-impact and other static tests to obtain measures of damage tolerance and residual strength after low-velocity impact. Subjecting specimens to repeated impacts can be employed to monitor residual strength and damage progression of composites. Belingardi [227] studied the testing of thick glass reinforced plastics laminated composites via repeated impacts, with an emphasis on the comparison between the more traditional hand lay-up manufacturing technique and a viable alternative such as vacuum infusion. He reported that no significant differences exist in the force, energy curves and damage parameter for tests in which no perforation occurs. When the impact energy causes determine laminate perforation, hand laid specimens survived more impacts before perforating, absorbing more total energy. Zhu [228] investigated the endurance of hard coatings under impact loading conditions. He concluded that two main failure modes, namely adhesive and cohesive failure, can be found in repeated impact loading. Adhesive failure is associated with adhesion of the coating, while cohesive failure is associated with toughness. The failure mode can be changed with different impact velocities even at the same loading force. To achieve cohesive failure for a tough coating, the increase of the impact velocity is efficient when the energy-cycles rather than the load-cycles relation is a more suitable index to indicate the damage resistance of coatings. Baucom [229] examined the damage progression and the absorption and dissipation of energy in 2D and 3D woven composite systems subjected to repeated impact up to the moment of complete perforation. It was reported that the 3D systems survived more strikes before perforating, and these systems absorbed more total energy than the 2D laminates and energy dissipation increased significantly for both systems, as damage progressed. Morais [230-231] investigated the influence of laminate thickness on the resistance to repeated low energy impacts of glass, carbon and aramid fabrics reinforced composites, at two levels of impact energy. The results obtained show that below a certain energy level the cross section of the laminate is the most relevant variable that determines the impact resistance. When the energy level of the impactor is increased, fiber characteristics become relevant. The glass fabric reinforced composite showed the steepest increase in impact resistance with increasing laminate thickness. Baucom [232] in another paper examined the effects of reinforcement geometry on damage progression in woven composite panels under repeated drop-weight impact loading conditions. It was concluded that the radial spread of damage was smallest for the 2D laminates and largest for the 3D woven composites. The 3D composites had the greatest resistance to penetration and dissipated more total energy than the other systems. Morais [233] used the low velocity impact tests results conducted on carbon–epoxy composites to develop a simple phenomenological equation relating the number of repeated low energy impacts and the duration of the impact event. Duration of the impact (t) was correlated against the number of repeated impact (N_i) by the quadratic equation

$t = a_3.N_i^{\ 2} + a_2.Ni + a_1$ **(1.2.3.1)**

where the coefficients a_1, a_2, a_3 are determined using the experimental data. Additionally, the damage parameter D was estimated using the following equation:

$D = 1 - E^* / E$ **(1.2.3.2)**

where E^* is the current stiffness and E is the initial stiffness for the undamaged material. It was concluded that the terms in the quadratic equation are structure dependent, varying as a function of the laminate stacking sequence. Hosur [234] evaluated the behavior of woven carbon/epoxy and woven glass/epoxy under repeated impact conditions. Laminates were subjected to repeated impact loads up to a maximum of 40 impacts at energy levels ranging from 10 to 50 J. He showed that there was a sudden drop in the peak load after a certain number of impacts. Absorbed energy also showed similar trend with respect to the number of impacts. The damage area increased with the number of impacts, but after a certain number of impacts it did not increase significantly. Mouritz [235] studied the flexural strength and interlaminar shear strength of stitched and non-stitched glass-reinforced plastic (GRP) laminates under conditions of increasing impact energy and increasing number of repeated impacts. He concluded that the strengths were reduced considerably with increasing number of impacts. The laminates suffered severe microstructural damage under repeated impacts, including shear cracking of the resin, delaminations, and crushing and fracture of glass fibres.

d) Projectile Shape

Studies in the literature show that the nose shape of the projectile plays an important part in penetration of targets at velocities below the dynamic yield strength of projectile material; the more blunt the nose shape, the higher the ballistic-limit velocity. At target impact velocities that exceed the dynamic yield strength of the projectile material, the nose shape has a negligible effect on the ballistic limit velocity [236]. The effect of the projectile shape varies with various parameters such as thickness of the target plate, impact velocity of the projectile, target thickness to projectile diameter ratio and nose angle or nose radius of the projectile. The deformation behavior of aluminum plates of various thicknesses was studied experimentally and numerically by Gupta [237]. The aluminum plates were impacted by blunt, ogive and hemispherical nosed projectiles. In another research [238], Gupta used the same approach to study the impact behavior of layered aluminum plates. He also studied the impact behavior of thin aluminum plates [239]. Ulven [240] investigated to what extent projectile geometry influenced damage propagation and evolution during ballistic impact normal to carbon/epoxy composite panels. It was reported that conical projectile high velocity impact resulted in the greatest amount of energy absorbed at ballistic limit followed by flat, hemispherical, and fragment simulating projectile impact. Cour-Plais [241], Schäfer [242] and Christiansen [243] studied the shape effects in hyper-velocity impact. Wen [244] derived simple equations for the penetration and perforation of FRP laminates by rigid projectiles with different nose shapes. It was shown that the theoretical predictions are in good agreement with experimental observations for FRP laminates struck normally by rigid projectiles with, conical, hemispherical and ogival shape. Chen and Medina [245] studied the development of damage in B/Al composite laminates subjected to high-velocity impact using the smoothed particle hydrodynamics (SPH) method. It was concluded that projectile shape significantly affects the progression and final state of the damage mechanisms in the composite targets. Turgutlu and associates [246] studied the effect of projectile nose geometry on weld interfaces during the impact spot welding of copper flyer plates (FP) to brass parent plates (PP).

e) Damage Evaluation

Polymer composites can be susceptible to impact damage during manufacturing and in service. These damages can be in the form of matrix cracks caused by tension or shear debonding between the fiber and matrix, delamination at the interface of adjacent plies with different fiber directions and fiber breakage and pull-out from the matrix. These damages can have an adverse effect on material performance and structural integrity. Therefore damaged composites should be carefully examined. Damage detection techniques applied to composite structures are classified into two categories: nondestructive and destructive techniques.

Nondestructive Techniques**:**

a) Liquid penetration [247]: Paint based chemicals are applied on the surface of the composite. A chemical penetrates into the composite where damage exists.
b) Visual inspection: Damaged specimen is inspected by eye.
c) Optical Microscopy: If the damage on the surface of the composite is very small and cannot be seen by the naked eye, optical microscopy can be employed to examine the surface.
d) Ultrasonic scan [248-251]: This method is the most common damage detection method used by researchers. Recently Aymerich [252] used ultrasonic evaluation to detect matrix damage. Other researchers made a ply-by-ply damage detection using ultrasonic technique [253-254]. Mouritz, et al. [255] applied the pulse-echo ultrasonic technique to thick GRP composites while Dong, et al. [256] adopted an

ultrasonic inspection system to explore on-line damage detection. However, the technique encounters difficulty to locate the through the thickness damage when composite specimens suffer large deformation.

e) Radiographic analysis: It is very powerful method to detect delamination as well as major cracks [257-259].

f) Acoustic emission [260-261]: It can be used to monitor damage initiation and progression. However, method cannot give any information about damage size and location.

g) Dynamic photoelasticity: The optical Coherent Gradient Sensing (CGS) technique combined with high-speed photography can obtain qualitative information regarding the stress field and observe the progression of damage [262-263]. The particular geometry of specimens and test set-up used here limit the application of this technique.

h) Others: Nunes [264] developed an automated digital analysis procedure to determine size and shape parameters that characterize the damaged areas. The procedure developed proved to be robust and sensible enough to cope with subtle variations in the damaged areas. Zhang [265] used Electronic Speckle Pattern Interferometry (ESPI) to visualize and quantify the internal damage in terms of thickness, density and uniformity degradations of fringe patterns. Takeda [266] applied small-diameter fiber Bragg grating (FBG) sensors for the monitoring of delamination induced by low-velocity impact. FBG sensors were embedded into carbon fiber reinforced plastic (CFRP) laminates. After impact, reflection spectra from the embedded FBG sensors were measured and compared with C-Scan.

They found that using small-diameter FBG sensors was effective for the monitoring of delamination. Roh [267] presented a study which deals with the detection of the strains and optimization of shape memory alloys (SMA) under low velocity impact.

Destructive Techniques:

De-ply technique and cross-sectional micrographs are two available destructive techniques [268-269]. In the de-ply technique [270], the damaged composite specimen is soaked in a solution to allow the solution to penetrate into the internal cracks. Then the specimen is treated under high temperature for a certain time, resulting in partial pyrolysis of the polymer matrix. The individual plies are then separated. Under an optical microscope, delamination, matrix cracking and fiber breakage can be detected. The results from de-ply are very accurate and reliable. However, this method is time-consuming and not suitable for thermoplastic matrix. In the cross-sectional technique [271-272], the damaged specimen is sectioned into a sufficient number of thin strips at different locations and orientations over the whole damaged zone. A series of microscopic images can be taken and a 3D map constructed. The damage distribution through the whole damaged zone can then be established. Using cross-sectional micrographs, more detailed damage information can be obtained than any nondestructive assessment. Like the de-ply technique, cross-sectional micrograph is time-consuming. Extreme precautions should be taken to avoid causing new damage during sectioning. It is worth to note that a combination of the above damage assessment techniques is needed to understand the full damage in most cases. The principle of choosing suitable techniques is dependent on the damage patterns and the researcher’s objectives [273-276].

1.2.4 Objective and distinction of our study

(a) Study the effect of hybridization on the impact response of woven composites with applications to armors. Specifically, graphite composites are prone to penetration. Whether penetration can be prevented by adding glass layers?

(b) Develop a finite element model to predict the behavior of hybrid woven composites (by using a user-defined material model). Testing is very expensive and time consuming. Once the finite element model is verified, then it can be used to study the behavior of other composites.

(c) Prediction of ballistic limit velocity using combined experimental and numerical approach.

(d) Study the effect of impactor shape on the impact response of composite.

(e) Study effect of glass fabric thickness on the performance of woven glass/graphite hybrid composites.

(f) Study the effect of repeated impacts on the performance of the woven composites.

Obviously, there is limited literature available on the mechanical and impact behavior of glass/graphite fiber hybrid composites. In particular, tensile, low-impact and ballistic impact behaviour of plain-woven S2-Toughened Glass/ IM7 Graphite fiber, SC79 epoxy matrix hybrid composites at room temperatures, which are the focus of our research, have not been studied yet. Also a literature review shows that there is no proper model developed that can simulate the impact behavior of our material.

2. Experimental set-up and the materials

2.1 Tensile test set-up

In this study, all of the tensile tests were performed using an MTS 810 97-KN universal testing system. The system is mostly used for general-purpose static and low-cycle fatigue tests. All of the tensile tests in our study were displacement controlled. However, MTS 810 is capable of conducting force, strain and displacement controlled tests. The hydraulic grips with varying gripping pressure allow the user to arrange the grip pressure for a specific material.

Figure 2.1 Tensile test machine and the environmental chamber

The tensile tests can be conducted at different temperatures using an environmental chamber. The temperature can be varied between –129 to 316°C. Internal heater provides the high temperatures. On the other hand, the low temperatures can be obtained using liquid nitrogen or liquid carbon dioxide. The test results are recorded (in voltage) using data acquisition card and software system. The proper conversions should be made to obtain force-time and displacement-time histories.

2.2 Drop-weight impact tester

In this study, all the low impact tests are performed using Instron-Dynatup 8250 impact test machine, a typical drop-weight impact tester with pneumatically assisted system (Fig. 2.2). We can control the impact velocity in a range of 0.61 m/sec to 13.41 m/sec by changing the drop height or using pneumatic assist while the drop weight varies from 2.5kg up to more than 45kg. Accordingly, the impact energy can vary from 0.67 Joules to around 440 Joules. The shape of impactor nose can be different, however most tests in this study were performed using a hemispherical impactor with diameter of 16 mm.

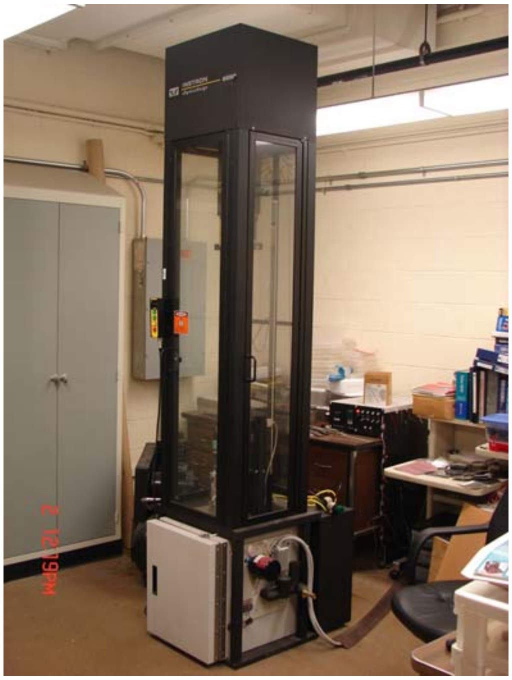

Figure 2.2 Dynatup impact tester.

With the attached environmental chamber, we can conduct the testing in either high or low temperature environment. The temperature range is from -50°C to +175° C. 1.3 kW open coil heater provides the high temperatures. The low temperatures are achieved through the use of either liquid nitrogen or liquid carbon dioxide. Specimens are clamped circumferentially with a 76 mm diameter fixture. There is a pneumatic break to prevent multiple strikes during each test. Using Dynatup 930-I data acquisition system, we can record the time histories of impact loads which are measured using a load cell located just above the impact nose and the impact velocity which is measured by one pair of photoelectric-diodes system attached to the base of the test machine.

However, with Dynatup 930-I data acquisition system, only load (the resistive force of the specimen) vs. time and initial impact velocity (just prior to impact) can be measured directly. Using the equations of motion, energy absorbed by the specimen, velocity of impactor and deflection at the impact center can be derived and recorded into file. The procedures are as follows (assuming data starts at t=0):

Notation	
v_i	Impact velocity measured by photodiodes.
$p(t)$	Load value measured by 930-I at time t.
m	Total mass of impactor (impact tower and nose)
g	Acceleration of gravity
$f(t)$	Total force acting on the impactor at time t.
$a(t)$	Resultant acceleration of the impactor at time t.
$v(t)$	Velocity of the impactor at time t.
$x(t)$	Deflection (position) of the impactor at time t.
$K(t)$	Kinetic energy of the impactor at time t.
$V(t)$	Potential energy of the impactor at time t.
$E_a(t)$	Energy absorbed by the specimen at time t.
$E(t)$	Total energy of the impactor /specimen system at time t.

Table 2.1 Notations used in drop impact tests

$$f(t) = mg - p(t) \tag{2-1}$$

$$a(t) = \tfrac{f(t)}{m} = g - \tfrac{p(t)}{m} \tag{2-2}$$

$$v(t) = v_i + \int a(t)dt = v_i + gt - \tfrac{1}{m}\int p(t)dt \tag{2-3}$$

$$x(t) = \int v(t)dt = v_i t + \tfrac{1}{2}gt^2 - \tfrac{1}{m}\int(\int p(t)dt)dt \tag{2-4}$$

$$E(t) = K(t) + V(t) + E_a(t) = K(0) \tag{2-5}$$

while $K(0) = \tfrac{1}{2}mv_i^2$ and the potential energy can be neglected, since the displacement is small. Therefore the energy absorbed by specimen can be computed as below

$$E_a(t) = K(0) - K(t) = \tfrac{1}{2}m\{v_i^2 - [v(t)]^2\} \tag{2-6}$$

2.3 Ballistic Gas-Gun

The ballistic impact tests were performed using an in house designed gas-gun (Fig.2.3). The 22 caliber copper bullet with plastic sabot was used as a projectile (Fig.2.5). The gun consists of helium tank, temporary gas storage vessel, solenoid valve and stainless-steel barrel. The fixture (Fig.2.4) with the front protective pipe was used to clamp the specimens. The specimens with two different dimensions were clamped from both ends during the ballistic impact tests (Fig.2.6).

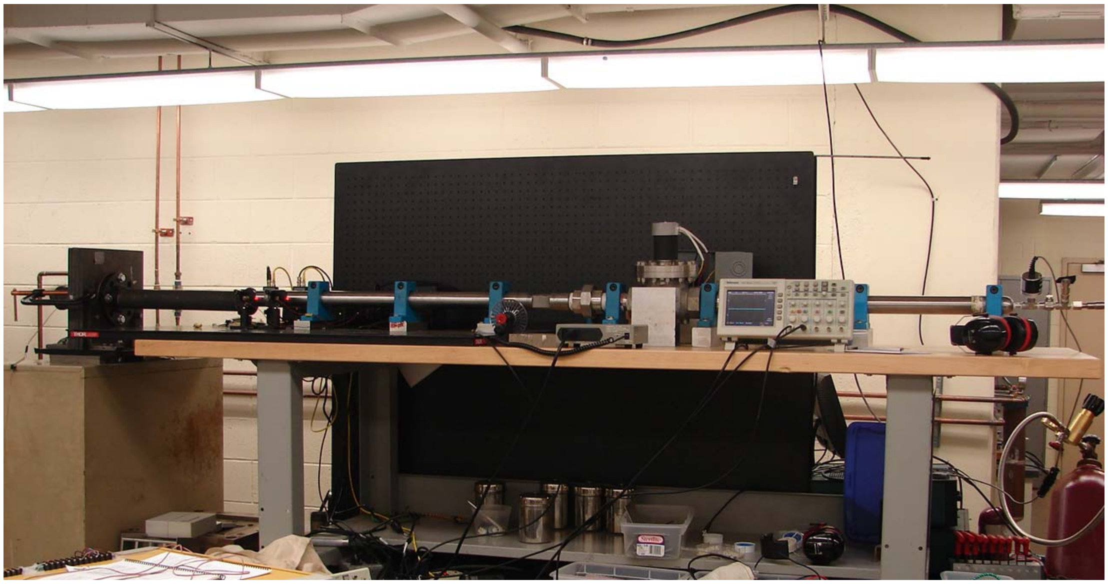

Figure 2.3 Ballistic impact test set-up

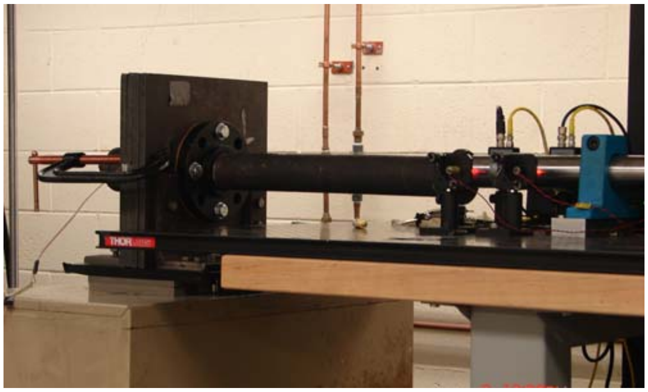

Figure 2.4 Fixture

Figure 2.5 Sabot and bullet

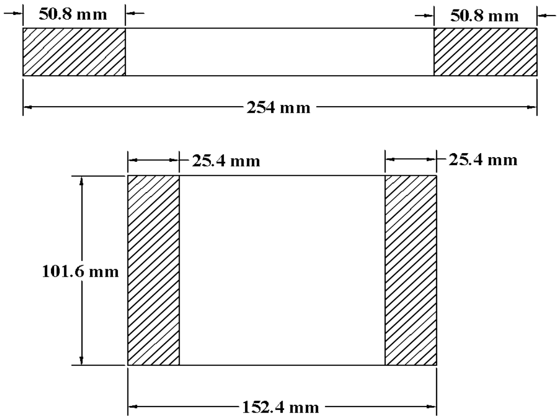

Figure 2.6 Ballistic impact test specimens

Compressed helium was used to propel the projectile. Varying the helium pressure controls the initial velocity of the projectile. Two holes were drilled on the barrel for velocity measurement. Two laser beams continuously feed the optical sensors. When the projectile passes through the holes, it blocks the lasers and the oscilloscope captures the voltage change. The velocity of the projectile is than calculated from the distance between the two sensors divided by the time that projectile spends traveling between the two holes. Figure 2.7 shows the two sensors and the voltage time histories captured with oscilloscope. However, the initial velocity is the only parameter that could be measured during the ballistic impact tests. The force-time histories and the deflection-time histories can not be measured with our set-up.

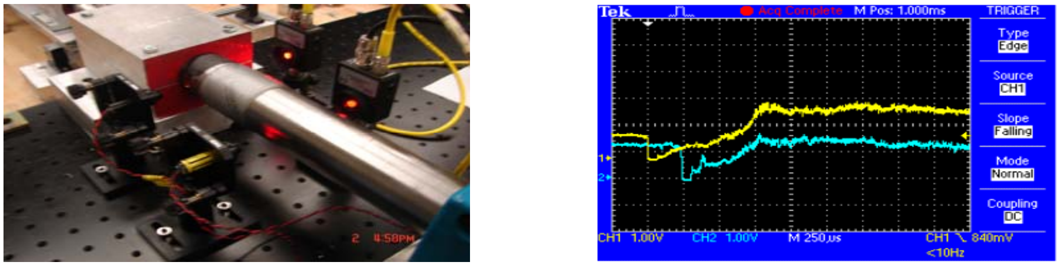

2.7.(a) Lasers and optical sensors

2.7. (b) Voltage-time histories

Figure 2.7 The velocity measurement during ballistic impact

2.4 Ultrasonic Damage Evaluation System

We use UltraPAC, an advanced, modular and expandable ultrasonic system offered by Physical Acoustics Corporation (Figure 2.8), to do the damage evaluation for the impacted specimens. The through-transmission (Fig. 2.9) techniques are used in this study. Flat and focused transducers (0.25 inch-diameters) of various frequencies (5 to 25 MHz) can be chosen for different specimens. Lower frequency transducers give better result when scanning thick specimens. Pulse-echo techniques are very sensitive and accurate for flat specimens, but they are not valid for large deformed specimens. For specimens with large deformation we must use through-transmission techniques.

Figure 2.8 The UltraPAC system

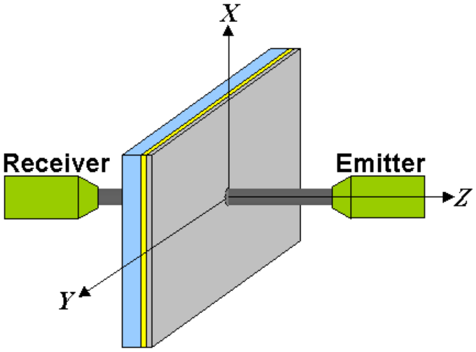

Figure 2.9 Through-transmission technique

2.5 The materials and the specimens

The materials used in this research are woven S2-glass/toughened epoxy, woven IM7-graphite/toughened epoxy and woven S2-glass, IM7-graphite/toughened epoxy hybrid composites. S2-glass fabrics (S2-4533 6000) and IM7-graphite fabrics (IM7-GP 6000) were supplied by the Hexcel Corporation. The matrix, SC-79 toughened epoxy resin, which has Part A (Batch number: SC79A012307) and Part B (Batch number: SC79B012507), was supplied by Applied Poleramic Inc. The manufacturing of the composite was done by EDO Fiber Innovations. The vacuum assisted resin transfer molding (VARTM) technique was used to stack the plain woven fabrics together (Fig.2.10). The specimens were cured at 177^0 C. Fiber volume fraction for all types was 60%. The final thickness of the specimens was 6.35 mm.

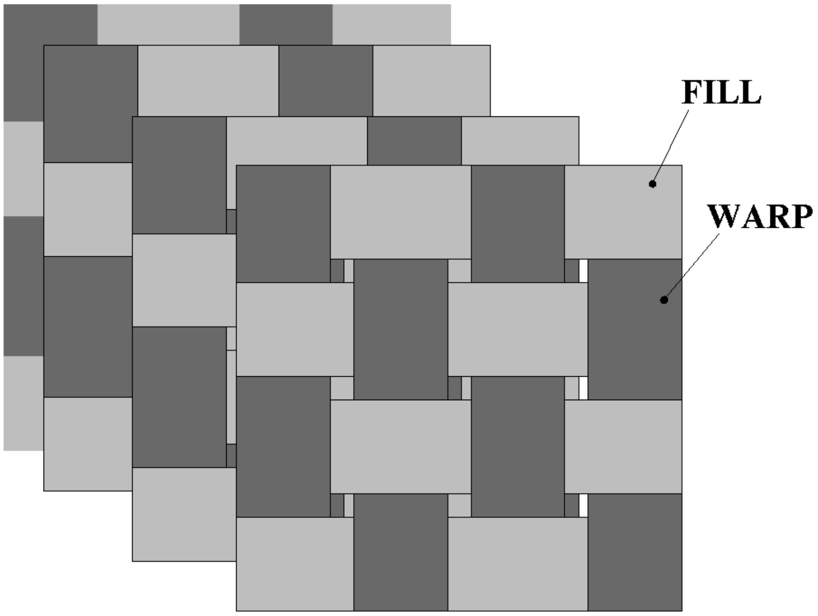

Figure 2.10 Plain-woven fabrics

Four different stacking sequences were used. The first type contains 37 layers of glass fabrics and was named as GL specimen (2.11.a). The second type had glass fabrics outside and graphite fabrics inside. The glass outer skins contain 9 layers of glass fabric at each side and 18 in total. The graphite core contains 16 layers of graphite fabrics. This specimen was named as GL/GR/GL specimen (2.11.b**).**

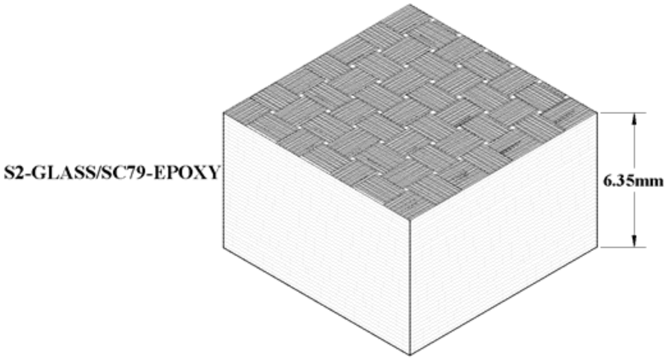

Figure 2.11 a) Woven S2-glass/ SC79 Epoxy composite

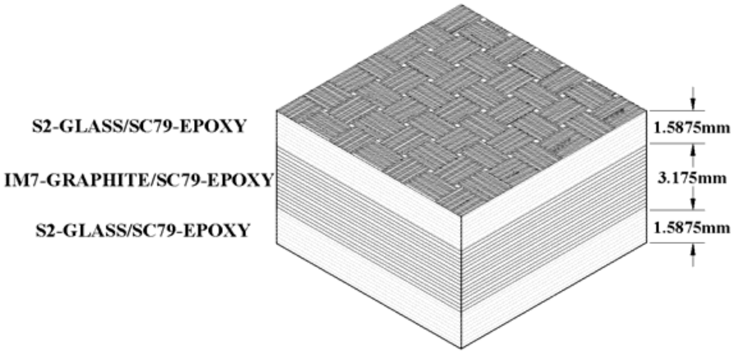

Figure 2.11 (b) Woven S2-glass, IM7-graphite/ SC79 Epoxy hybrid composite

The third type had graphite skin outside and glass core inside. While the graphite skin contained 8 layers of fabric at each side glass core had 16 layers of glass fabric. In total 32 layers of fabrics were used. This type was named as GR/GL/GR specimen (2.11**.**c**).** The fourth type contained 28 layers of graphite fabrics and was named as GR specimen (2.11.d). Although the thickness was constant for all types, the number of the fabric layers used in each composite varies due to the different thickness of graphite and the glass fabric.

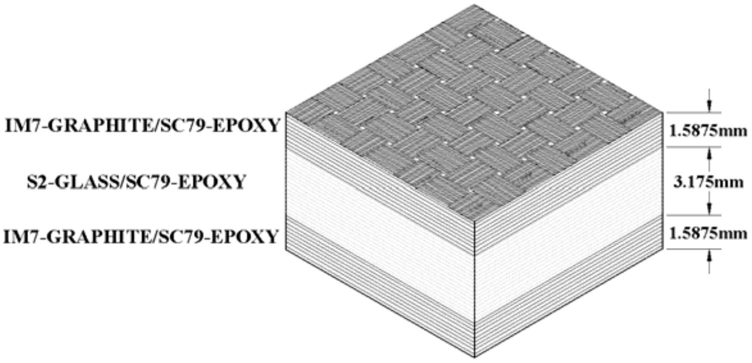

Figure 2.11 (c) Woven IM7-graphite, S2-glass / SC79 Epoxy hybrid composite.

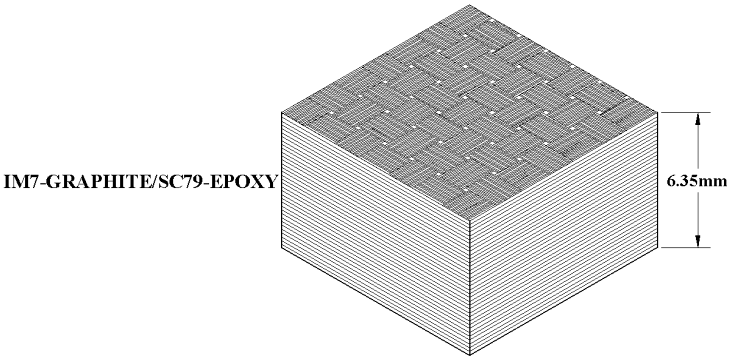

Figure 2.11 (d) Woven IM7-graphite/ SC79 Epoxy composite

After manufacturing process was completed, the 457.2 by 1524 mm composite panels were cut into the test specimens. All of the tensile tests and some of the ballistic tests were conducted using strip specimens (2.12.a). Rectangular specimens were also used for ballistic tests (2.12.c). On the other hand, all drop-impact tests were conducted on square specimens (2.12.b).

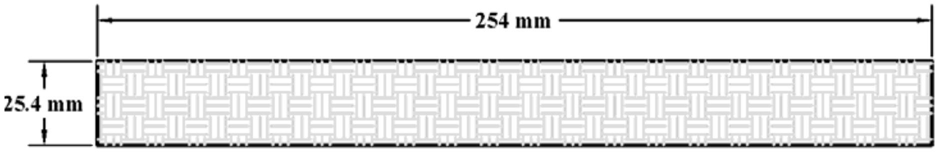

Figure 2.12 (a) Tensile and ballistic test specimen dimensions

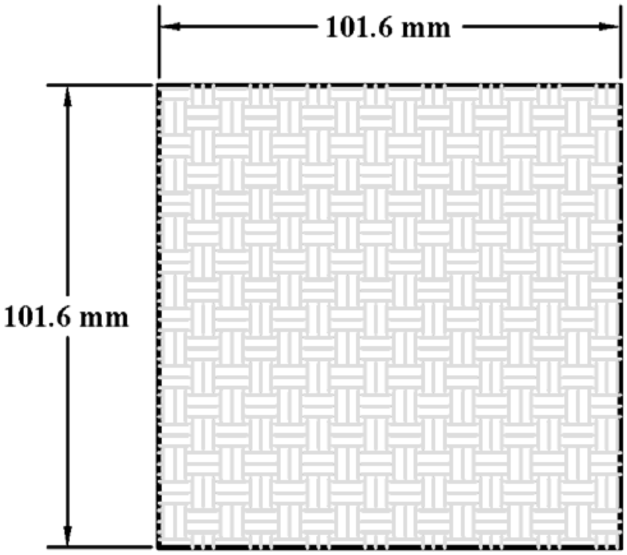

Figure 2.12 (b) Low impact test specimen dimensions.

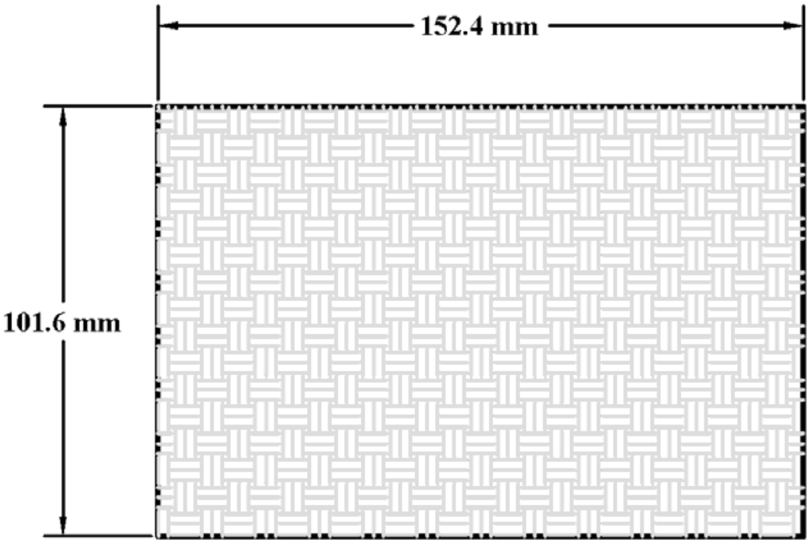

Figure 2.12 (c) Ballistic impact test specimen dimensions.

3. Tensile tests on woven hybrid composites

3.1 Experimental studies

The strip specimens with four different lay-ups were tested under uniaxial tension at room temperatures using a universal testing machine. Both loading and elongation histories were recorded through a National Instruments (NI)-DAQ based Lab View data acquisition system. In addition, a digital camera was used to capture the surface strain progression. The longitudinal and shear modulus of each specimen were calculated. Due to the woven fiber structure, the transverse modulus of the composites was assumed to be the same as the longitudinal modulus. Thus, tensile tests for transverse direction were not carried out. For each lay-up configuration multiple tests were conducted.

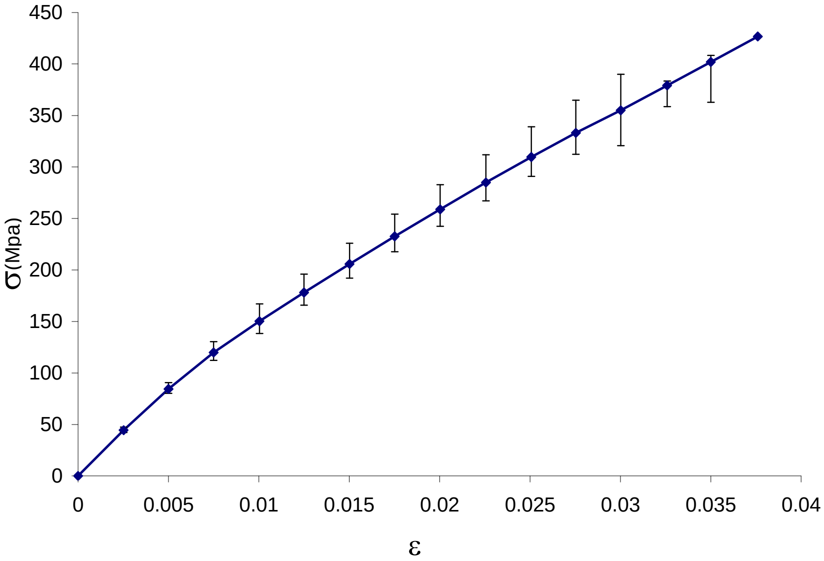

Figure 3.1 (a) Longitudinal and transverse stress-strain curves for GL specimens

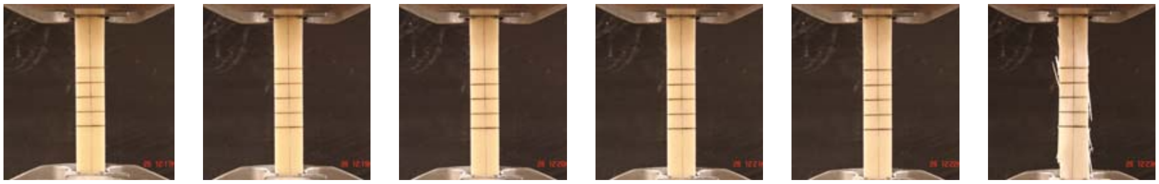

ε=0 ε=0.008 ε=0.016 ε=0.024 ε=0.032 ε=0.038

Figure 3.1 (b) Optical pictures of GL specimen taken during room temperature tensile testing at different strain levels.

Figure 3-1.a shows the longitudinal stress-strain relations of GL specimen. Even though each test did not exhibit identical result, similar trend for all three tests was observed. Each curve has a linear portion corresponding to the undamaged state, followed by a second linear portion with a smaller angle of slope. Figure 3.1.b shows the optical pictures taken at different strain levels during the test. Figure 3.2.a shows the stress-strain relation of GL specimen with +45/-45 fiber orientation. All curves had linear increase at the beginning that was followed by a nonlinear portion. The complete failure was observed when the stress was around 180 MPa. Optical pictures are shown in Figure 3.2.b.

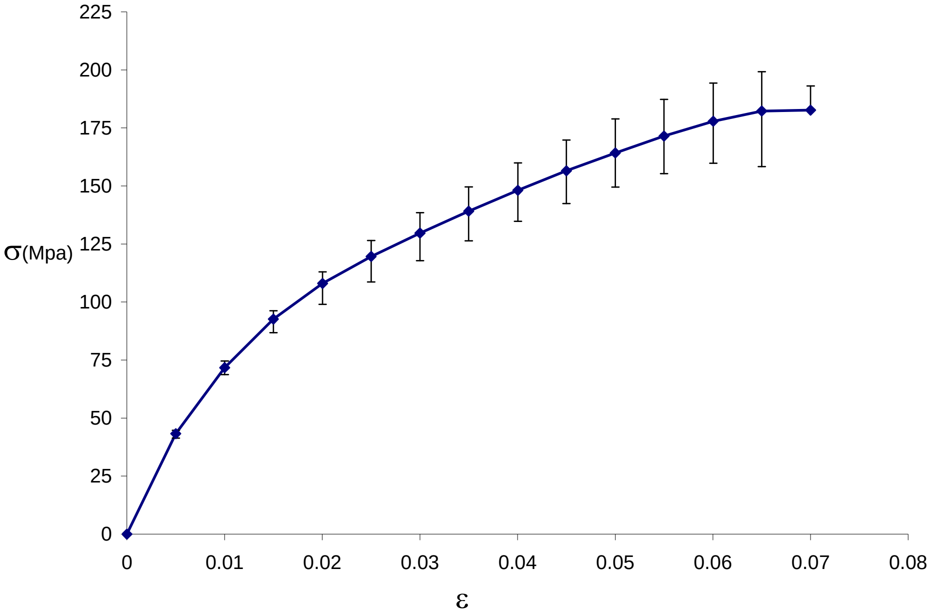

Figure 3.2 (a) Stress-strain relations for +45/-45 GL specimens

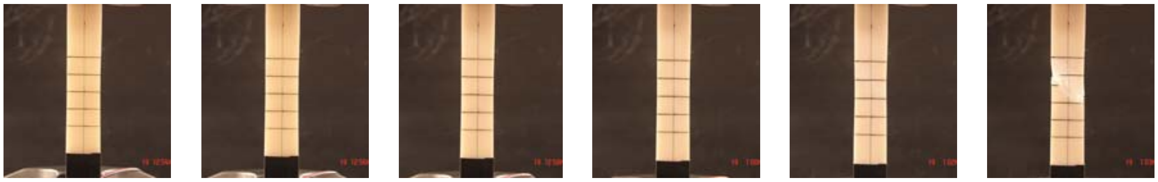

ε=0 ε=0.016 ε=0.032 ε=0.048 ε=0.064 ε=0.066

Figure 3.2 (b) Optical pictures of GL specimen (+45/-45 fiber orientation) taken during room temperature tensile testing

The hybrid specimens' longitudinal stress-strain curves had three stages. A linear portion at the beginning was followed by a second linear portion with a smaller angle of slope. During the third stage, the graphite part in the hybrid specimen was fractured first and the stress dropped to 100 MPa. However, the glass part in the hybrid composite was still undamaged.Thus, the stress increased linearly up to 180 MPa until the glass part in the hybrid specimen fractured. Figure 4.3.a shows the stress strain relations of the GR-GL-GL-GR specimen. Optical pictures of the same test are shown in Figure 3.3.b. Optical pictures clearly show that graphite part fractured first (ε=0.032) and the glass part fractured later (ε=0.041).

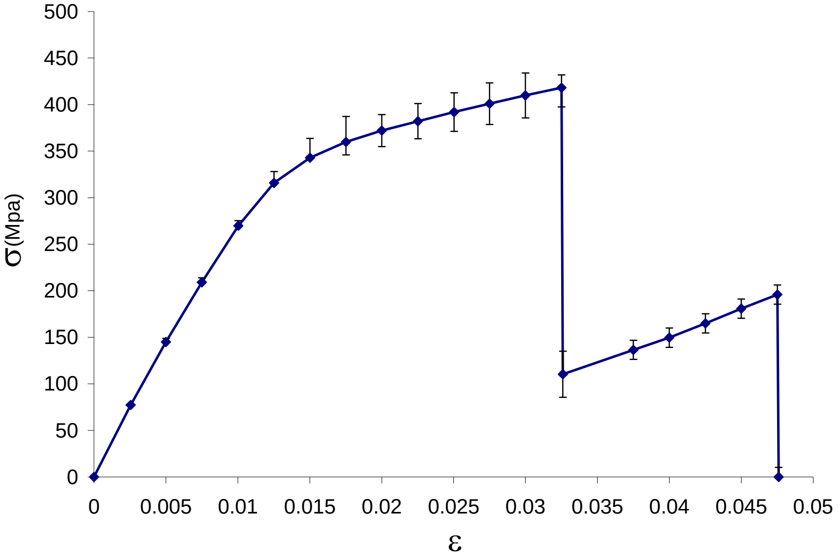

Figure 3.3 (a) Longitudinal and transverse stress-strain curves for GR/GL/GR specimens.

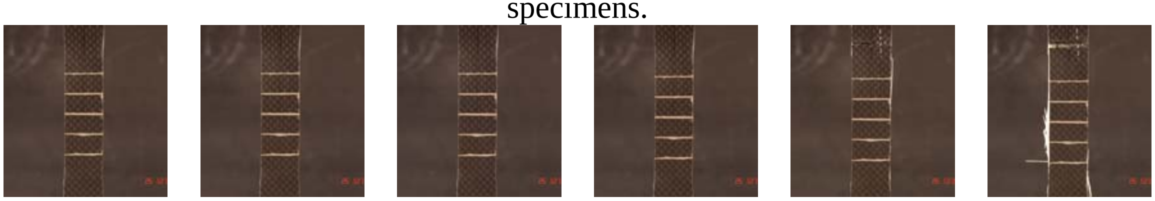

ε=0 ε=0.008 ε=0.016 ε=0.024 ε=0.032 ε=0.041

Figure 3.3 (b) Optical pictures of GR/GL/GR specimen (+45/-45 fiber orientation) taken during room temperature tensile testing at different strain levels.

We did not observe the two-stage failure for shear tests of hybrid specimens. Shear tests exhibit a linear portion at the beginning followed by a second linear portion with smaller slope. Graphite and glass failed together. The shear stress-strain relations of GR/GL/GR specimen and optical pictures taken during the test are shown in Figs.3.4.a and 3.4.b respectively.

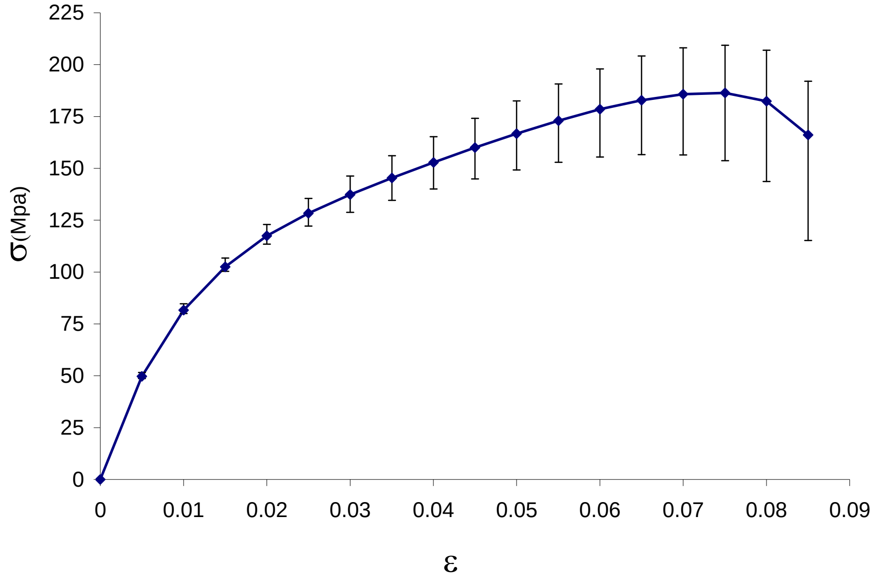

Figure 3.4 (a) Stress-strain relations for +45/-45 GR/GL/GR specimens

ε=0 ε=0.024 ε=0.048 ε=0.072 ε=0.089

Figure 3.4 (b) Optical pictures of GR/GL/GR (+45/-45 fiber orientation) specimen taken during room temperature tensile testing at different strain levels.

The behavior of GL/GR/GL specimens was similar to the other hybrid type as explained above. The longitudinal and shear stress strain relations are shown in Figs. 3.5.a and 3.5.b respectively.

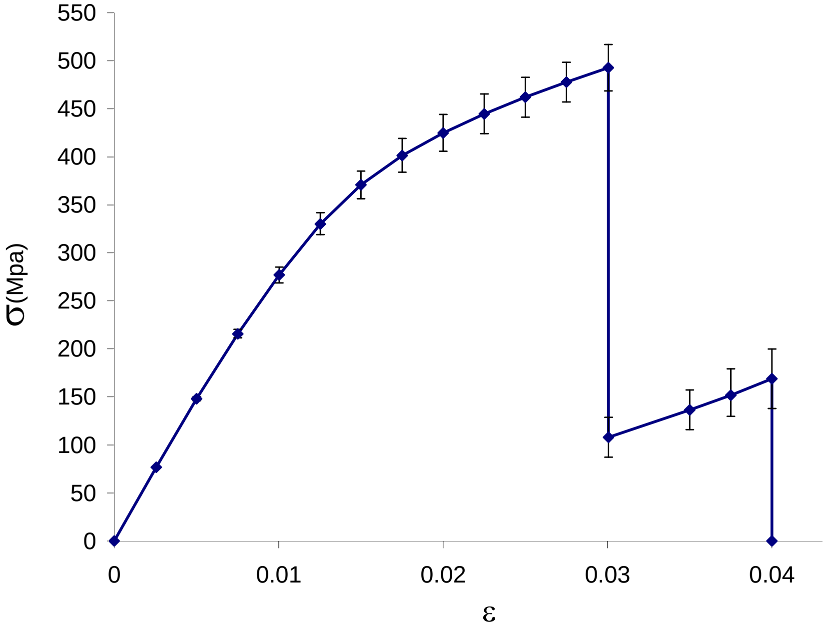

Figure 3.5 (a) Longitudinal and transverse stress-strain curve for GL/GR/GL specimens.

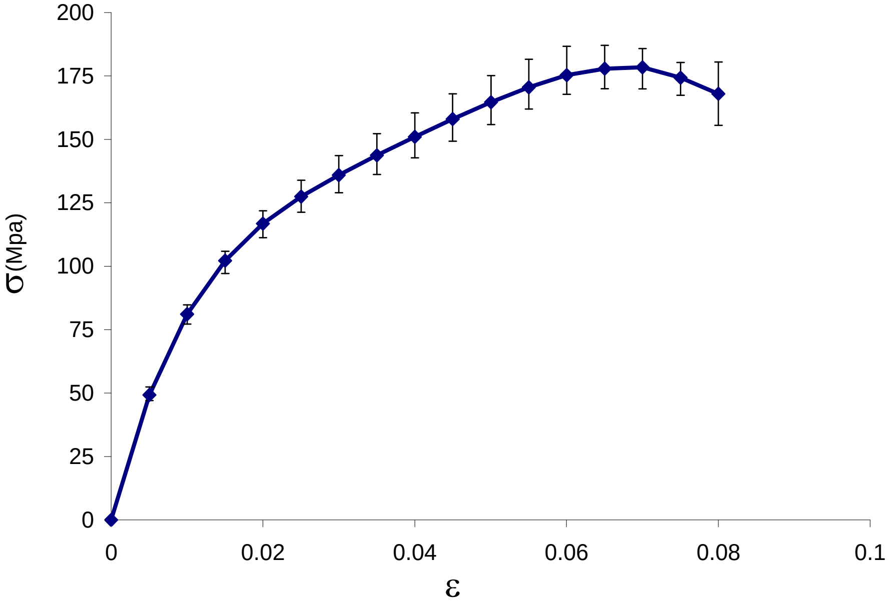

Figure 3.5 (b) Stress-strain curve for +45/-45 GL-GR-GL specimens

The tensile tests of GR composites at longitudinal direction exhibited linear stress-strain relation (Fig.3.6.a). All four tests conducted provided high consistency. The GR specimens were completely damaged when the tensile stress was around 600 MPa. The stress-strain relations for +45/-45 GR specimen are shown in Figure 3.6.b.

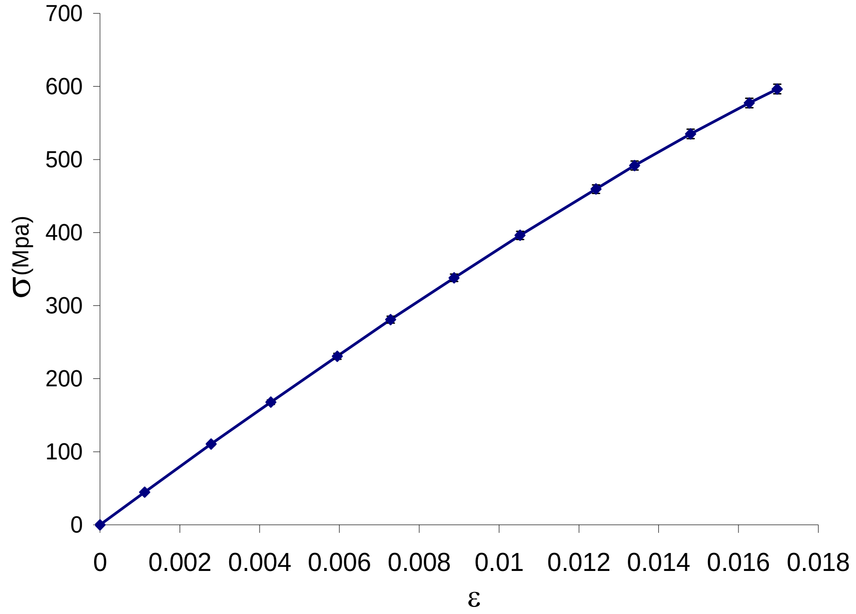

Figure 3.6 (a) Longitudinal and transverse stress-strain curves for GR specimens.

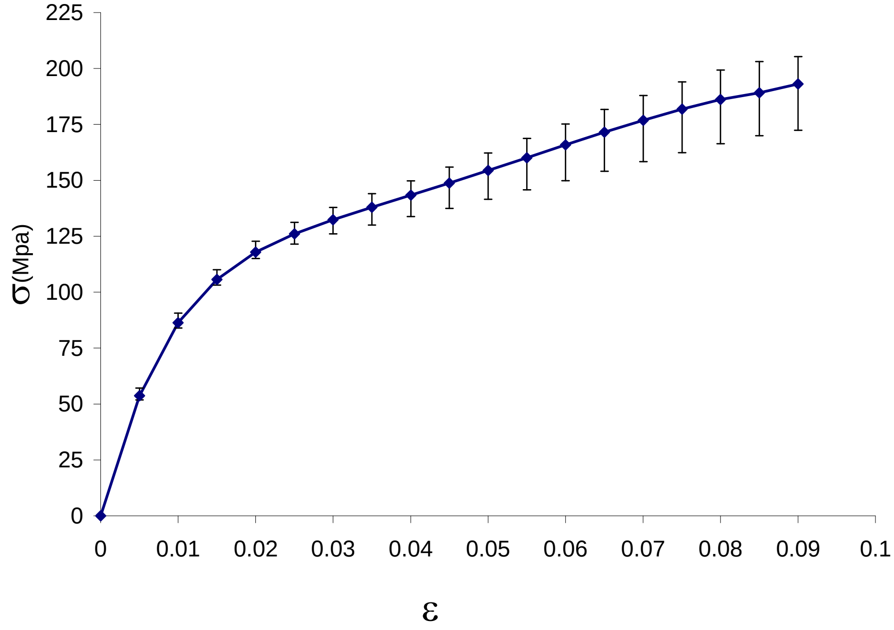

Figure 3.6 (b) Stress-strain curves for +45/-45 for GR specimens

The Rule of Mixtures for a single-fiber composite is:

$$E_c = V_f E_f + V_m E_m$$

where E_c, E_f, E_m are the Young's moduli of the composite, fiber, and matrix, respectively, and Vf, Vm are the fiber and matrix volume fractions.The Rule of Hybrid Mixtures (RoHM) of a hybrid composites can be written as:

$$E_{hc} = V_{f1}E_{f1} + V_{f2}E_{f2} + V_m E_m$$

where E_{hc}, E_{fi}, V_{fi} (i = 1,2) are the Young's moduli of the hybrid composite, constituent fibers, and the volume fractions of the constituent fibers, respectively. It is expected that the properties of hybrid composites should be somewhere between the properties of single fiber composites. Table 3.1 shows the material properties of non-hybrid and hybrid composites as measured.

Table 3.1 Material properties of woven hybrid composites

TYPE	$E_1=E_2$ ***(GPa)***	σ_{max} ***(MPa)***	ε_{max}	E_{xy}***(GPa)***
GL	17.047	426	0.0376	8.6665
GL/GR/GL	29.036	492.838	0.03	9.793
GR/GL/GR	27.582	458.152	0.0325	9.938
GR	36.434	596.528	0.0169	10.739

While the stiffness of GL composite was 17.047 GPa, it was 36.434 GPa for GR composite. The stiffness of GL/GR/GL and GR/GL/GR composites were 29.036 and 27.582 GPa respectively. The strength of the hybrid composites also lay somewhere between GL and GR composites. The stiffness of +45/-45 (E_{xy}) composites exhibited similar behavior. The longitudinal failure strain values of hybrid composites were a little higher than those for GL and GR composites. During the tensile test of hybrid composites, the glass and graphite reinforced parts of the composites initially acted together (Fig.3.7). As soon as the tensile strain reached 0.03, the graphite reinforced part of the composite failed and the tensile stress dropped. The remaining glass fiber reinforced part of the composite continued to elongate under low stress. While the failure strain for GL/GR/GL composite was 0.04, GR/GL/GR composite failed at 0.05.

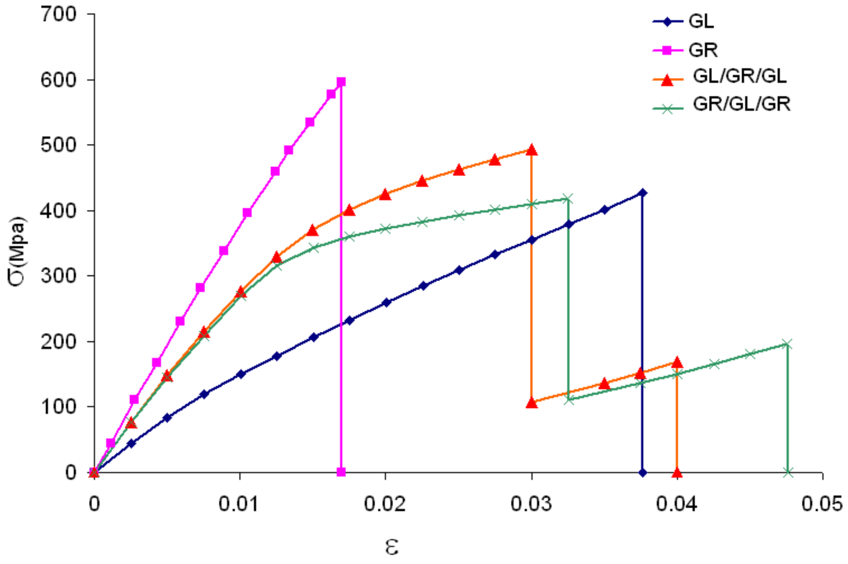

Figure 3.7 Longitudinal and transverse stress-strain curves of hybrid and non-hybrid composites

3.2 Determination of material properties

The LS-DYNA elastic orthotropic material model (MAT22), that is the Chang-Chang material model, requires nine constant to be entered to define orthotropic material. These constants are: Young's modulus in longitudinal direction (E_1), transverse Young's modulus (E_2), Young's modulus in thickness direction (E_3), shear moduli in three planes (G_{12}, $G13$, $G23$) and the generalized Poisson's ratios (v_{12}, v_{13}, v_{23}). E_1 and E_2 were assumed to be same due to the woven structure of the composites and obtained from tensile tests. E_3 was assumed to be same as that for matrix material and obtained from manufacturer. G_{12} was calculated using the relation

$G_{12}=\dfrac{1}{\dfrac{4}{E_{12}}-\dfrac{1}{E_1}-\dfrac{1}{E_2}+\dfrac{2\gamma_{12}}{E_1}}$ relation. E_{12} in this equation is the initial slope of the stress-strain curve obtained from tensile tests of the specimens with +45/-45 fiber orientation. The shear moduli in the remaining two planes were obtained through the relations $G_{13}=G_{23}=\dfrac{E_3}{2(1+\nu_{13})}$. The Poisson's ratios ν_{12} and $\nu_{13}=\nu_{23}$ were obtained from three strain-gages mounted on woven glass (4.8.a) and woven graphite (3.8.b) composite specimens for the tensile tests.

<table>
<tr><th colspan="2">Glass (a)</th><th>Graphite (b)</th></tr>
<tr><td>Composite Specimens</td><td></td><td></td></tr>
<tr><td>$\nu_{12}=-\varepsilon_2/\varepsilon_1$</td><td>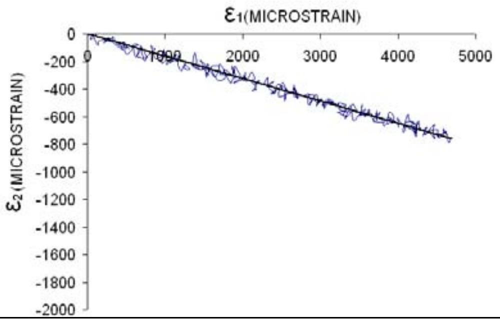 </td><td>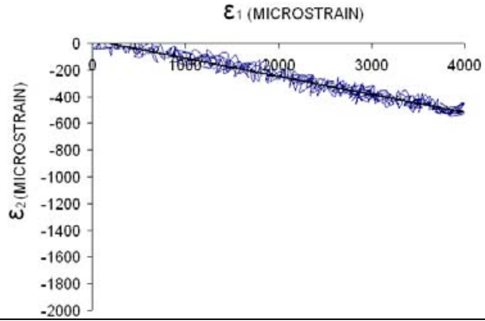 </td></tr>
<tr><td colspan="2">$\nu_{12}=0.13$</td><td>$\nu_{12}=0.12$</td></tr>
<tr><td>$\nu_{13}=\nu_{23}=-\varepsilon_3/\varepsilon_1$</td><td>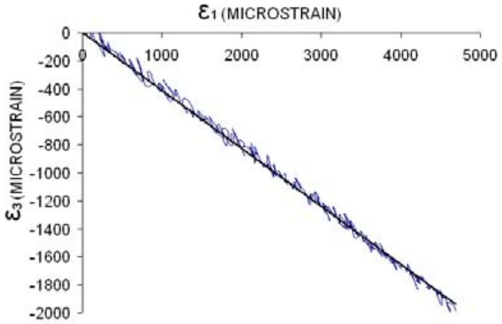 </td><td>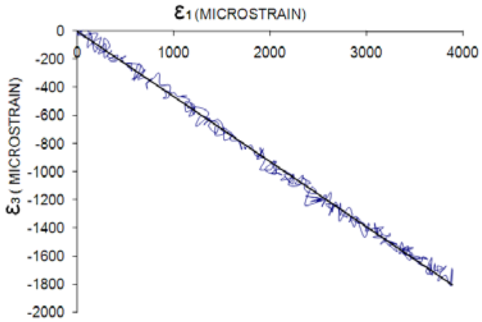 </td></tr>
<tr><td colspan="2">$\nu_{13}=\nu_{23}=0.413$</td><td>$\nu_{13}=\nu_{23}=0.427$</td></tr>
</table>

Figure 3.8 Poisson ratio measurements of woven glass (a) and woven graphite (b) toughened epoxy composites

The mechanical properties of woven glass and woven graphite composites are shown in Table 3.2. The linear orthotropic material model (MAT22) has some limitation due to absence of nonlinearity. The user-defined material model, which requires an entire curve to be entered, is expected to simulate better the nonlinear behavior of woven glass and woven graphite composites. However the tensile tests only provided complete E_1 and E_2 curves. E_3 was assumed to be same as that of matrix material and a linear curve was generated using the mechanical properties provided by the manufacturer. Using the relations $G_{12} = \dfrac{1}{\dfrac{4}{E_{12}} - \dfrac{1}{E_1} - \dfrac{1}{E_2} + \dfrac{2\gamma_{12}}{E_1}}$ and $G_{13} = G_{23} = \dfrac{E_3}{2(1+\nu_{13})}$ only the initial slope of the curve can be obtained. The entire curve for G_{12} was generated by scaling the stress-strain curve obtained from tensile tests of the specimens with +45/-45 fiber orientation (Fig.3.9.a and b).

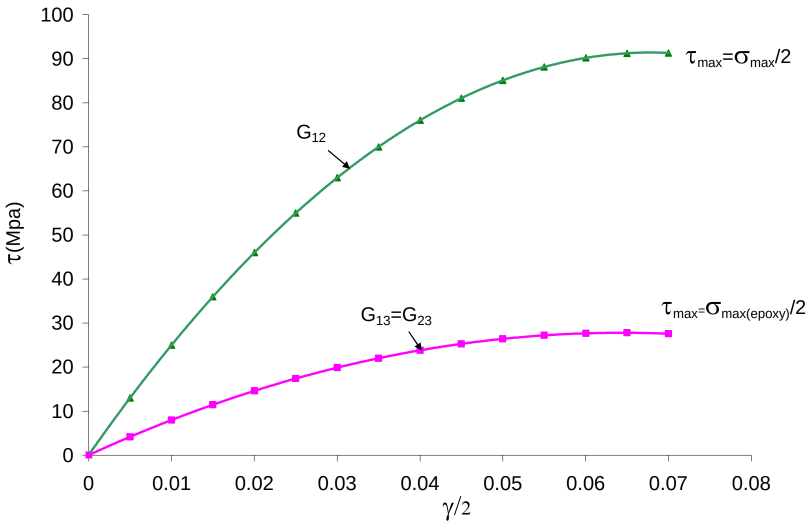

Figure 3.9 (a) Generating G_{12}, G_{13} and G_{23} curves for woven glass composite

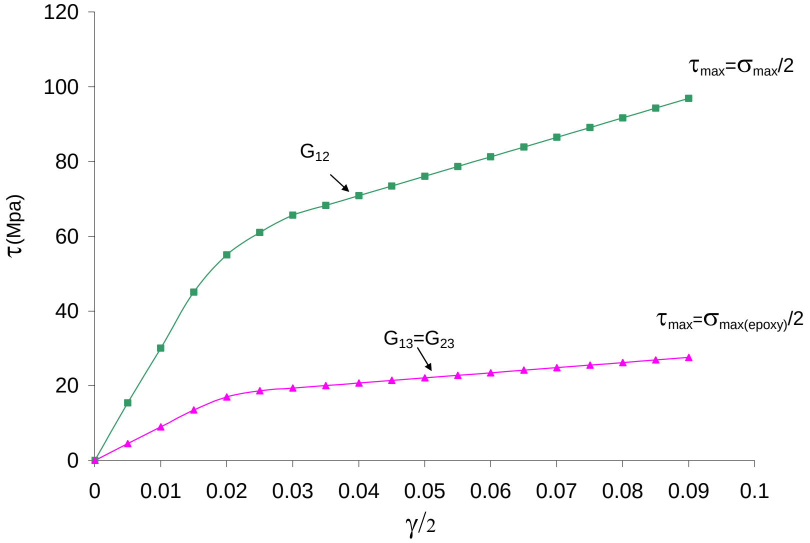

Figure 3.9 (b) Generating G_{12}, G_{13} and G_{23} curves for woven graphite composite

The initial slope was determined and the shear strength was calculated using the relation, $\tau_{\max} = \dfrac{\sigma_{\max}}{2}$. Same approach was used for generating the $G_{13}= G_{23}$ curve; the shear strength of this curve was obtained using the relation $\tau_{\max} = \dfrac{\sigma_{\max}(epoxy)}{2}$.

Table 3.2 Elastic mechanical properties of woven glass and graphite fibers-reinforced toughened epoxy.

	E_1=E_2 *(GPa)*	E_3 *(GPa)*	G_{12} *(GPa)*	G_{13}=G_{23} *(GPa)*	ν_{12}	$\nu_{13}=\nu_{23}$	ρ *(kg/mm³)*
Glass	17.04	3.06	2.742	1.091	0.13	0.413	$1.756\ 10^{-6}$
Graphit	36.43	3.06	3.08	1.071	0.12	0.427	$1.458\ 10^{-6}$

The curves representing the material properties of woven glass and woven graphite composites are shown in Figure 3.10.

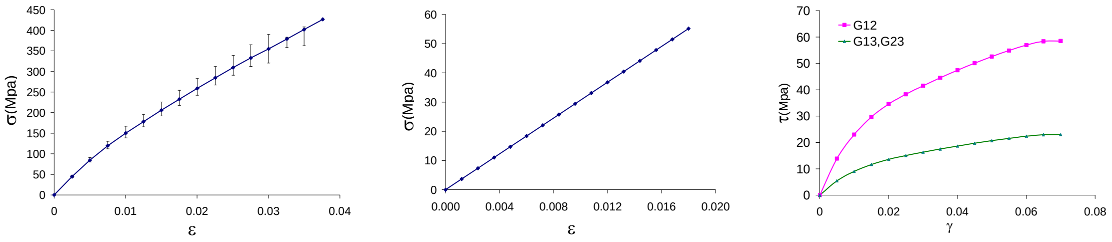

$E_1=E_2$ **E_3** **G_{12},G_{13} *and* G_{23}**

(a)

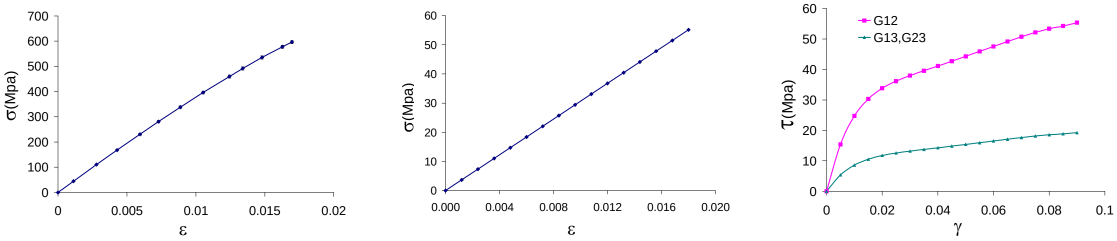

$E_1=E_2$ **E_3** **G_{12},G_{13} *and* G_{23}**

(b)

Figure 3.10 Nonlinear longitudinal, transverse and in-plane shear stress-strain curves with their slopes representing Young's and shear moduli, respectively.

(a) Glass (b) Graphite

3.3 CONCLUSIONS OF TENSILE TESTS

a) While the longitudinal and transverse stress-strain relations of GL, GL/GR/GL and GR/GL/GR composites exhibited non-linear behavior; the stress-strain relations for GR composite were almost linear.

b) During the tensile tests of hybrid composites, fracture of graphite was followed by fracture of glass fabrics. Thus the longitudinal and transverse stress-strain relations showed two stages. This two-stage failure was not seen during the tensile test of +45/-45 hybrid composites.

c) The over-all mechanical properties of hybrid composites were between those of GL and GR composites.

4. LOW-VELOCITY IMPACT TESTS ON WOVEN HYBRID COMPOSITES

The low velocity impact studies in this thesis can be categorized into three groups:

a) Effect of impact energy level on the response of composites, b) Effect of impactor shape on the response of composites and c) Effect of repeated impact on the performance of composites. Low impact tests at four different energy levels were carried out using a pressure-assisted Instron-Dynatup 8520 instrumented drop-weight impact tester. Figure 4.1 shows the schematic drawings of the experimental set-up for the low-velocity impact tests.

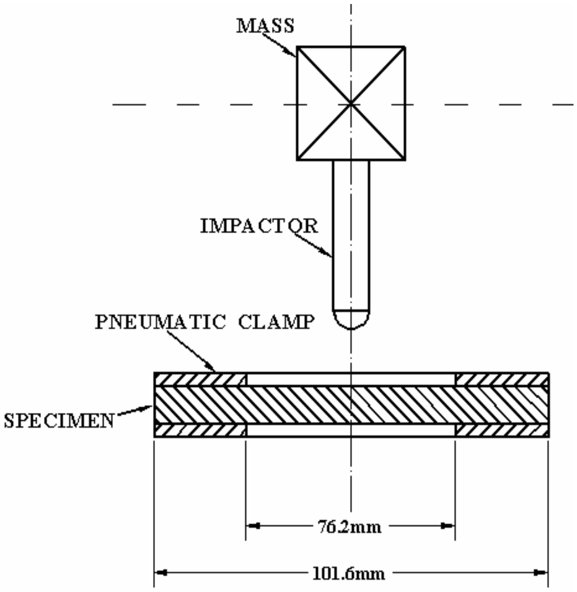

Figure 4.1 Schematic diagram of the set-up for drop-weight impact tests.

4.1 Effect of impact energy level on the low-velocity impact response of composites

During all impact tests, a 5.1 kg weight was attached to the steel impactor with a hemispherical tup of 16 mm diameter for a total of 6.15 kg. Simply placing the mass at the highest position of the impact tester and dropping it freely due to gravity results in a velocity of 3.9 m/s. To obtain higher impact velocities, the mass was held first at the highest position of the impact tester and the pneumatic assistance option was then deployed to increase the impact energy. In this study, various pressure levels were used to obtain impact velocities of 4.4, 4.8 or 6.3 m/s, respectively. As shown in Fig.4.2, two strain gages (one in the longitudinal direction and another in the transverse direction) were mounted 25.4 mm away from the center of the composite panel, where the impactor would drop. The specimen was then clamped circumferentially along a diameter of 76.2 mm in a pneumatic-actuated clamping fixture. Details of the parameters conducted in the drop-impact tests during this study are given in Table 4.1.

During the test, the time histories of impact force and the ensuing dynamic strains were recorded. For post-mortem observation, optical pictures of the front and back surface of the damaged composites were first taken. The impacted specimens were then scanned using an immersion ultrasonic system. The through transmission technique using a pair of 5 MHz focused and flat transducers was employed to detect the internal delamination in the damaged composite panel. Finally, the specimen was machined carefully into two halves along a central line to reveal the damage inside.

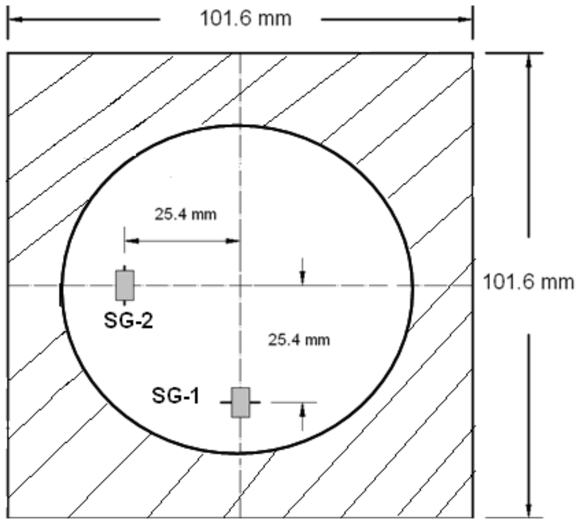

Figure 4.2 The strain-gage-mounted square composite specimen for drop-weight impact test

Table 4.1 Parameters of drop-weight impact tests.

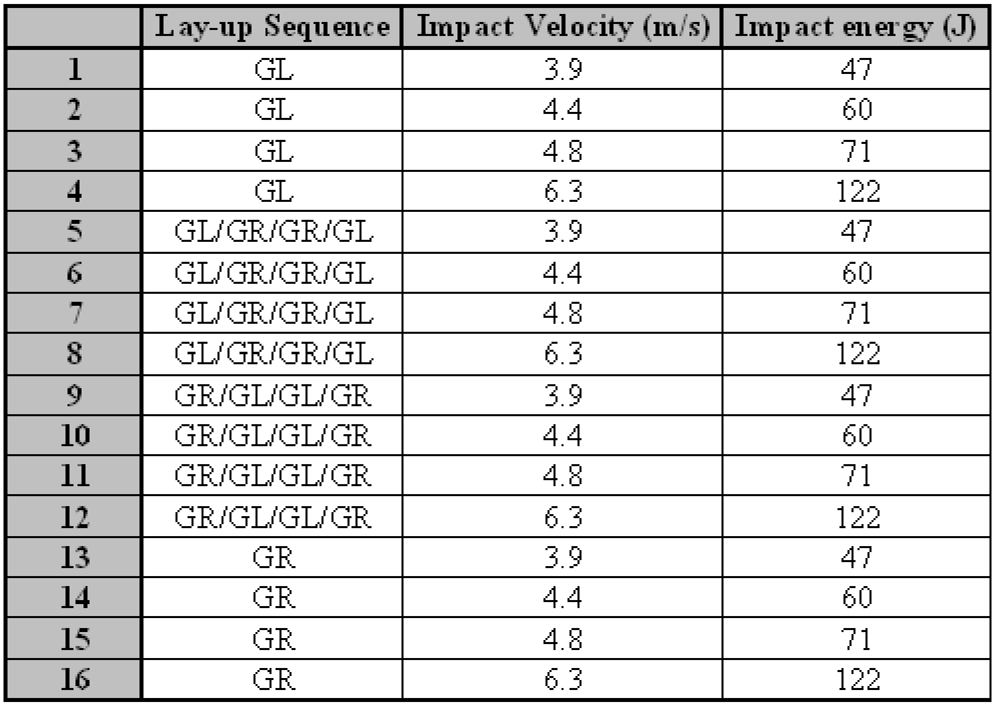

	Lay-up Sequence	Impact Velocity (m/s)	Impact energy (J)
1	GL	3.9	47
2	GL	4.4	60
3	GL	4.8	71
4	GL	6.3	122
5	GL/GR/GR/GL	3.9	47
6	GL/GR/GR/GL	4.4	60
7	GL/GR/GR/GL	4.8	71
8	GL/GR/GR/GL	6.3	122
9	GR/GL/GL/GR	3.9	47
10	GR/GL/GL/GR	4.4	60
11	GR/GL/GL/GR	4.8	71
12	GR/GL/GL/GR	6.3	122
13	GR	3.9	47
14	GR	4.4	60
15	GR	4.8	71
16	GR	6.3	122

(a) Experimental results

Various factors (such as lay-up configuration, laminate thickness, impactor size and shape, constituent properties, temperature, impact velocity and energy, etc.) can affect the impact response and damage pattern. Among the four lay-up sequences tested, the GL specimens were the strongest. As shown in Figure 4.3, for impact velocities up to 4.4 m/s only horizontal and vertical front surface cracks were created in GL specimens and no back surface splitting occurred. When the composites were impacted at higher velocity, e.g., 4.8 or 6.3 m/s, in addition to the front surface cracks, some back surface splitting was also observed. The length of the front surface crack increased with increasing impact velocity. Impact tests were conducted on two groups of hybrid composites. The first, called GL/GR/GL, has two glass layers as the outer skins and a graphite layer as the inner core; whereas the second, called GR/GL/GR, consists of graphite layers as the face sheets and a glass layer as the core material.

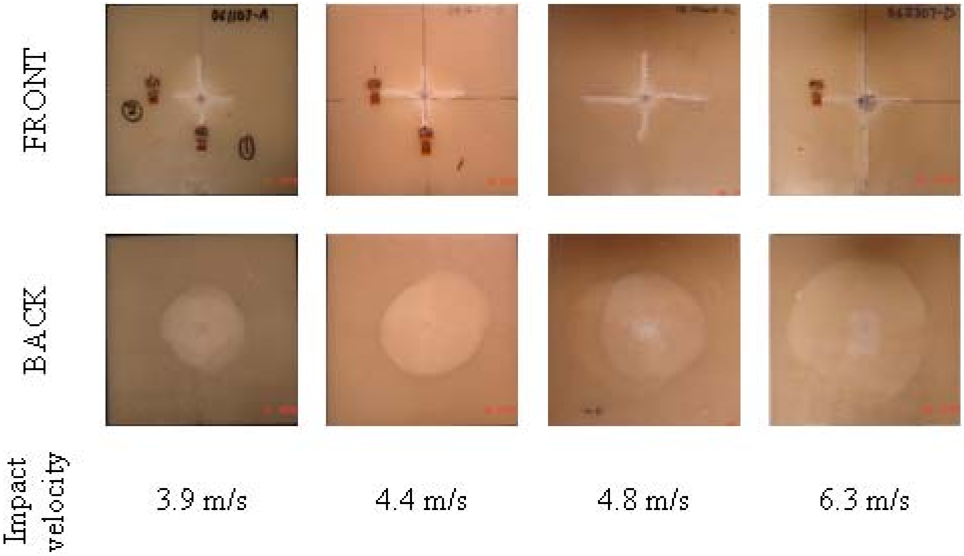

Figure 4.3 Optical fractographs of non-hybrid GL composite specimens after drop-weight impact by an impactor of 6.15 kg with a hemispherical tup of 16 mm diameter at various impact velocities.

As shown in Fig.4.4, drop-weight impact tests of GL/GR/GL hybrid composites created less horizontal and vertical front surface cracks compared to the afore-mentioned GL composite specimens. Only impact tests conducted at 6.3 m/s created some penetration and back surface splitting on the hybrid composite. The remaining three tests did not create severe back surface splitting.

On the other hand, drop-weight tests conducted on the second hybrid composite group, i.e. the GR/GL/GR specimens, generated extended horizontal and vertical front surface cracks for all specimens tested, as depicted in Fig. 4.5.

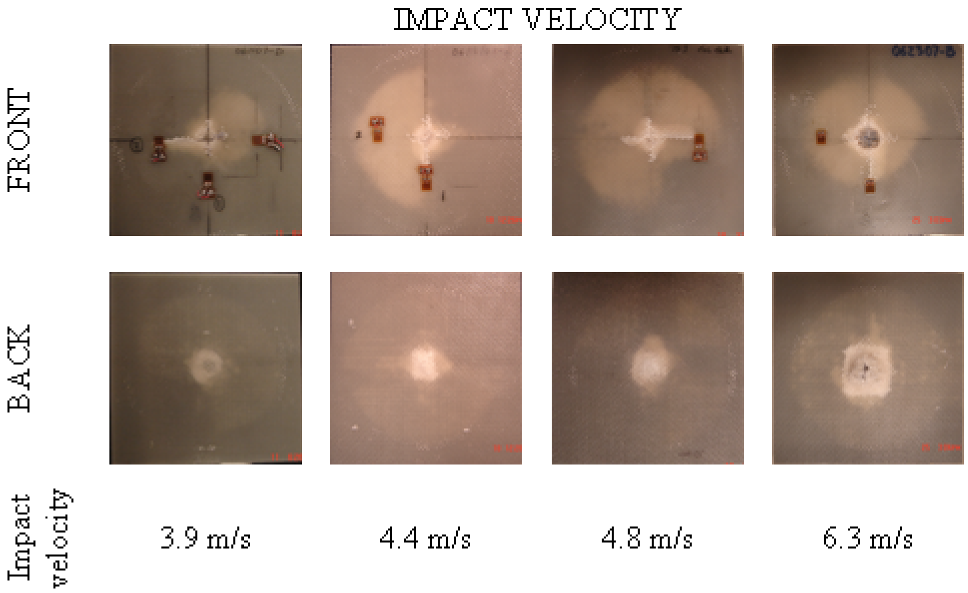

Figure 4.4 Optical fractographs of hybrid GL/GR/GL composite specimens after drop-weight impact by an impactor of 6.15 kg with a hemispherical tup of 16 mm diameter at various impact velocities.

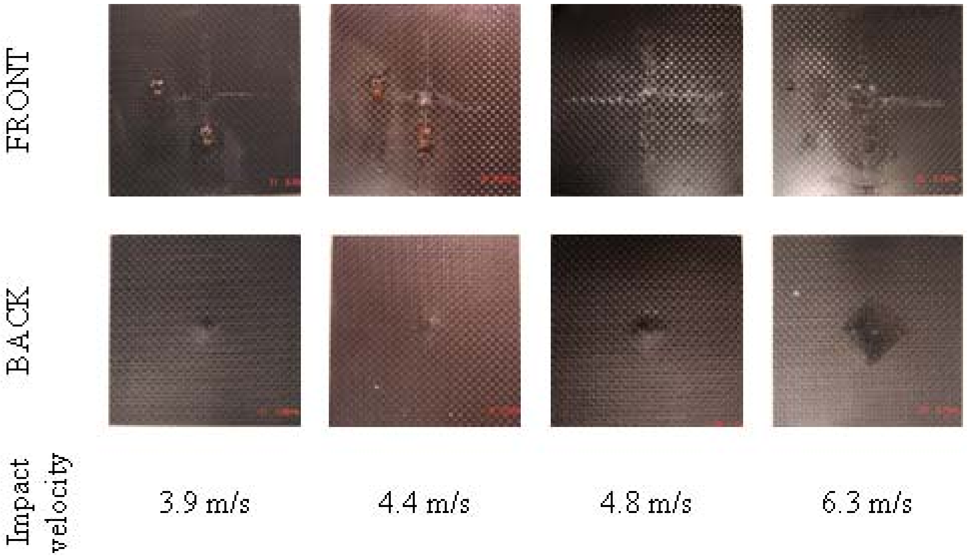

Figure 4.5 Optical fractographs of hybrid GR/GL/GR composite specimens after drop-weight impact by an impactor of 6.15 kg with a hemispherical tup of 16 mm diameter at various impact velocities.

Back surface splitting was not severe during the first three tests conducted at velocities up to 4.8 m/s. However for the impact test conducted at 6.3 m/s some penetration and back surface splitting was observed. It should be noted that drop-weight impact tests on both groups of hybrid composites were performed under similar conditions. However, the difference in stacking sequence results in appreciable differences in the size of the generated horizontal and vertical front surface cracks as well as the severity of penetration and back surface splitting. Finally, as shown in Fig. 4.6, the GR non-hybrid composite was the weakest compared to the other configurations tested. All four tests created penetration and back surface splitting. During impact tests at 4.8 and 6.3 m/s, perforation was observed; impactor did not bounce back and was stuck in the composite. When the horizontal and vertical front surface cracks were studied after impact, it was seen that the size of the cracks was very similar to that observed for GL non-hybrid composites.

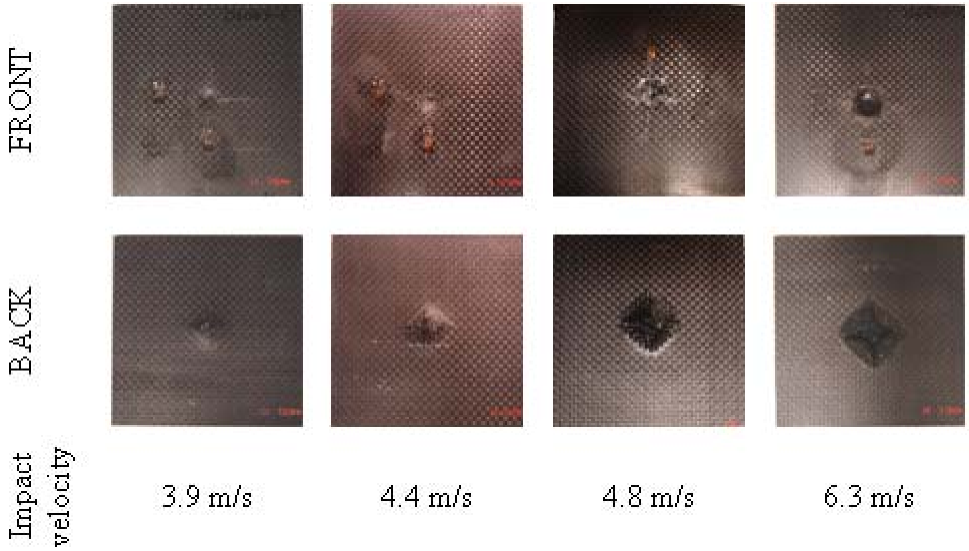

Figure 4.6 Optical fractographs of non-hybrid GR composite specimens after drop-weight impact by an impactor of 6.15 kg with a hemispherical tup of 16 mm diameter at various impact velocities.

(b) Impact force

It should be noted that the Dynatup 930-I data acquisition system, accompanying the Instron-Dynatup 8520 instrumented drop-weight impact tester, can only measure the initial velocity of the impactor and force *vs*. time directly. The remaining parameters, such as absorbed energy, velocity of impactor and deflection, are calculated using equations of motion. The shapes of the force-time histories of the non-hybrid GL composites for the first three tests conducted at velocities up to 4.8 m/s were quite similar, as depicted in Fig. 4.7. An almost linear increase of up to 10 KN was followed by an oscillating increase with a decreasing slope. After the maximum point was reached, the force decreased following almost a linear and non-oscillating curve and eventually became zero. The entire impact event took about 4.2 to 5 ms and the maximum force occurred around 2.5 ms. On the other hand, for the drop-impact conducted at 6.3 m/s, the force-time history exhibited a different pattern. The linear increase was followed by an oscillating increase as it was seen in first three tests until a sudden drop around 19 KN was observed. Knowing that sudden drop occurred around 2 ms, it is noted that it was a little earlier than the other three cases when the maximum force was reached around 2.5 ms.

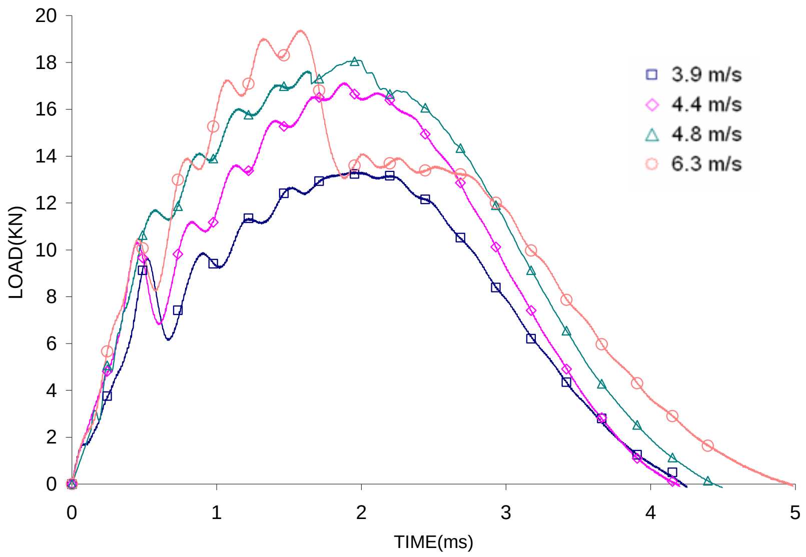

Figure 4.7 Time histories of the impact forces of non-hybrid GL composites.

Impact force-time histories of hybrid GL/GR/GL and GR/GL/GR specimens showed quite similar shapes during the first three impacts up to 4.8 m/s, Figs. 4.8 and 4.9. The linear increase at the beginning was followed by an oscillating increase and the force gradually returned to zero after reaching a maximum point. Just like in the non-hybrid GL case, during the impact tests of both hybrid composites at 6.3 m/s, a sudden drop right before maximum force were observed.

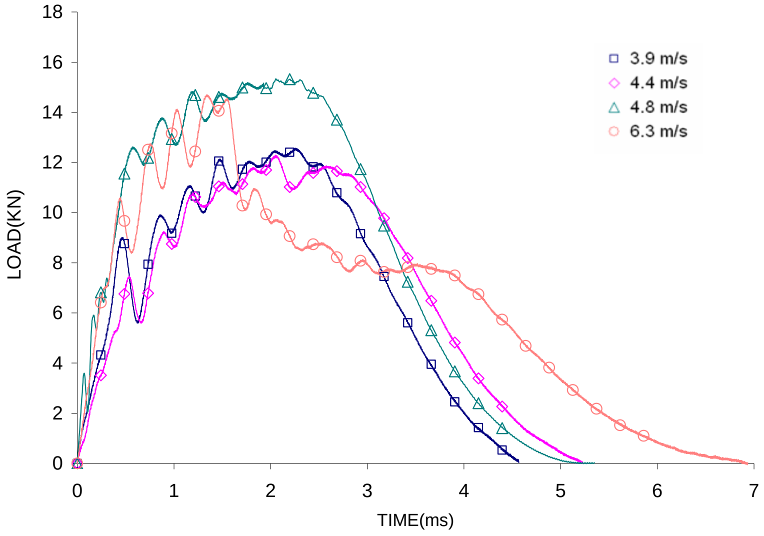

Figure 4.8 Time histories of the impact forces of hybrid GL/GR/GL composites.

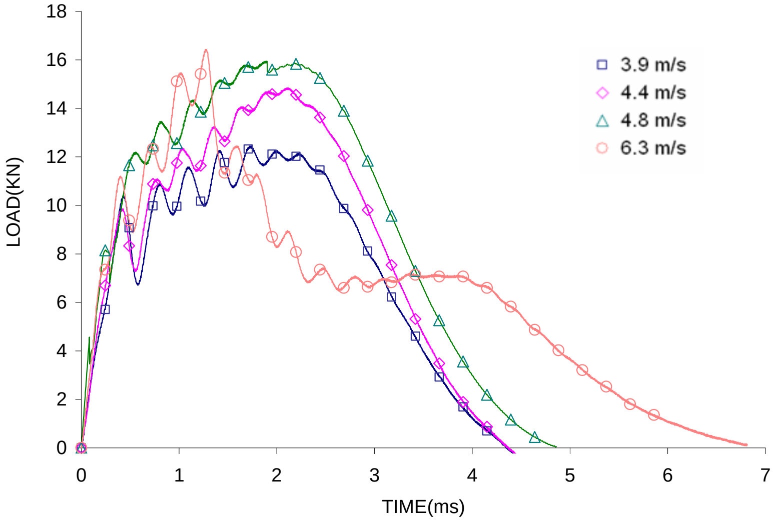

Figure 4.9 Time histories of the impact forces of hybrid GR/GL/GR composites.

During all four tests conducted on the non-hybrid GR specimens, a sudden drops right after the linear increase was observed (Fig. 4.10). In these tests, the oscillating increase that was commonly observed during the tests of the other three composite types was not seen. Drops in the force-time histories happened very early. Maximum force values were very low compared to those observed during the impact of the other three composite types.

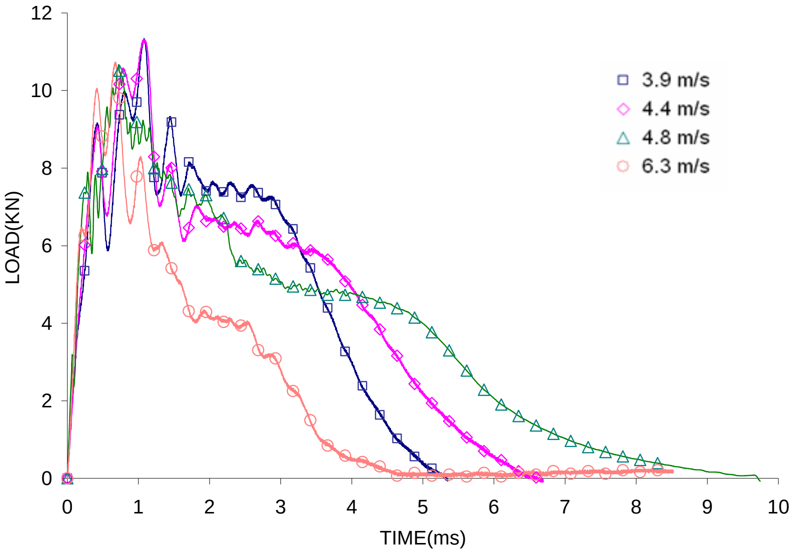

Figure 4.10 Time histories of the impact forces of non-hybrid GR composites.

Once the force-time histories of the drop impact tests and optical pictures of the impacted composites were evaluated, it can be concluded that impact tests, which created back surface splitting, exhibited sudden drops at their force-time histories; whereas the force-time histories of tests, which produced no or very little back surface splitting, did not show any significant drop. The force generated due to the contact of impactor-composite was linear at the beginning, because the impactor was just pushing the specimen down and no damage had been formed yet. As soon as some damage appeared in the composite, the force-time history started to show oscillations. This damage could be in the form of delamination, front surface cracks or front surface indentation. If the energy of the impactor was high enough, back surface splitting was also observed. The back surface splitting reduced the resistance (i.e., the out-of-plane stiffness) of the composite appreciably; thus resulting in the sudden drop of force-time history. If the remaining resistance of the composite was strong enough, the impactor would be pushed back and rebound happened. During the impact of GR at 4.8 m/s and 6.3 m/s, the composite lost its resistance and the impactor was able to move further and perforate the composite. For comparison, the maximum forces created during impact tests are summarized in Fig. 4.11. The results indicate that while GL sustained the highest force, GR composite resisted the lowest. Hybrid composites performed better than GR composite but the maximum force produced by these composites was a little less than that of the GL composite. The maximum force increased with increasing impact velocity during testing of GL and hybrid composites while the maximum forces produced by GR specimens were almost the same for the four impact tests conducted at various velocities.

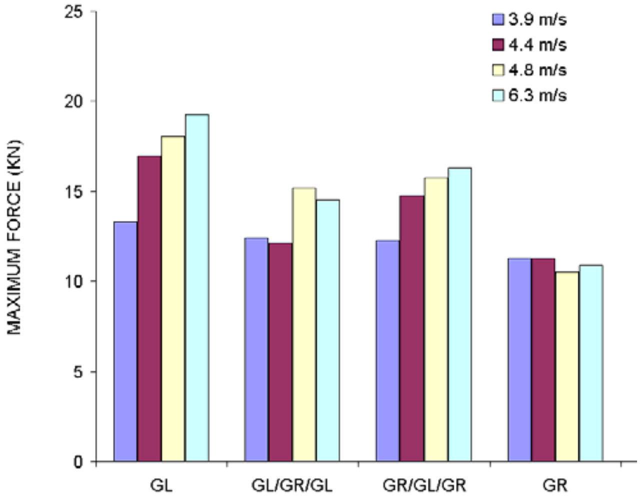

Figure 4.11 Comparison of maximum impact forces.

(c) Impact energy

Usually drop-weight impact tests result in three distinct interaction modes between the composite panel and the impactor depending on the level of energy. If the energy absorbed by the composite is very little, the impactor bounces back. If most of the energy of impactor is absorbed by the composite through various modes of damage, no rebound occurs. Finally, in the case of high energy level, perforation can be observed. A typical energy curve for drop-weight impact test where rebound of the impactor occurs is illustrated in Fig. 4.12. For this study, most of the energy-time histories, as shown in Fig. 4.13, are similar to the one depicted in Fig. 4.12, because except for the non-hybrid GR case, rebound occurred for all other composites during the impact tests conducted. Rebound was also observed during the impact tests of GR composites at 3.9 and 4.3 m/s impact velocities. The energy-time histories of GR composites when impacted at 4.8 and 6.3 m/s, Fig. 4.13(d), were different than those for the other specimens. At 4.8 m/s the impactor penetrated the composite and no rebound occurred. The test at 6.3 m/s created perforation in the composite and no rebound occurred either.

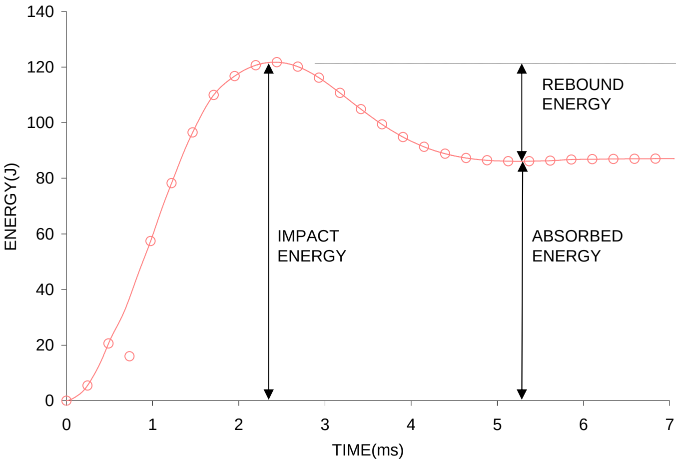

Figure 4.12 A typical energy curve for drop-weight impact test when the impactor rebound occurs.

Figure 4.14 summarizes the comparison of absorbed energies for the above drop-weight impact tests. As indicated in the figure, the GR composite always absorbed more energy compared to the other types. Energy absorption of the composites increased with increasing impact velocity. Energy absorption of GL and hybrid composites was very close during impact tests at the same velocity.

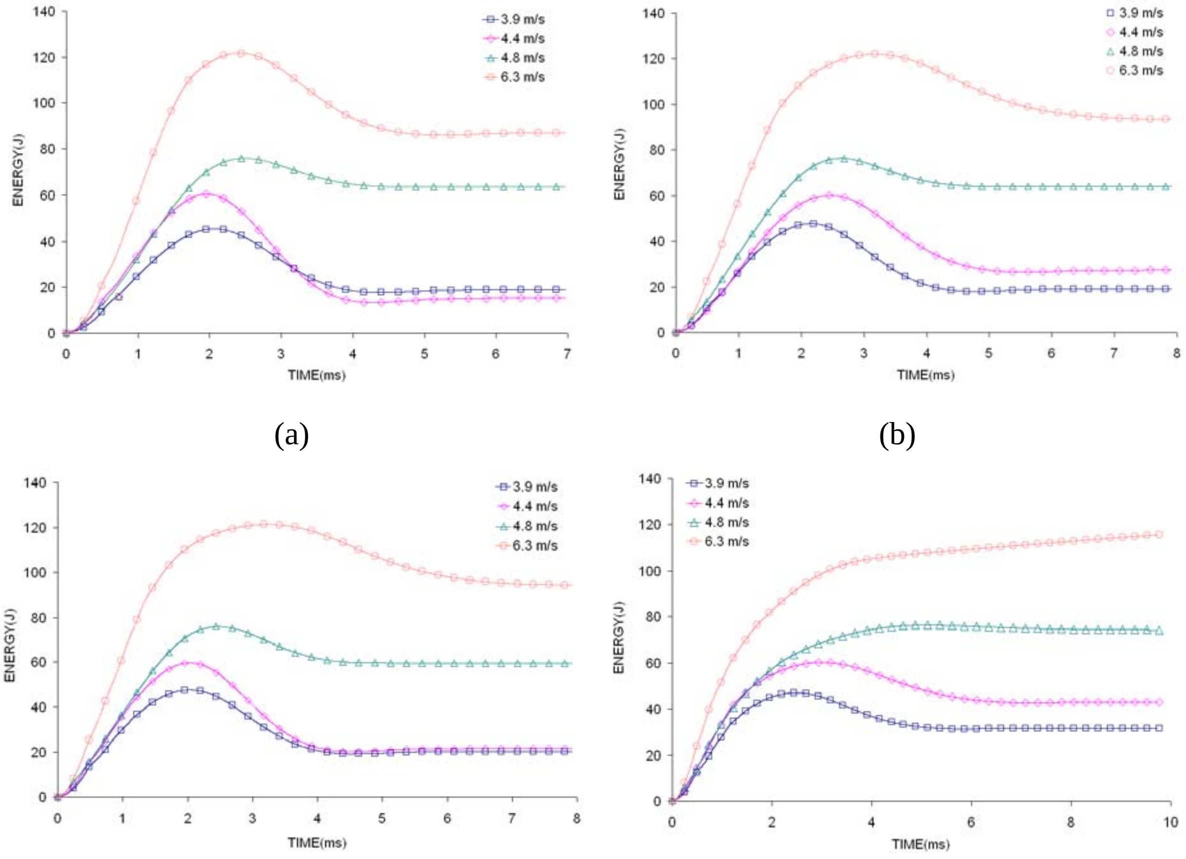

(a) (b)

(c) (d)

Figure 4.13 Energy-time histories of (a) GL, (b) GL/GR/GL, (c) GR/GL/GR and (d) GR for the impact tests conducted at impact velocities of 3.9, 4.4, 4.8 and 6.3 m/s, respectively.

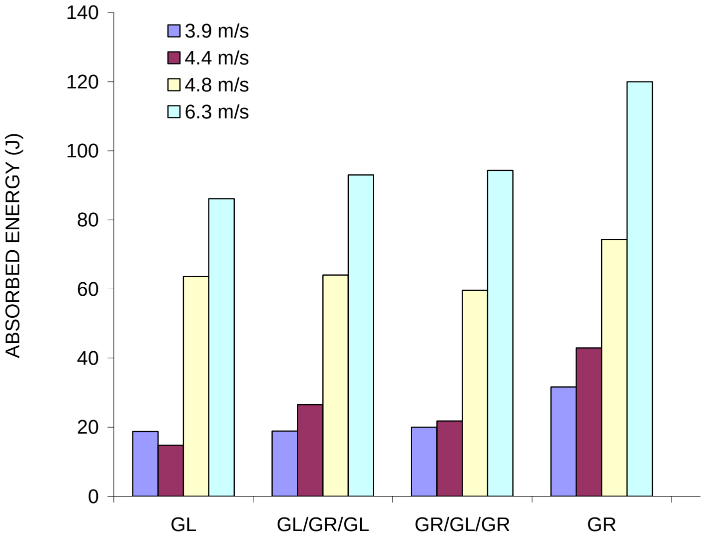

Figure 4.14 Comparison of energy absorption.

(d) Delamination

Figure 4.15 shows sectional views of composites, which highlightes various modes of damage resulting from drop-weight impact at 6.3 m/s. As depicted in Fig. 4.15(a), delamination in the non-hybrid GL composite was very localized on the impact (compression) side and widened on the back (tension) side of the composite. Similarly, delamination in the non-hybrid GR was much localized on the compression side; however the damage did not exhibit much spreading in the tension side, Fig. 4.15(b). On the other hand, drop-impact tests created quite extended delamination in the hybrid GL/GR/GL and GR/GL/GR composites, Fig.4.15(c) and (d) respectively, especially at the interface between GL and GR layers. Both hybrid composites delaminated more than the two non-hybrid composites. However splitting that occurred between hybrid layers was more severe in the GL/GR/GL composite compared to that in the GR/GL/GR composite. It is clear that hybrid composites were more susceptible to delamination, especially at the interfaces of GL and GR layers. This may be due to greater incompatibility between dissimilar layers. The ultrasonic C-scans of the impacted composites, as shown in Fig. 4.16 further prove that hybrid composites delaminated more than non-hybrid composites. Delamination in hybrid composites where GL was used as the outer skin was more pronounced compared to these in the other hybrid composites when GR was used as the face sheet (Fig.4.17). For the two non-hybrid composites, the GL composites delaminated more than the GR composites. Delamination in the GL and the two hybrid composites increased with increasing velocity. It should be noted that during these tests rebound was observed. Even impacted at 3.9 m/s, severe delamination was observed in the two hybrid composites and the delaminated area changed very little with changing velocity. However, the impact test of 3.9 m/s created small delamination in the non-hybrid GL and increasing velocity resulted in a significant increase of delaminated area.

Finally, delamination in GR did not increase with increasing velocity. Even though there was some increase between the first and second tests, impact tests conducted at 4.4 m/s and 6.3 m/s created less delamination than impacts at 3.9m/s and 4.4 m/s. This may be due to the occurrence of deep penetration and perforation in the more brittle GR composite when it was impacted at higher velocities: 4.8 and 6.3 m/s. During these two tests, the impactor penetrated into the composite and no rebound was observed.

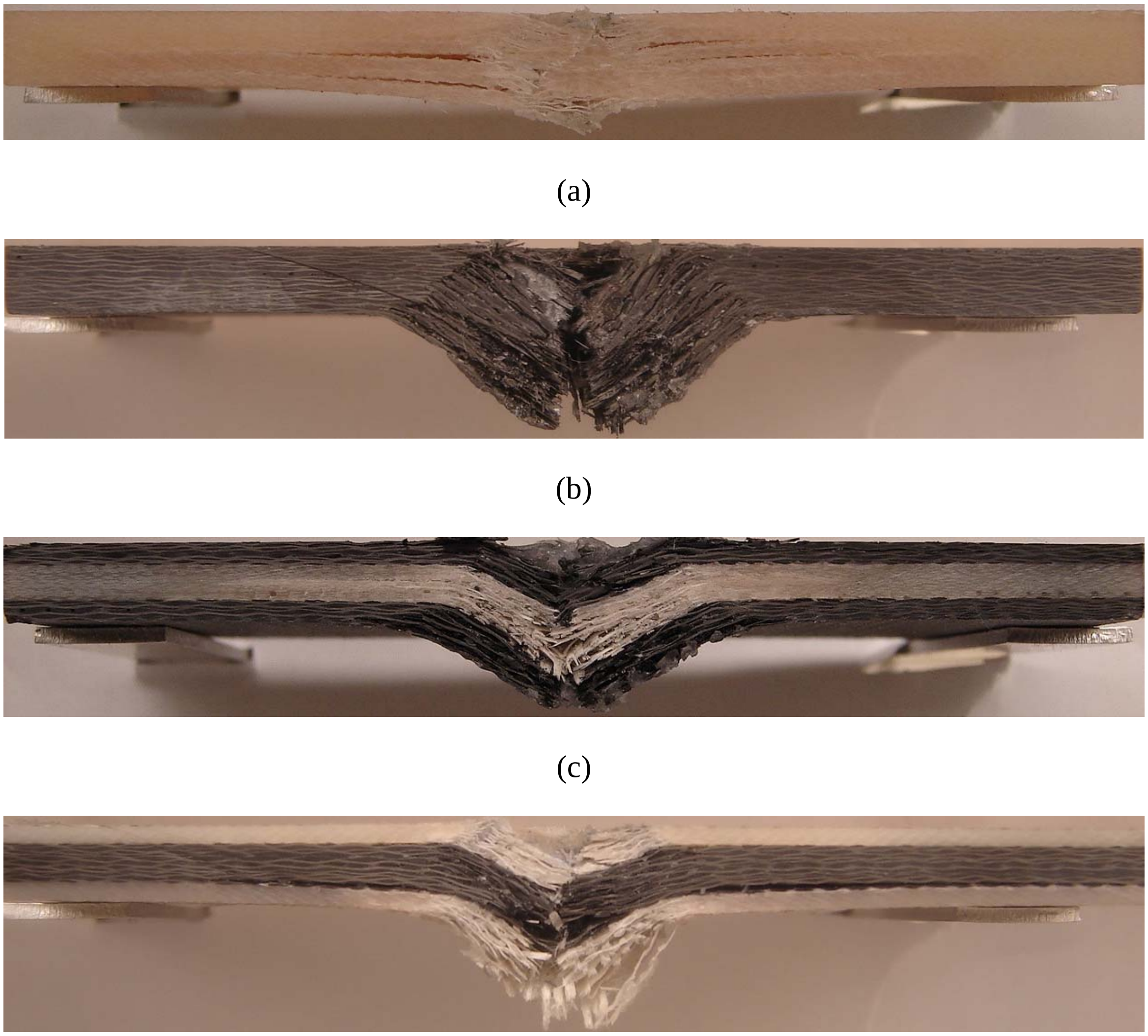

(a)

(b)

(c)

(d)

Figure 4.15. Optical fractographs of sectioned composites after drop impact conducted at 6.3 m/s: (a) non-hybrid GL, (b) non-hybrid GR, (c) hybrid GR/GL/GR and (d) hybrid GL/GR/GL.

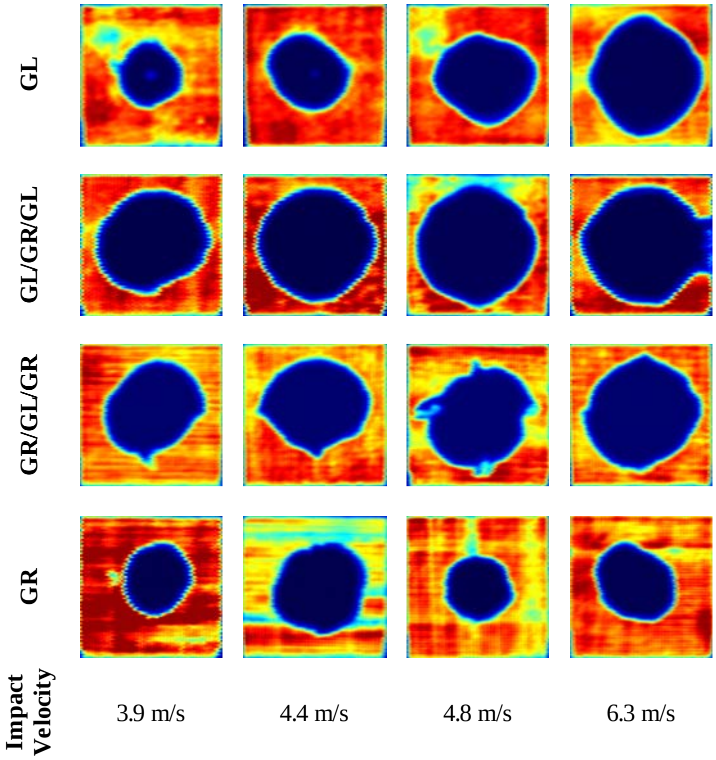

Figure 4.16 Ultrasonic C-scan images of the four types of composites impacted at various velocities.

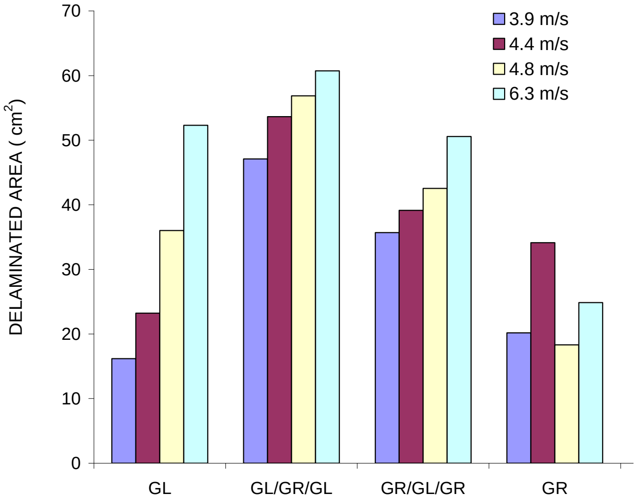

Figure 4.17 Comparison of the delaminated areas of the impacted composites.

(e) Contact duration

The contact durations of drop-impact tests are shown in Fig. 4.18. Contact durations produced by the non-hybrid GL composite were shorter than the other composite types. For the two hybrid composites, the GL/GR/GL type produced a little more contact time compared to the GR/GL/GR type; but both contact durations were definitely more than that for the GL composite. Contact durations increased with increasing impact velocity for the three composites afore.

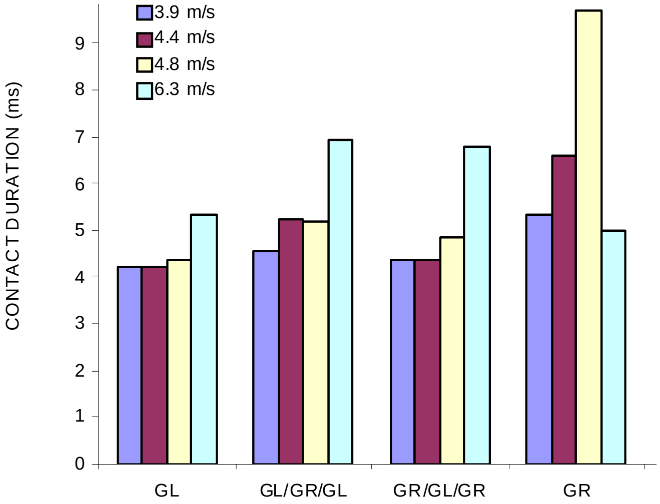

Figure 4.18 Comparison of contact durations.

On the other hand, the GR composite exhibited some inconsistency in contact duration. This again can be explained by the inherent brittleness of the non-hybrid GR composite. It should be noted that rebound was observed during testing of the GL and the two hybrid composites. If the deformation of the composite is not severe, the impactor will travel until its entire energy is spent and then it bounces back. Increasing velocity increases energy of the impactor and it will travel more to spend the extra energy. This will increase the engagement time of impactor and composite. However during the impact tests of GR severe penetration and even perforation was observed when the composite was impacted at higher velocities: 4.8 and 6.3 m/s. Impact test of GR specimens conducted at 4.8 m/s produced very long contact duration compared to other specimens. If impactor penetrates the composite, the friction between impactor and composite mainly governs the contact duration. During penetration, fibers and the matrix material are either pushed to the sides or ahead at the tip of the impactor. However, the impactor still cannot easily move forward due to the friction forces. Energy spent for friction within a unit time can be less than the energy spent for damaging the composite and that may cause some increase in contact duration. For the impact GR test at 6.3 m/s, contact duration was recorded as 5 ms. However, the impact force did not return to zero at 5 ms. It actually never returned to zero during the data acquisition time allowed by the equipment. This can be explained by the fact that when the data acquisition time ended, the impactor was still moving and the small force seen in the graph was due to the loose contact between the impactor and the hole perforated in the composite.

4.2 Effect of impactor shape on the low-velocity impact response of composites

During this study, the specimens with $+45^{o}/-45^{o}$ fiber orientation were impacted by four types of impactors (Fig.4.19 (a, b, c, d)) at a velocity of 4.1 m/s. The resultant damages created by various impactors were compared and the effect of impactor shape on the low-velocity impact response of woven glass-graphite/epoxy composites was studied. In addition, in order to study the effect of impactor angle on the low velocity impact response of woven composites, Charpy-type straight-line impactor (Fig.4.19 (d)) was used by rotating it 45^{o} around the z-axis. Two strain gages (one in longitudinal direction and the second in transverse direction) were mounted 25.4 mm away from the center (Fig.4.2). After each impact test, specimen was removed from fixture and pictures of front and back surface, were taken. Specimens were also scanned ultrasonically. The parameters of impactor test to study effect of impactor shape are shown in Table 4.2.

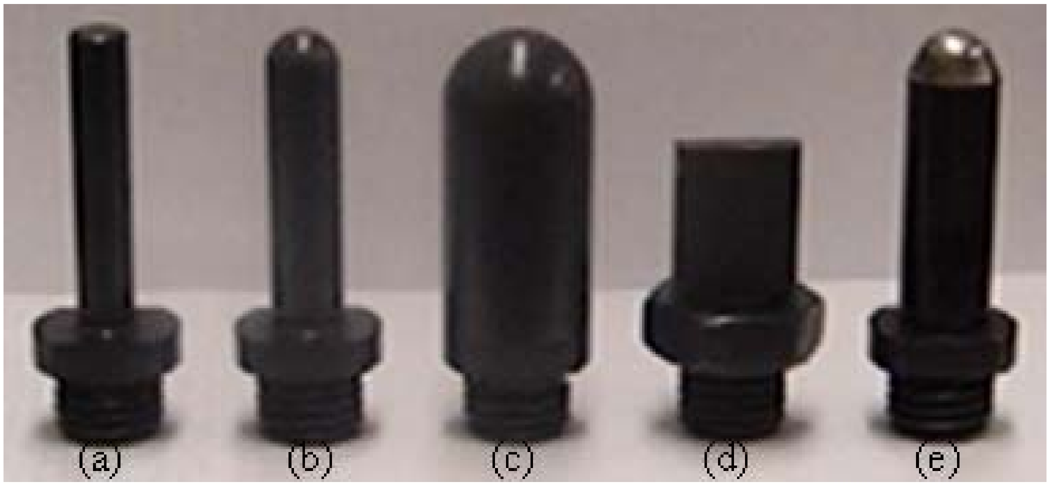

Figure 4.19 The impactors: a) 10mm flat-ended cylindrical b) 0.5” spherical c) 1” spherical d) Charpy-straight line e) 16 mm hemispherical (for repeated impact tests only)

Table 4.2 Parameters of low velocity impact tests conducted to study effect of impactor shape

	Lay-up sequence	**Impact tests**	**Impact Energy**	**Drop-weight**
Effect of impactor shape	GL	5	52J	6.15 kg
	GL/GR/GR/GL	5	52J	6.15 kg
	GR/GL/GL/GR	5	52J	6.15 kg
	GL	5	52J	6.15 kg

(a) Experimental results and discussion

Among the four lay-up sequences tested, The GL specimens sustained the highest impact force of 13-15KN (Fig.4.20 (a)) and no back-surface splitting was observed during all five-impact tests. However front-surface cracks in various shapes were observed (Fig.4.20 (b)).

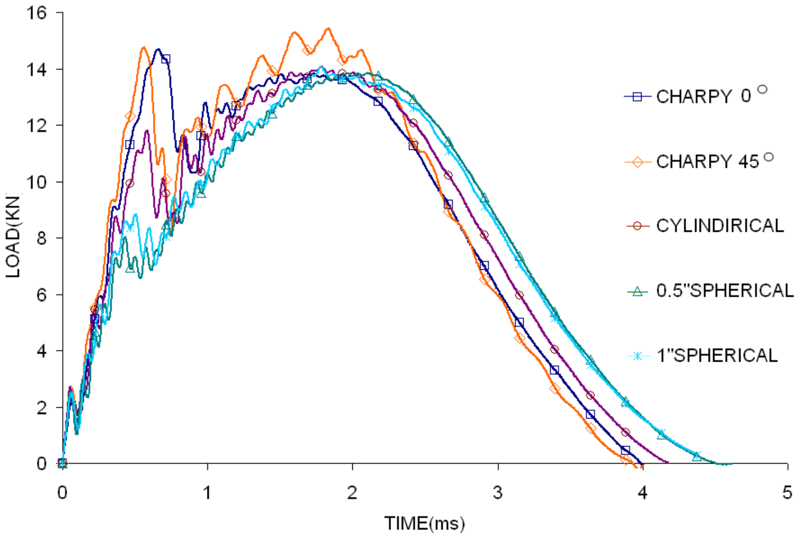

(a) Impact force

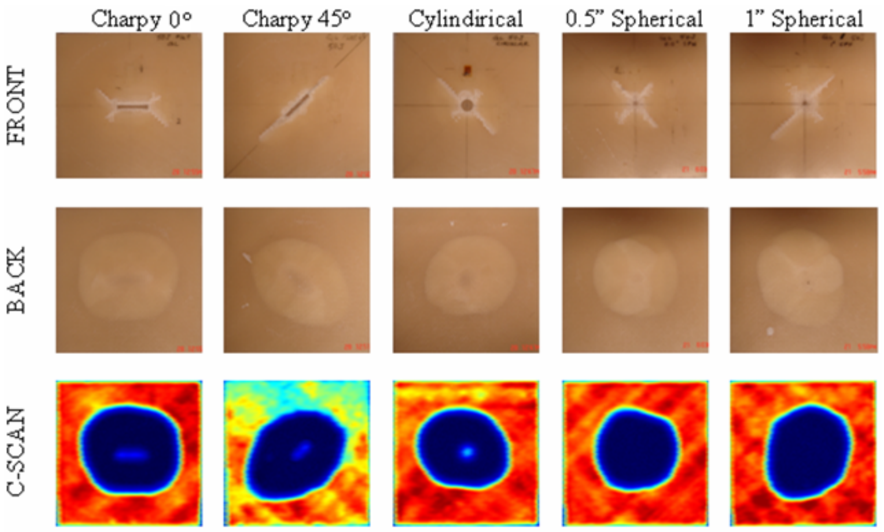

(b) Optical pictures and ultrasonic C-scans

Figure 4.20 (a) Impact force histories of GL specimen when impacted by various shapes of impactor. (b) Optical pictures and ultrasonic C-scans of impacted composites

The GR specimens sustained around 8-12 KN force (Fig.4.21 (a)). Except for the Charpy impactor, the remaining impactors penetrated into the composite and back-surface splitting was observed. Perforation was observed during the test conducted with the 0.5” spherical impactor (Fig.4.21 (b)).

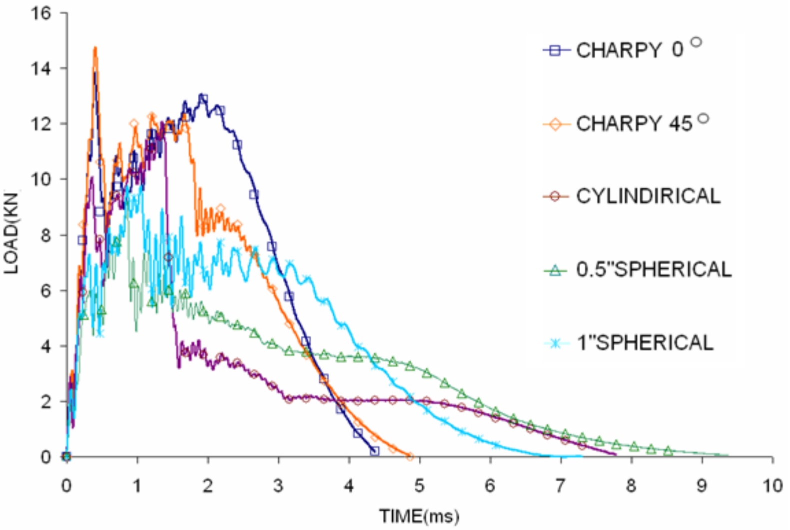

(a) Impact force

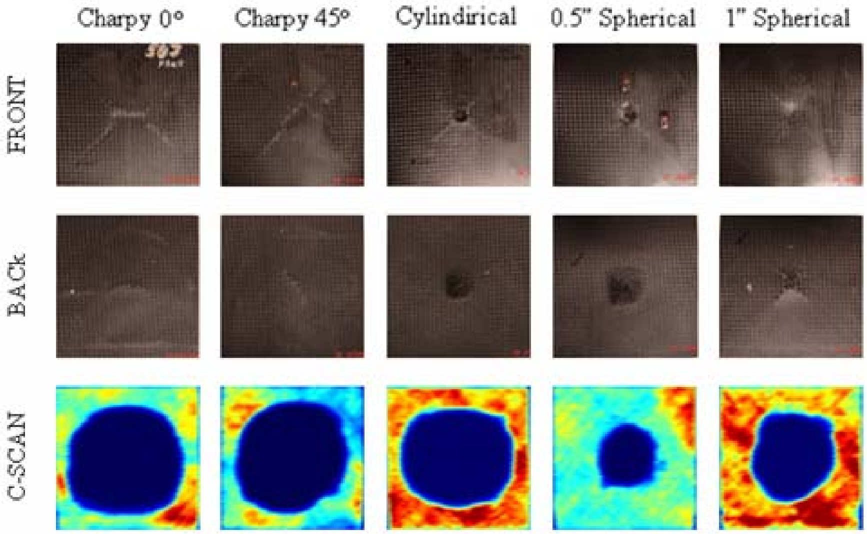

(b) Optical pictures and ultrasonic C-scans

Figure 4.21 (a) Impact force histories of GR specimen when impacted by various shapes of impactor (b) Optical pictures and ultrasonic C-scans of impacted composites.

The GL/GR/GR/GL specimens are one of the two hybrid specimens. They performed very close to the GL specimens and sustained 11-15 KN (Fig.4.22 (a)). No back-surface splitting occurred and some front surface crack was observed. (Fig.4.22 (b))

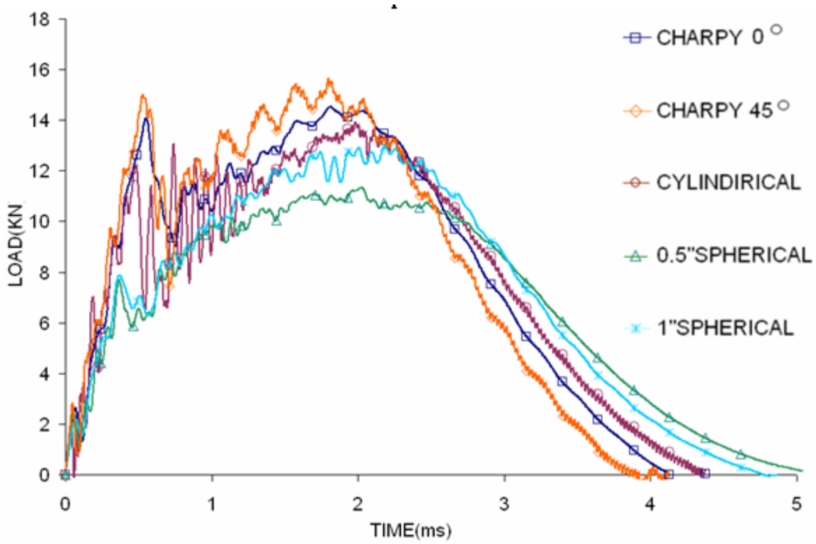

(a) Impact force

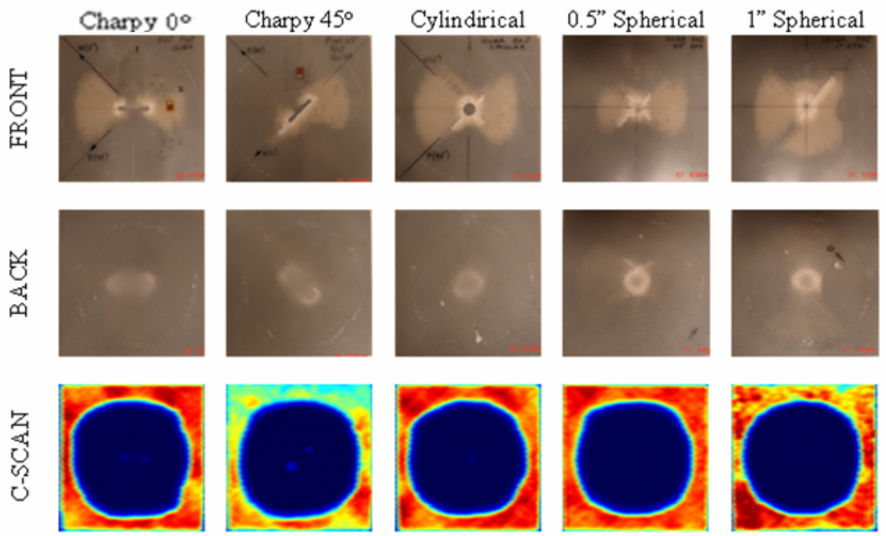

(b) Optical pictures and ultrasonic C-scans

Figure 4.22 a) Impact force histories of GL/GR/GL specimen when impacted by various shapes of impactor. b) Optical pictures and ultrasonic C-scans of impacted composites

The other hybrid specimen, GR/GL/GR, sustained 11-13 KN of impact force (Fig.4.23 (a)) and some penetration at the front surface was observed (Fig.4.23 (b)). Whenever back-surface splitting happens, usually drop at the force-time histories is witnessed. In most cases this drop happens before the maximum force is reached. Force-time histories of GR/GL/GR did not show such a drop. However optical pictures of back surfaces showed some initiation of splitting.

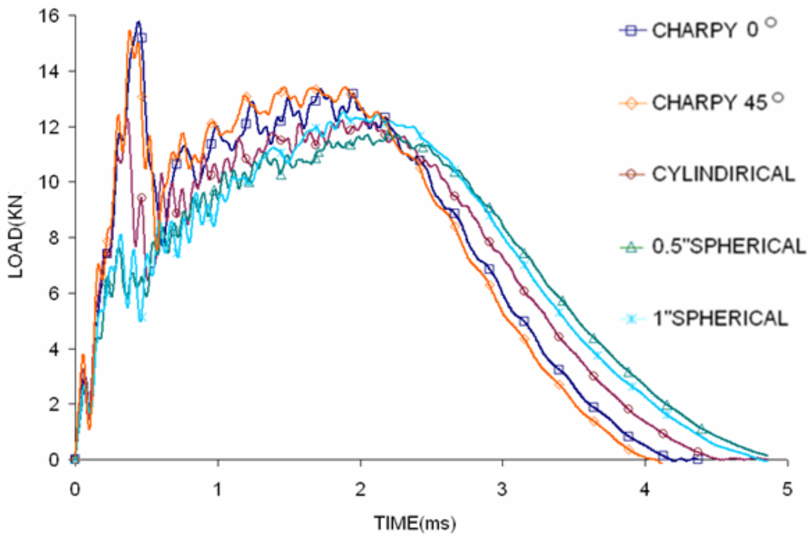

(a) Impact force

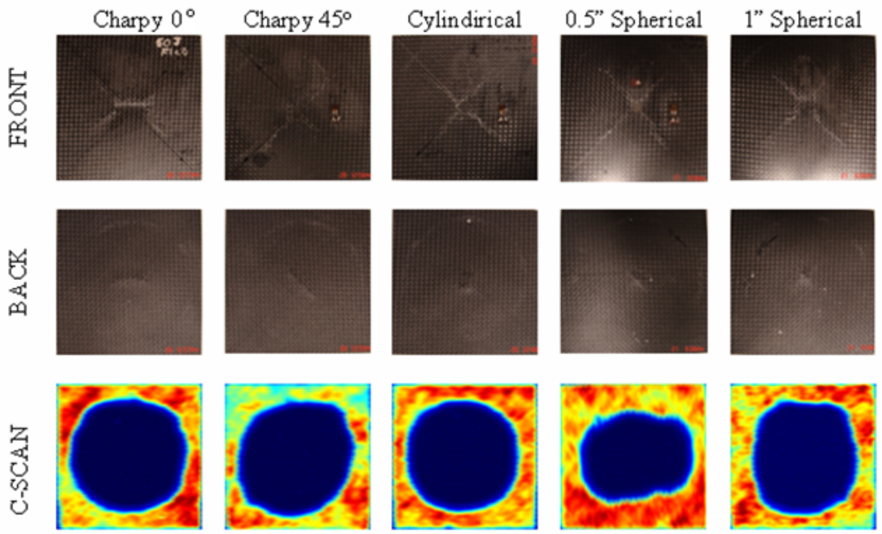

(b) Optical pictures and ultrasonic C-scans

Figure 4.23 (a) Impact force histories of GR/GL/GR specimen when impacted by various shapes of impactor. (b) Optical pictures and ultrasonic C-scan's of impacted composites

(b) Delamination

Resultant damages of low-velocity impacts are mostly in the form of delamination. Delamination created by different shapes of impactor did not vary significantly. In case of GL specimen, delaminated areas ((Fig.4.20 (b)) caused by Charpy and 1” spherical impactor were almost the same. A little less delamination was created when GL specimens were impacted by cylindrical and 0.5” impactors. Changing impactor angle created almost the same amount of delamination. However, while the shape of the delaminated area created by 0^o degree Charpy impactor was circular, the Charpy impactor at 45^o created an oval shape delaminated area. Delamination of hybrid specimens did not vary with changing impactor shape and orientation (Fig. 4.22(b) and 4.23(b)). GR specimens (Fig.4.21 (b)) delaminated most when impacted by Charpy and cylindrical impactor. The 1” spherical impactor created a little less delamination. During the impact of GR specimens by 0.5” spherical impactor very little delamination was created. This is because of the perforation observed in this case. During perforation, the specimen cannot deflect as much as it can during no perforation cases. Energy of the impactor is mostly used for penetration and less energy is left for delamination.

(c) Impact force

Changing impactor orientation did not have significant effect on impact force. However, when composites were impacted by 45^o Charpy impactor, more oscillations at force time histories were observed in comparison with force time histories obtained when using 0^O Charpy impactor.

When a typical force-time history of drop-weight impact is reviewed (Fig.4.24), three parameters appear to be significant. Initial peak, maximum force and contact duration.

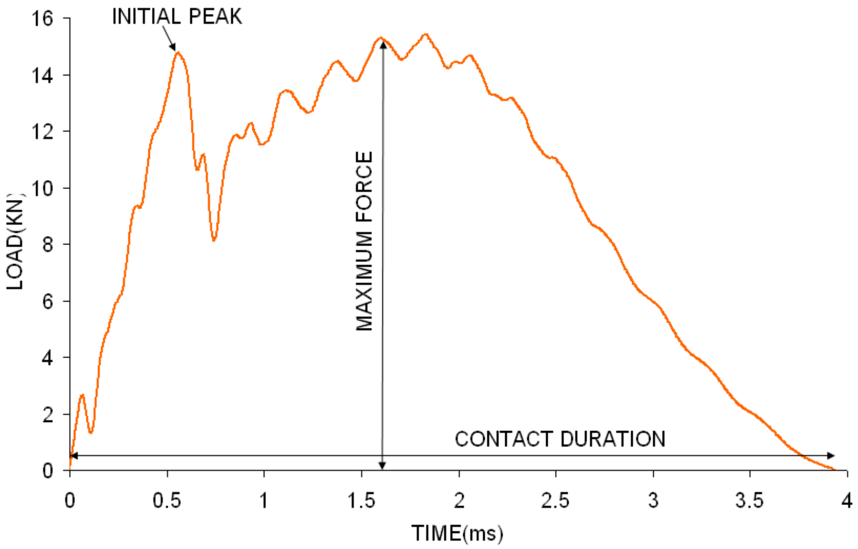

Figure 4.24 Typical force-time history of drop-weight impact test

Initial peak value of the impact force represents starting point of the damage. Drop-weight impact tests conducted using Charpy impactor had the highest initial peak for all lay-up sequences (Fig.4.25). On the other hand both spherical impactors had the lowest initial peak values. The results of the tests conducted using flat-ended cylindrical impactor lay somewhere in between. It can be said that the damage created by Charpy impactor was delayed because when the impactor touches the specimen, the contact is along the line and many fibers are active in terms of load sustainment. However when using spherical impactors, contact starts at a point and few fibers are active for load sustainment. Thus damage is quicker. Initial peak values obtained using flat-ended cylindrical impactor lay somewhere in between the initial peaks of Charpy and spherical impactors. The contact area of cylindrical impactor is between the contact area of the Charpy and that of the spherical impactor. Figure 4.26 shows the maximum force values recorded during the drop-weight impact tests using impactors of various shapes. While

Charpy impactor produced the highest impact force, spherical impactors produced the lowest and the force produced by cylindrical impactors was somewhere in between.

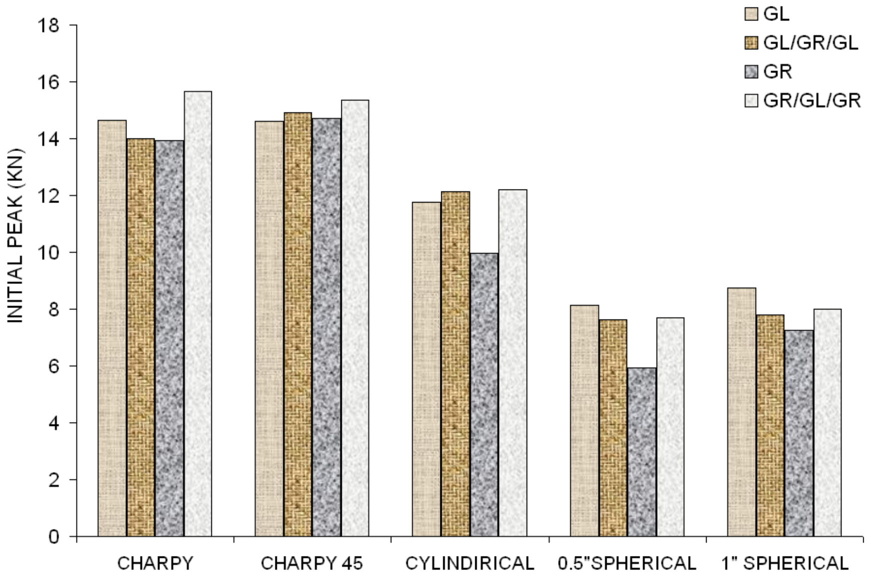

Figure 4.25 Comparison of initial peak forces for composites were impacted using impactors of various shapes.

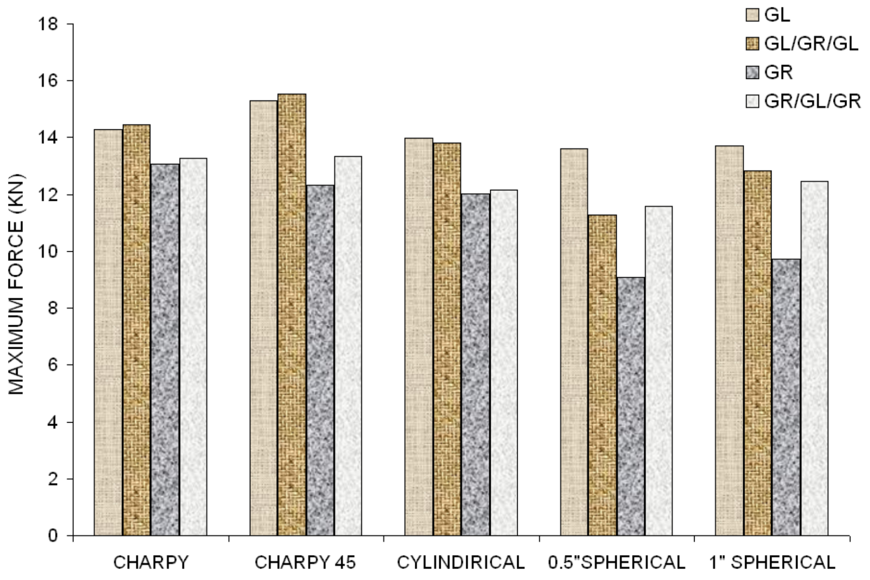

Figure 4.26 Comparison of maximum impact forces for composites impacted using impactors of various shapes

(d) Contact duration

Comparison of contact durations (Fig.4.27) shows that contact time for GR specimen especially when cylindrical and spherical impactors were used is quite different than the others. It should be noted that GR specimen was severely damaged during these impacts when the impactor penetrated into the specimen. Impact test conducted using 0.5" spherical impactor, caused complete perforation. If impactor penetrates into the composite, contact duration is mainly governed by the friction between impactor and composite. During penetration, fibers and matrix materials are either pushed to the sides or pushed ahead at the tip of the materials. After damaging the composite, not much resistance comes from composite.

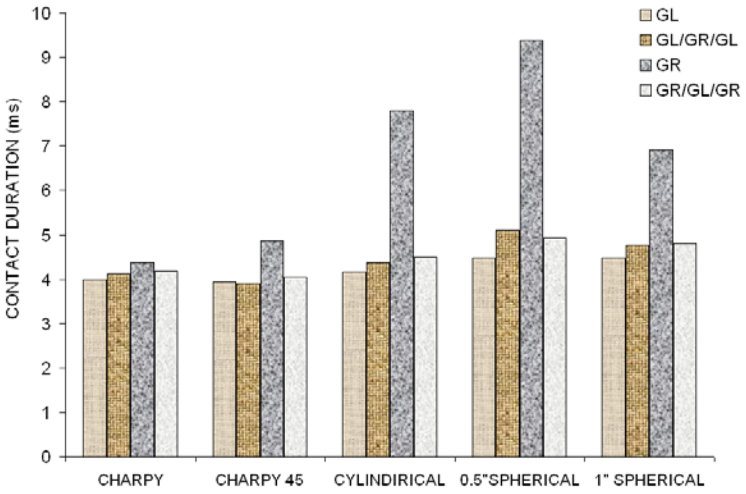

Figure 4.27 Comparison of contact durations for composites impacted using impactors of various shapes.

However impactor still cannot easily moves forward due to the friction forces. Energy spent for friction in unit time can be less than energy spent for damaging the composite and that may cause some increse in contact duration. For GL and hybrid specimens the contact duration was shortest when Charpy impactor was used. Using spherical impactors resulted in longest contact duration. Contact duration produced by cylindrical impactor was somewhere between the durations produced by Charpy and spherical impactors.

4.3 Effect of repeated impact on the low-velocity impact response of composites

This part of the study focused on the repeated impact response of woven hybrid composites. Specimens with 4 lay-up configurations were repeatedly impacted using 6.15 kg hemispherical impactor (Fig.4.19 (e)) at 3.1m/s. The impact energy was around 30 J. The reason for choosing low impact energy compared to the energy level used in the first part of the study was to avoid creating very fast damage accumulation in the composite. Quick damage accumulation in the composite would not show the progression of the damage clearly. Impact event was repeated until complete perforation. Specimen was removed from fixture after every 4 impacts, optical pictures of front and back surface were taken and specimen was scanned ultrasonically. No strain gage was mounted on the specimens. Table 4.3 shows detailed information about drop weight impact tests.

Table.4.3 Parameters of low velocity impact tests conducted to study effect of repeated impact

Lay-up sequence	Impact tests	Impact Energy	Drop-weight
GL	69	30J	6.15 kg
GL/GR/GR/GL	69	30J	6.15 kg
GR/GL/GL/GR	33	30J	6.15 kg
GR	6	30J	6.15 kg

(a) Experimental results and discussions

The woven composites with four different lay-up sequences were impacted repeatedly until perforation. The GL specimen was impacted 69 times and no perforation was observed (Fig.4.28).

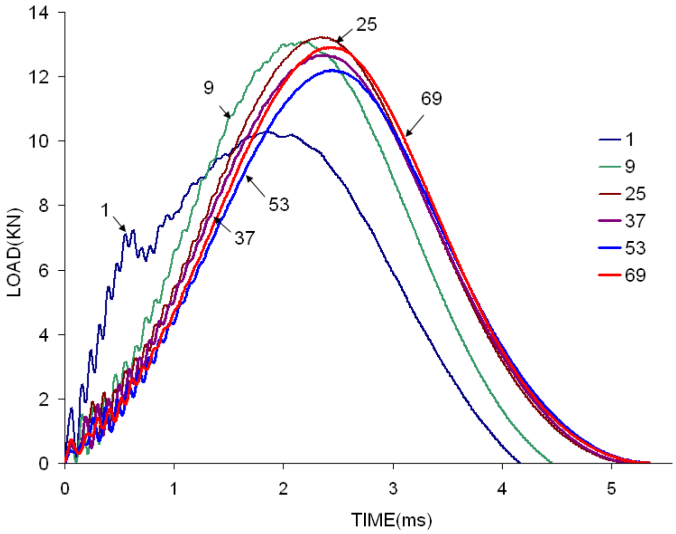

(a) Impact force

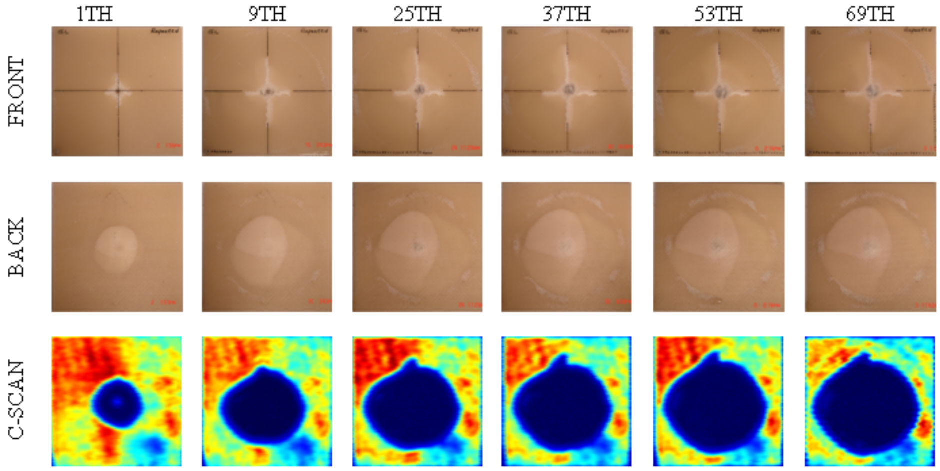

(b) Optical pictures and ultrasonic C-scans

Figure 4.28 (a) Impact force histories of GL specimen when repeatedly impacted by hemispherical impactor (b) Optical pictures and ultrasonic C-scans of composite after impact # 1, 9,25,37,53 and 69.

Perforation was observed at the first hybrid GL/GR/GL composite after 69 impacts. The second hybrid type GL/GR/GL composite survived up to 33 impacts. The GR specimen was the weakest and lasted for only 6 impacts.

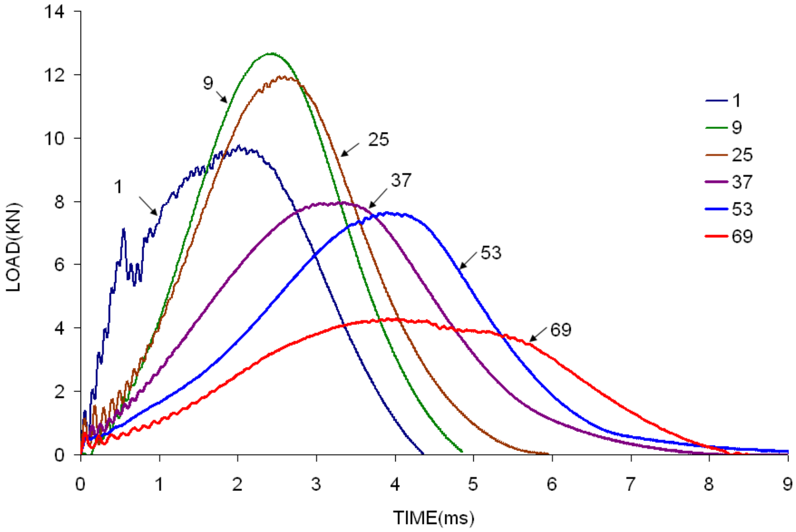

(a) Impact force

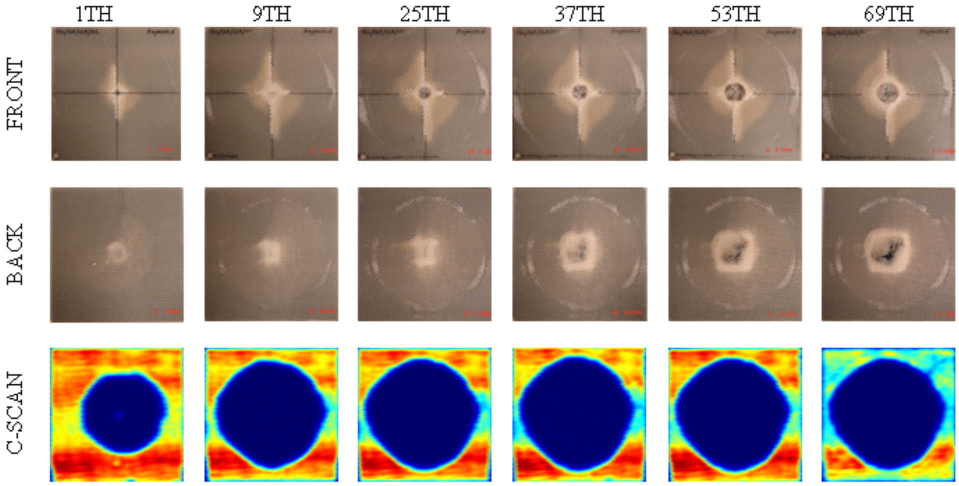

(b) Optical pictures and ultrasonic C-scans

Figure 4.29 (a) Impact force histories of GL/GR/GR/GL specimen when repeatedly impacted by hemispherical impactor b) Optical pictures and ultrasonic C-scans of composite after impact # 1, 9,25,37,53 and 69.

During the impact of three types of specimen, which contain glass fabrics (Fig.4.28 (a), 4.29(a), 4.30(a)) contact force increased after the first impact test. That was not the case for the GR specimen (4.31(a)). It can be said that glass fabrics were compacted after impact and became even stronger.

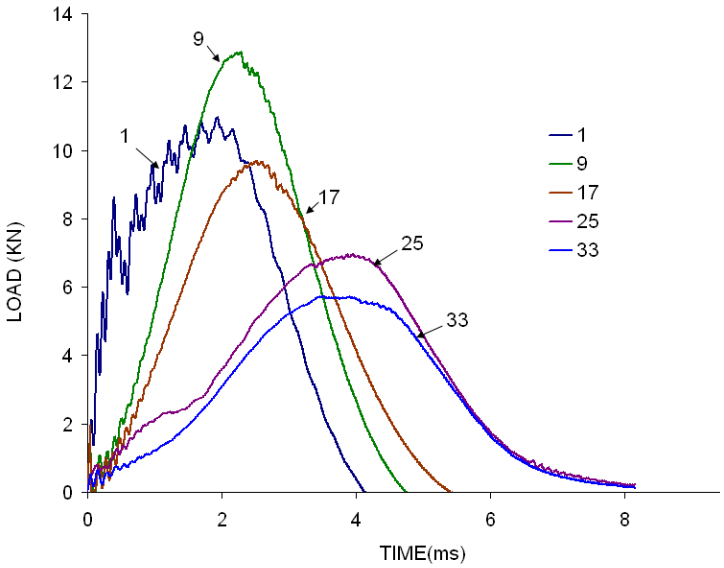

(a) Impact force

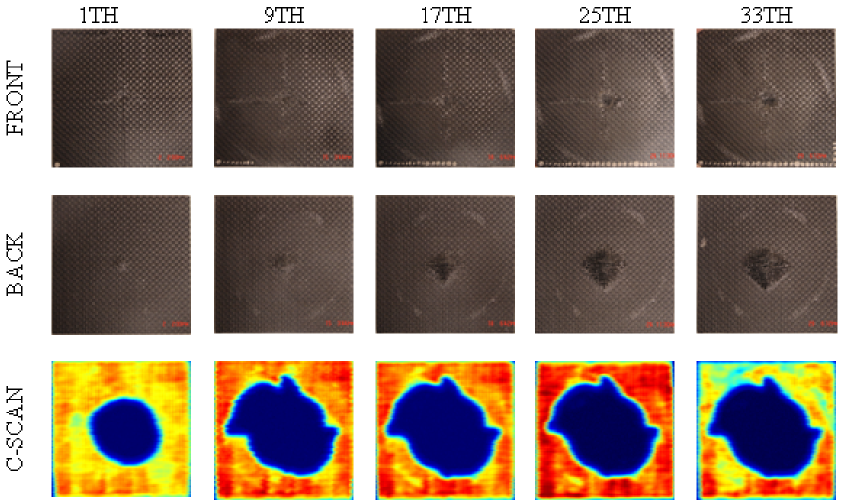

(b) Optical pictures and ultrasonic C-scans

Figure 4.30 a) Impact force histories of GR/GL/GR specimen when repeatedly impacted by hemispherical impactor b) Optical pictures and ultrasonic C-scans of composite after impact #1, 9, 17, 25 and 33

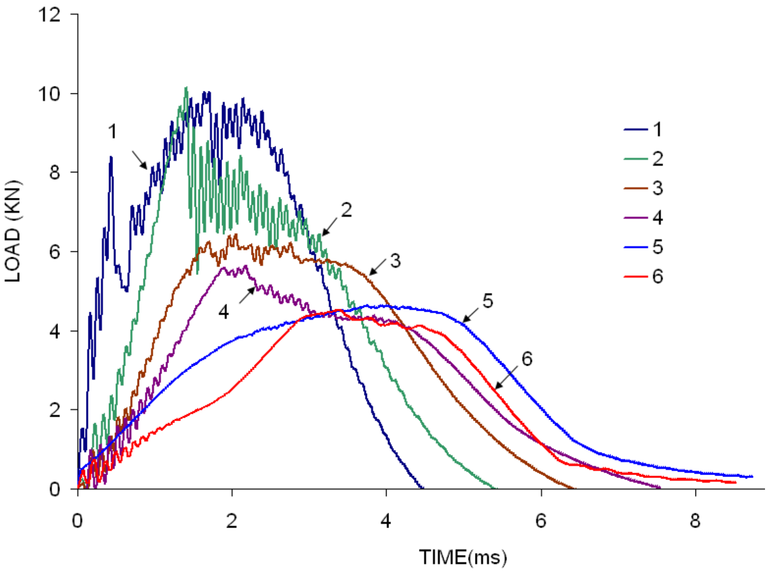

(a) Impact force

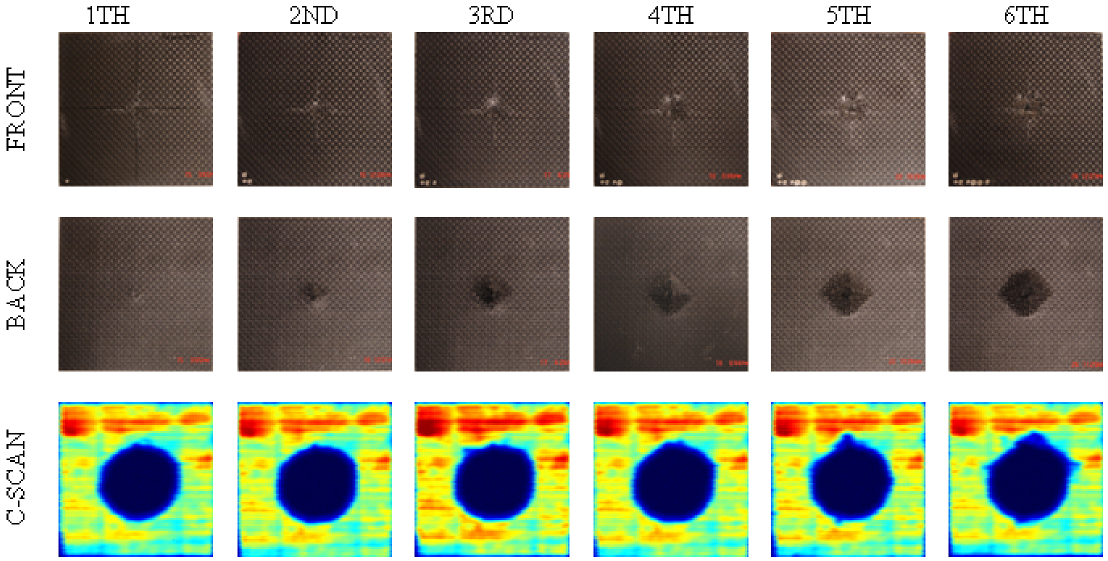

(b) Optical pictures and ultrasonic C-scans

Figure 4.31 a) Impact force histories of GR specimen when repeatedly impacted by hemispherical impactor. b) Optical pictures and ultrasonic C-scans of composite after impact # 1, 2,3,4,5 and 6.

(b) Impact force

During the impact test of GL composite, the peak 10KN contact force produced by the first impact increased to 13KN after 9 impacts and remained almost the same up to 69 impacts (Fig.4.28 (a)). Contact duration also increased up to 25 impacts and then remained constant. The force-time history of first impact showed initial peak value around 7KN. The rest of the impacts did not show such a peak value. It might be said that most of the damage was created by the first impact. Even though front surface crack propagated with increasing number of impacts, the impactor did not penetrate into the composite further after first impact.

Figure 4.29(a) shows the contact force histories for a GL/GR/GL specimen under repeated impacts. The first impact produced 9.5 KN of contact force. The contact force went up to 13 KN first, and then dropped down to 4 KN and eventually perforation occurred. Front surface crack propagated up to the ninth impact and remained the same for the rest of the impacts.

Figure 4.30(a) shows the contact force histories for a GR/GL/GR specimen impacted repetitively. The first impact produced 10.5 KN of contact force. Successive impacts increased the impact force up to 13 KN first, decreased it to 5 KN later and eventually perforation occurred. Front surface crack propagated up to the ninth impact and remained the same for the rest of the impacts. Back surface splitting occurred after nine impacts.

In the case of repeatedly impacting GR specimens (Fig.4.31 (a)), the first impact produced 10KN and back surface splitting was observed right after the second impact. The impactor penetrated more into the composite after repeated impacts and complete perforation occurred after the sixth impact. Fig.4.32 shows comparison of maximum forces. During the first twelve impacts, maximum force produced by GL composite increased from 10.3 KN to 13.8 KN and no significant change was observed afterwards.

Maximum force of GL/GR/GL composite increased from 10 KN to 13 KN during first ten impacts and became 5KN at the end of the 69 impacts. The GR/GL/GR hybrid composite exhibited similar response to GL/GR/GL composite but perforation was observed after 33 impacts and maximum force decreased to 5.8 KN. For the GR specimen the maximum force slightly increased after the first impact and rapid decreased was observed. The maximum force was 4KN when perforation observed.

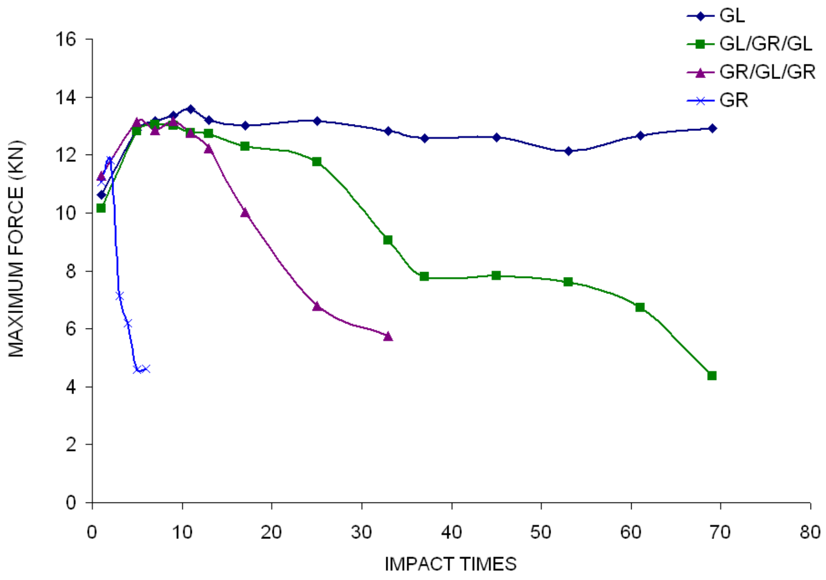

Figure 4.32 Comparison of maximum forces during repeated impact.

(c) Delamination

The successive impacts caused extended delamination during the test of GL composite (Fig. 4.28(b)). For the hybrid composites, delaminated area increased up to the ninth impact did not change significantly afterwards (Fig.4.29 (b), Fig.4.30 (b)). Due to the penetration and perforation, delaminated area of GR composite did not change during the six impacts (Fig.4.31 (b)). If penetration or perforation is observed substantial portion of the impact energy is used for damage creation and less energy is used for deflection. Thus, the resulting delaminated area is smaller. Figure 4.33 shows progression of delamination with repeated impacts. It is clear that non-hybrid composites delaminated less than hybrid composites. Delamination observed during repeated impact tests of GL/GR/GL hybrid composite was more than the delamination of the other hybrid composite.

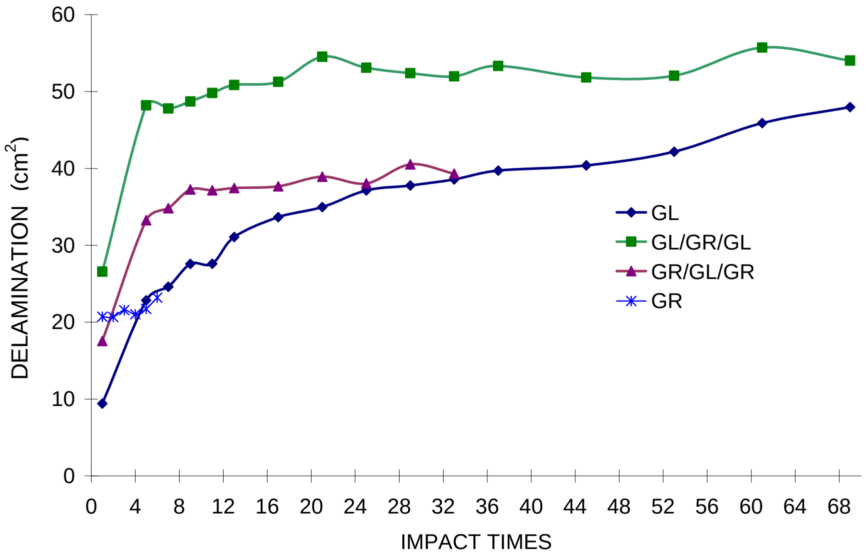

Figure 4.33 Comparison of delaminated areas

(d) Energy

Energy-time histories for impacted composites clearly show the impact energy, rebound energy and absorbed or transferred energy (Fig.4.12). Energy-time histories were recorded during all impact events but Figure 4.34 shows energy-time histories of selected impacts to have less crowded graphs. The absorbed energy of GL, GL/GR/GL and GR/GL/GR composites initially decreased with repeated impacts (Fig.4.35) and all had a very similar trend. The curves were separated after the tenth impact. The results indicate that, while the energy absorbed by GL composite increased at the lowest rate, the absorbed energy of GR/GL/GR increased at the highest rate. The GL/GR/GL composite behaved somewhere between GL and GR/GL/GR composites. On the other hand, successive impacts resulted in very rapid increase of absorbed energy in case of GR composites.

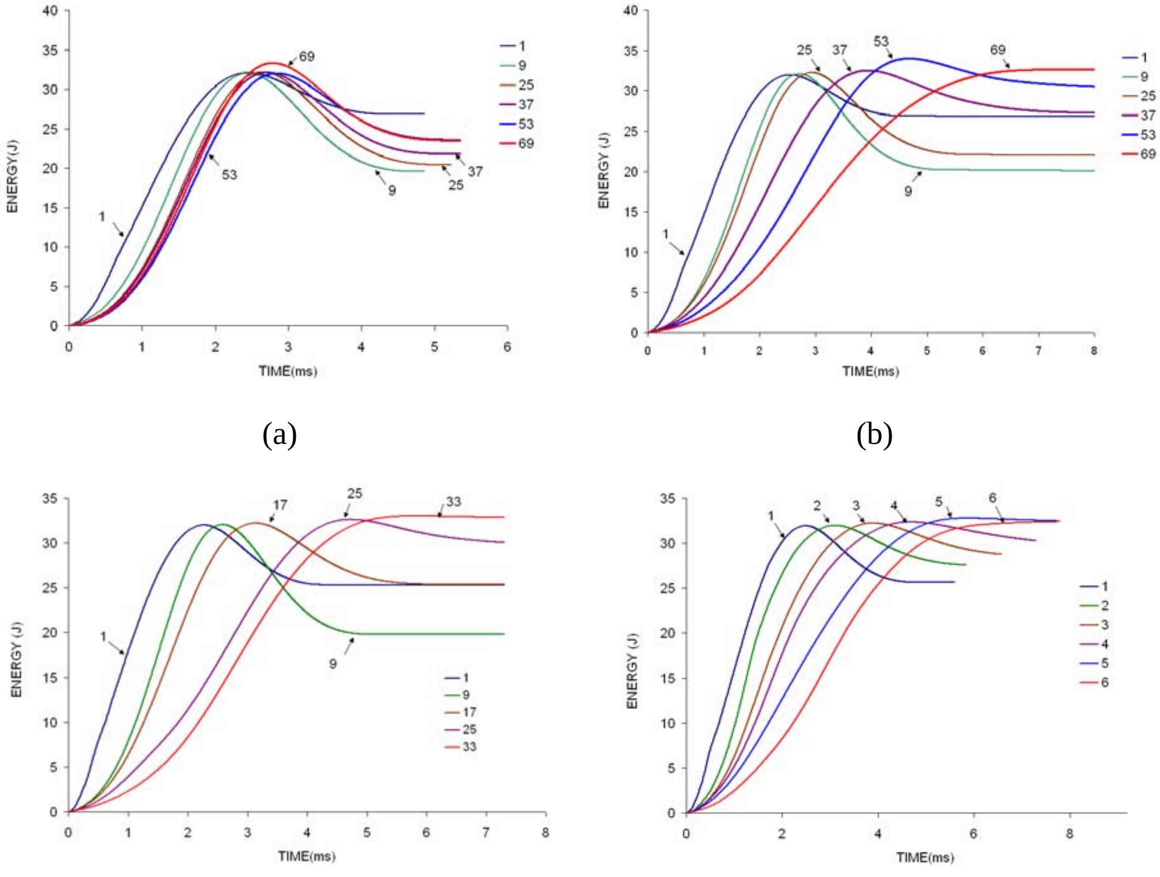

(a)

(b)

(c)

(d)

Figure 4.34 Energy-time histories of a) GL, b) GL/GR/GL, c) GR/GL/GR and d) GR composites

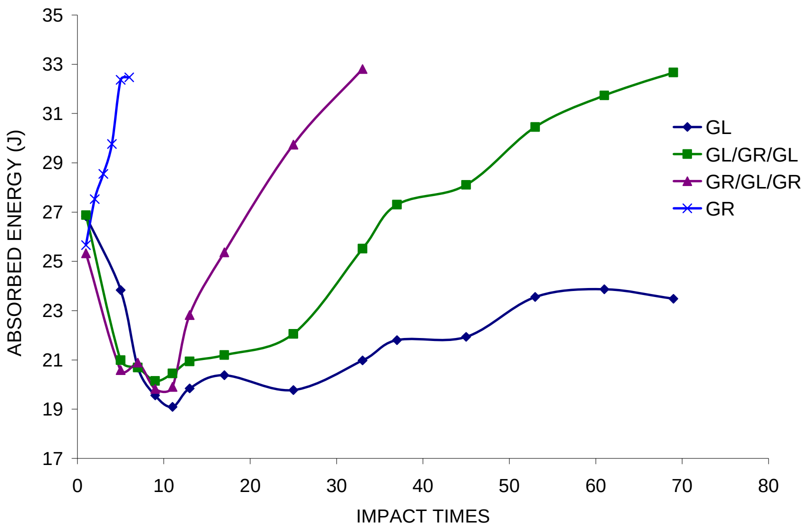

Figure 4.35 Comparison of absorbed energy-time histories

4.4 CONCLUSIONS OF DROP-WEIGHT IMPACT STUDIES

a) Among the four lay-up sequences tested, GL composite was the strongest, while GR was the weakest. Both hybrid specimens performed better than GR but not as well as GL. Between the two types of hybrid composites, the glass-skin/graphite-core type performed a little better than the graphite-skin/glass-core type.

b) The process of hybridization gives us control of certain parameters such as impact force and damage to the composite. However hybrid composites are prone to delamination especially between dissimilar layers.

c) Charpy impactor produced highest initial force peak, highest contact force and least contact duration. Spherical impactor generated lowest initial force peak and contact force but highest contact duration. Performance of the cylindrical impactor stands somewhere between that of Charpy and spherical impactor. This is true for non-perforation cases. If perforation occurs, specimen usually gets damaged before it can reach the maximum contact force and the contact duration is usually higher than that for non-perforation cases.

d) Placing Charpy impactor at 45^o did not create significant difference in the performance of composite when compared with the 0^o orientation case. However, more oscillations in force time histories for all cases were observed.

e) Changing the diameter of spherical impactor did not have any effect on the performance of the composite. Both spherical impactors produced very similar results.

f) Changing impactor shape did not affect delamination significantly. Shape of the delaminated area for GL was changed when impactor angle changed. In case of perforation the composite delaminated less.

g) Repeated impacts caused very quick damage accumulation for GR and very slow damage accumulation for GL. Progression of the damage for hybrid GL/GR/GL specimen was slower compared to that of the hybrid GR/GL/GR type.

h) Hybrid composites delaminated very quickly during the first impact. Delamination remained the same for the rest of the repeated impacts. Delaminated area of GL increased slowly after each successive impact. Delamination of the GR specimen was almost constant during six impacts before perforation.

5. BALLISTIC IMPACT TESTS ON WOVEN HYBRID COMPOSITES

The ballistic impact tests were conducted using an in-house high pressure gas gun. High pressure helium, once released by a fast acting solenoid valve, provides the force needed to accelerate a 22-caliber copper bullet through the gun barrel to the desired speed. Near the muzzle of the gun barrel, two sets of diode laser-amplified photo diode pairs form two optical paths separated by 101.6 mm. The voltage changes caused by the projectile traversing through the two optical paths were recorded and used to estimate the projectile speed.

Initial ballistic impact tests were conducted using composite beams made of toughened epoxy (i.e., cured at 350°F, 1 hour 15 minutes) reinforced by uni-directional S2 glass fibers (44% fiber volume fraction) machined into simple strip specimens. The panels had 24 layers (approximately 6.35 mm in thickness), which were stacked with different lay-up configurations. The ballistic impact tests on woven composites were conducted on two different geometries. While the panels with 101.6 mm by 152.4 mm were clamped over a length of 25.4 mm on both sides (5.1(b)), the composite beams with 25.4 mm by 254 mm were clamped over a length of 50.8 mm at both ends (5.1(a)). Two strain gages, marked as SG-1 and SG-2 were mounted on the impact side of the specimens. For the panel, the distance of the SG-1 and SG-2 from the center of the panel was 25.4 mm. For the composite beams, one of the strain gages was 25.4 mm and the other was 38.1 mm away from the center. During the ballistic impact test, the projectile sometimes might not directly hit at the center. A strain gage can not survive the impact if the impingement is too close to it. Having one strain gage on each side allowed us to obtain at least one good strain measurement. Once an experiment was completed, only the panels were ultrasonically C-scanned. The optical pictures of impacted specimens were taken. The specimens were also cut longitudinally at the center for comparison. Table 1 summarizes the specimen lay-up configurations and the impact velocities of six ballistic impact tests. Two strain-gages were mounted on the impact side.

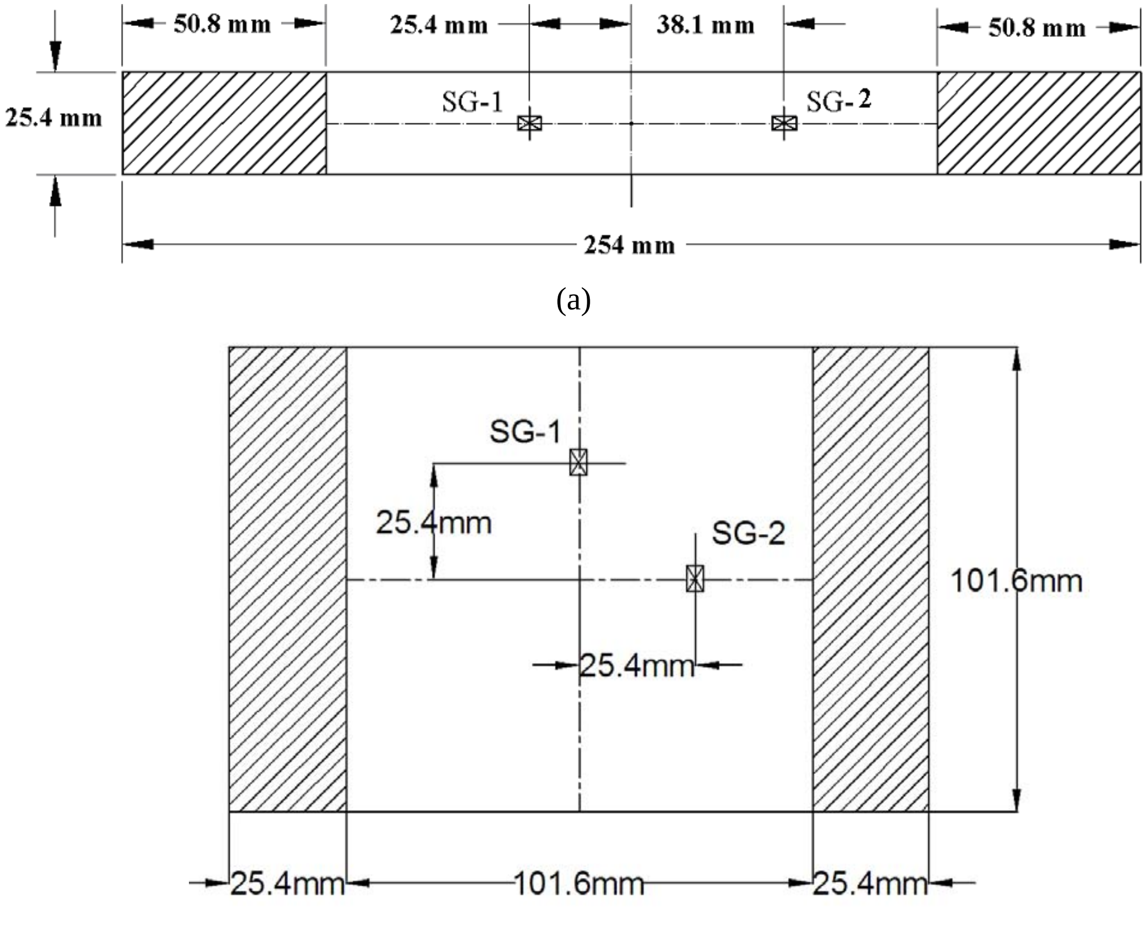

(a)

(b)

Figure 5.1 A typical (a) composite beam and (b) composite panel specimen mounted with two strain-gages on the ballistic impact side

5.1 Ballistic impact tests on S2-glass fiber/toughened epoxy composite beams

The six ballistic impact tests were conducted on the composite with two different lay-up sequences. The Table 5.1 shows the parameters of the ballistic impact tests.

It should be noted that the ballistic limit (V_{50}) of the composites cannot be determined using these few experimental data. The classical ballistic limit calculations are done using at least ten experimental data.

Table 5.1 Parameters of ballistic impact tests on glass/epoxy composites

Test	**Lay-up sequence**	**Impact velocity, V_I (m/s)**	**Projectile Penetration**
1	$\left[0^\circ_3/90^\circ_3\right]_{2S}$	120	Partial
2	$\left[0^\circ_3/90^\circ_3\right]_{2S}$	298	Partial
3	$\left[0^\circ_3/90^\circ_3\right]_{2S}$	465	Full
4	$\left[0^\circ_3/45^\circ_3/90^\circ_3/-45^\circ_3\right]_S$	390	Full
5	$\left[0^\circ_3/45^\circ_3/90^\circ_3/-45^\circ_3\right]_S$	423	Full
6	$\left[0^\circ_3/45^\circ_3/90^\circ_3/-45^\circ_3\right]_S$	442	Full

Five of the experiments should preferably be partial penetration and the remaining five full penetration. However our approach is to use Finite Element analysis to calculate the ballistic limit velocity. Thus these experiments were mainly used for validating our FE models. Figures 5.2 to 5.4 show the dynamic strain histories, post-impact optical micrographs and the deformed 22-caliber copper projectile for three ballistic impact tests described in Table 5.1. As shown in Fig. 5.2, no delamination was observed for Ballistic Test 1. $\left[0^\circ_3/90^\circ_3\right]_{2S}$ cross-ply beam was impacted at 120 m/s. Only the top layers of the composite were slightly damaged and the deformation of the projectile was not severe; whereas the Ballistic Test 2, $\left[0^\circ_3/90^\circ_3\right]_{2S}$ cross-ply beam was impacted at 298 m/s and the 22-caliber copper projectile penetrated into the composite. As shown in Fig. 5.3, higher dynamic strains were produced; delamination was observed; and the projectile deformed more significantly.

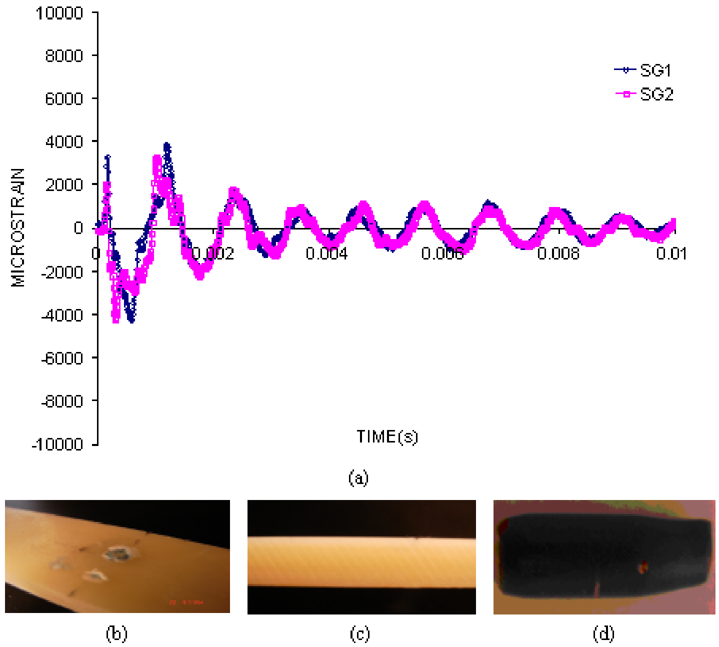

Figure 5.2 Dynamic strain histories and the post-mortem specimen and after-impact projectile of Ballistic Test 1: $\left[0^\circ_3/90^\circ_3\right]_{2S}$ cross-ply S2 glass-toughened epoxy composite beam impacted at 120 m/s by a 22 caliber copper projectile: (a) Dynamic strains, (b) Perspective view, (c) Side view and (d) Deformed projectile

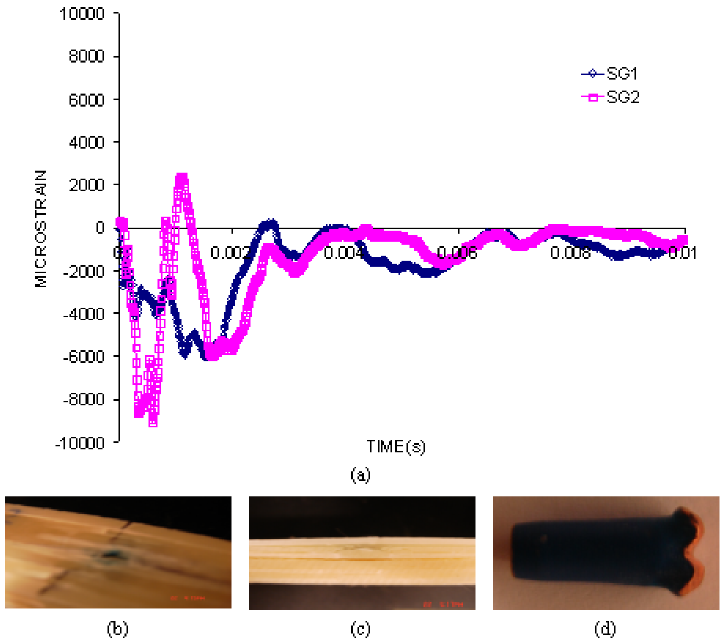

Figure 5.3 Dynamic strain histories and the post-mortem specimen and after-impact projectile of Ballistic Test 2: $\left[0^\circ_3/90^\circ_3\right]_{2S}$ cross-ply S2 glass-toughened epoxy composite beam impacted at 298 m/s by a 22 caliber copper projectile: (a) Dynamic strains, (b) Perspective view, (c) Side view and (d) Deformed projectile

For the ballistic Test 6: $\left[0^\circ_3/45^\circ_3/90^\circ_3/-45^\circ_3\right]_S$ quasi-isotropic beam, the specimen was impacted at 422 m/s. It was observed that the projectile penetrated completely and exited from the back side of the composite. There was serious damage to the composite as well as to the projectile itself. Figure 5.4 shows the strain histories, top surface and side views of the composite after impact, and the deformed projectile. Delamination occurred between all layers and was more severe around the center. The length of the delamination for all layers except the last three was approximately 30 mm. The last three layers delaminated more than the others.

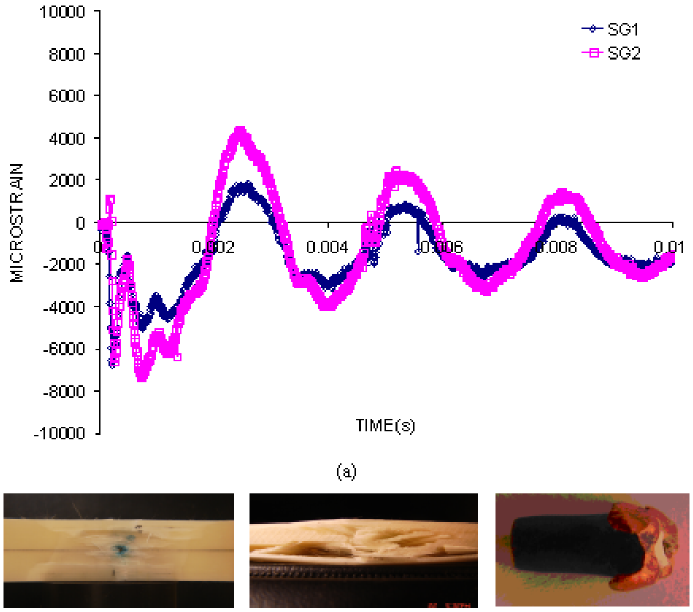

(a)

(b) (c) (d)

Figure 5.4 Dynamic strain histories and the post-mortem specimen and after-impact projectile of Ballistic Test 6: $\left[0^\circ_3/45^\circ_3/90^\circ_3/-45^\circ_3\right]_S$ quasi-isotropic S2 glass-toughened epoxy composite beam impacted at 442 m/s by a 22 caliber copper projectile: (a) Dynamic strains (b) Perspective view (c) Side view (d) Deformed projectile

5.2 Ballistic impact tests on woven hybrid composite panels

Six ballistic impact tests were conducted on each composite type. Among these six tests, at least two of them were full penetration tests. The interval of V_{50} velocity for all panels was roughly estimated using experimental data. The parameters of ballistic impact tests conducted on panel composites are shown in Table 5.2

Table 5.2 Parameters of ballistic impact tests on woven composite panels.

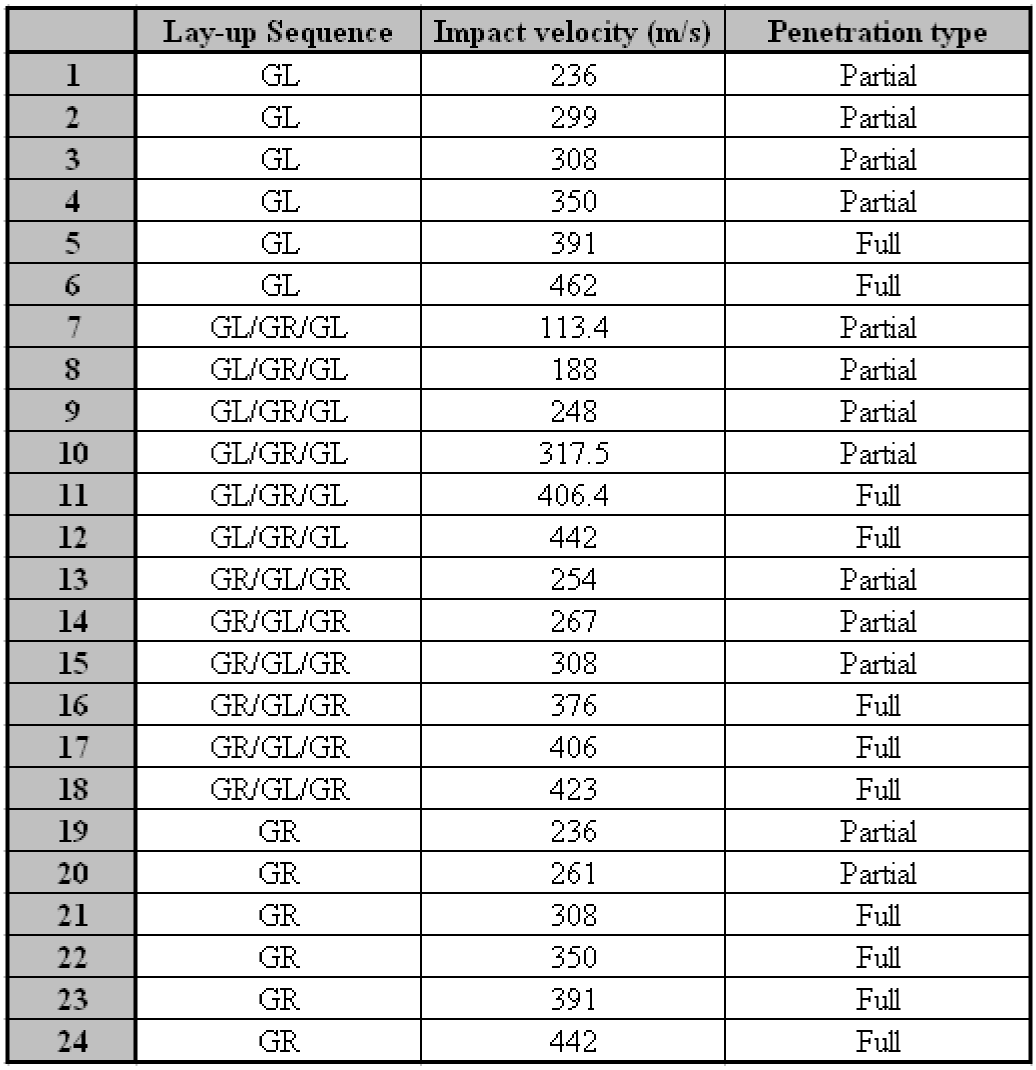

	Lay-up Sequence	Impact velocity (m/s)	Penetration type
1	GL	236	Partial
2	GL	299	Partial
3	GL	308	Partial
4	GL	350	Partial
5	GL	391	Full
6	GL	462	Full
7	GL/GR/GL	113.4	Partial
8	GL/GR/GL	188	Partial
9	GL/GR/GL	248	Partial
10	GL/GR/GL	317.5	Partial
11	GL/GR/GL	406.4	Full
12	GL/GR/GL	442	Full
13	GR/GL/GR	254	Partial
14	GR/GL/GR	267	Partial
15	GR/GL/GR	308	Partial
16	GR/GL/GR	376	Full
17	GR/GL/GR	406	Full
18	GR/GL/GR	423	Full
19	GR	236	Partial
20	GR	261	Partial
21	GR	308	Full
22	GR	350	Full
23	GR	391	Full
24	GR	442	Full

(a) Experimental results

Figure 5.5(a, b, c and d) shows optical pictures of impacted composites. The GL composite exhibited partial penetration during the ballistic impact tests conducted at 236.6, 299, 308 and 350 m/s (Fig.5.5 (a)). The impact velocities 391 and 442 m/s resulted in full penetration of projectile. The length of the vertical and horizontal front surface cracks increased with increasing velocity for partial penetration cases. However increasing velocity resulted in smaller horizontal and vertical cracks for full penetration cases. No back surface splitting occurred for non perforation cases. However, full penetration caused localized back surface splitting at 391 and 462 m/s.

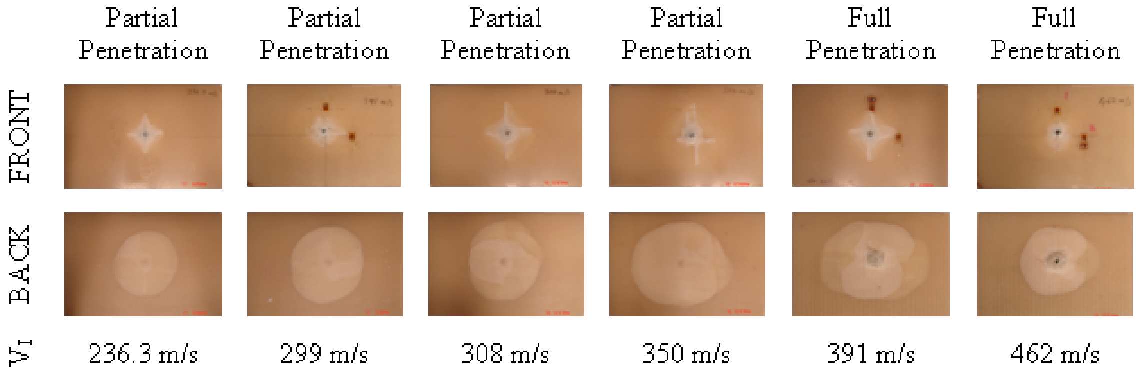

Figure 5.5 (a) Optical pictures of GL composite specimen after impact

During the ballistic impact test of GL/GR/GL composites, while velocities up to 248 m/s resulted in partial penetration, 317.5, 406.4 and 442 m/s impact velocities caused full penetration of projectile (Fig.5.5 (b)). The front surface cracks increased with increasing velocity and were only observed for partial penetration cases. Localized back surface splitting was observed for full penetration cases. On the other hand, the impact velocities 188 and 248 m/s also initiated some back surface splitting.

The second hybrid composite, GR/GL/GR, was partially penetrated during ballistic tests conducted at 254,267 and 308 m/s (Fig.5.5(c)). The remaining three velocities caused full penetration. Back surface splitting was significant especially during ballistic tests at 376, 406 and 423 m/s. The opening created due to impact was wider and the glass fabrics which were used at the inner layers became visible.

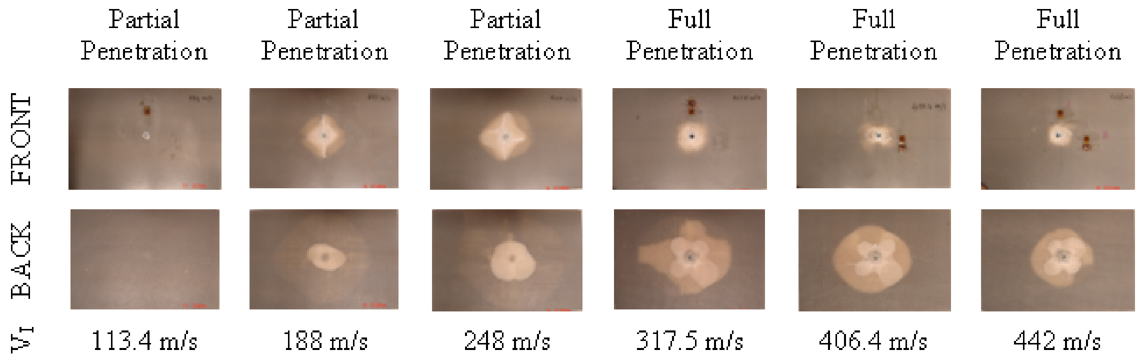

Figure 5.5(b) Optical pictures of GL/GR/GL composite after impact

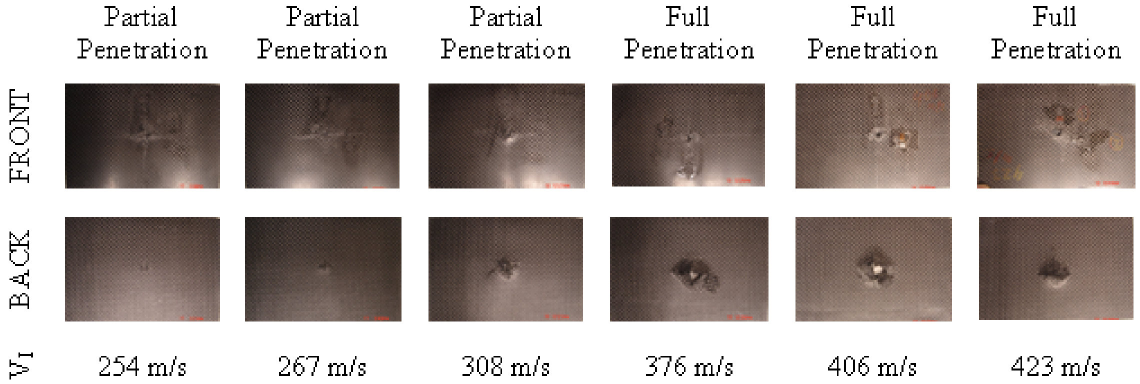

Figure 5.5(c) Optical pictures of GR/GL/GR composite after impact

The four ballistic tests on GR composites exhibited full penetration (Fig.5.5(d)). The only velocities which resulted in partial penetration were 236 m/s and 261 m/s. The horizontal and vertical front surface cracks were only observed for partial penetration cases. The back surface splitting was not as severe as that for GR/GL/GR composites but definitely wider than those seen for GL and GL/GR/GL composites.

(b) Dynamic strains

The ballistic impact event takes place in an extremely short time. Accordingly the frequency of the strain amplifier frequency should be high enough to capture the strains in such a short time. The strain amplifier used in this study has a maximum frequency of 100 KHz. In other words, it was only able to record the strain data for every 10µs.

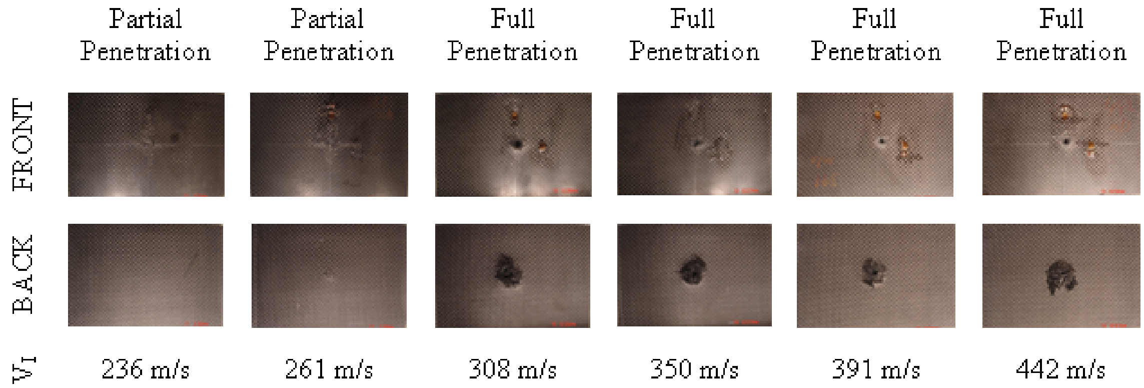

Figure 5.5(d) Optical pictures of GR composite after impact

Assuming that ballistic impact event takes 100µs, the dynamic strain curve from experiment would have captured only 10 data points, resulting in significant undersampling. Thus, the strain curve constructed using these data points can not represent the real response of the composite. The strain measurements obtained are mainly for vibration of impacted composite beam. They are not able to capture the transient response of composite during ballistic impact. Figure 5.6 shows the dynamic strain histories of composites of four lay-up sequences. The velocities in this figure are chosen as close as possible to each other to enable comparison.

The equation for wave speed can be written as:

$c = \sqrt{\frac{E}{\rho}}$ (E is the Young’s modulus and ρ is density of the material).

The wave speed of GR composites would be higher than the wave speed of GL composites due to their mechanical properties (Table 5.3). Knowing that all strain-gages were mounted 25.4 mm away from the impact location at longitudinal and transverse directions, the strain recording obtained during the ballistic impact tests of GR composite should start little quicker. On the other hand, because of the higher stiffness of GR composites, amplitude of strain output should be smaller compared to that of the GL composites.

Table 5.3 Mechanical properties of woven glass and graphite composites

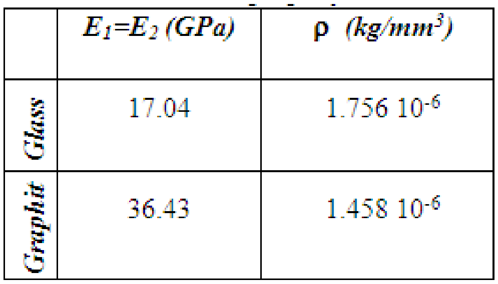

	$E_1=E_2$ (GPa)	ρ (kg/mm³)
Glass	17.04	$1.756\ 10^{-6}$
Graphit	36.43	$1.458\ 10^{-6}$

Figure 5.6 shows the strain histories of four lay-up sequences. It is clear that GR strain measurements started little earlier compared to the strain histories of GL composite. The strain histories of hybrid composites were somewhere between those of GL and GR composites. Comparing the magnitudes of the signals, it is observed that, GL composite had the highest and GR composite had the lowest magnitude. However, while the magnitude of the GR/GL/GR composite was close to that of GR, the magnitude of GL/GR/GL was close to that of GL composite.

(c) Delamination

Figure 5.7 shows the fractographs of sectioned composites after ballistic impact conducted at various velocities. The delamination in GL composite was very localized on the impact side and widened once it moved to the tension side of the composite (5.7(a)). Ballistic impact tests created quite extended delamination in hybrid composites especially at the interface of GL and GR layers (Fig.5.7.b-c). This may be due to greater incompatibility between dissimilar layers. Both hybrid composites delaminated more than non-hybrid composites. However splitting that occurred between hybrid layers were more severe in GL/GR/GL composite (Fig.5.7 (b)) compared to that in GR/GL/GR composite (Fig.5.7(c)).

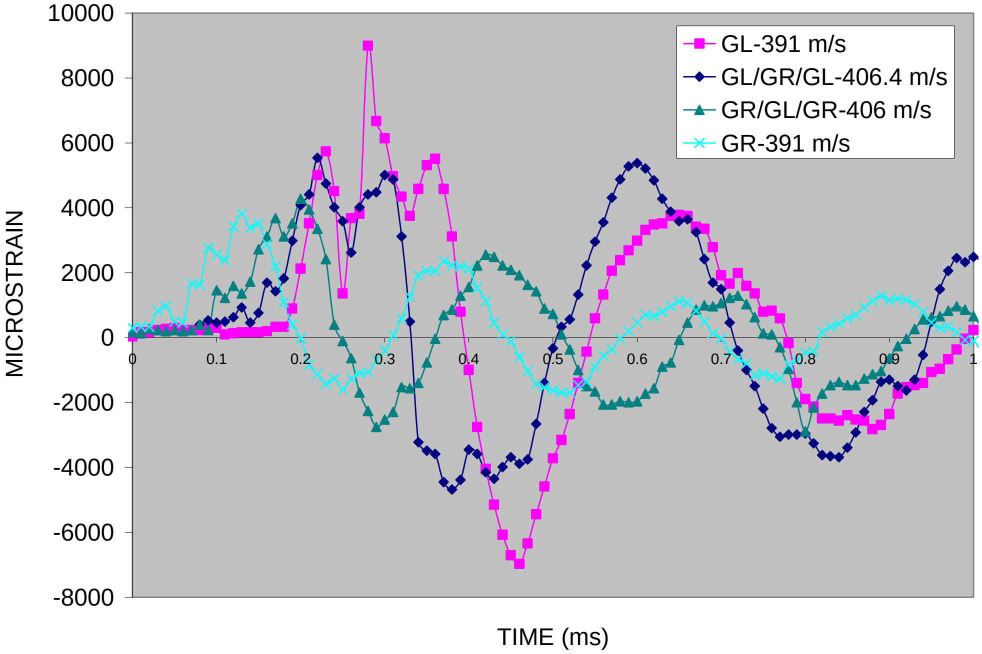

Figure 5.6 Dynamic strain histories of GL (impacted at 391 m/s), GL/GR/GL (impacted at 406.4 m/s), GR/GL/GR (impacted at 406 m/s) and GR (impacted at 391 m/s) composites.

Delamination in GR was much more localized and did not exhibit much spreading on the tension side (Fig.5.7 (d)).

Figure 5.8 shows ultrasonic C-scans of impacted composites. The C-Scans show that hybrid composites delaminated more than non-hybrid composites. Delamination in hybrid composite where GL was used as an outer skin was more pronounced compared to that in the other hybrid composite. All C-Scan images exhibited increased delamination up to the certain velocity and gradual decrease was observed after that critical velocity.

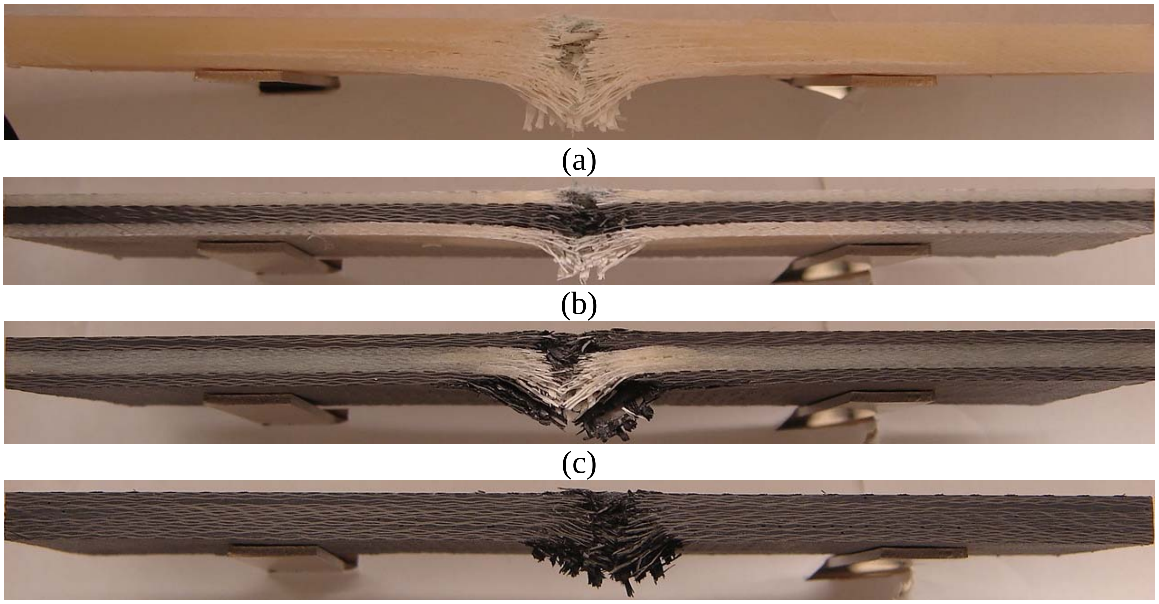

(a)

(b)

(c)

(d)

Figure 5.7 Fractographs of sectioned composites after ballistic impact conducted at various velocities: (a) non-hybrid GL impacted at 391 m/s, (b) hybrid GL/GR/GL impacted at 406.4 m/s, (c) hybrid GR/GL/GR impacted at 406 m/s and (d) non-hybrid GR impacted at 391 m/s

These critical velocities were 350 m/s for GL, 248 m/s GL/GR/GL, 308 m/s for GR/GL/GR and 261 m/s for GR composites. All these caused partial penetration and higher velocities for the same composite caused full penetration. Thus, it can be said that delaminated area increases with increasing velocity for partial penetration cases. However it decreases with increasing velocity for full penetration cases. The C-Scan images themselves suggest the possible range for ballistic limit velocity V_{50}.

(d) Ballistic Limit V_{50} estimation

The classical V_{50} determination requires at least ten ballistic tests having half of them cause partial penetration and the other half cause full penetration. However our approach is using FE analysis to determine V_{50}, the ballistic limit velocity. The experimental data were used to validate the FE models. Once the experimental results were plotted on the same graph (Fig.5.9), the intervals (between dashed lines) of V_{50} were very clear. The interval of GL composite was definitely higher than that for GR composite and the interval of the hybrid composites laid between that of GL and GR composites.

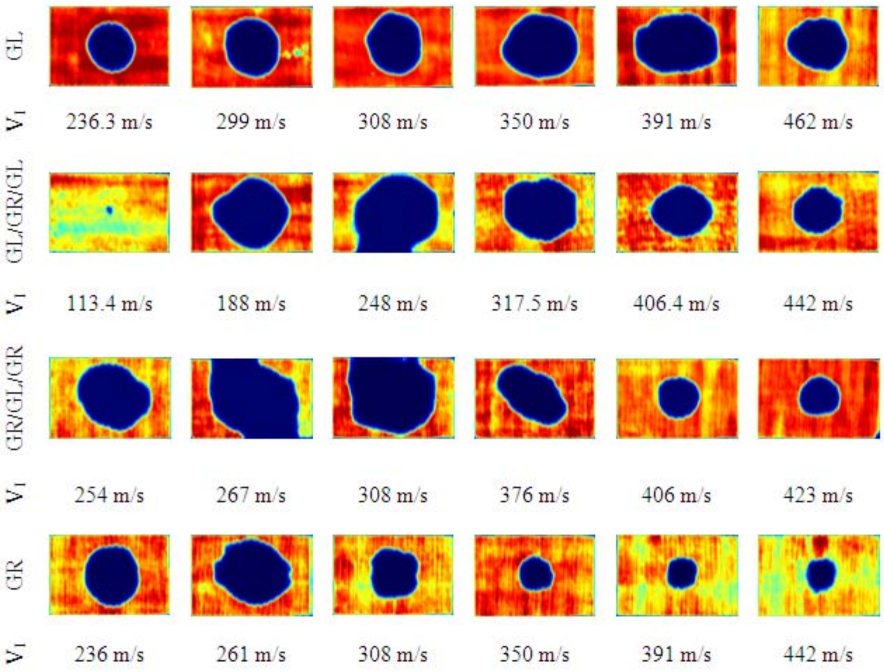

Figure 5.8 Ultrasonic C-scan images of impacted composites

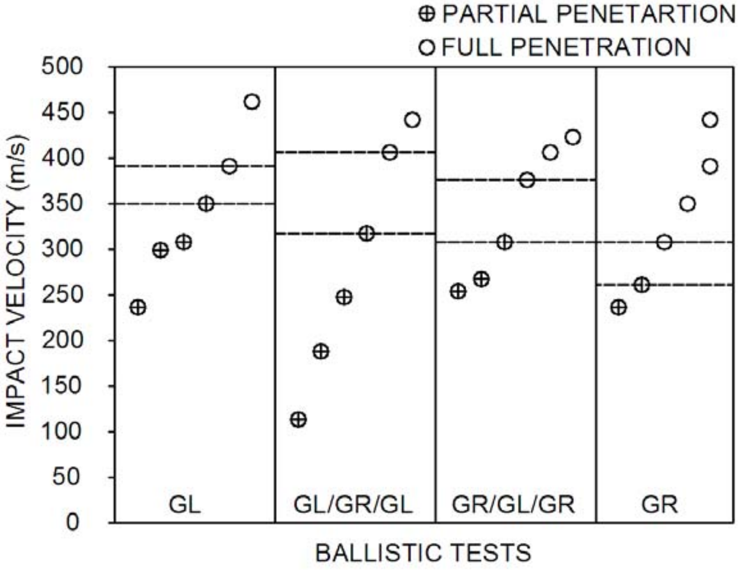

Figure 5.9 Interval of V_{50} for hybrid and non-hybrid composite panels

5.3 Ballistic impact tests on woven composite beams

(a) Experimental results

The parameters of ballistic tests conducted on composite beams are shown in Table 6.4. The number of tests conducted for GL, GL/GR/GL, GR/GL/GR and GR were six, five, five and four respectively. Only one full penetration case for each lay-up type was obtained and interval of the V_{50} was estimated. Due to highly extended delamination in composite beams no ultrasonic C-scan images were taken.

Figure 5.10-5.13 shows the optical pictures of impacted composite beams. The images only show the portion with 25.4 mm width and 50.8 mm length at impact location. The only impact velocity that resulted in full penetration was 442 m/s (Fig.5.10). During the ballistic impact test conducted at 363 m/s and 390 m/s, the projectile got stuck into the composite beams.

None of the partial penetration cases exhibited back surface splitting. The fabrics at the tension side were completely broken in the transverse direction during the ballistic test conducted at 442 m/s. Figure 5.11 shows the optical pictures of GL/GR/GL composites impacted at various velocities. Figure 5.12 shows the impacted GR/GL/GR hybrid specimens. The impact velocities up to 308 m/s resulted in partial penetration. Remaining two impact velocities created full penetration. The projectile passed through the GR composite beam during the ballistic impact at 236 m/s (Fig.5.13). Without creating a hole, because it was broken into two pieces due to bending and that allowed the projectile to pass through. Due to brittle nature of graphite, the GR composite beam does not allow much deflection. Significant back surface splitting occurred during the ballistic impact test conducted at 230 m/s but no full penetration was observed.

Table 5.4 Parameters of ballistic impact tests conducted on woven composite beams

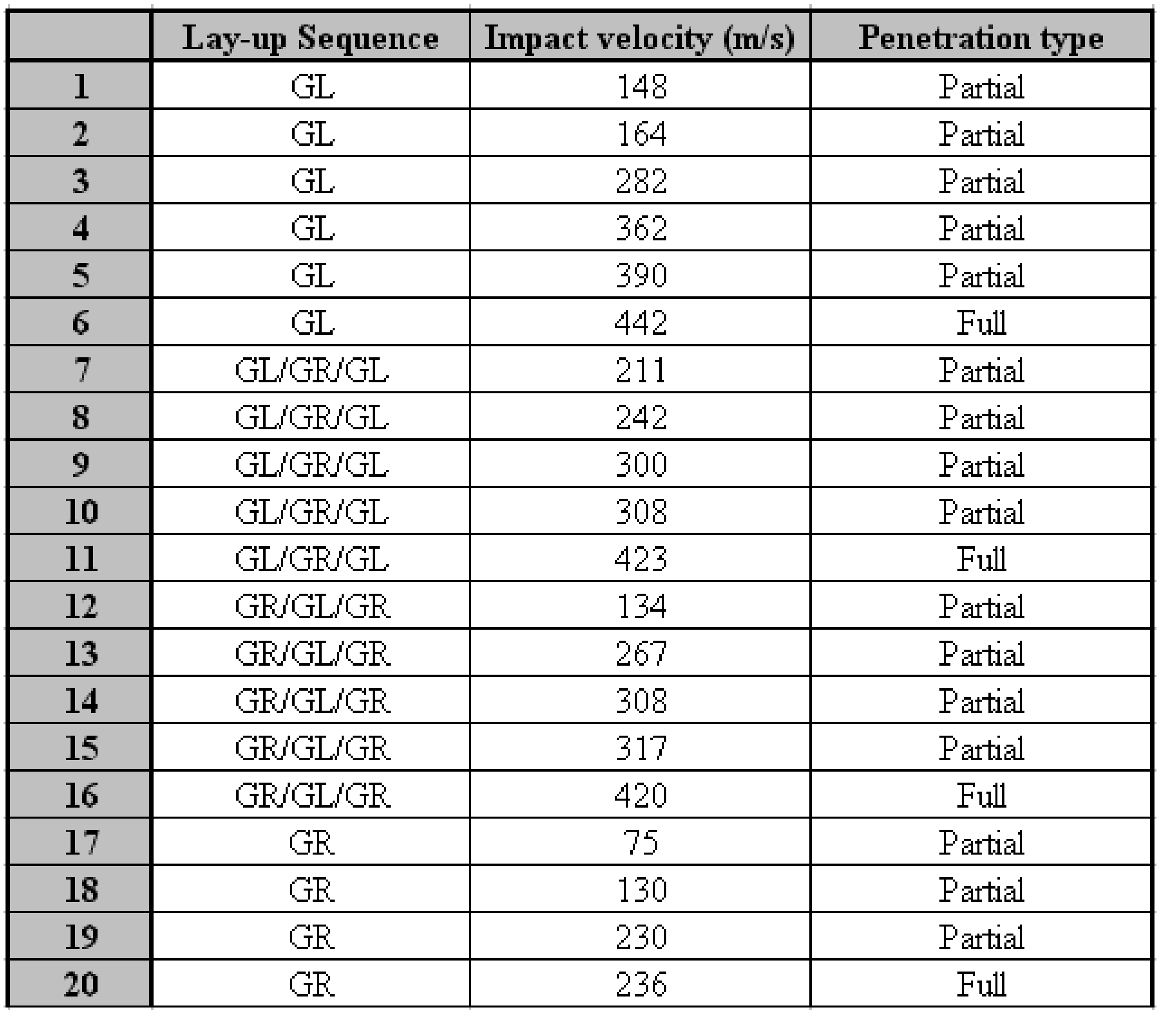

	Lay-up Sequence	Impact velocity (m/s)	Penetration type
1	GL	148	Partial
2	GL	164	Partial
3	GL	282	Partial
4	GL	362	Partial
5	GL	390	Partial
6	GL	442	Full
7	GL/GR/GL	211	Partial
8	GL/GR/GL	242	Partial
9	GL/GR/GL	300	Partial
10	GL/GR/GL	308	Partial
11	GL/GR/GL	423	Full
12	GR/GL/GR	134	Partial
13	GR/GL/GR	267	Partial
14	GR/GL/GR	308	Partial
15	GR/GL/GR	317	Partial
16	GR/GL/GR	420	Full
17	GR	75	Partial
18	GR	130	Partial
19	GR	230	Partial
20	GR	236	Full

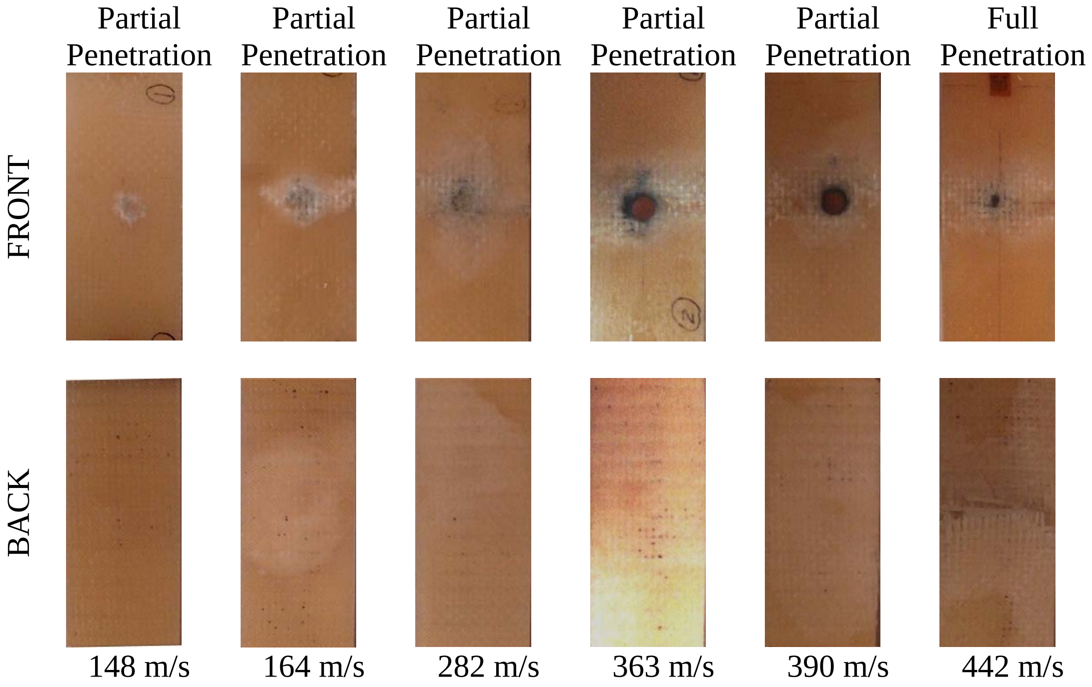

Figure 5.10 Optical pictures of GL composite beams after impact

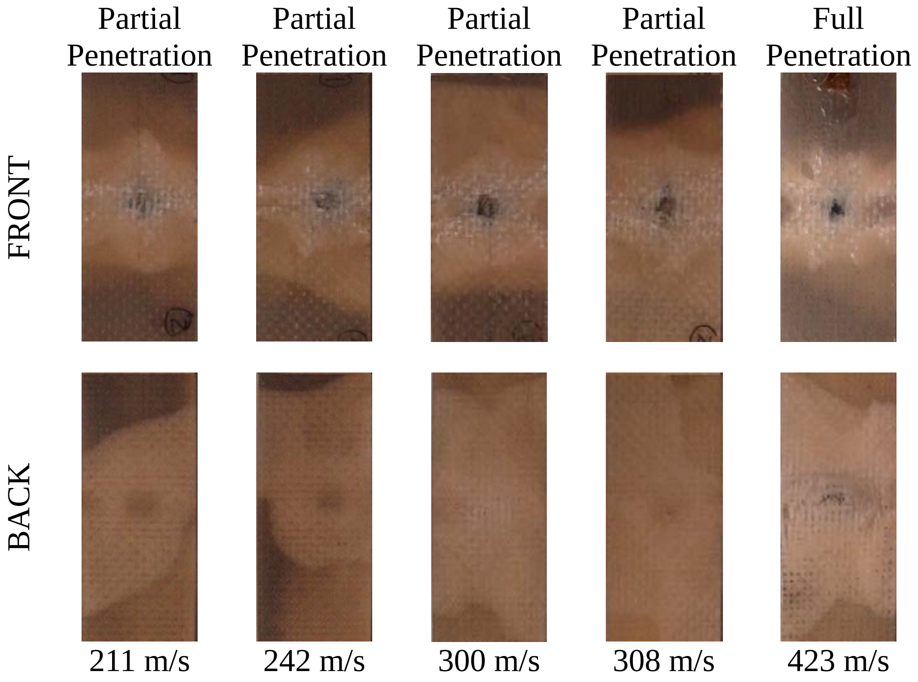

Figure 5.11 Optical pictures of GL/GR/GL composite beams after impact

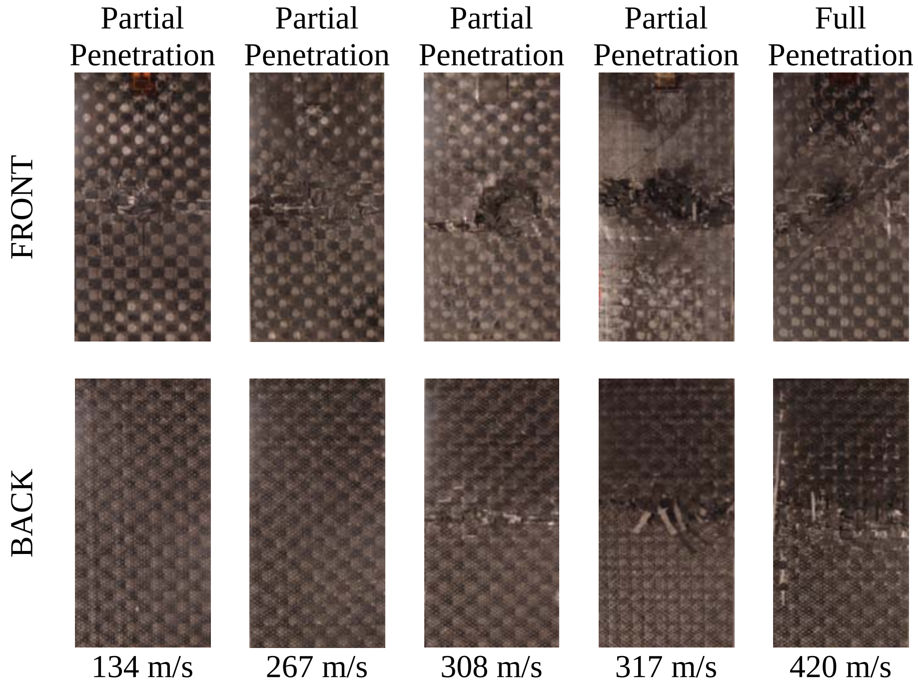

Figure 5.12 Optical pictures of GR/GL/GR composite beams after impact

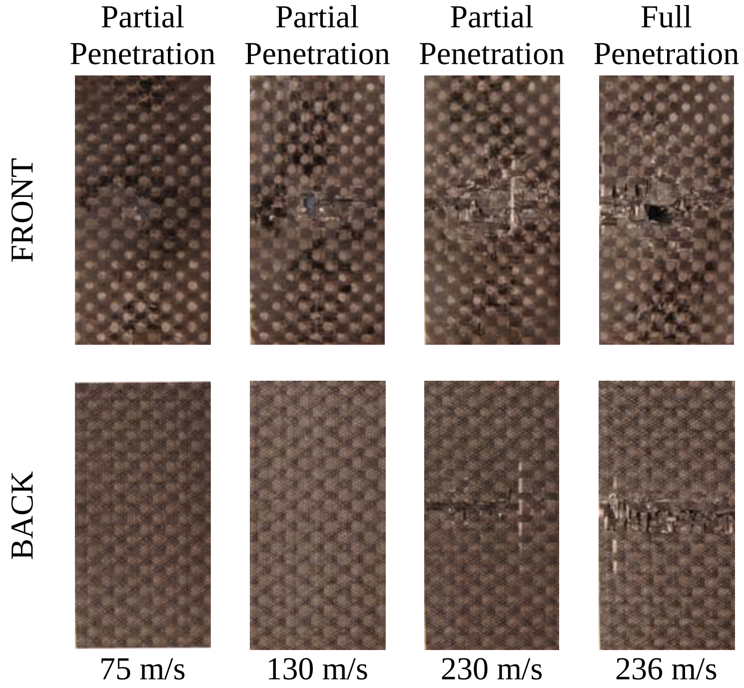

Figure 5.13 Optical pictures of GR composite beams after impact

(b) Delamination

Figure 5.14 shows the fractographs of longitudinally sectioned impacted composites. Two impacted composites, one partially and one fully penetrated, were considered for each lay-up sequence. Delamination of GL composites when partially penetrated was concentrated at both impact and tension sides. However fully penetrated composites mostly delaminated at the tension side. The delamination between dissimilar layers in hybrid composites was significant. The graphite fabrics in both hybrid composites were cut into half in the transverse direction due to ballistic impact. The impact velocity 236 m/s created a transverse cut in GR composite and localized delamination was observed. The impact velocity of 230 m/s initiated a partial transverse cut and projectile was not able to pass through the composites. Localized delamination was also observed for this case. When delaminations of composite beams were compared, it was observed that GR composites delaminated less than GL and hybrid composites. Delamination of the GL composites was more than that of GR composites and less than that of hybrid composites. The hybrid composites were vulnerable to delamination especially between dissimilar layers.

(c) Ballistic Limit V_{50} Estimation

Figure 5.15 shows the interval of V_{50} for hybrid and non-hybrid composite beams. The interval of V_{50} for GL, GL/GR/GL, GR/GL/GR and GR composites were 390-442 m/s, 308-423 m/s, 317-420 m/s and 230-236 m/s respectively. While the ballistic resistance of GL was highest, that of GR was lowest. The ballistic resistance of hybrid composites was somewhere between the resistance of GL and GR composite beam.

V_I=390 m/s V_I=442m/s V_I=308m/s V_I=423m/s V_I=317m/s V_I=420m/s V_I=230m/s V_I=236m/s

(a) (b) (c) (d)

Figure 5.14 Fractographs of sectioned composites after ballistic impact conducted at various velocities: (a) non-hybrid GL impacted at 391 m/s, (b) hybrid GL/GR/GL impacted at 406.4 m/s, (c) hybrid GR/GL/GR impacted at 406 m/s and (d) non-hybrid GR impacted at 391 m/s

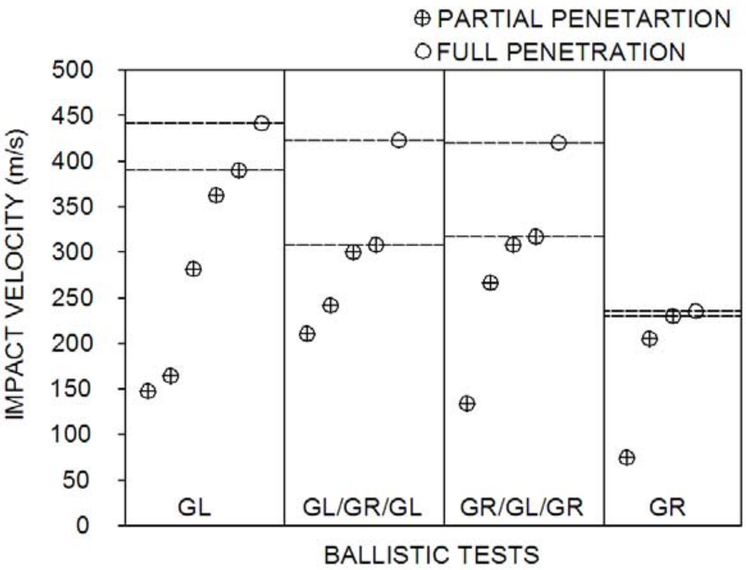

Figure 5.15 Interval of V_{50} for hybrid and non-hybrid composite beams

5.4 CONCLUSIONS OF BALLISTIC IMPACT STUDIES

a) During ballistic impact tests delamination, matrix failure, fiber breakage and projectile deformation were observed

b) Hybrid composites delaminated more than non-hybrid composite and delamination between dissimilar layers was significant

c) Delamination increased with increasing velocity for partial penetration cases and it decreased with increasing velocity for full penetration cases.

d) The interval of the ballistic limit velocity can be estimated using ballistic tests and Ultrasonic C-Scans.

6. FINITE ELEMENT ANALYSIS

The finite element code LS-DYNA was used to simulate low velocity and ballistic impact response of composites. The finite element models were validated using experimental data. The finite element models for ballistic tests were validated using experimentally obtained strain-time histories and post-impact damage patterns. The force time histories and energy time histories were also used for validating finite element models of low-velocity impact tests. Once the finite element model was validated, it was used to simulate different cases. The composite layers, impactors and projectiles were modeled using 8-node solid element. The only one quarter of the geometry was modeled for most cases because symmetry.

6.1 Finite element models

6.1.1 Material Models

(a) MAT_COMPOSITE_DAMAGE (MAT_022): It is also called the Chang-Chang composite damage model. This model is for an orthotropic material where optional brittle failure for composites can be defined [20-21]. Three failure criteria are possible in this model:

(1) Matrix cracking:

$$\left(\frac{\sigma_2}{S_2}\right)^2 + \left(\frac{\tau_{12}}{S_{12}}\right)^2 \geq 1 \qquad (6.1)$$

where σ_2 and S_2 are the tensile stress and the associated tensile strength in the transverse direction whereas τ_{12} and S_{12} are the in-plane shear stress and the associated shear strength between fibers and matrix. Once this type of failure occurs, the material constants E_2 (Young's modulus in the transverse direction), G_{12} (in-plane shear modulus in the 1-2 plane), ν_{12} and ν_{21} (generalized Poisson's ratios in the 1-2 plane) are set to zero.

(2) Fiber breakage:

$$\left(\frac{\sigma_1}{S_1}\right)^2+\left(\frac{\tau_{12}}{S_{12}}\right)^2\geq 1 \qquad (6.2)$$

where σ_1 and S_1 are the tensile stress and the associated tensile strength in the longitudinal direction whereas τ_{12} and S_{12} are again the in-plane shear stress and the associated shear strength between fibers and matrix. After fiber breakage, E_1 (Young's modulus in the longitudinal direction), E_2, G_{12}, ν_{12} and ν_{21} are all set to zero.

(3) Compressive failure:

$$\left(\frac{\sigma_2}{2S_{12}}\right)^2+\left(\frac{\tau_{12}}{S_{12}}\right)^2+\left[\left(\frac{C_2}{2S_{12}}\right)^2-1\right]\frac{\sigma_2}{C_2}\geq 1 \qquad (6.3)$$

where C_2 is the transverse compressive strength. When this type of failure occurs, the material constants E_2, ν_{12} and ν_{21} are all set to zero.

This material was only used for simulating the ballistic tests conducted on S2-glass fiber/toughened composites.

(b) MAT_USER_DEFINED_MATERIAL-MODELS (MAT_43): The material models that can be used for composites such as Chang-Chang model (MAT_22) and Composite MSC (MAT_161, MAT_162) only require inputting nine elastic constant for orthotropic materials. However our experimental curves exhibited nonlinear behavior for woven glass and woven graphite composites. Using only the initial slope of the curves may not represent the exact behavior of nonlinear orthotropic material. There is also nonlinear orthotropic material (MAT_40), that allows inputting experimental curves but this model is not recommended by LS-DYNA due to due to its instability. On the other hand user-defined material subroutine can be incorporated into LS-DYNA. The user-defined subroutines can be in two formats: scalar or vectorized. In case of vectorized subroutine, a group of elements is processed at a time. However in case of scalar subroutine, only one element at a time is processed by the subroutine. The failure criteria and erosion of the elements can also be programmed in the subroutine. The MAT_ADD_EROSION option can also be used without including erosion in the code. In our model, the curves obtained from tensile tests (Fig.3.10) were entered into LS-DYNA. When the stresses in all directions reach their respective critical values, which were defined by the entered experimental curves, that element fails and is eroded from further calculation. The vectorized subroutine was used and erosion was introduced using the MAT_ADD_EROSION option. The failure criteria used in our proposed model are as follows:

Longitudinal failure: $\sigma_1 \geq S_1$ (in tension) $|\sigma_1| \geq C_1$ (in compression) (6.4)

where σ_1 and S_1 are the tensile stress and tensile strength in longitudinal (fiber) direction. After longitudinal failure, E_1 (Young's modulus in the longitudinal direction), ν_{12}, ν_{21}, ν_{13} and ν_{31} (Poisson's ratios in the 1-2 and 1-3 planes) are all set to zero.

Transverse failure: $\sigma_2 \geq S_2$ (in tension) $|\sigma_2| \geq C_2$ (in compression) (6.5) where σ_2, S_2 and C_2 are the tensile stress, tensile strength and compressive strength in transverse (matrix) direction. After transverse failure, E_2 (Young's modulus in the transverse direction), ν_{12}, $\nu_{21,}\nu_{23}$ and ν_{32} (Poisson's ratios in the 1-2 and 2-3 planes) are all set to zero.

Out of plane normal failure: $\sigma_3 \geq S_3$ (in tension) $|\sigma_3| \geq C_3$ (in compression) (6.6)

where σ_3, S_3 and C_3 are the tensile stress, tensile strength and compressive strength in transverse (matrix) direction. After transverse failure, E_2 (Young's modulus in the transverse direction), ν_{13}, $\nu_{31,}\nu_{23}$ and ν_{32} (Poisson's ratios in the 1-2 and 2-3 planes) are all set to zero.

In-plane shear failure: $|\tau_{12}| \geq S_{12}$ (6.7)

where τ_{12} and S_{12} are the in-plane shear stress and the associated shear strength. The shear strength was obtained using the relation: After in-plane failure, G_{12} (in-plane shear modulus in the 1-2 plane), ν_{12}, ν_{21} (Poisson's ratios in the 1-2 plane) are all set to zero.

Out-plane shear failure: $|\tau_{13}| \geq S_{13}$ and $|\tau_{23}| \geq S_{23}$ (6.8)

where τ_{13}, τ_{23} and S_{13}, S_{23} are the out-plane shear stresses and strengths, respectively. After out-of-plane failure, G_{13}, G_{23} (out-plane shear modulus in the 1-3 and 2-3 plane), $\nu_{13,}$ ν_{31}, ν_{23} and ν_{32} (Poisson's ratios in the 1-3 and 2-3 planes) are all set to zero.

(c) MAT_PLASTIC_KINEMATIC (MAT_003): This model is used for isotropic and kinematic hardening plasticity with the option of including rate effects. Here l_o and l are undeformed and deformed lengths of uniaxial tension specimen and E_t is the slope of the second arm of the bilinear stress strain curve (Fig.6.1). This material was used for the 22 caliber copper bullet.

(d) Rigid Material

The rigid material provides a convenient way of turning one or more parts into a rigid body. Elements which are rigid are bypassed in the element processing and no storage is allocated for storing history variables, thus rigid material is very cost efficient. Young's modulus, *E,* Poisson ratio ν are used for determining the sliding interface parameters if the rigid body interacts in a contact definition. This material was used for impactors of low velocity impact tests.

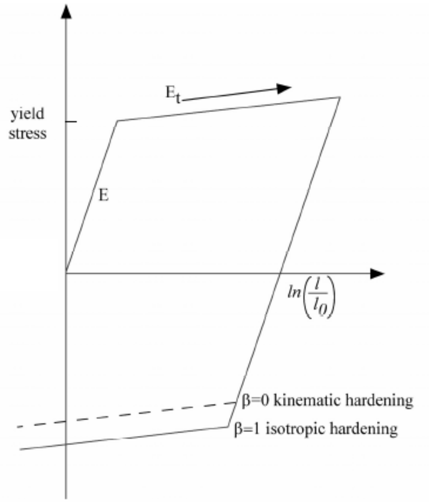

Figure 6.1 Elastic-plastic behavior with kinematic and isotropic hardening. (Picture is taken from LS-DYNA theoretical manual [12].

6.1.2 Contact and delamination Model

Delamination between the composite layers is governed by the criterion:

$$\left[\frac{\max\left(0,\sigma_n\right)}{NFLS}\right]^2+\left(\frac{\sigma_s}{SFLS}\right)^2\geq 1 \qquad (6.9)$$

where σ_n and σ_s are normal and shear stresses acting on the layer interface, respectively, while *NFLS* and *SFLS* are normal and shear strengths of the layer interface, respectively. This criterion was incorporated into LS-DYNA through

CONTACT_AUTOMATIC_SURFACE_TO_SURFACE_TIEBREAK

Additionally, ERODING_SURFACE_TO_SURFACE contact model was used between the impactor and the composite. This model allows elements to be eroded when certain failure criteria are met. In this study strain-based failure criterion was used for element erosion; that is, when $\varepsilon \geq \varepsilon_{\text{erosion}}$, the element was eroded and removed from calculation. The contact and delamination models as well as the erosion option were used for all composites.

6.2 Finite element simulations for low-velocity impact tests

6.2.1 Effect of impact energy levels on the low velocity impact response of woven composites

Figure 6.2 shows the LS-DYNA finite element meshes used simulating drop-weight impact onto (a) a woven GL composite (b) a woven hybrid GL/GR/GL composite (c) a woven hybrid GR/GL/GR composite and (d) a woven GR composite. 18 layers for GL, 14 layers for GR and 16 layers for hybrid composites were created. Fine mesh around the center and course mesh away from center was used.

(a) Comparison of Force-Time histories

Since Dynatup 930-I data acquisition system can only measure force (the resistive force of the specimen) vs. time and initial impact velocity (just prior to impact) directly, experimental force-time histories would be the most valuable data to obtain for comparisons. Force-time histories were compared for the impact tests conducted at 3.9m/s velocity. Comparison of FEM and experimental force-time histories exhibited good agreement (Fig.6.3).

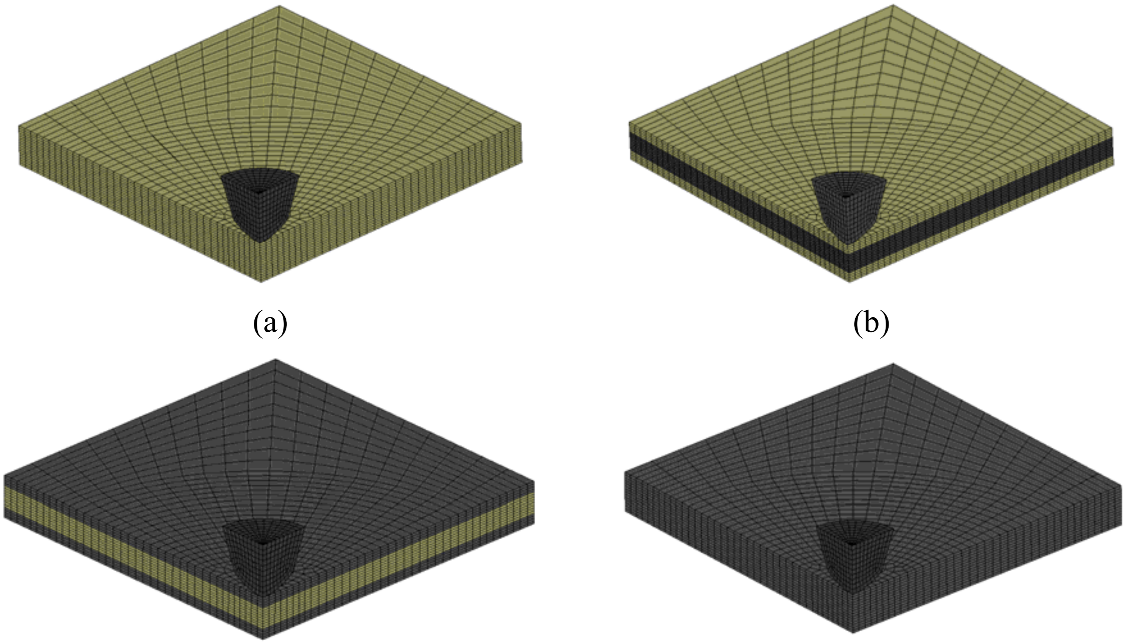
(a) (b)

(c) (d)

Figure 6.2 Finite element simulation models. (a) Drop-weight impact model for the GL specimen (b) Drop-weight impact model for the GL/GR/GL specimen (c) Drop-weight impact model for the GR/GL/GR specimen d) Drop-weight impact model for the GR specimen

FEM force-time histories of GL composite showed little late damage initiation and bigger contact compared to experimental result (Fig.6.3 (a)). FEM calculations produced somewhat longer contact duration for hybrid composites (Fig.6.3 (b-c)). Predicted force-time histories of GR composites showed slight mismatch especially during the period following the sudden drop (Fig.6.3 (d)). Predicted contact duration of this test was also smaller than the experimental one.

(b) Comparison of Energy-Time histories

Dynatup 930-I data acquisition system calculates the total energy of impactor/specimen system at time t using the equation

$$E(t) = K(t) + V(t) + E_a(t) = K(0) \qquad (6.10)$$

where *E(t)* is the total energy of the impactor /specimen system at time t, *K(t)*, kinetic energy of the impactor at time t, *V(t),* potential energy of the impactor at time t, and *E_a(t),* the energy absorbed by the specimen at time t. $K(0) = \frac{1}{2}mv_i^2$ and the potential energy can be neglected, since the displacement is small. Therefore the energy absorbed by specimen can be computed as follows:

$$E_a(t) = K(0) - K(t) = \frac{1}{2}m\{v_i^2 - [v(t)]^2\} \qquad (6.1)$$

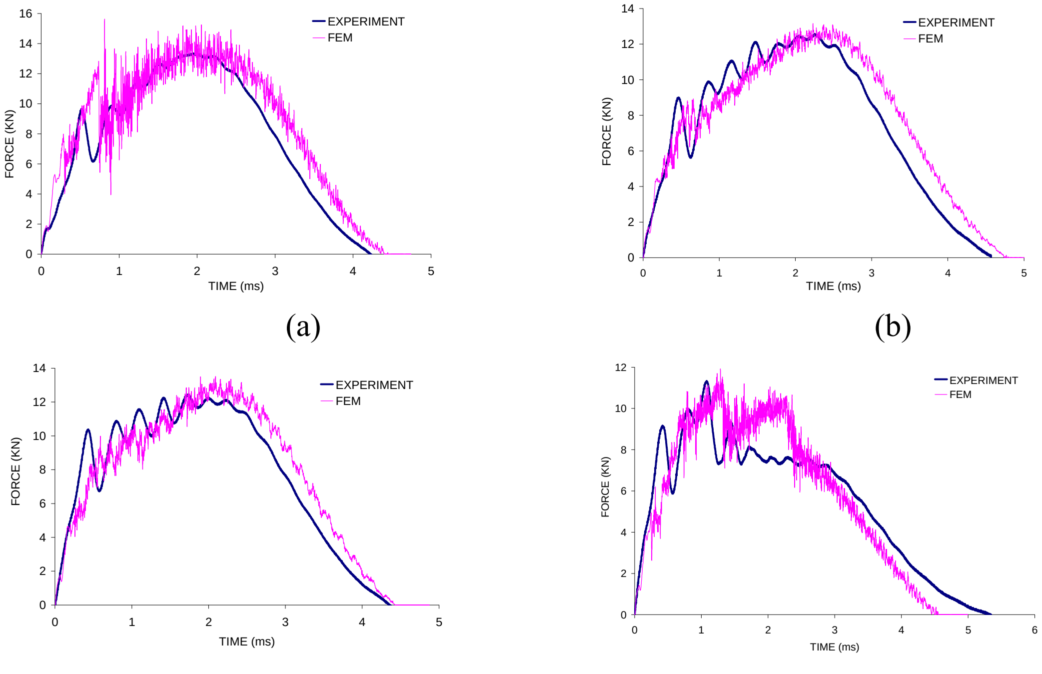

(a) (b)

(c) (d)

Figure 6.3 Comparison of FEM and experimental force-time histories for (a) GL,(b) GL/GR/GL, (c) GR/GL/GR, (d) GR composite plates impacted at 3.9 m/s.

where v_i is the impact velocity measured by photodiodes and $v(t)$ is the velocity of the impactor at time t. On the other hand, LS-DYNA calculates the internal energy of each composite layer. Figure 6.4(a) shows internal energy of the sixteen layers. Once these internal energies of each composite layer are summed, the absorbed energy histories of GL/GR/GL composite impacted at 4.4 m/s can be determined. Figure 6.4(b) shows that the experimental and FEM calculated energy time histories are in good agreement.

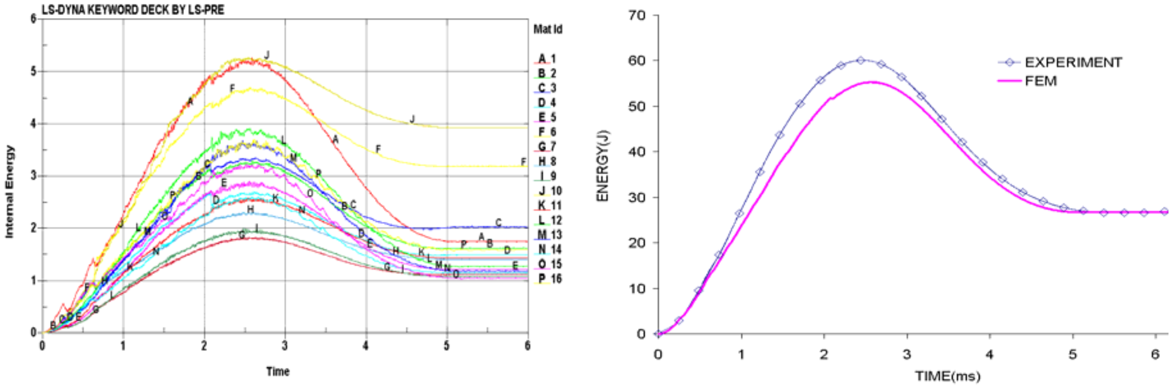

(a) (b)

Figure 6.4 (a) FEM calculated internal energy of laminates
(b) Comparison of energy time histories of drop impact test for
GL/GR/GL conducted at 4.4 m/s

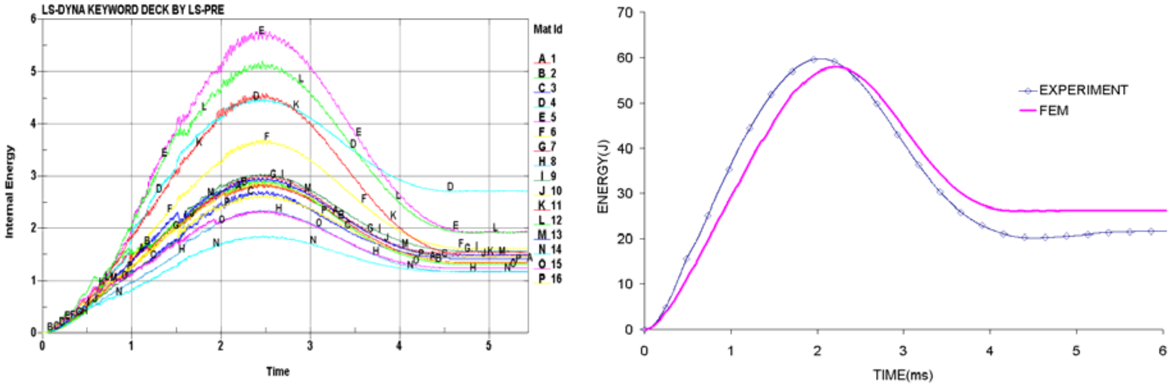

(a) (b)

Figure 6.5 (a) FEM calculated internal energies of each composite layer
(b) Comparison of energy time histories of drop impact
tests for GR/GL/GR conducted at 4.4 m/s

Figure 6.5(a) shows internal energy histories of layers of GR/GL/GR impacted at 4.4 m/s. Comparison of FEM calculated and experimental absorbed energy histories exhibited slight mismatch. FEM predicted absorbed energy history showed delays and predicted greater final absorbed energy (Fig. 6.5(b)).

(c) Comparison of Strain-Time histories

The experimental curves of strain were smoother than the FEM results and exhibited time delays. This can be explained with the fact that experimental impact force and strain measurements were obtained through a load cell and strain gage amplifiers, where actual readings might have been filtered. Figure 6.6(a) shows strain time histories of GL/GR/GL composite impacted at 4.8 m/s. SG-1 and SG-2 in these figures represent the strain-time histories captured by strain-gages mounted at location 1 and location 2 respectively. FEM calculated strain outputs are in agreement with experimental strains. Duration of the strain recording both from experiment and FEM calculations was around 5ms. FEM results successfully captured sudden strain decrease for SG-1 at 1.5 ms. The nonlinear strain increase for SG-2 was also successfully simulated by the FEM model. Slight magnitude mismatches between experimental and FEM results for both locations were also evident.

Figure 6.6(b) shows strain time histories of GR/GL/GR composite impacted at 4.8 m/s. FEM calculated strains are in agreement with the experimental results. While predicted strain for SG-2 location was almost the same as the experimental one, predicted strain for SG-1 location did not successfully capture the initial portion of the experimental data.

(d) Comparison of post-impact damage patterns

Post impact damage pattern comparisons were made for GR and GL/GR/GR/GL composites. Impacted specimens were cut into half at impact location. Even though just one quarter of the composite was modeled for FEM calculations, half of the composite is shown for comparison. During the impact tests conducted on GR composite, rebound was observed at impact velocities of 3.9 m/s and 4.4 m/s. Perforation was seen at 6.3 m/s impact velocity and no perforation, no rebound occurred during the impact test at 4.8 m/s. FEM simulations predicted these behavior very accurately (Fig.6.7(a)). Due to the erosion option used in FEM calculations, element was eroded and removed from calculations once failure criterion was met. However during experiment, damaged material still was in place after impact event.

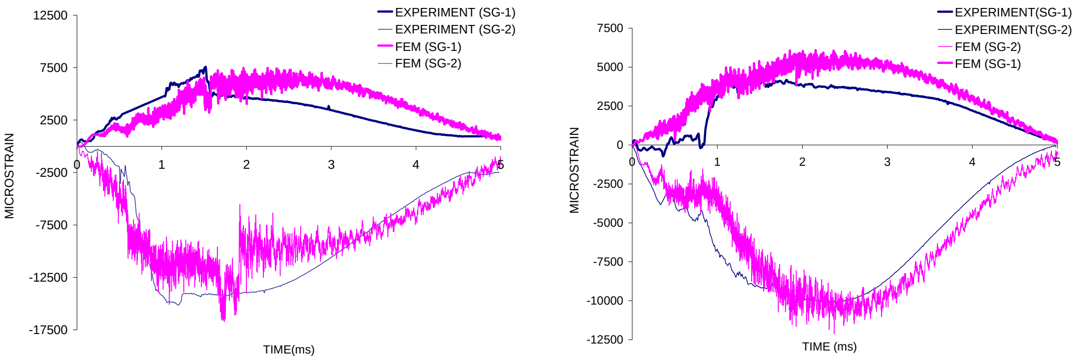

(a) (b)

Figure 6.6 Comparison of dynamic strain histories of (a) GR/GL/GL/GR and (b) GL/GR/GR/GL composite plates impacted at 4.8 m/s.

Figure 6.7(b) shows damage pattern comparisons for GL/GR/GL composite. The first three impacts did not create significant damage in the hybrid composite. Impact tests conducted at 6.3 m/s, created damage. FEM results also showed no significant damage during the first three and some damage for the last experiment. Optical pictures of impacted specimens showed delamination especially between dissimilar layers. FEM model successfully predicted delamination for all experiments.

	EXPERIMENT	FEM
(1)		
(2)		
(3)		
(4)		

Figure 6.7 (a) Comparison of post impact damage patterns of FEM and experimental results for drop-weight tests where GR specimen was impacted at (1) 3.9 m/s, (2) 4.4 m/s (3) 4.8 m/s and (4) 6.3 m/s using 16mm hemispherical impactor.

	EXPERIMENT	FEM
(1)		
(2)		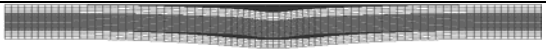
(3)	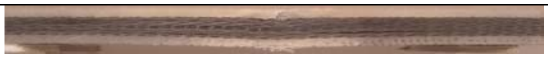	
(4)		

Figure 6.7 (b) Comparison of post impact damage patterns of FEM and experimental results for drop-weight tests where GL/GR/GL specimen impacted at (1) 3.9 m/s, (2) 4.4 m/s (3) 4.8 m/s and (4) 6.3 m/s using 16mm hemispherical impactor.

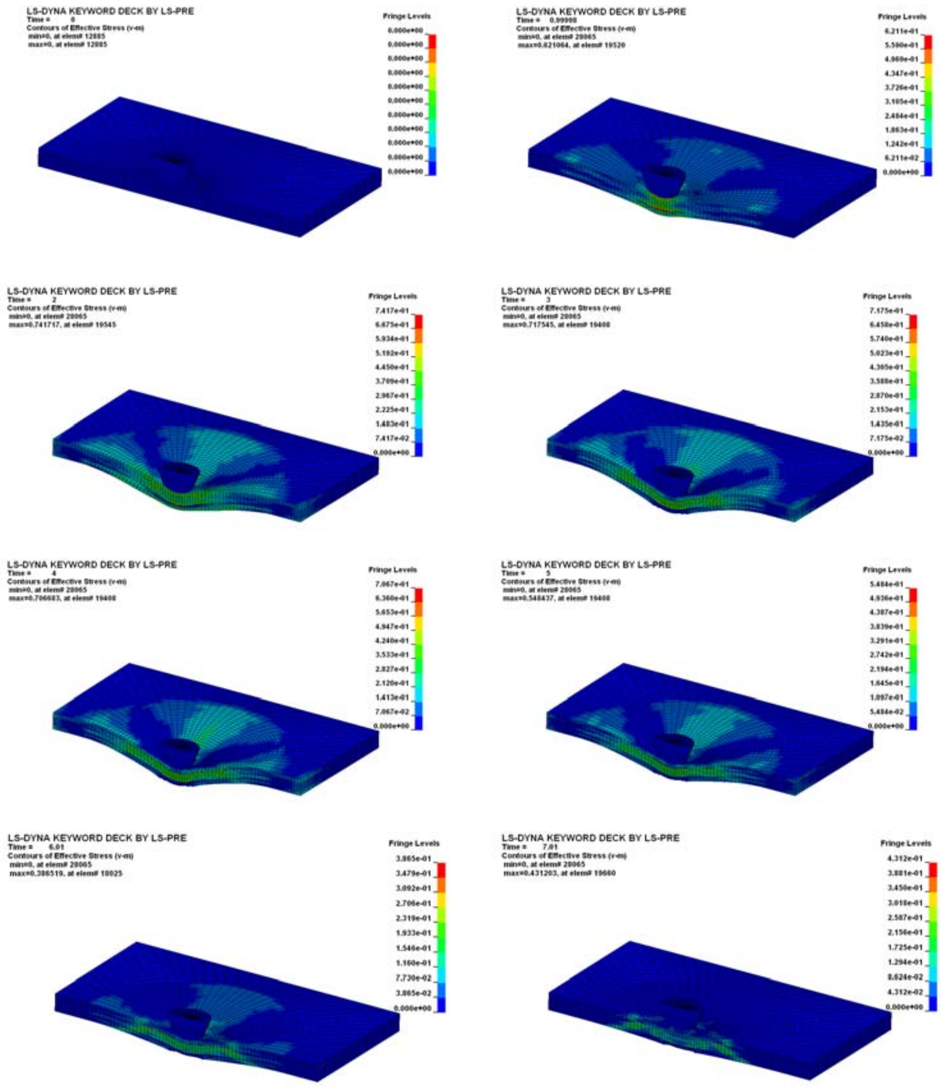

Figure 6.8 Damage progression and stress counters of FEM simulation for hybrid woven GR/GL/GR composite plate impacted at 4.8 m/s. (Time interval between each plot is 1ms)

Figure 6.8 shows damage progression and stress counters of FEM simulation for hybrid woven GR/GL/GL/GR composite plate impacted at 4.8 m/s.

(e) Effect of glass fabric thickness on the low velocity impact response of hybrid composites

It is known that graphite reinforced composites are attractive for aerospace applications because of their light weight, but it is also a reality that they are vulnerable to impact. One of the goals in this study was to see the effect of hybridization on the impact performance of graphite reinforced composites. The GL/GR/GL composite that was used during the experimental study had 1.5875 mm glass fabrics reinforced layers on each side and 3.175 mm graphite fabrics as inner layers. The experimental results showed that using glass fabrics as outer layer improved the impact performance of graphite composites. However one of the major concerns in aerospace application is weight and using glass fabrics will definitely increase the weight of the composite. Can the performance of the graphite reinforced composite be improved without increasing the weight too much? To answer this question, experiments have to be conducted on GL/GR/GL composites with various lay-up sequences. Another approach can be predicting the results for various geometry using validated FEM model without going through costly experiments. As shown above force, strain, absorbed energy histories and damage patterns obtained from experiments and FEM predictions were in very good agreement. Once FEM model is validated, it can then be employed in engineering design. Therefore three more FEM models were created for GL/GR/GL composites. The models had 0.396875, 0.79375 and 1.190625 mm glass fabrics as outer layer respectively. The model with 1.5875 mm glass fabrics had already been created for validation purposes. Figure 6.9 shows the new FEM models for GL/GR/GL (b, c, d) composites and also previously created GL/GR/GL (e), GR (a), GL (f) composites and their weight. As it is clear from Figure 6.9, adding glass fabrics increases the weight. The response of the GL/GR/GL composites with various lay-up sequences were predicted using FEM models. Figure 6.10 shows FEM predicted force-time histories of GR and GL/GR/GL composites of various thicknesses. Adding glass fabrics improved the performance of the composite. Predicted force-time histories of GR composites impacted at 3.9 m/s indicated sudden drops that represent damage created in the composite following the linear increase

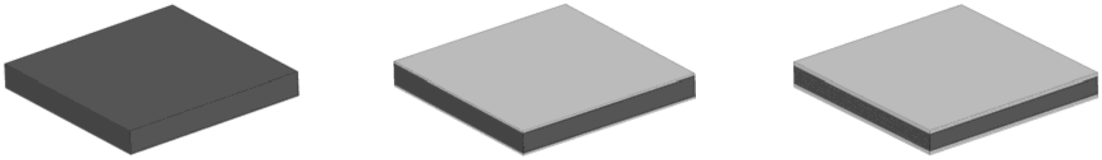

(a) $GR_{6.35mm}$ Weight=95.585gr

(b)$GL_{0.397mm}/GR_{5.55mm}/GL_{0.397mm}$ Weight=98.077gr

(c)$GL_{0.794mm}/GR_{4.76mm}/GL_{0.794mm}$ Weight=100.567gr

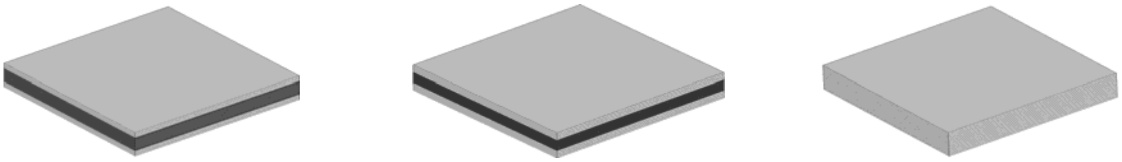

(d)$GL_{1.19mm}/GR_{3.97mm}/GL_{1.19mm}$ Weight=103.062gr

(e)$GL_{1.587mm}/GR_{3.17mm}/GL_{1.587mm}$ Weight=105.555gr

(f)$GL_{6.35mm}$ Weight=115.524gr

Figure 6.9 FEM models for GR (a), GL (f) and GL/GR/GL (b, c, d and e) composites and their weight

One layer of glass fabrics delayed the damage but adding 2, 3 and 4 layers of glass fabrics prevented the damage. The maximum force sustained by the composite slightly decreased by adding more glass fabrics. GL/GR/GL composite with one outer layer of glass fabrics produced almost the same contact duration as GR composite. All remaining GL/GR/GL composites produced around 5ms contact duration. Predicted force time histories of GR composite impacted at 6.3 m/s showed sudden drops at around 1ms (Fig.6.10(b)). Experimental force-time histories of the same test also showed similar behaviors (Fig.4.10) due to perforation observed during this experiment. Adding more layers of glass onto the GR composite reduced the damage and perforation was prevented. GL/GR/GL composites with one and two layers of glass fabrics produced around 9 ms contact duration. Remaining composites produced around 6 ms contact duration.

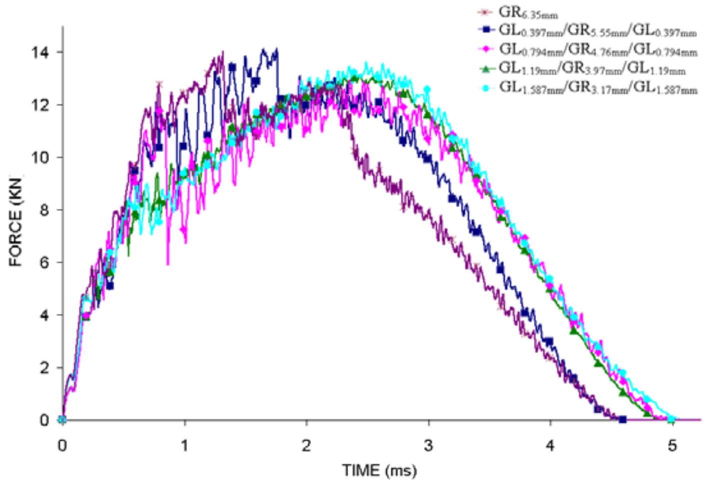

(a)

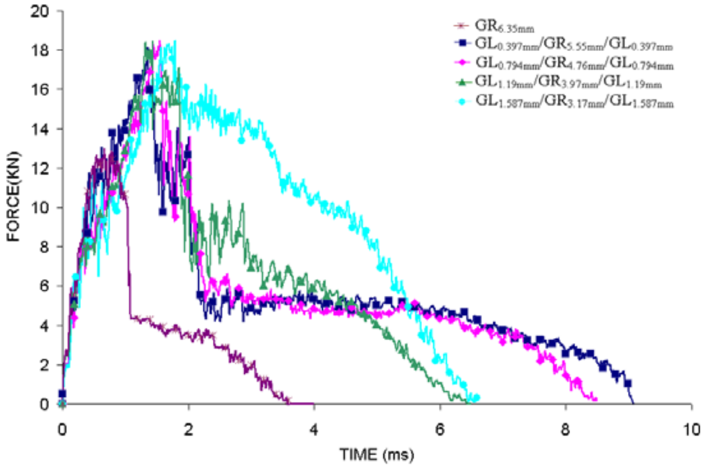

(b)

Figure 6.10 Comparison of FEM predicted force-time histories of GL/GR/GL composites of various thicknesses and GR composites impacted at (a) 3.9 m/s (b)6.3 m/s

FEM predicted damage patterns in Fig 6.11 clearly show improvement for the performance of the composite due to addition of glass fabric layers. Adding even one layer of glass fabric onto GR composite made significant improvement (Fig.6.11 (a-5)). Predicted perforation of GR impacted at 6.3 m/s was prevented by adding glass fabrics (Fig.6.11 (b)). As figure 6.11 shows, improvement is clearly evident. Adding more layers of glass fabrics reduced the damage but increased the weight of the composite.

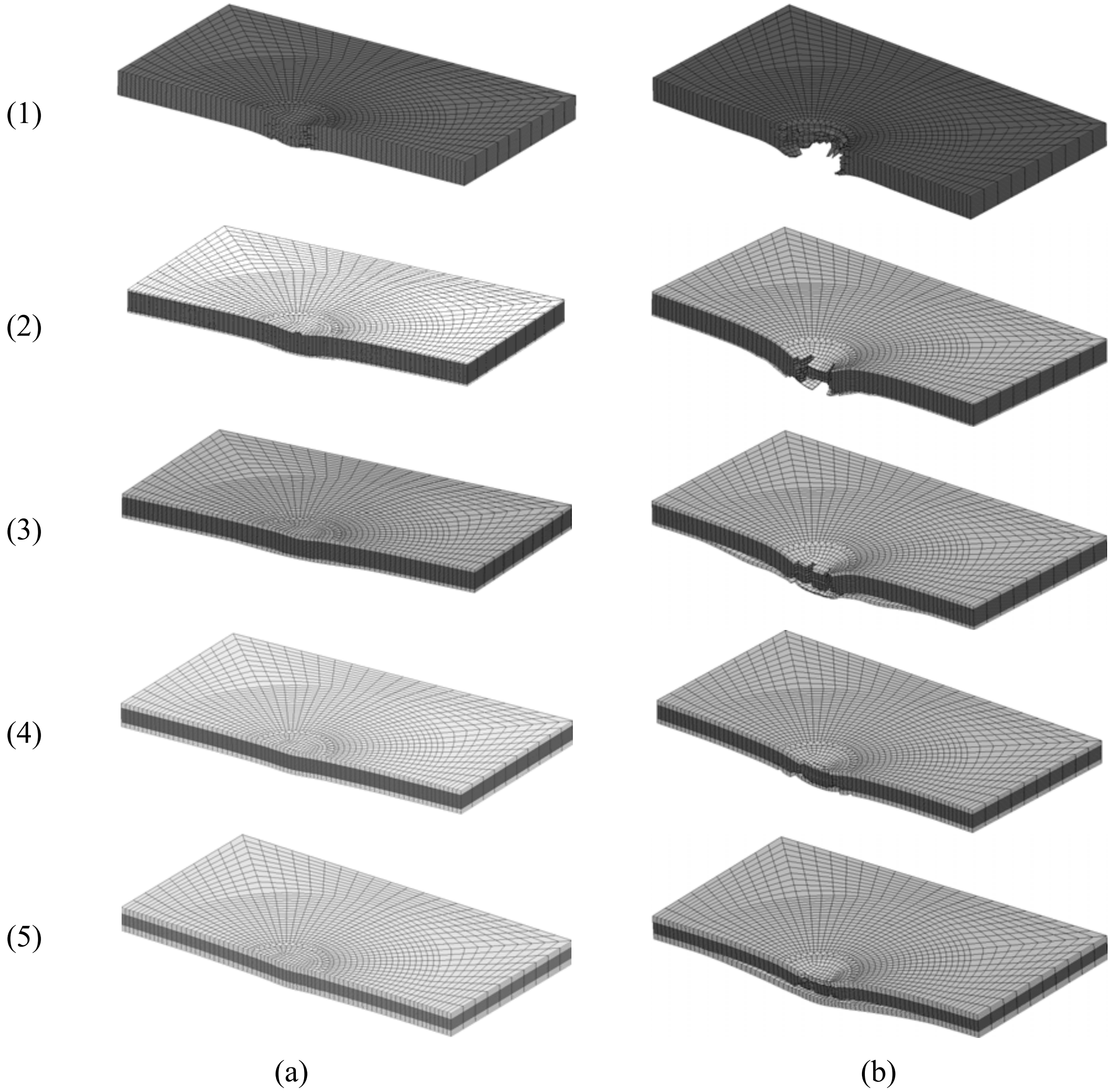

Figure 6.11 FEM predicted damage patterns of
(1) $GR_{6.35mm}$, (2)$GL_{0.397mm}/GR_{5.55mm}/GL_{0.397mm}$, (3)$GL_{0.794mm}/GR_{4.76mm}/GL_{0.794mm}$, (4)$GL_{1.19mm}/GR_{3.97mm}/GL_{1.19mm,}$(5) $GL_{1.587mm}/GR_{3.17mm}/GL_{1.587mm}$ composites impacted at (a) 3.9 m/s and (b) 6.3 m/s.

6.2.2 Finite element simulations of low velocity impact tests conducted using different shape of impactors

Figure 6.12 shows the LS-DYNA finite element meshes simulating drop-weight impact onto (a) a woven GL composite(cylindrical impactor) (b) a woven hybrid GL/GR/GR/GL composite (0.5” spherical impactor) (c) a woven GR composite (1” spherical impactor) and (d) a woven hybrid GR/GL/GL/GR composite (Charpy impactor). 18 layers for GL, 14 layers for GR and 16 layers for hybrid composites were created. Fine mesh around the center and course mesh away from center was used. Due to symmetry, only a quarter plate was used.

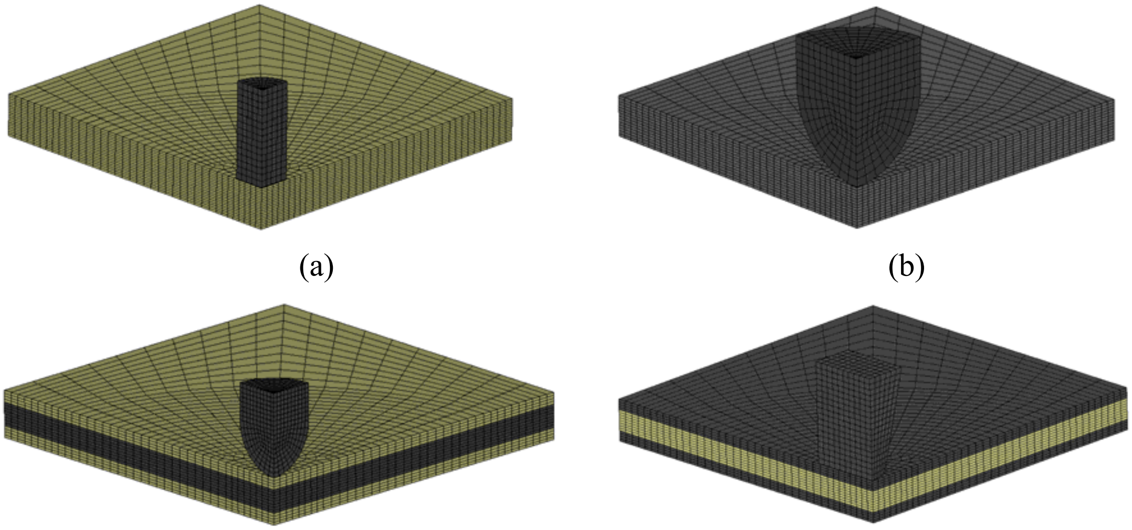

(a) (b)

(c) (d)

Figure 6.12 Finite element simulation models.(a) Drop-weight impact model for the GL (cylindrical impactor) (b) Drop-weight impact model for the GR(1” spherical impactor) (c) Drop-weight impact model for the GL/GR/GL (0.5” spherical impactor) (d) Drop-weight impact model for the GR/GL/GR (Charpy impactor)

(a) Comparison of Force-Time and Strain-Time histories

Figures 6.13 and 6.14 show force and strain histories of GL/GR/GL specimens. Force time histories obtained from experiment and FEM had almost the same initial slope but

FEM results gave a little higher initial peak force and damage initiation started with a delay. The contact duration of FEM was exactly the same as the experimental contact duration (6.13(a)). Predicted strain for strain-gage at location 1 had same magnitude with the experimental strain. However the nonlinear portion seen at experimental strains was not well predicted by FE model. The predicted strains for the strain-gage at location 2 agreed well with experimental strains (6.13(b)). The predicted force time histories of GL/GR/GL specimens when impacted by Charpy impactor had lower initial peak and little higher maximum force compared to experimental force-time histories (Fig.6.14 (a)).The predicted contact duration was exactly the same as the experimental contact duration. The predicted strain-time histories at both locations showed good agreement with experimental strains. However the predicted strains showed some flattening after 3.5 ms that was not observed in experimental strains.

It should be noted that for all cases experimentally obtained force and strain histories were smoother compared to FEM calculated results. This can be due to the fact that force time history is obtained through load cell and some filtering might have been applied to the original readings. By the same token, the strain-output is obtained using strain-gage amplifier where some filtering due to electronic circuitry is very possible.

Figure 6.15 shows the damage progression of GR specimen when impacted by 1” spherical impactor. Note that because the specimen has $+45^{o}$ $/-45^{o}$ fiber orientations, impactor caused higher stresses at $+45^{o}$ and -45^{o} directions.

(b) Post-impact damage patterns

FE predicted post impact damage patterns of GL/GR/GL composite are shown in Figure 6.16. The figures were captured right after contact force became zero. The images were captured at (a) 5 ms, (b) 5.11m/s, (c) 4.87 ms, (d) 4.36 ms. None of the impactors created significant damage on the GL/GR/GL composites. Delamination was the dominant failure mode for all cases. The delamination created by cylindrical, spherical with 25.4 mm diameter and Charpy impactors (Figure 6(a, c, d)) did not create splitting between the layers. However the spherical impactor with 12.7 mm diameter created significant splitting between the layers (Figure 6(b)). The same impactor also created indentation on the surface of the composites. The indentation created by the remaining three impactors was not significant.

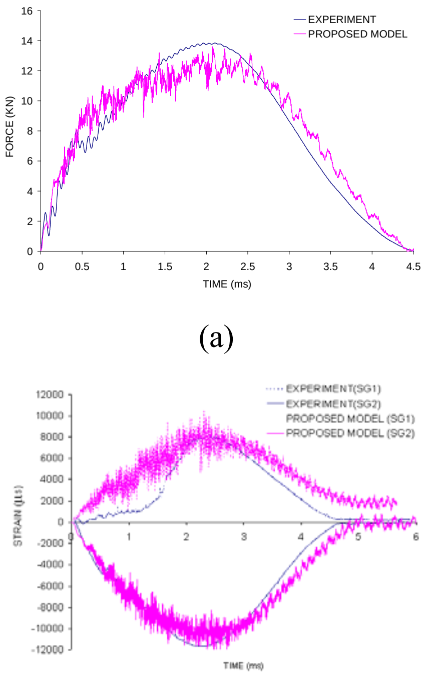

(a)

(b)

Figure 6.13 Comparison of (a) impact force and (b) strain histories for hybrid woven GL/GR/GL composite plate impacted at 4.1 m/s by a 6.15 kg 12.7 mm diameter spherical impactor.

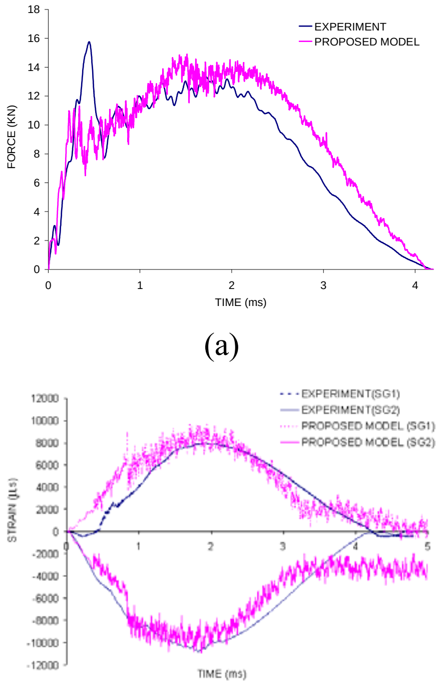

(a)

(b)

Figure 6.14 Comparison of (a) impact force and (b) strain histories for hybrid woven GL/GR/GL composite plate impacted at 4.1 m/s by a 6.15 kg Charpy impactor.

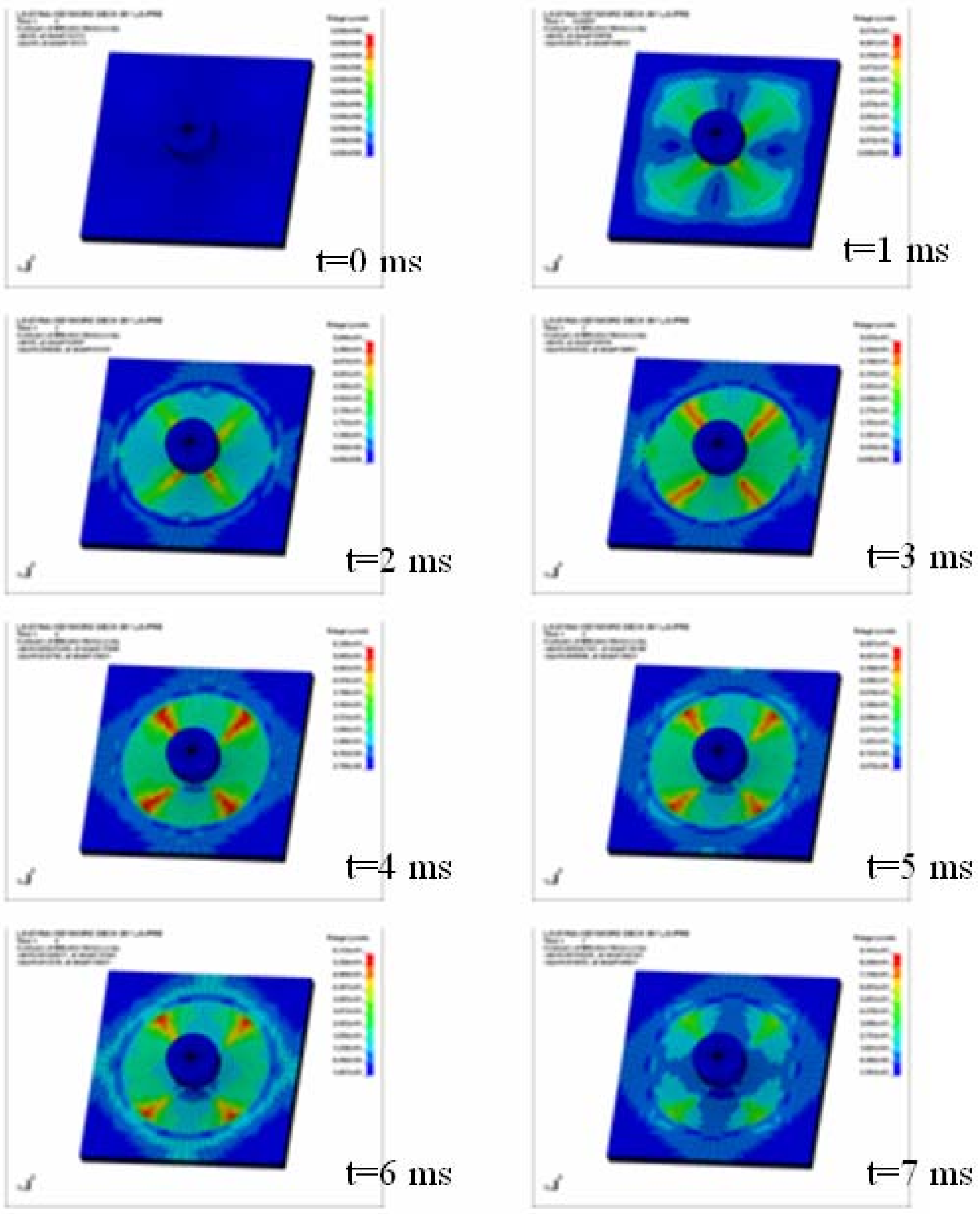

Figure 6.15 Damage progressions and stress counters of FEM simulation for hybrid woven GR composite plate impacted at 4.1 m/s by a 6.15 kg 25.4mm diameter spherical impactor. (Time interval between each plot is 1ms)

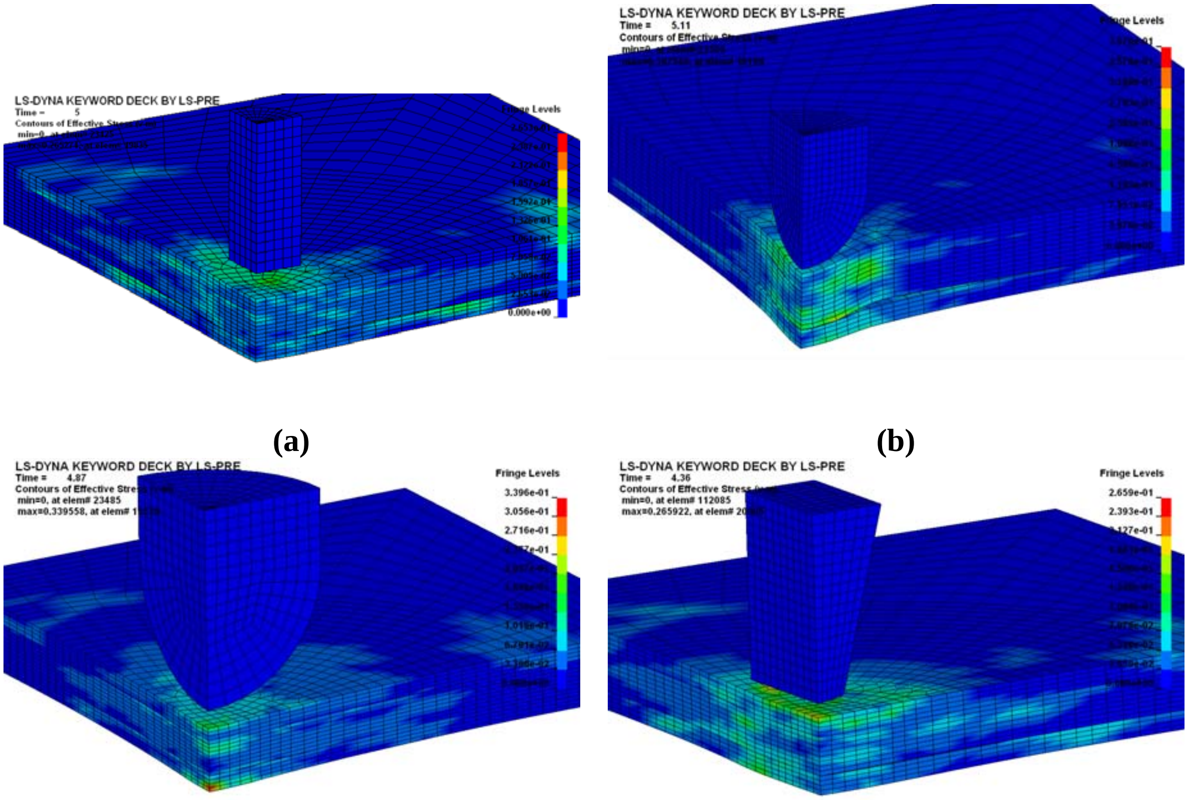

(a) (b)

(c) (d)

Figure 6.16 FE predicted post impact damage patterns for drop-weight tests where GL/GR/GL specimen impacted at 4.1 m/s using (a) cylindrical, (b) spherical with 12.7mm diameter, (c) spherical with 25.4 mm diameter (d) Charpy impactor.

6.3 Finite element simulations for ballistic impact tests

6.3.1 Simulations of ballistic tests on S2-glass fiber/toughened epoxy composite beams

Figure 6.17 shows the LS-DYNA finite element mesh simulating ballistic impact onto a $\left[0^{\circ}_{3}/90^{\circ}_{3}\right]_{2S}$ cross-ply composite beam and ballistic impact onto a $\left[0^{\circ}_{3}/45^{\circ}_{3}/90^{\circ}_{3}/-45^{\circ}_{3}\right]_{S}$ quasi-isotropic composite beam. Due to symmetry, only a quarter of the beam was modeled for ballistic impact onto $\left[0^{\circ}_{3}/90^{\circ}_{3}\right]_{2S}$ .Fine meshes at the vicinity of the impact and course meshes away from the center were generated. The composite beams tested had 24 layers; thus 24 layers of mesh and 23 interfaces were created.

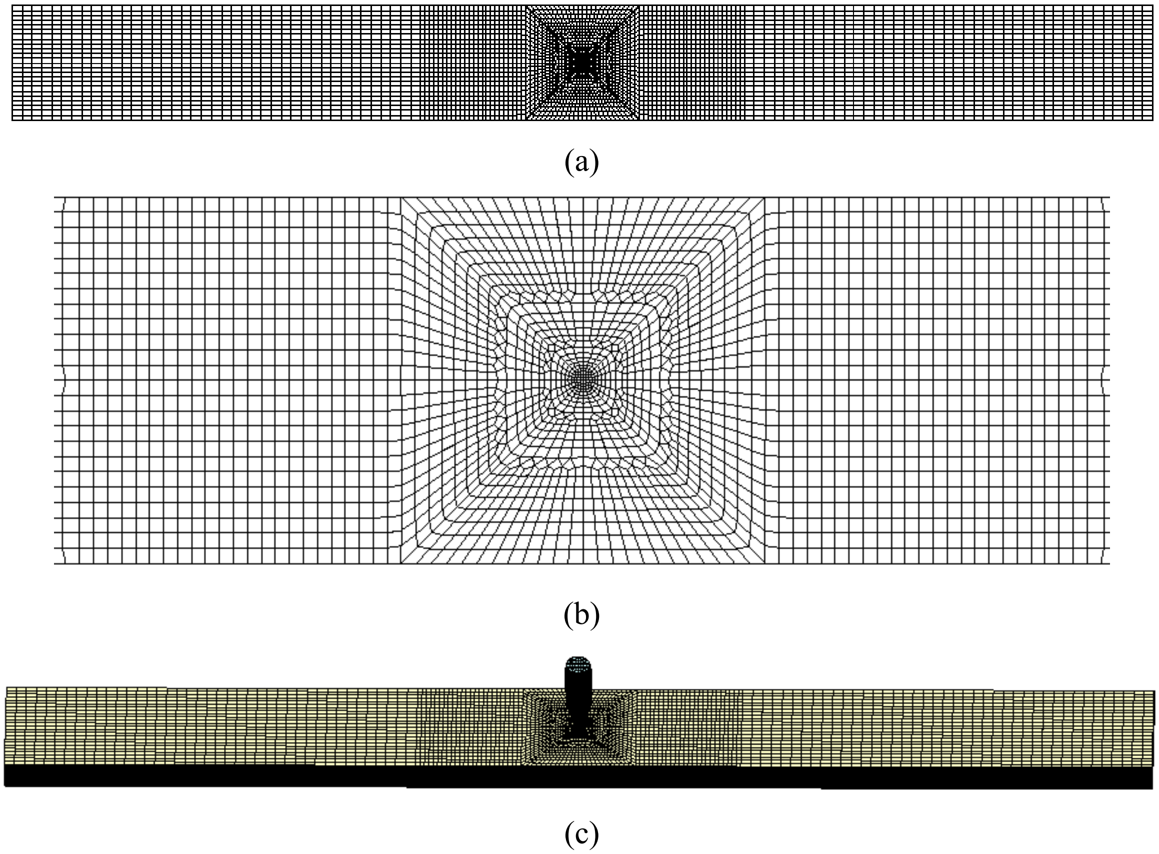

Figure 6.17 Finite element simulation model: (a) Top view, (b) Close-up view and (c) Perspective view.

(a) Determination of damping constant

Initial strain comparison between experimental and FE predicted dynamic strains, where damping is disregarded, exhibited some frequency mismatch. The dynamic strain histories recorded during ballistic impact tests showed damped response of the composite. It is also a known fact that in laminated structures such as composites, slipping between layers introduces high internal damping to the system. It was clear that damping had to be incorporated into FE model. However, the damping constant is not easy to determine. A reasonable approach to estimate damping was using the experimental strain output. Once damping was estimated, it was introduced into the FE model using DAMPING_FREQUENCY_RANGE option in LS-DYNA.

The strain output in Figure 6.18 shows the damped ballistic impact response of a $\left[0^\circ_3/45^\circ_3/90^\circ_3/-45^\circ_3\right]_S$ quasi-isotropic S2 glass-toughened epoxy composite beam impacted at 406 m/s by a 22 caliber copper projectile. The first three cycles of the dynamic strain history have damped frequencies of 327.8, 362.3 and 395.2 Hz, respectively. The gradual increase in the damped frequency indicates the nonlinear behavior of the composite beam due to ballistic damage. The average damped frequency of these three cycles is 361.8 Hz. In order to estimate the damping ratio, the fundamental damped frequency of the signal was determined as 366.2 Hz using Fast Fourier Transform (Fig.6.19).

The convenient half-power method was used for estimating the equivalent viscous damping in mechanical systems.

$$\zeta = \frac{\omega_2 - \omega_1}{2\omega_r} \qquad (6.12)$$

where $\omega_2 - \omega_1$ describes the bandwidth. The resonance frequency can be written as:

$$\omega_r = \omega_n \sqrt{1 - 2\zeta^2} \cong \omega_n \qquad (6.13)$$

When ω_n obtained from Fourier transform of experimental strain history was entered into equation (6.13), damping ratio was calculated as 0.12. The undamped natural frequency of the composite beam can also be calculated theoretically :

$$\omega_n = \alpha^2 (bD_{11} / \rho A L^4)^{1/2} \qquad (6.14)$$

In equation (6.14), b is the width, ρ the density, A the cross-sectional area, L the length, and D_{11} the bending stiffness of the composite beam and α is a constant depending on boundary conditions. The constants for simply-simply supported and clamped-clamped beams are 9.87 and 22.37, respectively. ω_n in equation (6.14) was calculated as 300 Hz for a simply-simply supported and 681 Hz for a clamped-clamped beam. Having experimental $\omega_n = 366.2$ Hz tells us that our boundary condition is most likely between simply-simply supported and clamped-clamped beams.

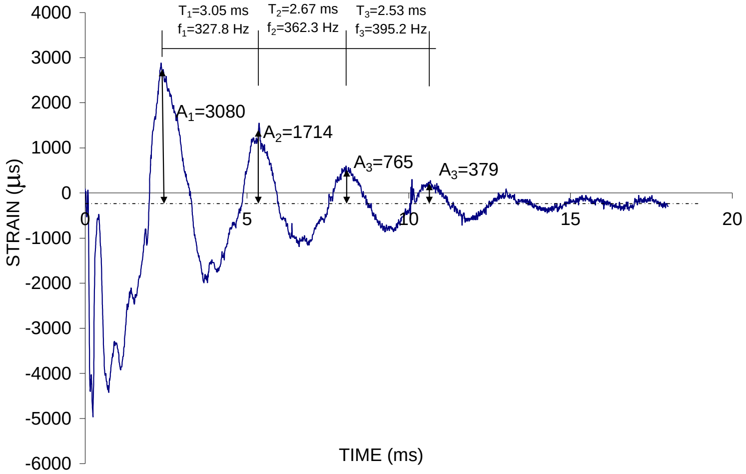

Figure 6.18 The dynamic strain history of a $\left[0^\circ_3/45^\circ_3/90^\circ_3/-45^\circ_3\right]_S$ quasi-isotropic S2 glass-toughened epoxy composite beam impacted at 406 m/s by a 22 caliber copper projectile.

Another approach to calculate the damping ratio is using logarithmic decrement:

$$\zeta = \frac{(\frac{1}{n-1})\ln(\frac{A_1}{A_n})}{\sqrt{4\pi^2 + [(\frac{1}{n-1})\ln(\frac{A_1}{A_n})]^2}} \qquad (6.15)$$

Where n is the cycle number and A_n the amplitude of the n^{th} cycle. The respective values of ζ for n=2, 3, 4 were calculated to be 0.093, 0.11 and 0.11. It is seen that the damping ratio obtained from logarithmic decrement was close to the one calculated using the half-power approach.

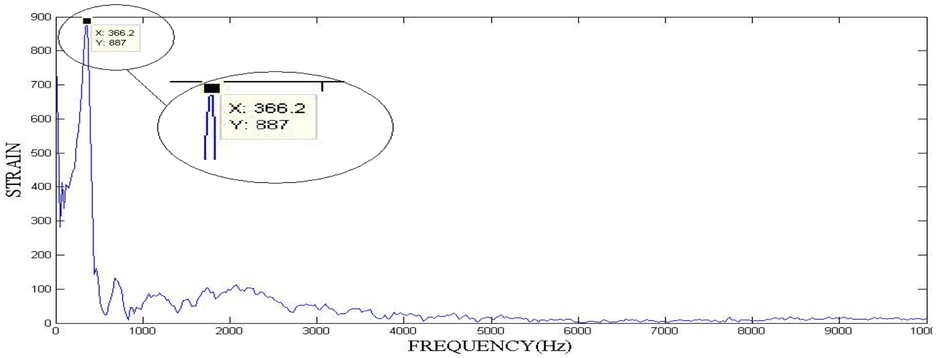

Figure 6.19 The associated Fast-Fourier Transform of dynamic strain history.

(b) Comparison of Strain-Time histories

In this study FE predictions were compared with experimental results mainly for dynamic strain histories and post-impact damage patterns, since it was not possible to obtain force and energy-time histories experimentally. Comparison of force-time histories and energy-time histories were made for two FE Models. As shown in Fig.6.20 (a, b, c) the dynamic strains obtained from experiments and FE results especially those for the user defined material model are in good agreement. The strains obtained using the Chang-Chang model exhibited some magnitude and frequency mismatch in comparison with experimental data. This may be because the nonlinear material behavior could not be represented perfectly by the linear Chang-Chang model.

It should be noted that the strain comparisons made here are mainly for vibration of impacted composite beams. It would be better to compare the transient response of composite during ballistic impact. However ballistic impact takes place in an extremely short time. In order to capture strains in such a short time, the frequency of the strain amplifier should be high enough.

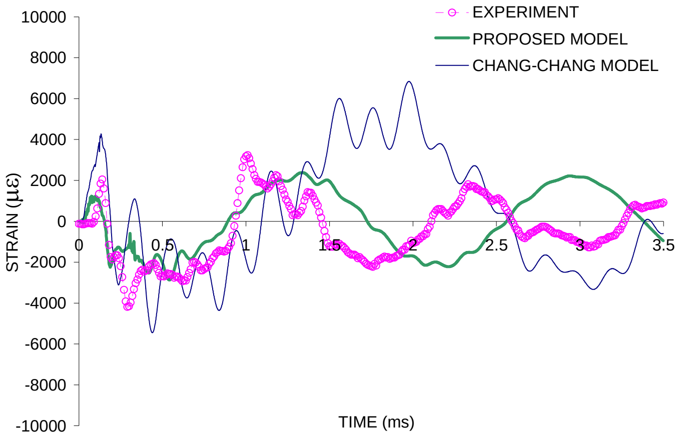

Fig.6.20 (a) Ballistic Test 1: $V_0 = 120$ m/s

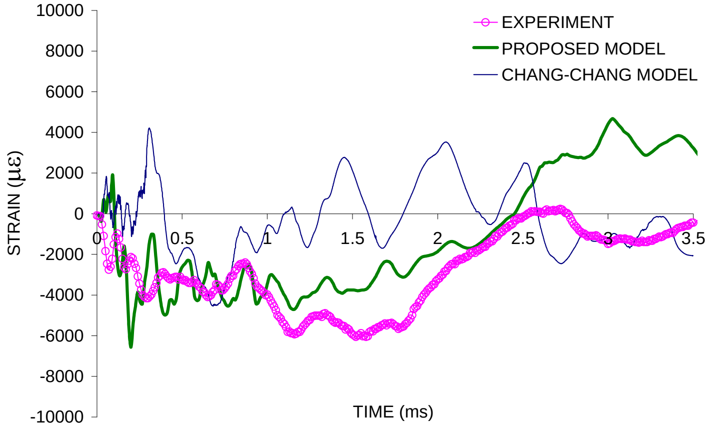

Fig.6.20 (b) Ballistic Test 2: $V_0 = 298$ m/s

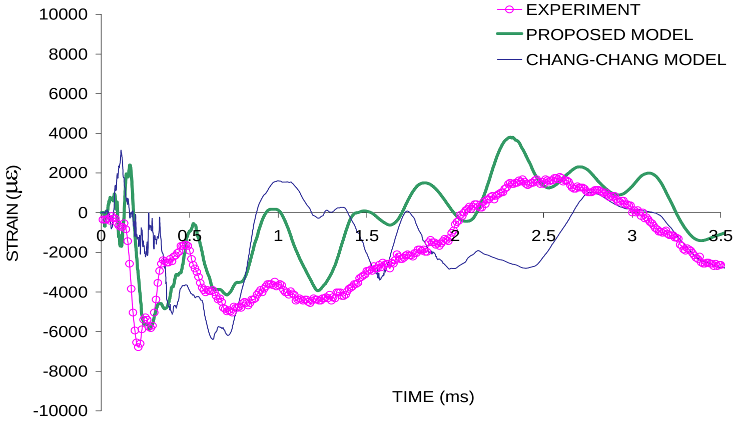

Fig.6.20 (c) Ballistic Test 3: $V_0 = 442$ m/s

Figure 6.20 Comparison of FE predictions and experimental results of dynamic strain histories for Ballistic Tests 1 and 2: $\left[0^\circ_3/90^\circ_3\right]_{2S}$ cross-ply and Test 3: $\left[0^\circ_3/45^\circ_3/90^\circ_3/-45^\circ_3\right]_S$ quasi-isotropic composite beams impacted by a 22-caliber copper projectile.

The strain amplifier used in this study has a maximum frequency of 100 KHz. In other words, it was only able to record the strain data every 10μs. Assuming that ballistic impact event takes 100μs, the dynamic strain curve from experiment would have captured only 10 data points, which would be significantly under sampling. The strain curve constructed using these data points cannot represent the real response of the composite. Due to such equipment-related barriers, the initial transient responses obtained from experiment and FE calculations are not compared. However the results obtained from FE calculations were recorded to better understand the phenomenon.

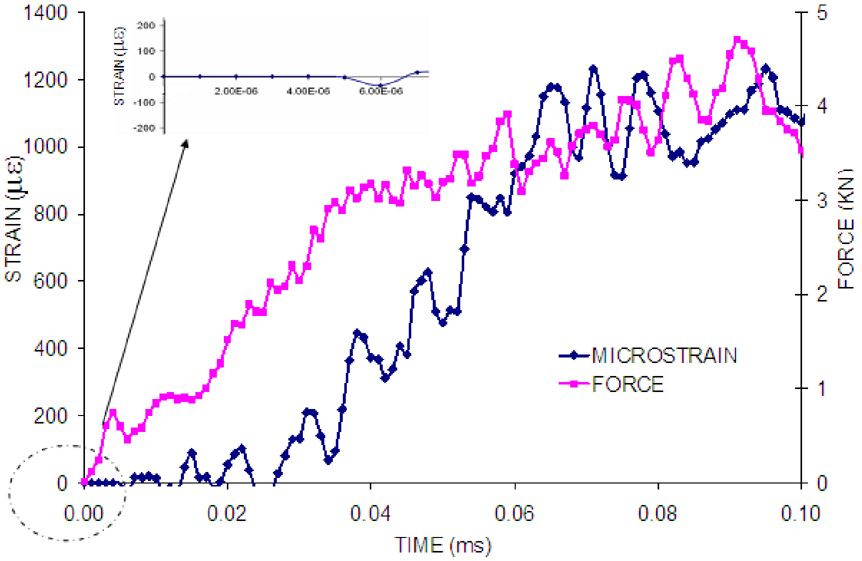

Figure 6.21 Dynamic force and strain histories for Ballistic Test 1
(first 100μs of impact event only)

For instance, FE calculated dynamic force and strain histories for Ballistic Test 1 were plotted just for the first 100μs (Fig.6.21). When t=0, projectiles started engaging the specimen and some contact force was generated. However no strain was recorded during the first 5μs. This can be explained by the fact that the element selected for strain output was 25.4 mm away from the contact location. It took about 5μs for the strain wave to propagate to that element. As soon as the strain wave reaches that element, some strain data were observed.

(c) Comparison of post-impact damage patterns

Once all ballistic impact tests were completed, composite beams were cut into half at impact location for further post-impact damage pattern examination and comparison (Fig.6.7). Optical picture of the composite impacted at 120 m/s (Fig.6.7.1.a) shows the damage up to the third laminate around the impact location, but no delamination was observed. FE prediction of damage and delamination for this test (Fig.6.7.1.b) by user-defined model agreed well with the experiment. However, the Chang-Chang model (Fig.6.7.1.c) predicted less damage to the composite. Optical picture of second composite (Fig.6.22.2(a)), which was impacted at 298 m/s, exhibited damage up to the sixth laminate and delamination mostly occurred between laminates where fiber orientation changes. User-defined model for this case predicted a little more penetration (Fig.6.22.2 (b)). However, delamination patterns were well agreed well with experiment. FE prediction by the Chang-Chang model showed almost no delamination and much localized damage (Fig.6.22.2(c)). The projectile fully penetrated during the impact test of $\left[0^\circ_3/45^\circ_3/90^\circ_3/-45^\circ_3\right]_S$ composite at 442 m/s. Matrix and fiber damage was very severe, delamination was observed between all laminae (Fig.6.22.3 (a)). Both FE models predicted very similar damage for this test (Figs.6.22.3 (b) and (c). Prediction by the Chang-Chang model exhibited more delamination and more damage around the center (Fig.6.22.3(c)). While the projectile that impacted $\left[0^\circ_3/90^\circ_3\right]_{2S}$ composite at 120 m/s (Fig.6.23.1 (a)) had slight damage at the tip, 298 m/s test (Fig.6.23.2 (a)) resulted in a compacted and split projectile. The projectile turned into a mushroom shape after 442 m/s test (Fig.6.23.3 (a)). The deformation predicted by Chang-Chang material model (Figs.6.23.1(c), 2(c), 3(c)) agreed less with experimental data compared to the deformation predicted by user-defined material model (Figs.6.23.1 (b), 2(b), 3(b))

1	$\left[0^\circ_3/90^\circ_3\right]_{2S}$, Impacted at 120 m/s			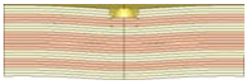
2	$\left[0^\circ_3/90^\circ_3\right]_{2S}$, Impacted at 298 m/s			
3	$\left[0^\circ_3/45^\circ_3/90^\circ_3/-45^\circ_3\right]_S$ Impacted at 442 m/s			
	Specimen	a) Experiment	b) User-defined Model	c) Chang-Chang Model

Figure 6.22 Comparison of FE predictions and experimental results of post-impact damage patterns.

However both FE material models were unable to predict splitting and the mushroom shape. This can be explained by the fact that an erosion criterion was used during FE analysis in order to maintain numerical stability. The elements were eroded when sufficient failure criterion was met. Thus the damaged part of the projectile was eroded and disappeared in FE analysis instead of being pushed to the sides and changing the shape of the projectile.

(d) Comparison of Force-Time histories

FE analysis predicted force-time histories (Fig.6.24) obtained through the two different material models were in agreement. Force histories produced by Chang-Chang model showed higher initial slope compared to user-defined material model. After reaching 9KN, pick contact force values dropped to 6KN and eventually returned to zero. User-defined material model predicted 8KN maximum force. Gradual decreases after maximum force was observed. Figure 6.25 shows force time histories and damage progression for $\left[0^\circ_3/90^\circ_3\right]_{2S}$ S2 glass-toughened epoxy composite beam impacted at 298 m/s by a 22 caliber copper projectile.

a)Experiment			
b)User-defined Model			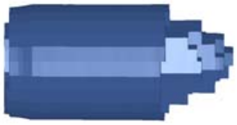
c)Chang-Chang Model			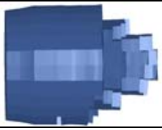
Projectile	1. Deformed projectile after impacting $\left[0^\circ_3/90^\circ_3\right]_{2S}$ composite at 120 m/s	2. Deformed projectile after impacting $\left[0^\circ_3/90^\circ_3\right]_{2S}$ composite at 298 m/s	3.Deformed projectile after impacting $\left[0^\circ_3/45^\circ_3/90^\circ_3/-45^\circ_3\right]_{S}$ composite at 442 m/s

Figure 6.23 Post impact damage pattern comparisons for projectiles.

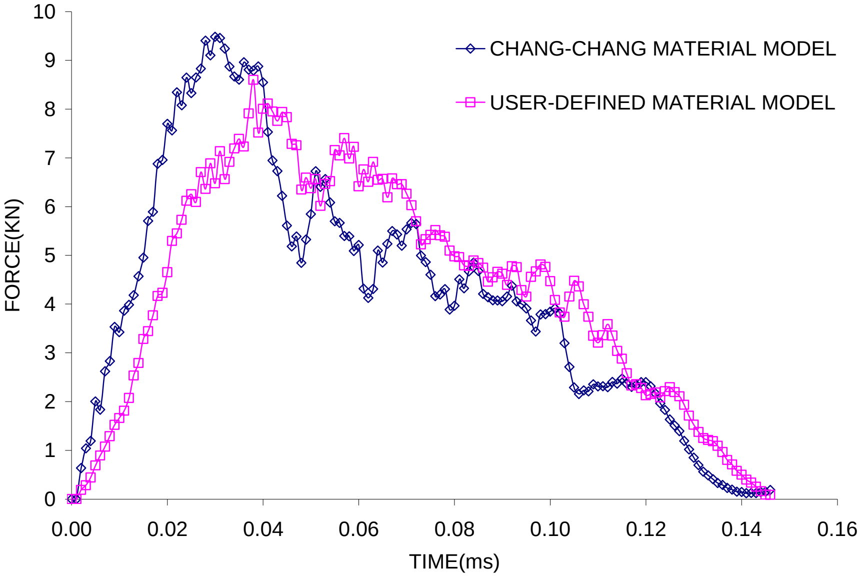

Figure 6.24 Comparison of FE predicted force-time histories for cross-ply S2 glass-toughened epoxy composite beam impacted at 298 m/s by a 22 caliber copper projectile

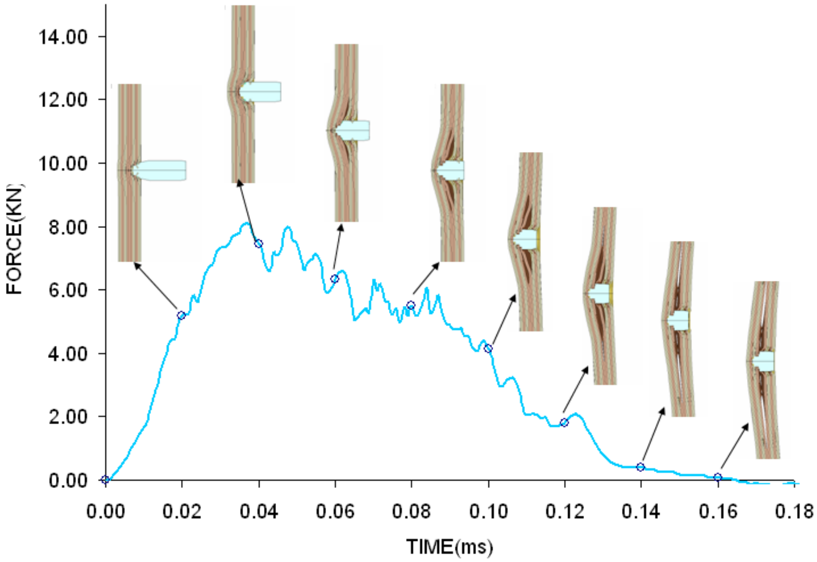

Figure 6.25 Comparison of FE predicted force-histories and damage progression for cross-ply S2 glass-toughened epoxy composite beam impacted at 298 m/s by a 22 caliber copper projectile.

(e) Comparison of Energy-Time histories

Impactor energy histories (Fig.6.26) produced by the two FE models were also in agreement. Energy of the impactor obtained using the Chang-Chang model decreased to zero with higher slope.

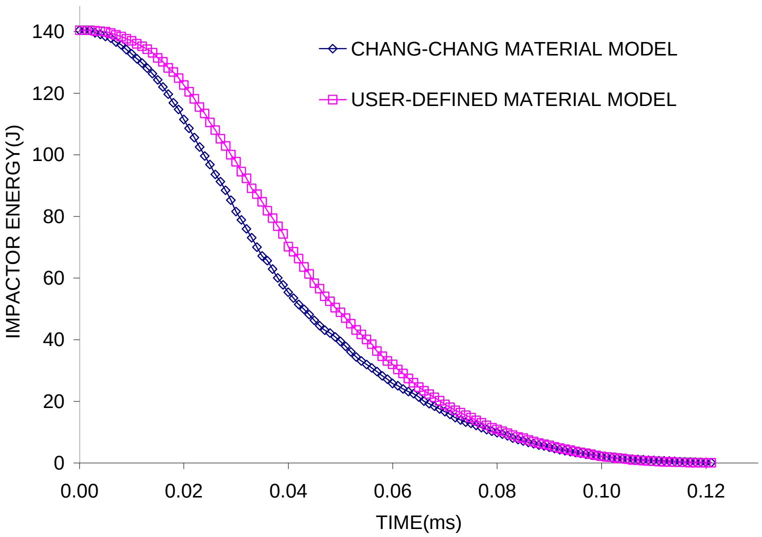

Figure 6.26 Comparison of FE predicted impactor energy-time histories for S2 glass-toughened epoxy composite beam impacted at 298 m/s by a 22 caliber copper projectile

(f) Determination of ballistic limit velocity V_{50}

As explained above, dynamic strain histories and damage patterns obtained from experiments and FE (user-defined material) predictions were in very good agreement. The proposed user-defined material model can then be employed in engineering design. For instance, we can use this model to predict the ballistic limit velocity V_{50} of the armors made of this toughened composite. Here V_{50} is defined as the velocity required for a projectile to reliably penetrate (i.e., 50% probability of penetration) a piece of armor. Figure 6.27 shows the damage progression for $\left[0^\circ_3/45^\circ_3/90^\circ_3/-45^\circ_3\right]_S$ S2 glass-toughened epoxy composite beam impacted at 442 m/s by a 22 caliber copper projectile.

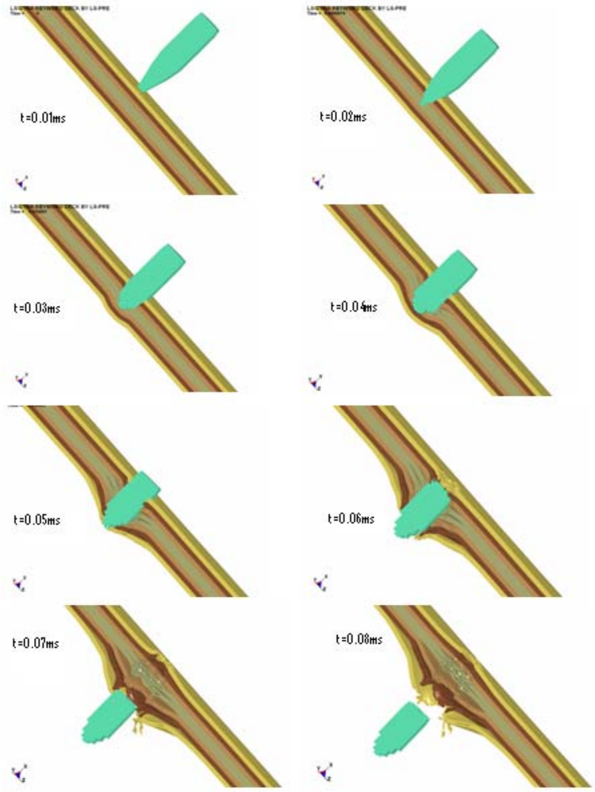

Figure 6.27 FE predicted damage progression for $\left[0^\circ_3/45^\circ_3/90^\circ_3/-45^\circ_3\right]_S$ S2 glass-toughened epoxy composite beam impacted at 442 m/s by a 22 caliber copper projectile.

Consider composite beams made of $\left[0^\circ_3/90^\circ_3\right]_{2S}$ S2 glass-toughened epoxy. Two ballistic impact tests, which were conducted at 120m/s and 290 m/s, showed partial penetration into $\left[0^\circ_3/90^\circ_3\right]_{2S}$ S2 glass-toughened epoxy. The two experimental results and the FE predicted number of damaged laminae at various speeds are shown in Fig 6.28. A linear relation between velocity and number of damaged layers was observed. Using this linear relationship, the velocity to damage all 24 lamina was calculated as 342m/s. V_{50} for this composite should be less than this number, because damaging all 24 layers may result in full penetration. On the other hand, during the ballistic impact test at 298 m/s, partial penetration was observed. It can be concluded that the V_{50} ballistic limit velocity should be between 298 and 342 m/s. Results of FE simulations at velocities between 298 and 342 m/s showed that the projectile partially penetrated, i.e. remained inside the composite, for velocities up to 320 m/s. All simulations above 320 m/s velocity showed full penetration. Thus, the predicted V_{50} ballistic limit of $\left[0^\circ_3/90^\circ_3\right]_{2S}$ S2 glass-toughened epoxy was 320 m/s. Using this approach, V_{50} can be calculated with sufficient accuracy. Once the relation between velocity and number of damaged layers is established, ballistic limit V_{50} for different thicknesses of the same composite can easily be estimated. Figure 6.29 shows FE predicted projectile penetration for $\left[0^\circ_3/90^\circ_3\right]_{2S}$ S2 glass-toughened epoxy composite impacted at the velocities above and below ballistic limit V_{50}. Our ballistic impact test set-up is not capable of capturing residual velocities. The V_{50} ballistic limit velocity can be estimated once impact and residual velocities are measured experimentally. It should be noted that for sufficient accuracy, an adequate number of experiments has to be conducted. Increasing number of experimental data also increases accuracy of estimation. Then, FE model that is validated using limited number of experiments can be run for different velocities.

The energy transferred to the composite can be written as:

$$E_{transferred} = \frac{1}{2} m_{bullet} ((V_{impact})^2 - (V_{residual})^2) \qquad (9)$$

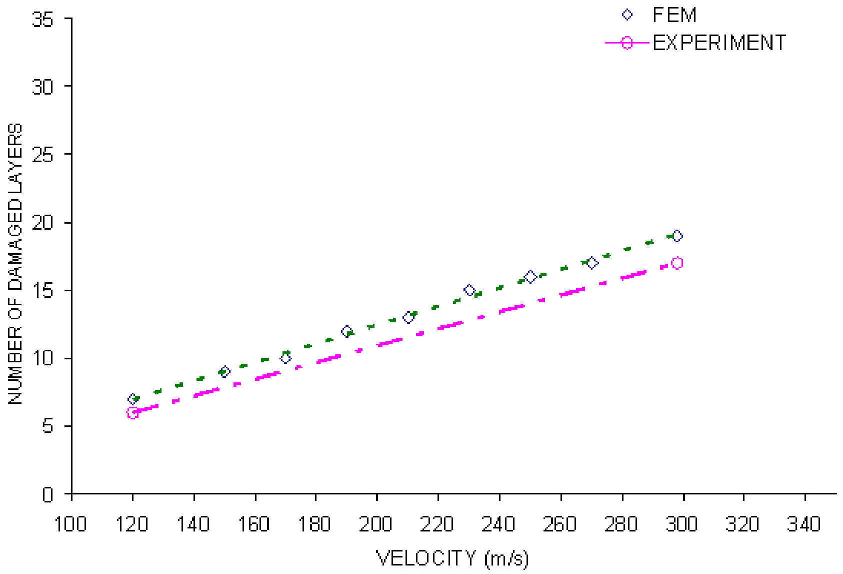

Figure 6.28 FE predicted and experimentally obtained number of damaged laminae at various velocities for $\left[0^\circ_3/90^\circ_3\right]_{2S}$ S2 glass-toughened epoxy composite beam impacted by a 22 caliber copper projectile.

When the residual velocity (V_R) become zero in this equation impact velocity (V_I) would be equal to $V_{50,}$ the ballistic limit velocity. Even though residual velocities could not be measured experimentally, they were plotted using FE analysis (Fig.6.30). The FE predicted velocity-time histories clearly indicate impact velocities (V_I) and residual velocities (V_R). It should be noted while the impact velocities below V_{50} produced negative and small V_R due to bounce-back of projectiles, the velocities above V_{50} produced positive V_R due to full penetration of projectile. The V_R velocities below V_{50} did not vary much. However slight change at impact velocity resulted in significant difference for V_R. Once V_R was plotted against V_I (Fig.6.31), V_{50} can be determined as the velocity where V_R became zero. It was estimated as 320 m/s, in agreement with the estimation obtained using the number of damaged layers approach.

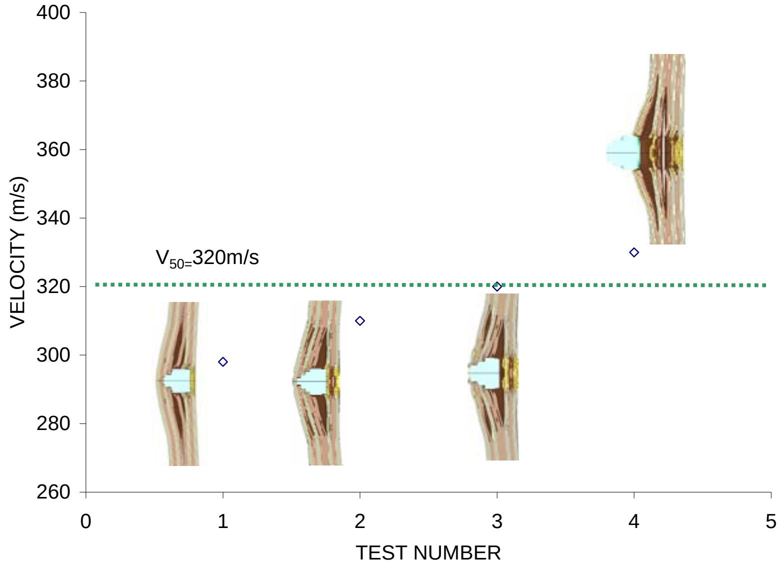

Figure 6.29 FE predicted projectile penetration for $[0_3^\circ/90_3^\circ]_{2S}$ S2 glass-toughened epoxy composite beam impacted at above and below V_{50}.

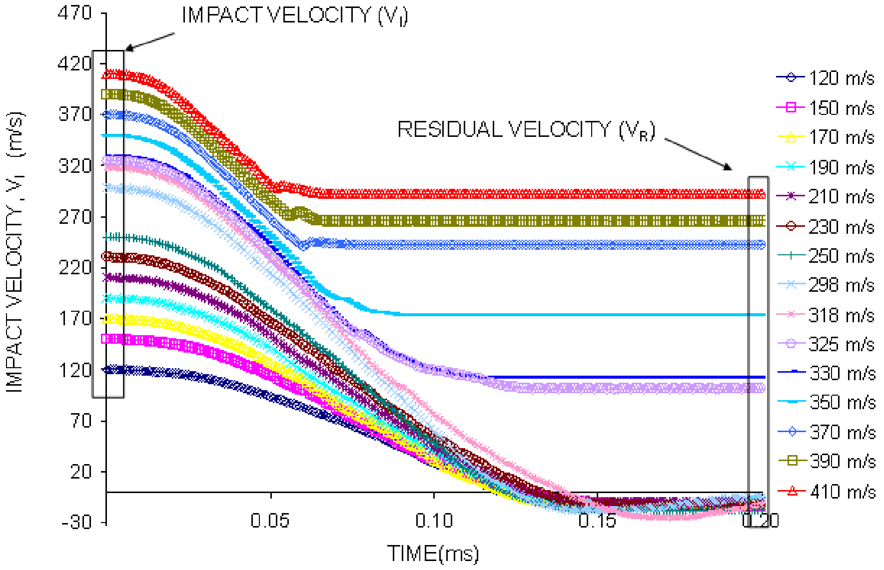

Figure 6.30 FE predicted velocity histories for $[0_3^\circ/90_3^\circ]_{2S}$ S2 glass-toughened epoxy composite beam impacted at above and below V_{50}.

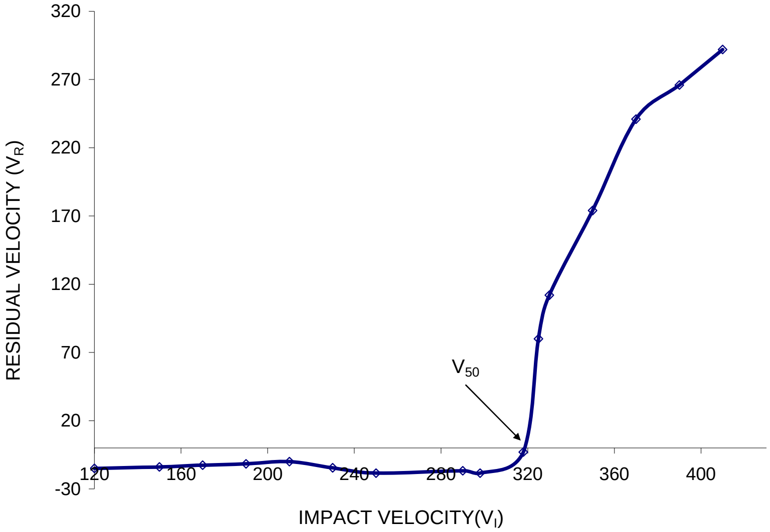

Figure 6.31 FE predicted residual velocity (*V_R*)-impact velocity (*V_I*) relation for $\left[0^\circ_3/90^\circ_3\right]_{2S}$ S2 glass-toughened epoxy composite beam impacted at above and below *V_{50}*.

The three experiments conducted for $\left[0^\circ_3/45^\circ_3/90^\circ_3/-45^\circ_3\right]_S$ composite beam were above 390m/s and full penetration of projectile was observed during all three tests.

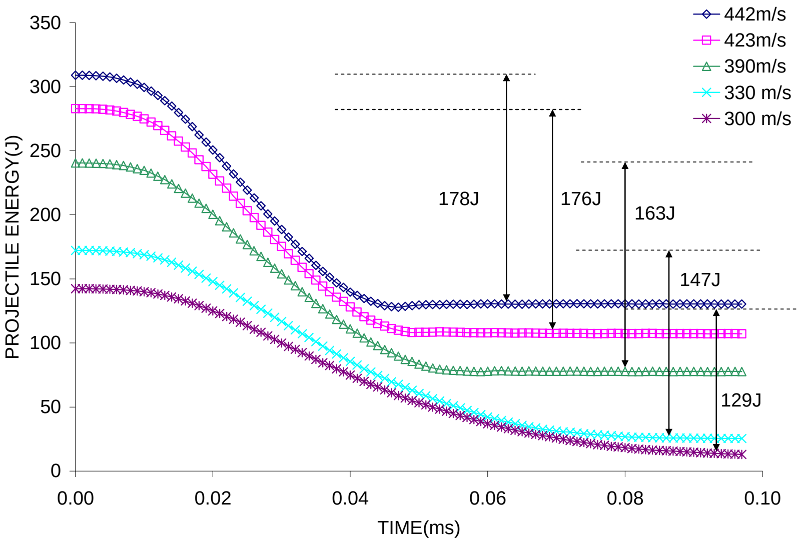

Figure 6.32 FE predicted projectile energy-time histories for $\left[0^\circ_3/45^\circ_3/90^\circ_3/-45^\circ_3\right]_S$ S2 glass-toughened epoxy composite beam impacted at above and below *V_{50}*.

In terms of V_{50} calculation, the only conclusion that can be drawn from these three experiments is that V_{50} was below 390 m/s. Figure 6.32 shows FE predicted energy time histories of $\left[0^\circ_3/45^\circ_3/90^\circ_3/-45^\circ_3\right]_S$ glass-fiber toughened epoxy composites.

FE predicted energy-time histories (Fig.6.33) show that transferred energy increases with increasing velocity. If all the kinetic energy of the projectile is transferred to the composite beam, there is a great chance for partial penetration. On the other hand all impact velocities up to V_{50} show partial penetration. The transferred energy (E_T) can be written as

$$E_{transferred} = E_{impact} - E_{residual} \qquad (6.16)$$

If there is no full penetration, $E_{residual}$ (E_R) in this equation become zero and the equation can be written as:

$$E_{transferred} = E_{impact} \qquad (6.17)$$

The velocity that satisfies equation (6.17) determines V_{50} ballistic limit velocity. Figure 24 shows FE predicted impact, residual and transferred energies for velocities above V_{50}. The critical velocity where impact energy (E_I) is equal to transferred energy (E_T) and the residual energy (E_R) is zero determines ballistic limit velocity V_{50}.

Since the critical velocity where impact energy (E_I) is equal to (E_T) determines V_{50}, the equation (6.17) can be written as:

$$\frac{1}{2} m_{bullet} ((V_{impact})^2 = f(V_{impact}) \qquad (6.18)$$

The function $f(V_{impact})$ here can be determined by curve-fitting to the E_T values shown in Figure 6.33 in it was obtained as:

$$f(V_{impact}) = a \ln(V_{impact}) - b \quad (14)$$

Once the function was determined, the V_{impact} value in equation (13) can be used for V_{50}.

Figure 6.34 shows V_R-V_I relations for $\left[0_3^\circ/45_3^\circ/90_3^\circ/-45_3^\circ\right]_S$ S2 glass-toughened epoxy composite beam. Only the impact velocities that resulted in full penetration, above V_{50}, were considered here. The critical point where V_R becomes zero determines the V_{50} here as 290 m/s.

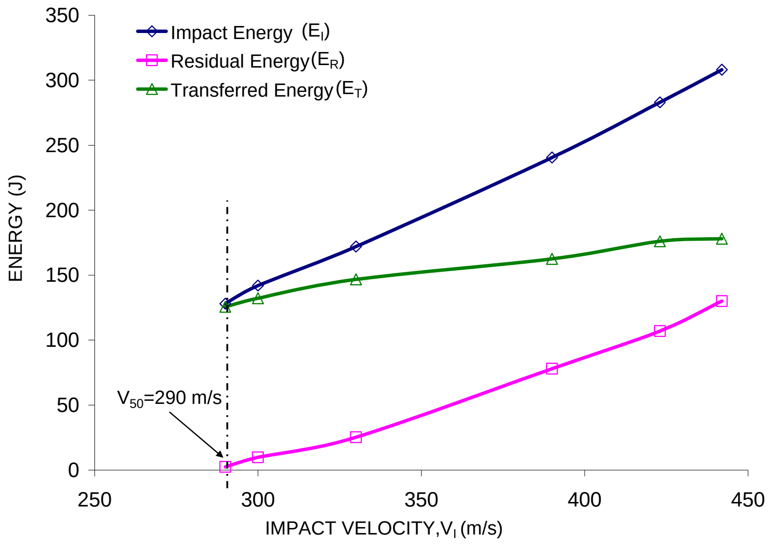

Figure 6.33 FE predicted projectile impact, residual and transferred energies for $\left[0_3^\circ/45_3^\circ/90_3^\circ/-45_3^\circ\right]_S$ S2 glass-toughened epoxy composite beam impacted at 442, 423, 390, 330, 300, and 290m/s, respectively.

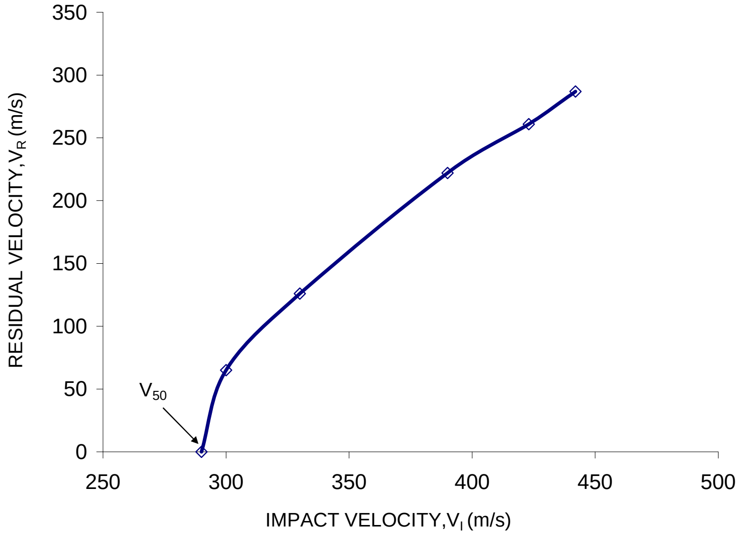

Figure 6.34 FE predicted residual velocity (V_R)-impact velocity (V_I) relation for $\left[0_3^\circ/45_3^\circ/90_3^\circ/-45_3^\circ\right]_S$ S2 glass-toughened epoxy composite

Figure 6.35 shows FE model predicted and experimentally obtained projectile penetration at velocities above and below V_{50}.

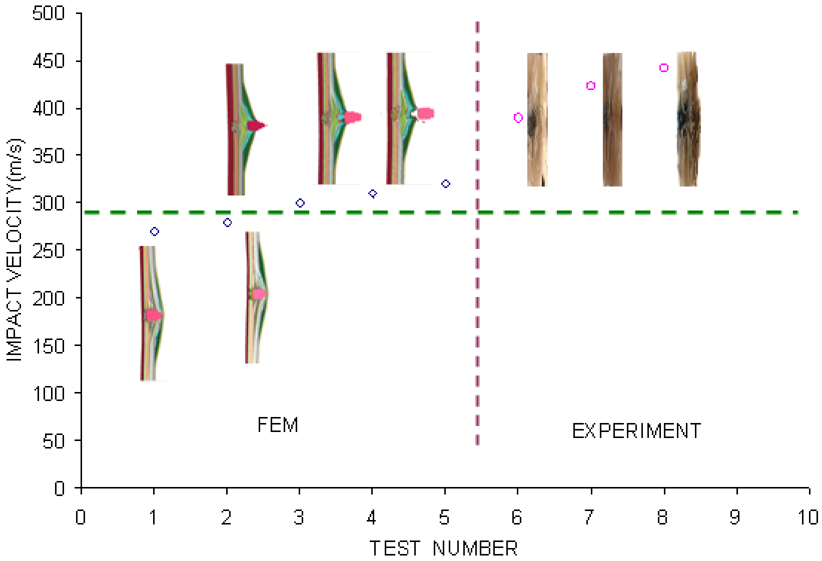

Figure 6.35 FE predicted and experimentally obtained projectile penetration for $\left[0^\circ_3/45^\circ_3/90^\circ_3/-45^\circ_3\right]_S$ S2 glass-toughened epoxy composite beam impacted at above and below V_{50}.

6.3.2 Finite element simulations of ballistic tests on woven composite panels

Figure 6.36 shows the LS-DYNA finite element meshes simulating ballistic impact onto (a) a woven GL composite (b) a woven hybrid GL/GR/GL composite (c) a woven GR composite and (d) a woven hybrid GR/GL/GR composite. Figure 6.36 (e) shows the close-up view of the projectile and plate. It should be noted that fine mesh around the center and course mesh away from center was created. Due to symmetry, only a quarter of the plate was used. 18 layers for GL, 14 layers for GR and 16 layers for hybrid composites were created.

(a) Comparison of Strain-Time histories

As it was mentioned before, dynamic strains obtained from experiments were compared with FE predicted strains. The experimental dynamic strains captured the vibration of composite panels. However they were unable to capture the transient response of the composites due to equipment related barrier. Figure 6.37 shows comparison of dynamic strain histories for GL composite impacted at 236 m/s. The experimental and FE predicted dynamic strain histories were in agreement However the magnitude of the predicted strains was higher than the magnitude of the experimental strains. The frequency of both signals was in good agreement

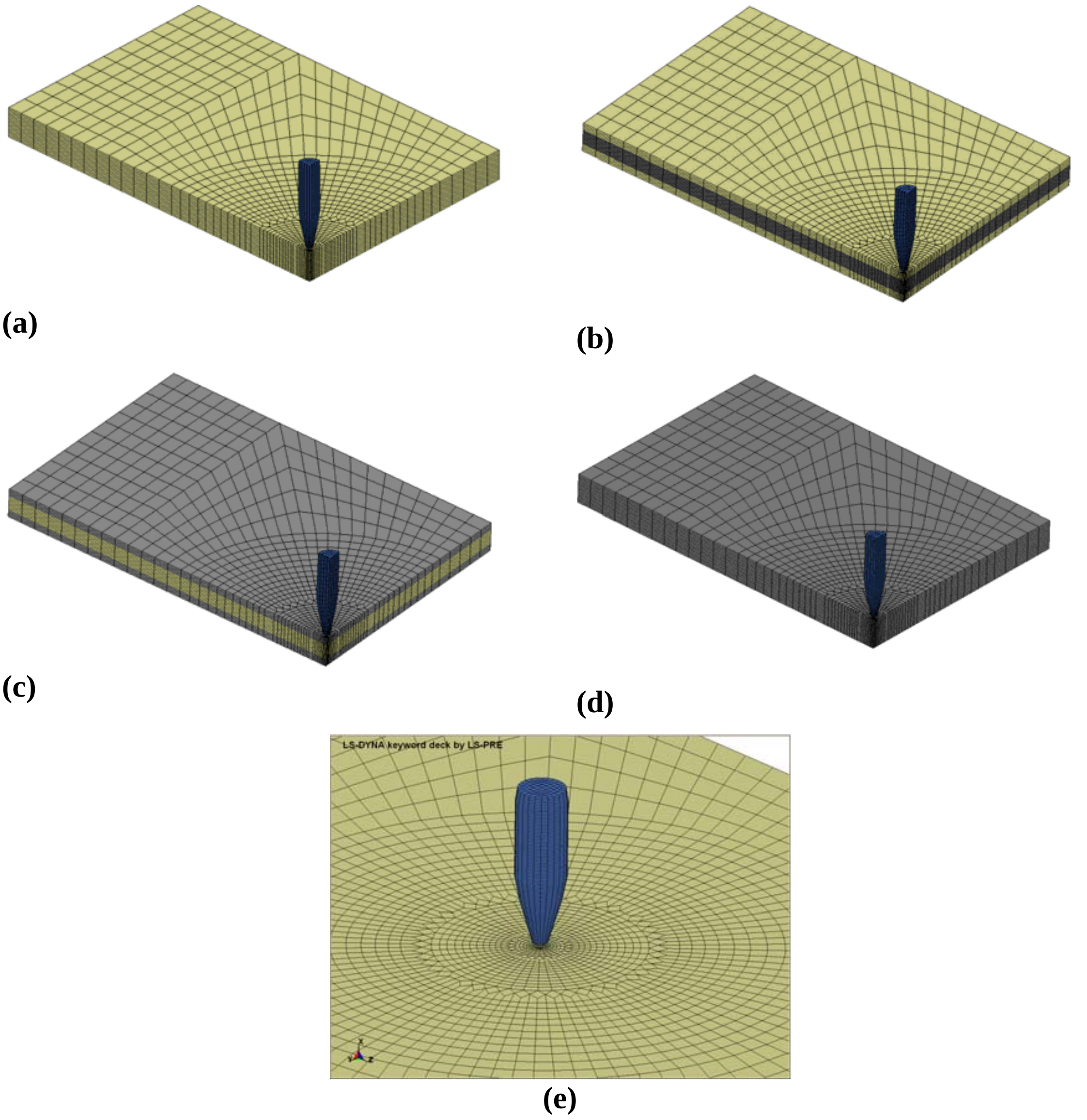

Figure 6.36 Finite element simulation model for composite panels: (a) GL, (b) GL/GR/GL, (c) GR/GL/GR, (d) GR and (e) Close-up view of top surface of composite and projectile

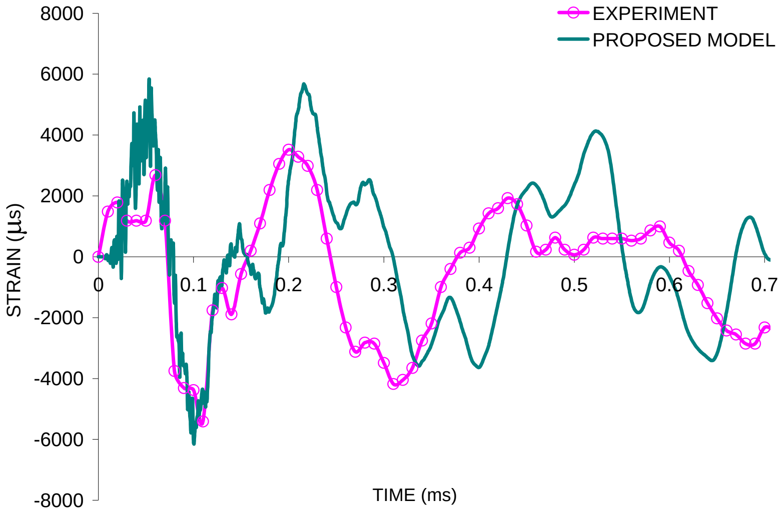

Figure 6.37 The dynamic strain history of GL composite panel impacted at 236 m/s by a 22 caliber copper projectile.

Figure 6.38 shows the strain comparison for GR composite impacted at 442 m/s. The magnitude and the frequency of the experimental and predicted strains were in very good agreement especially during the first two cycles. The frequency exhibited some mismatch starting from the thirds cycle.

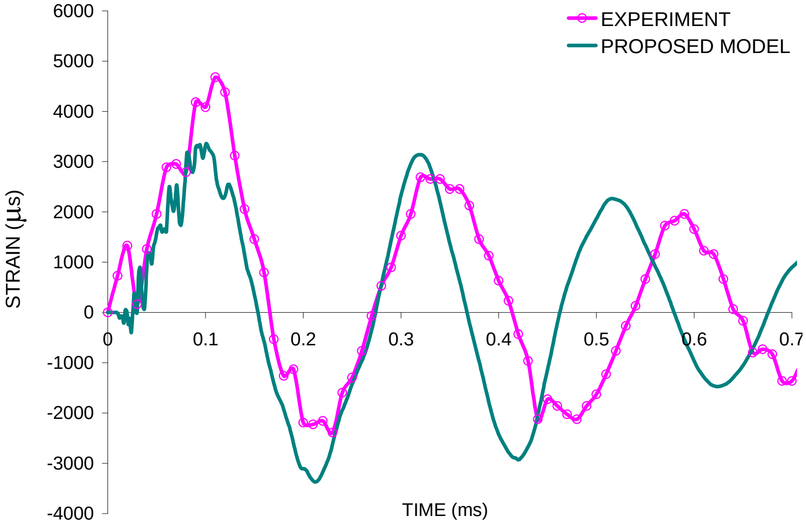

Figure 6.38 The dynamic strain history of GR composite panel impacted at 442 m/s by a 22 caliber copper projectile.

(b) Comparison of Force-Time histories

The force time histories could not be captured during experiments. However FE model provides the force-time histories of ballistic tests. Figure 6.39 shows the predicted force-time histories of GL composite impacted at various velocities. It is clear that the higher impact velocity produced lower contact time for three partial penetration cases. The magnitude of the forces for these cases did not show significant difference. On the other hand, the full penetration test at 385 m/s produced less impact force and less contact duration. The predicted force time histories of GL/GR/GL composite are shown in Figure 6.40. Once the three partial penetration tests are compared, it is seen that 113.4 m/s produced the highest impact duration and 300 m/s produced the lowest impact duration. The full penetration test (339 m/s) produced the lowest impact duration and the lowest impact force.

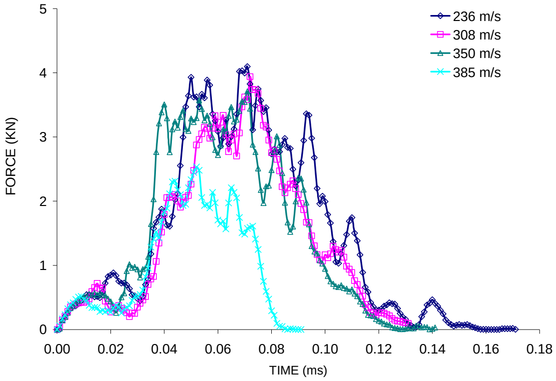

Figure 6.39 Comparison of FE predicted force-time histories of GL composite panel impacted by a 22 caliber copper projectile

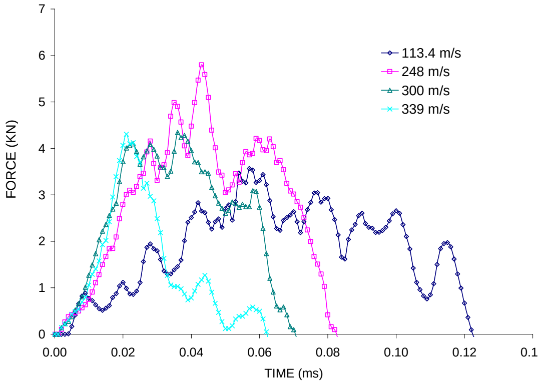

Figure 6.40 Comparison of FE predicted force-time histories of GL/GR/GL composite panel impacted by a 22 caliber copper projectile

During the ballistic impact event, if the projectile partially penetrated, the velocity of the projectile decreased and became zero before traveling the entire thickness of the composite. Thus typical force-time histories of partial penetration tests would have a linear increase at the beginning and return the zero after reaching maximum force. The drops that were observed in the force time histories represent the failure of the composite layers. As soon as a composite layer is damaged, the projectile loses its contact temporarily. Once the following layer is reached, the contact force starts to increase again. The projectile passes through the entire thickness in a very short time in case of full penetration. The contact between the projectile and the composite ends before the maximum force is reached. Thus the force and contact duration produced by full penetration tests are lower than those produced by partial penetration cases.

(c) Comparison of post-impact damage patterns

Figure 6.41 shows the comparison of experimentally obtained and FE predicted post impact damage patterns of ballistic impact tests for (a) non-hybrid GL impacted at 391 m/s, (b) hybrid GL/GR/GL impacted at 406.4 m/s, (c) hybrid GR/GL/GR impacted at 406 m/s and (d) non-hybrid GR impacted at 391 m/s. The finite element models successfully predicted the damage observed during the experiments. The significant delamination between dissimilar layers during the ballistic impact tests of hybrid composite was predicted by the finite element model. The broken fibers appeared at the tension side of the experimental pictures for all lay-up sequences, but were not seen in the FE prediction. This is because of the strain based element erosion criterion used in the FE model. The area where broken fibers are seen represents failed material. On the other hand the failed elements are eroded and removed from calculation in the FE model.

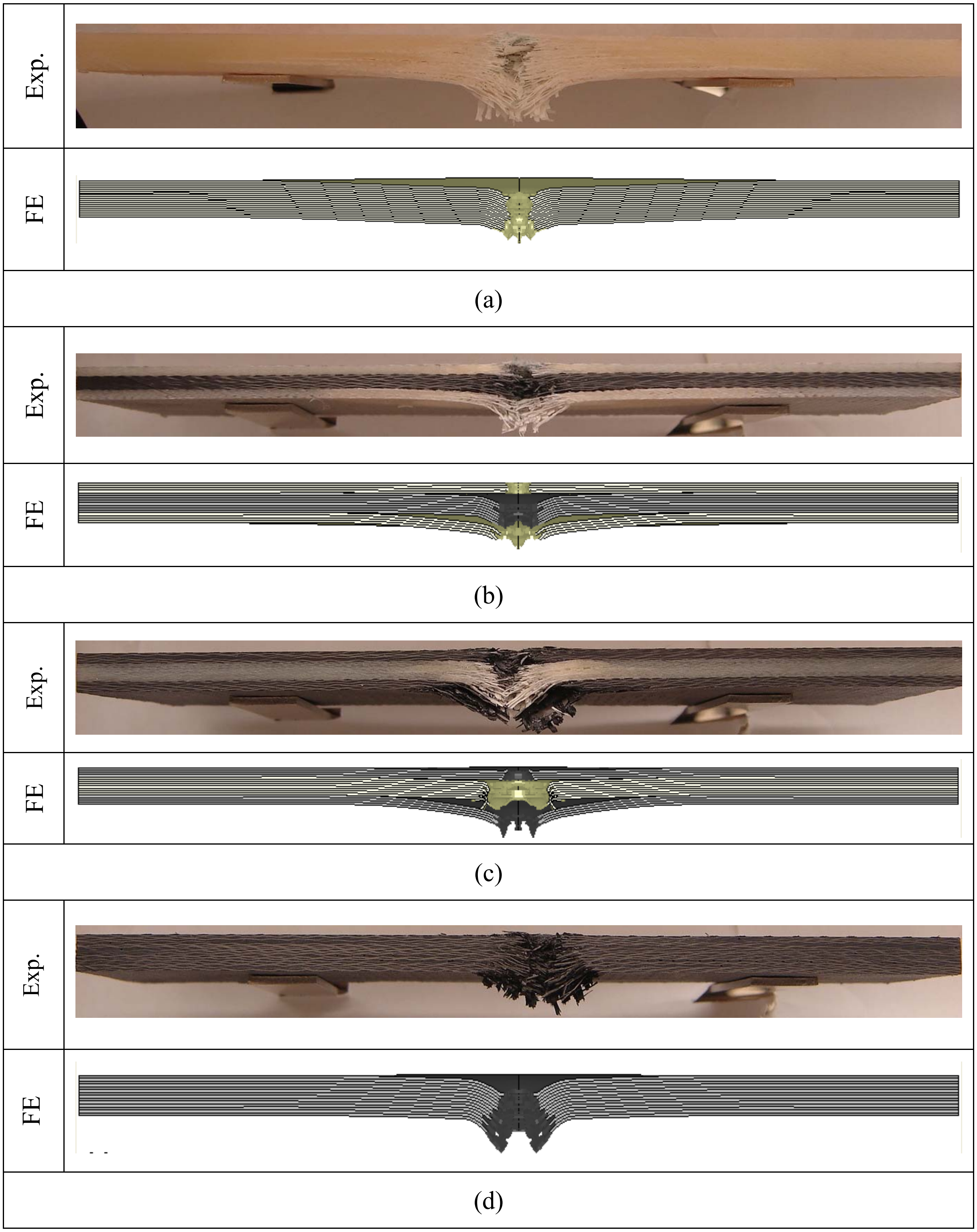

Figure 6.41 Comparisons of post impact damage patterns for (a) non-hybrid GL impacted at 391 m/s, (b) hybrid GL/GR/GL impacted at 406.4 m/s, (c) hybrid GR/GL/GR impacted at 406 m/s and (d) non-hybrid GR impacted at 391 m/s

(d) Determination of ballistic limit velocity, V_{50}

The ballistic limit velocity can be calculated using FE simulations. Two approaches were discussed in section 6.3.1.2. One of the approaches was using the residual velocities of ballistic impact tests. Once the residual velocities were calculated using FE model, the plot of residual velocities versus impact velocities clearly showed the ballistic limit of the composite. The critical impact velocity, V_I, where residual velocity, V_R, became zero was also the ballistic limit velocity, V_{50}. Figure 6.42 shows the V_R- V_I relations. The V_{50} for GL, GL/GR/GL, GR/GL/GR and GR composites was calculated as 378 m/s, 312 m/s, 312 m/s and 276 m/s respectively.

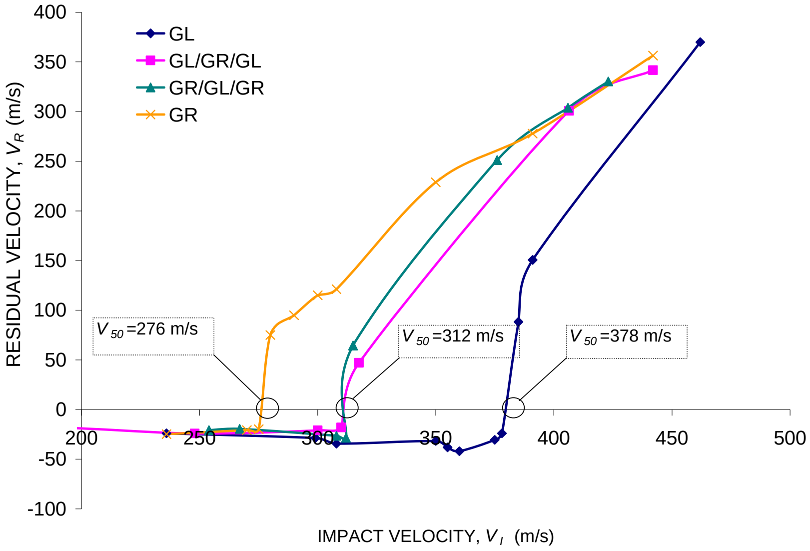

Figure 6.42 FE predicted residual velocity (V_R) and impact velocity (V_I) relations for GL, GL/GR/GL, GR/GL/GR and GR composite panels impacted at above and below V_{50}.

The second approach to calculate ballistic limit velocity, V_{50}, was using the various energies (Section 6.3.1.2). Once the impact energy, transferred energy and residual energy were plotted against impact velocity, the critical impact velocity where the impact energy is equal to the transferred energy and the residual energy is zero, is also the ballistic limit velocity V_{50}. Figure 6.43 shows the impact, residual and transferred energies for GL, GL/GR/GL, GR/GL/GR and GR composites. The ballistic limit velocity for each lay-up sequence is marked in Figure 6.43.

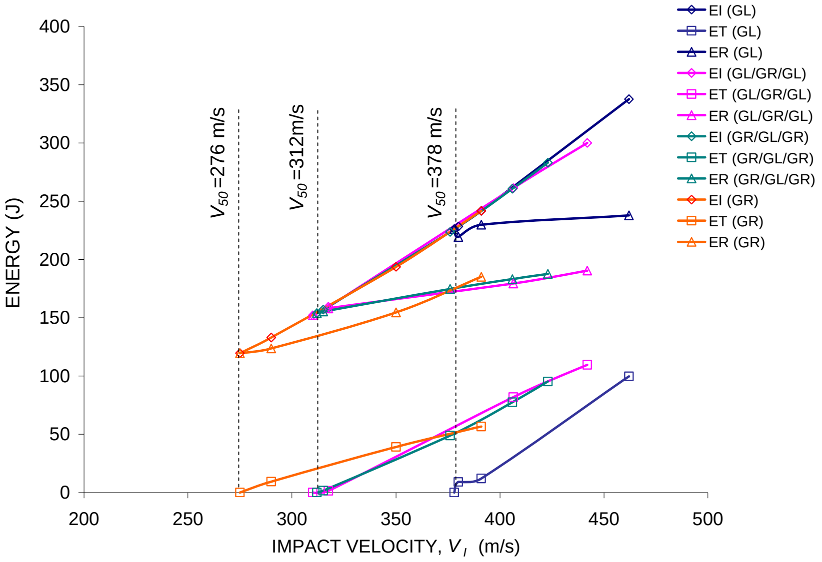

Figure 6.43 FE predicted projectile impact, residual and transferred energies for GL, GL/GR/GL, GR/GL/GR and GR composite panels impacted at above and below V_{50}.

(e) Effect of glass fabric thickness on the ballistic limit of hybrid composites

After validation, the FE model was used to calculate the ballistic limit velocity of the GL/GR/GL hybrid composites with various woven glass thicknesses. A similar study for the low-velocity impact tests was conducted in Section 6.2.1.2. During the ballistic tests, the only GL/GR/GL hybrid composite used in experiments was $GL_{1.58mm}/GR_{3.175mm}/GL_{1.58mm}$. This composite had a ballistic limit higher than that of GR composite and lower than that of GL composite. To be able to understand the effect of glass fabric thickness, more FE models were created. Figure 6.44 shows the non-hybrid GR (a), GL (f), hybrid GL/GR/GL composites with various lay-up sequences (b, c, d) and their weight. Each composite had 6.35 mm final thickness.

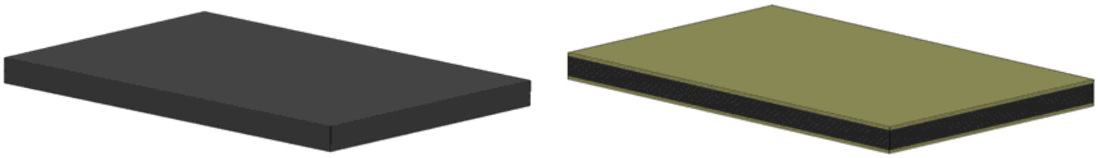

(a) $GR_{6.35mm}$
Weight=143.327gr

(b) $GL_{0.794mm}/GR_{4.76mm}/GL_{0.794mm}$
Weight=150.651gr

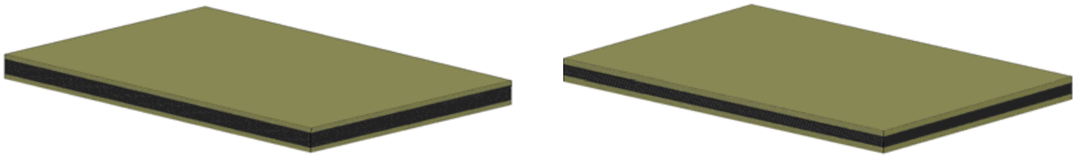

(c) $GL_{1.19mm}/GR_{3.97mm}/GL_{1.19mm}$
Weight=154.312gr

(d) $GL_{1.58mm}/GR_{3.175mm}/GL_{1.58mm}$
Weight=157.974gr

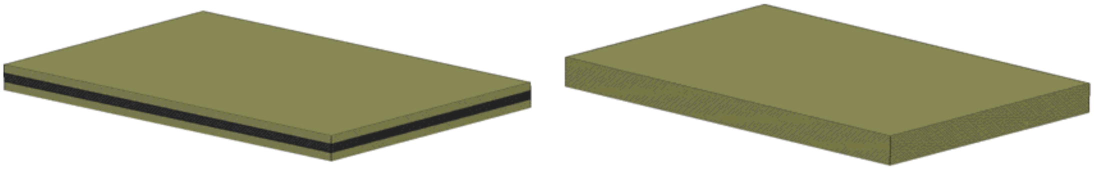

(e) $GL_{1.984mm}/GR_{2.38mm}/GL_{1.984mm}$
Weight=161.636gr

(f) $GL_{6.35mm}$
Weight=172.621gr

Figure 6.44 FEM models for GR (a), GL (f) and GL/GR/GL (b, c, d and e) Composites and their weight

The ballistic limit of composite was calculated using the residual velocity approach. Once the ballistic limit of each lay-up sequence is calculated (Figure 6.45), it was clear that adding the glass fabrics as outer layer increased the ballistic limit of the composite. While the ballistic limit of the GR composite was 276 m/s, adding two layers of glass fabrics as outer layers increased the ballistic limit to 277 m/s. In case of having three, four and five fabrics on each side of the hybrid composite, the ballistic limit velocity was calculated as 285,312 and 335 m/s respectively. The ballistic limit of the GL composites was also calculated as 378 m/s.

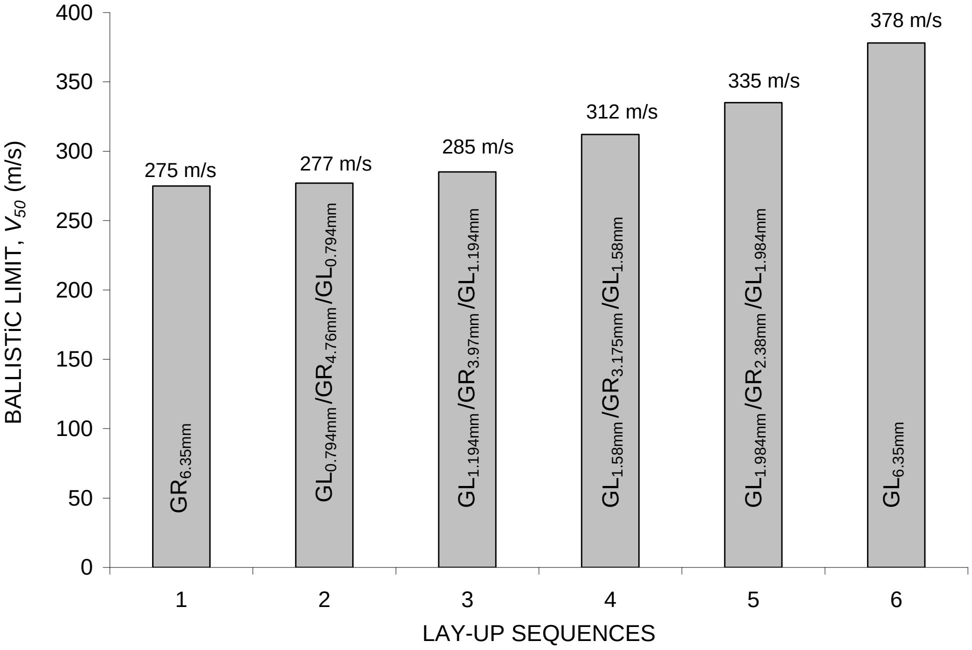

Figure 6.45 The ballistic limit velocity, V_{50} for (1) $GR_{6.35mm}$, (2)$GL_{0.794mm}/GR_{4.76mm}/GL_{0.794mm}$, (3) $GL_{1.19mm}/GR_{3.97mm}/GL_{1.19mm}$, (4) $GL_{1.984mm}/GR_{2.38mm}/GL_{1.984mm}$, (5) $GL_{1.58mm}/GR_{3.175mm}/GL_{1.58mm}$ (f) $GL_{6.35mm}$ composites

6.3.3 Finite element simulations of ballistic tests on woven composite beams

Figure 6.46 shows the finite element simulation model for (a) GL (b) GL/GR/GL (c) GR/GL/GR (d) GL composite beams. Figure 6.46 (e) shows the close-up view of the projectile and beam. It should be noted again, fine mesh around the center and course mesh away from center was created. Due to symmetry, only a quarter of the plate was used. 18 layers for GL, 14 layers for GR and 16 layers for hybrid composites were created. The mesh pattern at the tip of the projectile conformed to the mesh pattern of the composite beam at same location. The elements which were in contact were identical. Having the same mesh pattern at contact location helps the contact algorithm work better.

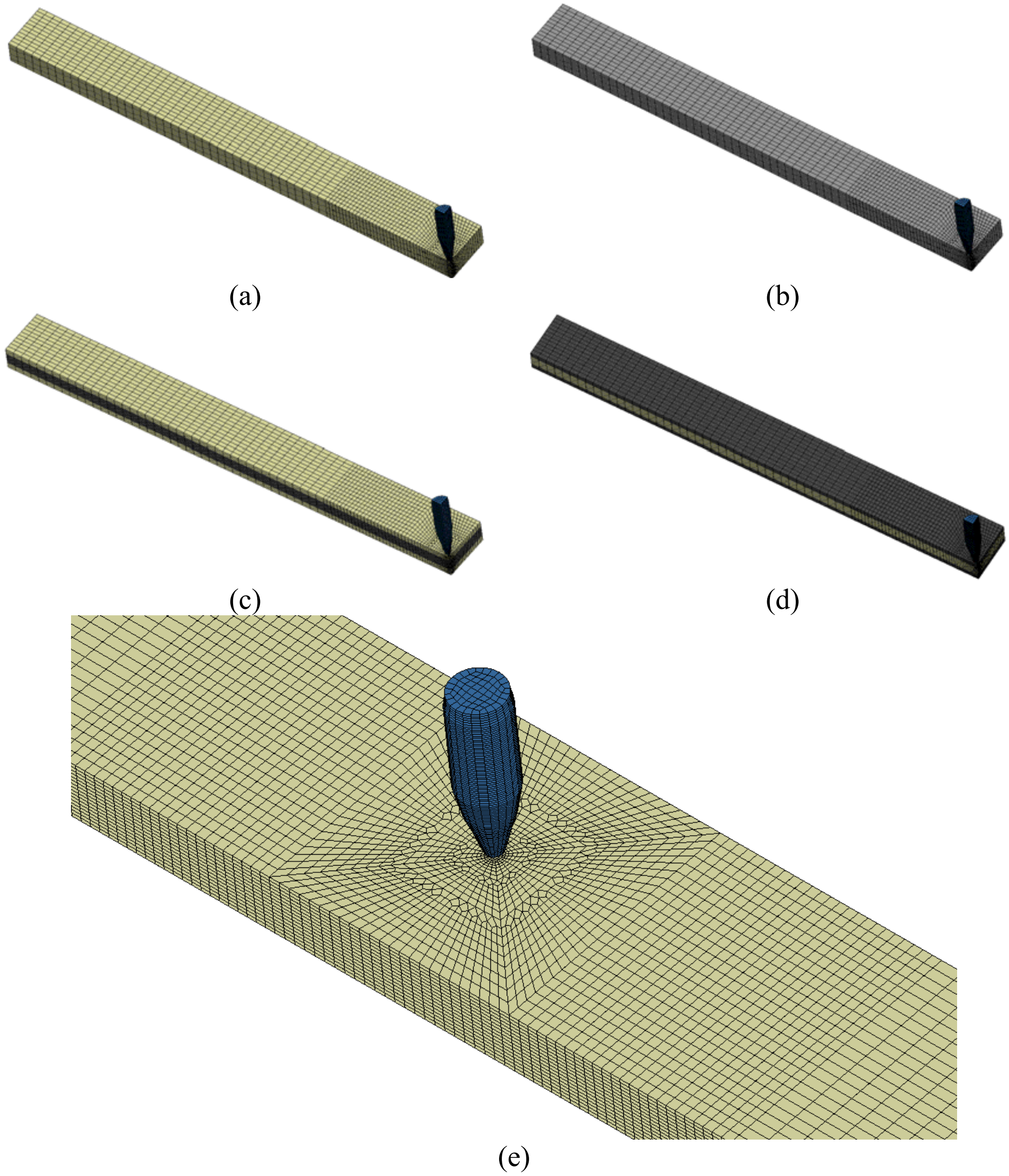

Figure 6.46 Finite element simulation model for composite beams: (a) GL, (b) GL/GR/GL, (c) GR/GL/GR, (d) GR and (e) Close-up view of top surface of composite and projectile

Comparison of Strain-Time histories

Figure 6.47 shows the strain-time histories of GL/GR/GL composite impacted at 308 m/s and GR/GL/GR composite impacted at 442 m/s. The predicted and experimentally obtained strain-time histories agreed well in terms of magnitude of the strains and frequencies. However the initial spike that was predicted by FE model was not captured by experiments.

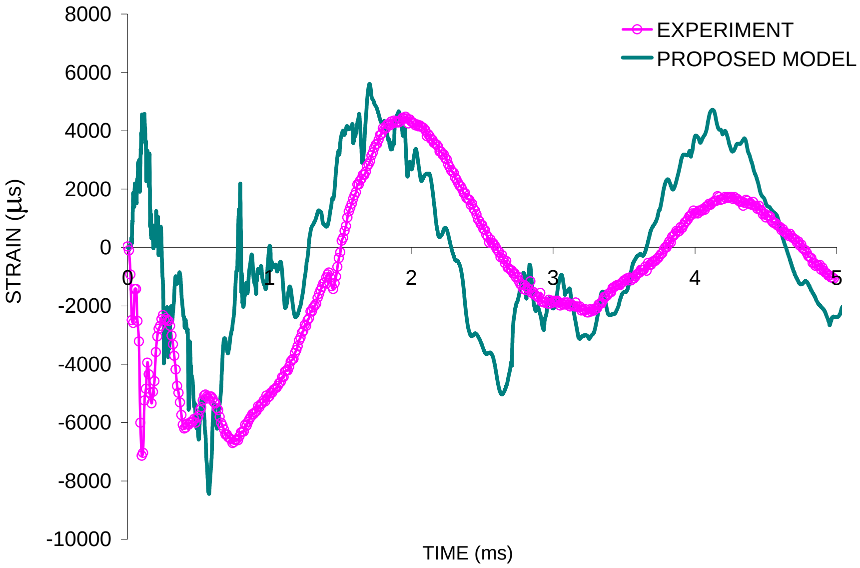

(a)

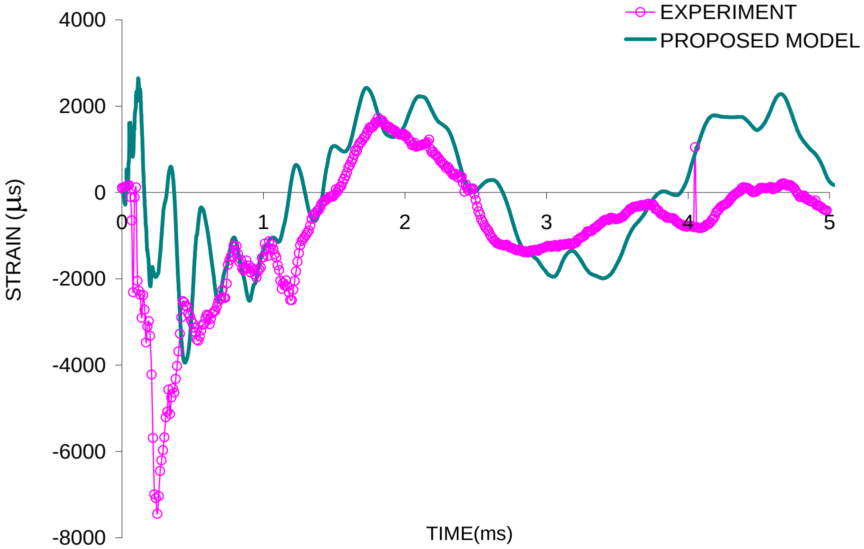

(b)

Figure 6.47 The dynamic strain histories of (a) GL/GR/GL composite beam impacted at 308 m/s (b) GR/GL/GR composite impacted at 442 m/s by a 22 caliber copper projectile

(b) Comparison of Force-Time histories

Figures 6.48 and 6.49 show the predicted force-time histories for GL and GL/GR/GL composites respectively. The contact duration for 130 m/s and 175 m/s tests were almost the same (Fig.6.48). The force-time histories for 175 m/s tests exhibited drop at 0.06 m/s but did not return to zero suddenly. The 236 m/s test where the composite beam broke into two pieces showed sudden drop at 0.055 m/s. The 350 m/s test also produced lower contact force and shorter contact duration. As it was explained earlier, due to excessive material failure the projectile looses its contact with the composite. Thus drops at the force-time histories were observed. If the projectile fully penetrated, it pushes the material ahead or to the side, and contact force quickly returns to zero.

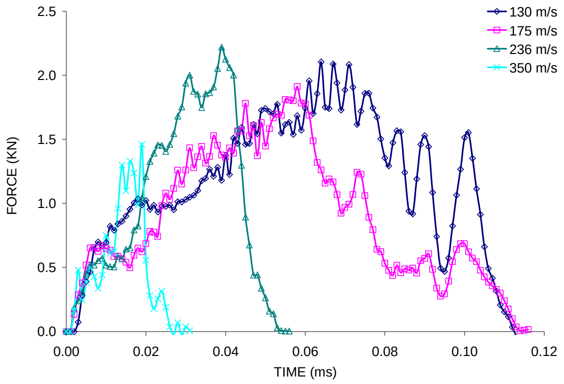

Figure 6.48 Comparison of FE predicted force-time histories GR composite beams impacted by a 22 caliber copper projectile

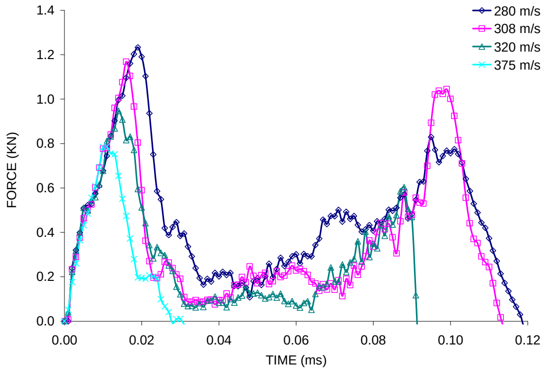

Figure 6.49 Comparison of FE predicted force-time histories GL/GR/GL composite panels impacted by a 22 caliber copper projectile**.**

The force-time histories for hybrid GL/GR/GL composites were quite different than those of non-hybrid GL composites. All partial penetration tests exhibited two stages. The contact forces increased to maximum value, decreased back to around 0.2KN, increased to another maximum value which was lower than the first peak and eventually returned to zero. The delamination between dissimilar layers for the hybrid composite was significant. As soon as the projectile passes through one of the hybrid layers, there might be duration until it reaches the second hybrid layer. During this duration, contact force decreases and it increases back when it reaches the second hybrid layer. The contact force produced by 320 m/s test returned to zero a little earlier. The full penetration case again created the lowest maximum force and contact duration compared to those created by partial penetration cases.

(c) Comparison of post-impact damage patterns

Comparisons were made for two ballistic tests conducted on hybrid composites and one ballistic test conducted on non-hybrid composite. The GL/GR/GL composite impacted at 308 m/s also created significant delamination between dissimilar layers (6.50(a)). The woven graphite fabrics at the inner layers and woven glass fabrics at impact side damaged significantly. The glass fabrics located at the tension side were not damaged and the projectile was stopped by those fabrics. The FE model prediction agreed well with the experimental results. The hybrid GR/GL/GR composite impacted at 317 m/s partially penetrated by projectile (6.50(b)). The optical pictures clearly show that woven graphite fabrics had significant damage but the projectile was stopped by the woven glass fabrics at the inner layers. The delamination between dissimilar layers was extended to the sides. The FE model sufficiently predicted similar damage and delamination of fabrics. The GR composite impacted at 236 m/s broke the composite at impact location (6.50(c)). The FE model simulated the same type of failure. However delamination that was observed during experiment was not reproduced in FE simulations.

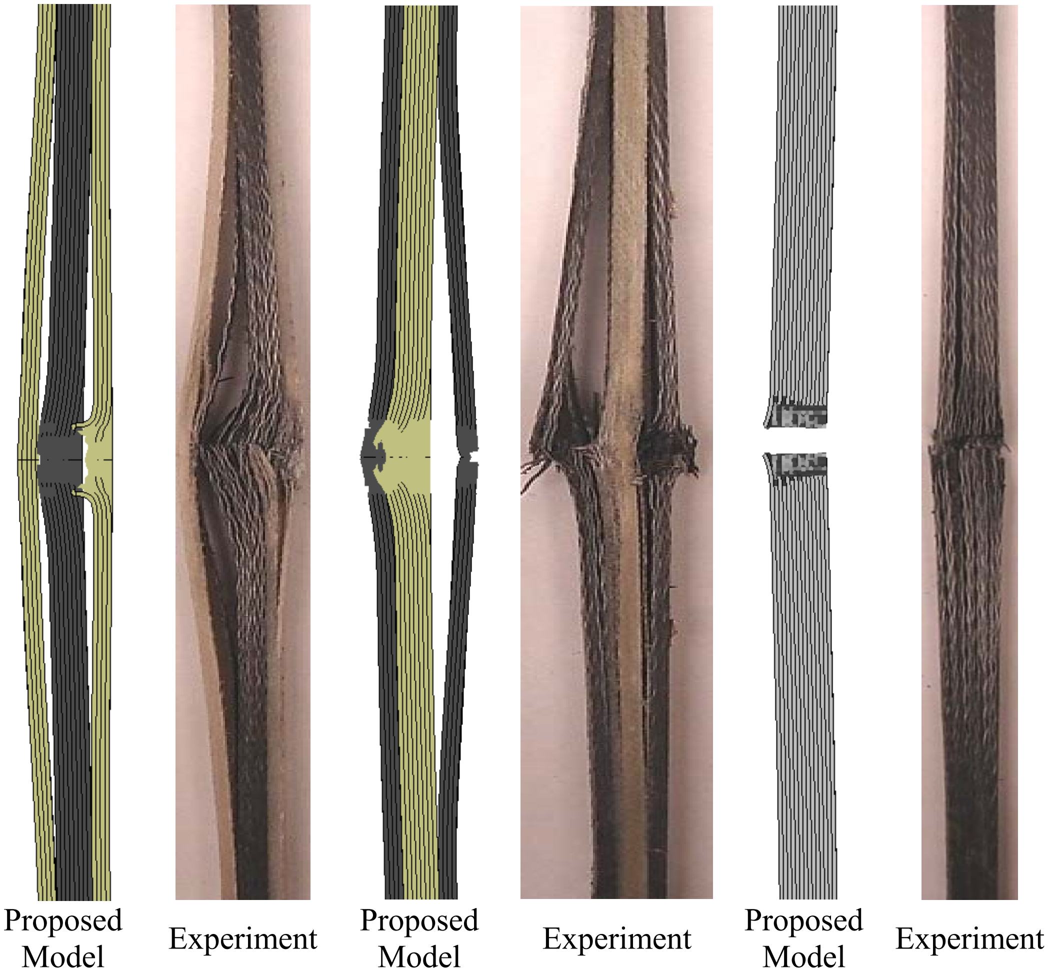

(a) GL/GR/GL composite impacted at 308 m/s

(b) GR/GL/GR composite impacted at 317 m/s

(c) GR composite impacted at 236 m/s

Figure 6.50 Comparisons of post impact damage patterns

(d) Determination of ballistic limit velocity, V_{50}

The ballistic limit of the composite beams was again calculated using residual velocity (Figure 6.51) and residual energy (Figure 6.52) approaches. The ballistic limit velocity, V_{50} for GL, GL/GR/GL, GR/GL/GR and GR composites was 232, 317.5, 317.5 and 395.5 m/s respectively.

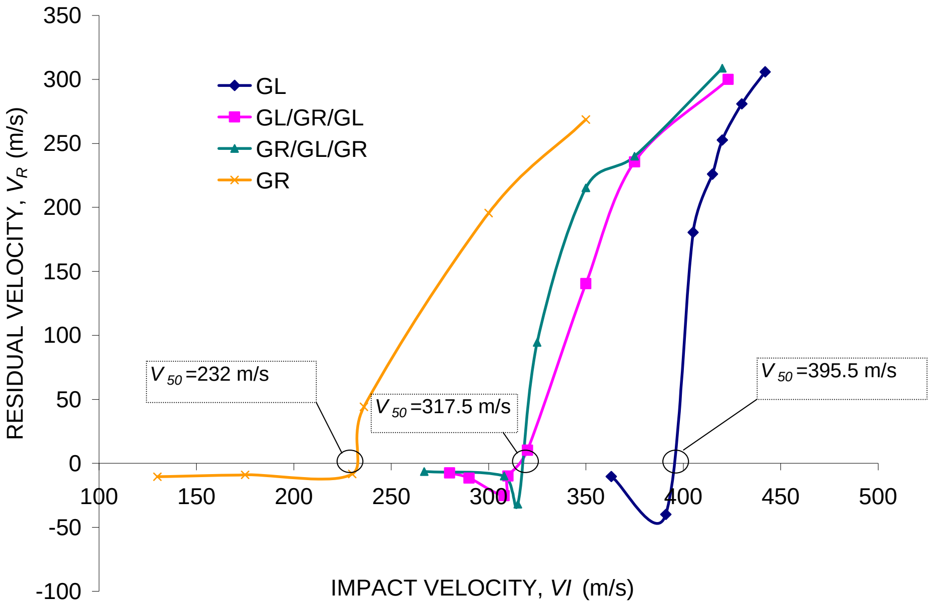

Figure 6.51 FE predicted residual velocity (V_R) and impact velocity (V_I) relations for GL, GL/GR/GL, GR/GL/GR and GR composite beams impacted at above and below V_{50}.

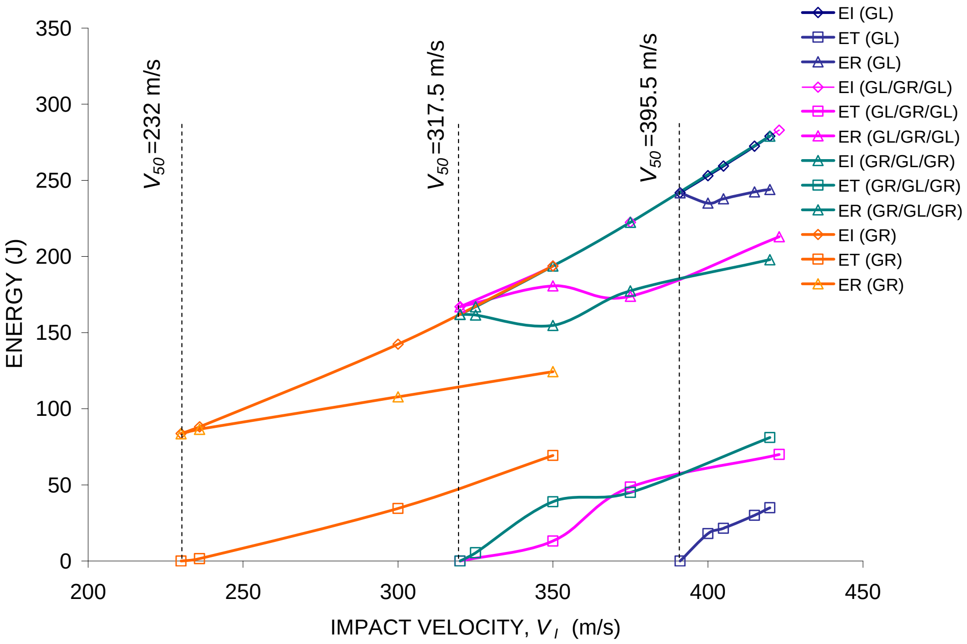

Figure 6.52 FE predicted projectile impact, residual and transferred energies for GL, GL/GR/GL, GR/GL/GR and GR composite beams impacted at above and below V_{50}.

6.3.4 Effect of geometry on the ballistic limit velocity

The experiments and analysis are usually conducted on certain geometries. In real applications, composites of various sizes and geometries may be used. The results obtained using certain geometries might not be exactly the same, when the geometry is changed. Throughout the study, two geometries of composites were ballistically impacted and analyzed using FE modeling. The ballistic limit velocities for both geometries were calculated using FE predicted residual velocities and energies. Once the predicted ballistic limit velocities of the two geometries were compared, the difference at ballistic limit velocity was evident (Figure 6.53). The ballistic limit velocities of GL, GL/GR/GL, GR/GL/GR composite beams were higher than those for composite panels. However the ballistic limit velocity of GR composite beam was lower than that of composite panel. Due to the brittle nature of GR composite, velocities higher than 236 m/s broke the composite at impact location. However GR composite panels did not exhibited breakage at the impact location. This can be explained with the fact that the composite beams had tendency of deflecting more than composite panels due to their smaller cross-section. Thus, some of the projectile energy was used for deflecting the composite. On the other hand, due to the narrow section of beams, delamination especially in hybrid composites was significant. It can be said that significant delamination observed composite beams also uses some of the projectile energy. Thus less energy is left for damaging the composite beam that increases the ballistic limit velocity. However the composite panels do not allow deflection as much as composite beams. Once the projectile impacts the panel, only small amount of energy is used for deflection and more of the energy is used for damaging the composite material.

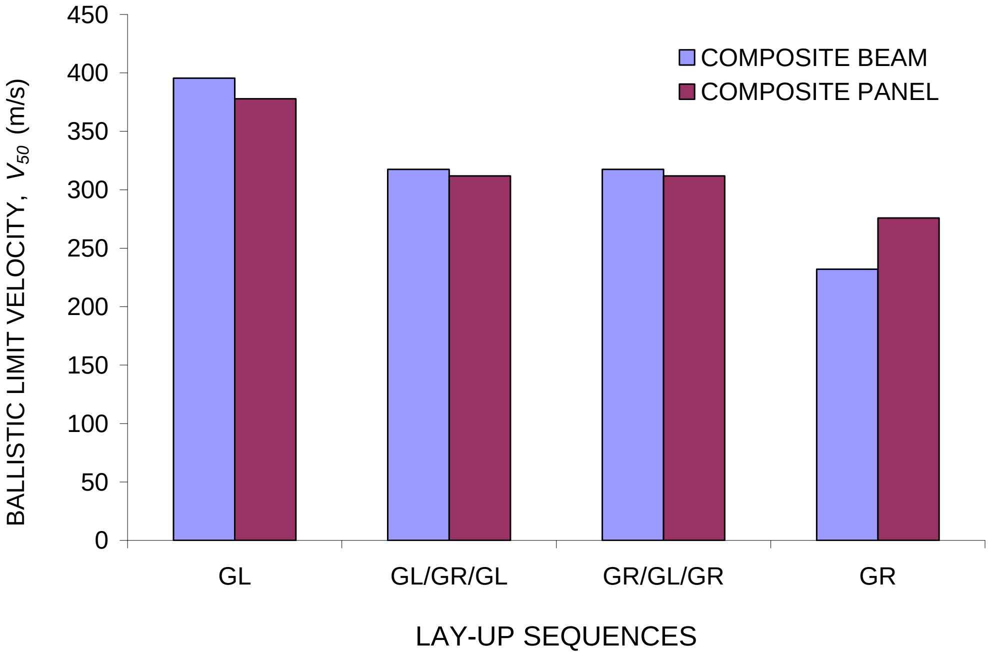

Figure 6.53 Comparison of FE predicted ballistic limit velocities, V_{50}

CONCLUSIONS OF FINITE ELEMENT STUDIES

(a) The proposed FE model successfully simulated the low-velocity and ballistic impact tests conducted on GL, GL/GR/GL, GR/GL/GR and GR composites.

(b) The FE model validated using experimental force, energy, strain histories and post-impact damage patterns. The experimental and FE predicted results agreed sufficiently both for low-velocity impact tests and ballistic tests.

(c) The effect of the woven glass fabrics thickness on the performance of the low-velocity response was simulated using FE model. It was concluded that adding glass fabrics will improve the low-velocity impact response of the GL/GR/GL composite while increasing the weight.

(d) The ballistic limit velocity of composites was calculated using FE predicted residual velocities and residual energies. The ballistic limit of the GL composite was the highest and that of GR composite was the lowest. The ballistic limits of the hybrid composites were the approximately the same and between those for GL and GR composites.

(e) The effect of the woven glass fabrics thickness on the ballistic lmit velocity was studied using an FE model. It was concluded that adding glass fabrics will increase the ballistic limit velocity of the GL/GR/GL composite while increasing its weight.

(f) The effect of the geometry on the ballistic limit velocity of the composites was studied using an FE model. The composite panles (101.66 mm in width and 152.4 mm in length) and composite beams (25.4 mm in width and 254 mm in length) were compared. The ballistic limit of composite beams for all lay-up sequences except for GR composites was higher than the ballistic limit for the composite panels.

GENERAL CONCLUSIONS

(a) Among the four lay-up sequences tested, GL composite was the strongest, while GR was the weakest one. Both hybrid specimens performed better than GR but not as well as GL. Between the two types of hybrid composites, the glass-skin/graphite-core type performed little better than the graphite-skin/glass-core type.

(b) The process of hybridization gives us control of certain parameters such as impact force and damage to the composite. However hybrid composites are prone to delamination especially between dissimilar layers.

(c) Nonlinear orthotropic user-defined damage model was successfully implemented into LS-DYNA. Dynamic force, strain histories and post impact damage patterns obtained from experiment and proposed FE model were in good agreement.

(d) FE predicted force-time histories and damage patterns showed that to reduce impact damage, the surface of GR composites can be covered by glass fabrics. Adding more fabrics improved the performance of the GR composite but this resulted in weight increase.

(e) The impactor shape had significant effect on the low-velocity impact response of woven composites

(f) Ballistic limit velocity V_{50} was estimated using FE model and a limited number of experimental tests.

CONTRIBUTIONS

(a) Novel hybridization technique was used to improve impact response of woven composites. It was shown that adding a glass layer improved the impact performance of the woven graphite composite.

(b) Development of FE model using a material model that is not available in LS-DYNA library. This way the real behavior of the material can be inputted in the FE code.

(c) Ballistic limit velocity V_{50}, which is the major concern for armor applications, can be estimated using the proposed FE model and a limited number of ballistic impact tests.

REFERENCES

1. Jones M. R., Mechanics of Composite Materials, Chapter 1.4., Applications of Composite Materials, Edwards Brothers, Ann Arbor, MI, 1998.

2. Naik K. N., Woven Fabric Composites, Introduction, Technomic Publishing Company Inc., Pennsylvania, 1994.

3. Chou TW. and Ko K. F. , Textile structural composites, Introduction to textile structures and their behavior, Elsevier Science Publishing Company, New York, 1989.

4. Hancox N.L., Introduction to fibre composite hybrids, Ch. 1 in Fibre Composite Hybrid Materials, Hancox NL (Ed), Applied Science Publishers, London, 1981.

5. Reyes G. and Kang H., Mechanical behavior of lightweight thermoplastic fiber–metal laminates, Journal of Materials Processing Technology, Volume 186, Issues 1-3, 7 May 2007, Pages 284-290.

6. Lee S.H., Noguchi H. and Cheong S.K., Tensile properties and fatigue characteristics of hybrid composites with non-woven carbon tissue, International Journal of Fatigue, Volume 24, Issues 2-4, February-April 2002, Pages 397-405.

7. Tsai K.H. , Chiu C. H. and Wu T.H., Fatigue behavior of 3D multi-layer angle interlock woven composite plates, Composites Science and Technology, Volume 60, Issue 2, 1 February 2000, Pages 241-248.

8. Belingardi G. and Cavatorta M.P., Bending fatigue stiffness and strength degradation in carbon–glass/epoxy hybrid laminates: Cross-ply vs. angle-ply specimens, International Journal of Fatigue, Volume 28, Issue 8, August 2006, Pages 815-825.

9. Belingardi G., Cavatorta M.P. and Frasca C., Bending fatigue behavior of glass–carbon/epoxy hybrid composites, Composites Science and Technology, Volume 66, Issue 2, February 2006, Pages 222-232.

10. Ni D.R., Geng L., Zhang J. and Zheng Z.Z., Fabrication and tensile properties of in situ TiBw and TiCp hybrid-reinforced titanium matrix composites based on Ti–B_4CC, Materials Science and Engineering: A, In Press, Corrected Proof, Available online 9 June 2007.

11. Kang T, Shin S. J., Jung K. and Park J. K., Mechanical, thermal and ablative properties of interply continuous/spun hybrid carbon composites, Carbon, Volume 44, Issue 5, April 2006, Pages 833-839.

12. Khatri S.C. and Koczak M.J., Thick-section AS4-graphite/E-glass/PPS hybrid composites: Part I. Tensile Behaviour. Composites Science and Technology, Volume 56, 1996, Pages 181-192.

13. Khatri S.C. and Koczak M.J., Thick-section AS4-graphite/E-glass/PPS hybrid composites: Part II. Flexural response. Composites Science and Technology, Volume 56, Issue 4, 1996, Pages 473-482.

14. Wan Y.Z., Chen G.C., Huang Y., Li Q.Y., Zhou F.G., Xin J.Y. and Wang Y.L., Characterization of three-dimensional braided carbon/Kevlar hybrid composites for orthopedic usage, Materials Science and Engineering A, Volume 398, Issues 1-2, 25 May 2005, Pages 227-232.

15. Park R. and Jang J., The effects of Hybridization on the mechanical performance of aramid/polyethylene intraply fabric composites, Composites Science and Technology, Volume 58, Issue 10, October 1998, Pages 1621-1628.

16. Muto N., Arai Y., Shin S. G., Matsubara H., Yanagida H., . Sugita M and T. Nakatsuji, Hybrid composites with self-diagnosing function for preventing fatal fracture Composites Science and Technology, Volume 61, Issue 6, May 2001, Pages 875-883.

17. Bosze E.J., Alawar A., Bertschger O., Tsai Y. and Nutt S.R., High-temperature strength and storage modulus in unidirectional hybrid composites, Composites Science and Technology, Volume 66, Issue 13, October 2006, Pages 1963-1969.

18. Dlouhy I., Chlup Z., Boccaccini D. N., Atiq S. and Boccaccini A. R., Fracture behaviour of hybrid glass matrix composites: thermal ageing effects, Composites Part A: Applied Science and Manufacturing, Volume 34, Issue 12, December 2003, Pages 1177-1185.

19. Schmitt-Thomas Kh.G., Yang Z.G. and Malke R., Failure behavior and performance analysis of hybrid-fiber reinforced PAEK composites at high temperature, Composites Science and Technology, Volume 58, Issue 9, September 1997, Pages 1509-1518.

20. Lipetzky P., Dvorak G.J. and Stoloff N.S., Tensile properties of a SiC/SiC composite Materials Science and Engineering A, Volume 216, Issues 1-2, 15 October 1996, Pages 11-19.

21. Shan Y., Lai K.F., Wan K.T., Liao K., Static and Dynamic Fatigue of Glass-Carbon Hybrid Composites in Fluid Environment, Journal of Composite Materials, Vol.36, No.02/2002.

22. Shan Y., Liao K., Environmental fatigue of unidirectional glass-carbon fiber reinforced hybrid composite. Composites: Part B 32 (2001) 355-363.

23. Zhang X.X., Deng C.F., Shen Y.B., Wang D.Z. and Geng L., Mechanical properties of ABOw+MWNTs/Al hybrid composites made by squeeze cast technique, Materials Letters, Volume 61, Issue 16, June 2007, Pages 3504-3506.

24. Mäder E., Gao S., Plonka R. and Wang J., Investigation on adhesion, interphases, and failure behaviour of cyclic butylene terephthalate (CBT)/glass fiber composites, Composites Science and Technology, In Press, Corrected Proof, Available online 10 May 2007.

25. Li G., Experimental study of hybrid composite cylinders, Composite Structures, Volume 78, Issue 2, April 2007, Pages 170-181.

26. Gajiwala H. M., Vaidya U. K., Sodah S. A. and Jeelani S., Hybridized resin matrix approach applied for development of carbon/carbon composites, Carbon, Volume 36, Issues 7-8, 1998, Pages 903-912.

27. Hussain M., Nakahira A. and Niihara K., Mechanical property improvement of carbon fiber reinforced epoxy composites by Al2O3 filler dispersion, Materials Letters, Volume 26, Issue 3, February 1996, Pages 185-191.

28. Hitchen S. A. and Kemp R. M. J., Development of novel cost effective hybrid ply carbon-fibre composites, Composites Science and Technology, Volume 56, Issue 9, 1996, Pages 1047-1054.

29. Gupta M., Lai M.O. and Lim C.Y.H., Development of a novel hybrid aluminum-based composite with enhanced properties, Journal of Materials Processing Technology, Volume 176, Issues 1-3, 6 June 2006, Pages 191-199.

30. Ho K. F., Gupta M. and Srivatsan T. S., The mechanical behavior of magnesium alloy AZ91 reinforced with fine copper particulates, Materials Science and Engineering A, Volume 369, Issues 1-2, 25 March 2004, Pages 302-308.

31. Wong W.L.E., Gupta M. and Lim C.Y.H., Enhancing the mechanical properties of pure aluminum using hybrid reinforcement methodology, Materials Science and Engineering: A, Volume 423, Issues 1-2, 15 May 2006, Pages 148-152.

32. Ko B.C.l and Yoo Y.C., The effect of aging treatment on the microstructure and mechanical properties of AA2124 hybrid composites reinforced with both SiC whiskers and SiC particles, Composites Science and Technology, Volume 59, Issue 5, April 1999, Pages 775-779

33. Thwe M.M., Liao K., Effects of environmental aging on the mechanical properties of bamboo-glass fiber reinforced polymer matrix hybrid composites, Composites: Part A 33 (2002) 43-52.

34. Velmurugan R. and Manikandan V., Mechanical properties of Palmyra / glass fiber hybrid composites Composites Part A: Applied Science and Manufacturing, In Press, Accepted Manuscript, Available online 11 July 2007.

35. Thwe M. M. and Liao K., Effects of environmental aging on the mechanical properties of bamboo–glass fiber reinforced polymer matrix hybrid composites, Composites Part A: Applied Science and Manufacturing, Volume 33, Issue 1, January 2002, Pages 43-52.

36. Jacob M., Thomas S. and K. Varughese T., Mechanical properties of sisal/oil palm hybrid fiber reinforced natural rubber composites, Composites Science and Technology, Volume 64, Issues 7-8, June 2004, Pages 955-965.

37. Paiva C. Z. Júnior, Carvalho L. H. , Fonseca V. M., Monteiro S. N. and d'Almeida J. R. M., Analysis of the tensile strength of polyester/hybrid ramie–cotton fabric composites Polymer Testing, Volume 23, Issue 2, April 2004, Pages 131-135.

38. Velde K. V. and Kiekens P., Effect of material and process parameters on the mechanical properties of unidirectional and multidirectional flax/polypropylene composites, Composite Structures, Volume 62, Issues 3-4, 2003, Pages 443-448.

39. Arbelaiz A., Fernández B., Cantero G., Llano-Ponte R., Valea A. and Mondragon I., Mechanical properties of flax fiber/polypropylene composites. Influence of fiber/matrix modification and glass fiber hybridization, Composites Part A: Applied Science and Manufacturing, Volume 36, Issue 12, December 2005, Pages 1637-1644.

40. Meguid S. A. and Sun Y., On the tensile and shear strength of nano-reinforced composite interfaces, Materials & Design, Volume 25, Issue 4, June 2004, Pages 289-296.

41. Yao W., Li J. and Wu K., Mechanical properties of hybrid fiber-reinforced concrete at low fiber volume fraction, Cement and Concrete Research, Volume 33, Issue 1, January 2003, Pages 27-30.

42. Scida D., Aboura Z., Benzeggagh M. L. and Bocherens E., Prediction of the elastic behaviour of hybrid and non-hybrid woven composites, Composites Science and Technology, Volume 57, Issue 12, 16 January 1998, Pages 1727-1740.

43. Ganesh V.K. and Naik N.K., Failure behavior of plain weave fabric laminates under on-axis uniaxial tensile loading: I-Laminate Geometry. Journal of Composite Material.1996, 30(16), 1748-1778.

44. Ganesh V.K. and Naik N.K., Failure behavior of plain weave fabric laminates under on-axis uniaxial tensile loading: II-Analytical Geometry. Journal of Composite Material. Volume 30, Issue 16, 1996, 1779-1782.

45. Ganesh V.K. and Naik N.K., Failure behavior of plain weave fabric laminates under on-axis uniaxial tensile loading: III-Effect of fabric Geometry. Journal of Composite Material, Volume 30, Issue 16, 1996, 1823-1856.

46. Falzon P.J., Herszberg I. and Karbhari V., Effects of compaction on the stiffness and strength of plain weave fabric RTM composites. Journal of Composite Material, Volume 30, Issue 11, 1996,Pages 1210-1247.

47. Falzon P.J., Herszberg I. and Bakeri A.A., Stiffness analysis of textile composites. Presented at 5th Australian Aeronautical Conference, Melbourne, 1193, pp. 219-224.

48. Ishakawa T. and Chou T.W., Stiffnes and strength behaviour of woven fabric composites. Journal of Material Science. Volume 17, 1982, Pages 3211-3220.

49. Ishakawa T. and Chou T.W., Elastic behavior of woven hybrid composites. Journal of Composite Materials, Volume 16, 1982, Pages 2-19.

50. Ishakawa T. and Chou T.W., One dimensional micromechanical analysis of woven fabric composites. AIAA J., , Volume 21, Issue 12, 1983, Pages 1714-1721.

51. Ishakawa T. and Chou T.W., In-plane thermal expansion and thermal bending coefficients of fabric composites. Journal of Composite Materials. Volume 17, 1983, Pages 92-104.

52. Ishakawa T., Matsushima M., Hyashi Y., and Chou T.W., Experimental confirmation of the theory of elastic moduli of fabric composites. Journal of Composite Materials. Volume 19, 1985,Pages 443-458.

53. Peng X.Q. and Cao J., A continuum mechanics-based non-orthogonal constitutive model for woven composite fabrics, Composites Part A: Applied Science and Manufacturing, Volume 36, Issue 6, June 2005, Pages 859-874.

54. Huang Z.M. and Ramakrishna S., Modeling inelastic and strength properties of textile laminates: a unified approach, Composites Science and Technology, Volume 63, Issues 3-4, February-March 2003, Pages 445-466.

55. Huang Z. M., The mechanical properties of composites reinforced with woven and braided fabrics, Composites Science and Technology, Volume 60, Issue 4, 1 March 2000, Pages 479-498.

56. Yu W. R., Pourboghrat F., Chung K., Zampaloni M. and Kang T. J.
Non-orthogonal constitutive equation for woven fabric reinforced thermoplastic composites, Composites Part A: Applied Science and Manufacturing, Volume 33, 2002, Pages 1095-1105.

57. Karakuzu R., Gülem T. and İçten B. M., Failure analysis of woven laminated glass–vinylester composites with pin-loaded hole, Composite Structures, Volume 72, Issue 1, January 2006, Pages 27-32.

58. Içten B. M. and Karakuzu. R., Progressive failure analysis of pin-loaded carbon–epoxy woven composite plates, Composites Science and Technology, Volume 62, Issue 9, July 2002, Pages 1259-1271.

59. Okutan B., Aslan Z. and Karakuzu R.,A study of the effects of various geometric parameters on the failure strength of pin-loaded woven-glass-fiber reinforced epoxy laminate, Composites Science and Technology, Volume 61, 2001, Pages 1491-1497.

60. Carvelli V. and Poggi C., A homogenization procedure for the numerical analysis of woven fabric composites, Composites Part A: Applied Science and Manufacturing, Volume 32, 2001, Pages 1425-1432.

61. Ge D. and Gu M., Mechanical properties of hybrid reinforced aluminum based composites, Materials Letters, Volume 49, Issue 6, July 2001, Pages 334-339.

62. Lin H. J. and Tsai C. C., Failure analysis of bolted connections of composites with drilled and moulded-in hole, Composite Structures, Volume 30, Issue 2, 1995, Pages 159-168.

63. Zinoviev P.A., Smerdov A.A., Ultimate properties of unidirectional fiber composites, Composites Science and Technology, Volume 59, 1999, Pages 625-634.

64. Tabiei, Y. Jiang, Woven fabric composite material model with material nonlinearity for nonlinear finite element simulation, International Journal of Solids and Structures, Volume 36, 1999, Pages 2757-2771.

64. Aminjikarai B., Tabiei A., A strain-rate dependent 3-D micromechanical model for finite element simulations of plain weave composite structures Composite Structures, Volume 81, 2007, Pages 407–418.

65. Tabiei A., Ivanov I., Materially and geometrically non-linear woven composite micro-mechanical model with failure for finite element simulations. International Journal of Non-Linear Mechanics, Volume 39, 2004, Pages 175– 188.

66. Tabiei A., Yi W., Comparative study of predictive methods for woven fabric composite elastic properties Composite Structures, Volume 58, 2002, Pages 149–164.

67. Ivanov I., Tabiei A., Three dimensional computational micro-mechanic model for woven fabric composites, Composite Structures, Volume 54, 2001, Pages 489-496.

68. Jiang Y., Tabiei A., Simitses G.J., A novel micromechanics-based approach to the derivation of constitutive equations for local/global analysis of a plain-weave fabric composite. Composites Science and Technology, Volume 60, 2000,Pages 1825-1833.

69. Naik N.K. , Shrirao P., Composite structures under ballistic impact, Composite Structures, Volume 66, 2004, Pages 579–590.

70. Starratt D., Sanders T., Cepus E. , Poursartip A., Vazir R., An effcient method for continuous measurement of projectile motion in ballistic impact experiments International Journal of Impact Engineering, Volume 24,2000, Pages 155-170.

71. Belingardi G., Vadori R., Low velocity impact tests of laminate glass-fiber-epoxy matrix composite material plates, International Journal of Impact Engineering, Volume 27,2002, Pages 213–229

72. Mili F., Necib B., Impact behavior of cross-ply laminated composite plates under low Velocities, Composite Structures, Volume 51, 2001, Pages 237-244.

73. Robb MD, Arnold WS, Marshall IH. The damage tolerance of GRP laminates under biaxial pre-stress. Composite Structures, Volume 32, 1995, Pages 141–149.

74. Alcock B., Cabrera N.O., Barkoula N.-M. , Peijs T., Low velocity impact performance of recyclable all-polypropylene composites, Composites Science and Technology,Volume 66, 2006, Pages 1724–1737.

75. Sutherland L.S., Guedes Soares C., Impact characterization of low fibre-volume glass reinforced polyester circular laminated plates, International Journal of Impact Engineering, Volume 31, 2005, Pages 1–23.

76. Caprino G., Spataro G. and Luongo S. D., Low-velocity impact behaviour of fibreglass–aluminium laminates, Composites Part A: Applied Science and Manufacturing, Volume 35, Issue 5, May 2004, Pages 605-616.

77. Dhakal H.N., Zhang Z.Y., Richardson M.O.W., Errajhi O.A.Z., The low velocity impact response of non-woven hemp fibre reinforced unsaturated polyester composites, Composite Structures, Composite Structures, Volume 81, Issue 4, December 2007, Pages 559-567.

78. Lin J.C., Chang L.C., Nien M.H., Ho H.L., Mechanical behavior of various nanoparticle filled composites at low-velocity impact, Composite Structures, Volume 74 2006, Pages 30–36.

79. Sun CT, Chattopadhyay S., Dynamic response of anisotropic laminated plates under initial stress to impact of a mass. Journal of Applied Mechanics, Volume 42,1975, Pages 693–708.

80. Sun CT, Chen JK. On the impact of initially stressed composite laminates. Journal of Composite Materials, Volume 19, 1985, Pages 490–504.

81. Whittingham B., Marshall I.H., Mitrevski T., Jones R., The response of composite structures with pre-stress subject to low velocity impact damage, Composite Structures, Volume 66,2004, Pages 685–698.

82. Ulven C.A, Vaidya U.K., Post-fire low velocity impact response of marine grade sandwich composites, Composites Part A, Volume 37, 2006, Pages 997–1004.

83. Anderson T., Madenci E., Experimental investigation of low-velocity impact characteristics of sandwich composites, Composite Structures, Volume 50, 2000, Pages 239-247.

84. Gustin J., Joneson A., Mahinfalah M., Stone J., Low velocity impact of combination Kevlar/carbon fiber sandwich composites, Composite Structures, Volume 69,200, Pages 396–406.

85. Mines R. A. W., Worrallt C. M. and Gibson A.G., Low velocity perforation behaviour of polymer composite sandwich panels, International Journal of Impact Engineering, Vol. 21, No. 10,199, Pages 855–879,

86. Schubel P.M., Luo J.J., Isaac M. Daniel, Low velocity impact behavior of composite sandwich panels, Composites Part A, Volume 36, 2005, Pages 1389–1396.

87. Serrano-Perez J.C., Vaidya U. K., Uddin N., Low velocity impact response of autoclaved aerated concrete/CFRP sandwich plates, Composite Structures, Volume 80, 2007, Pages 621–630.

88. Jiang D., Shu D., Local displacement of core in two-layer sandwich composite structures subjected to low velocity impact, Composite Structures, Volume 71, 2005, Pages 53–60.

89. Kim J.S., Chung S.K., A study on the low-velocity impact response of laminates for composite railway body shells, Composite Structures, Volume 77, 2007, Pages 484–492.

90. Avila A.F., Soares M.I., Neto A. S., A study on nanostructured laminated plates behavior under low-velocity impact loadings, International Journal of Impact Engineering, Volume 34,2007, Pages 28–41.

91. Belingardi G., Vadori R., Influence of the laminate thickness in low velocity impact behavior of composite material plate. Composite Structures, Volume 61, 2003, Pages 27–38.

92. Sutherland L.S., Guedes Soares C., Effect of laminate thickness and of matrix resin on the impact of low fibre-volume, woven roving E-glass composites, Composites Science and Technology, Volume 64, 2004, Pages 1691–1700.

93. Sutherland L. S. and Soares C.G., Impact tests on woven-roving E-glass/polyester laminates, Composites Science and Technology, Volume 59, Issue 10, August 1999, Pages 1553-1567.

94. Aslan Z., Karakuzu R., Okutan B., The response of laminated composite plates under low-velocity impact loading, Composite Structures, Volume 59, 2003, Pages 119–127.

95. Cantwell W.J., Geometrical effects in the low velocity impact response of GFRP Composites Science and Technology, Volume 67, 2007, Pages 1900–1908.

96. Atas C. and Liu D., Impact response of woven composites with small weaving angles International Journal of Impact Engineering, In Press, Corrected Proof, Available online 8 January 2007.

97. Imieliska K. and Guillaumat L., The effect of water immersion ageing on low-velocity impact behaviour of woven aramid–glass fibre/epoxy composites. Composites Science and Technology, Volume 64, Issues 13-14, October 2004, Pages 2271-2278.

98. Kim J.K., Sham M.L., Sohn M.S. and Hamada H., Effect of hybrid layers with different silane coupling agents on impact response of glass fabric reinforced vinylester matrix composites. Polymer, Volume 42, Issue 17, August 2001, Pages 7455-7460.

99. Bahei-El-Din Y.A., Zikry M.A., Impact-induced deformation fields in 2D and 3D woven composites, Composites Science and Technology, Volume 63, 2003, 923–942.

100. Hosur M.V., Adbullah M. and Jeelani S., Studies on the low-velocity impact response of woven hybrid composites, Composite Structures, Volume 67, Issue 3, March 2005, Pages 253-262.

101. Shim V.P.W. and Yang L.M., Characterization of the residual mechanical properties of woven fabric reinforced composites after low-velocity impact, International Journal of Mechanical Sciences, Volume 47, Issues 4-5, April-May 2005, Pages 647-665.

102. Qiu Y., Xu W., Wang Y., Zikry M.A. and Mohamed M.H., Fabrication and characterization of three-dimensional cellular-matrix composites reinforced with woven carbon fabric, Composites Science and Technology, Volume 61, Issue 16, December 2001, Pages 2425-2435.

103. Kinsey A., Saunders D.E.J. and Soutis C., Post-impact compressive behaviour of low temperature curing woven CFRP laminates, Composites, Volume 26, Issue 9, September 1995, Pages 661-667.

104. Shim V.P.W., Yang L.M., Characterization of the residual mechanical properties of woven fabric reinforced composites after low-velocity impact, International Journal of Mechanical Sciences, Volume 47, 2005, Pages 647–665.

105. Wang X., Hu B., Feng Y., Liang F., Mo J., Xiong J. and Qiu Y., Low Velocity Impact Properties of 3D Woven Basalt/ Aramid Hybrid Composites, Composites Science and Technology, In Press, Accepted Manuscript, Available online 28 June 2007.

106. Khojin A.S., Mahinfalah M., Bashirzadeh R. and Freeman B., Temperature effects on Kevlar/hybrid and carbon fiber composite sandwiches under impact loading, Composite Structures, Volume 78, Issue 2, April 2007, Pages 197-206.

107. Hosur M.V., Adbullah M. and Jeelani S., Studies on the low-velocity impact response of woven hybrid composites, Composite Structures, Volume 67, Issue 3, March 2005, Pages 253-262.

108. Hosur M.V., Abdullah M. and Jeelani S., Manufacturing and low-velocity impact characterization of hollow integrated core sandwich composites with hybrid face sheets Composite Structures, Volume 65, Issue 1, July 2004, Pages 103-115.

109. Khalili M.R., Malekzadeh K., Mittal R.K., Effect of physical and geometrical parameters on transverse low-velocity impact response of sandwich panels with a transversely flexible core., Composite Structures, Volume 77, 2007, Pages 430–443.

110. Shivakumar, K.N., Elber, W., and Illg, W. Prediction of impact force and duration due to low-velocity impact on circular composite laminates. J. Applied Mechanics, Volume 52, 1985, Pages 674-680.

111. Abrate, S. Modeling of impacts on composite structures. Composite Structures, Volume 51, 2001, Pages 129-138.

112. Abrate, S. Impact on Composite Structures. Cambridge University Press, Cambridge, UK, 1998.

113. Jime´nez O., Sullcahuaman J.A., Sa´nchez-Soto M., Martinez A.B., Low energy impact evaluation using non conservative models, International Journal of Solids and Structures, Volume 42,2005, Pages 5758–5764.

114. Christoforou A.P., Elsharkawy A.A., Guedouar L.H., An inverse solution for low-velocity impact in composite plates, Computers and Structures, Volume 79,2001, Pages 2607-2619.

115. Davies G.A.O., Hitchings D., Wang J., Prediction of threshold impact energy for onset of delamination in quasi-isotropic carbon/epoxy composite laminates under low-velocity impact, Composites Science and Technology, Volume 60,2000, Pages 1-7.

116. Davies GAO, Zhang X. Impact damage prediction in carbon composite structures. International Journal of Impact Engineering, Volume 16, 1995, Pages149-70.

117. Malekzadeh K., Khalilib M.R., Mittal R.K., Response of composite sandwich panels with transversely flexible core to low-velocity transverse impact: A new dynamic model International Journal of Impact Engineering, Volume 34, 2007, Pages 522–543

118. Chun L and Lam K.Y.,Dynamic Response of Fully Clamped laminated composite plates subjected to low-velocity impact of a mass, International Journal of Solids Structures, Volume 35, No. 11, 1998, Pages 963- 979.

119. Choi I. H., Lim C.H., Low-velocity impact analysis of composite laminates using linearized contact law, Composite Structures, Volume 66,2004, Pages 125–132.

120. Guinarda S., Allix O., D. Degeorgesa G., Vineta A., A 3D damage analysis of low-velocity impacts on laminated composites, Composites Science and Technology, Volume 62,2002, Pages 585–589.

121. Palazotto P.A.N., Herup E.J., Gummadi L.N.B., Finite element analysis of low-velocity impact on composite sandwich, Composite Structures, Volume 49,2000, Pages 209-227.

122. Moura M.F.S.F., Goncalves J.P.M., Modelling the interaction between matrix cracking and delamination in carbon–epoxy laminates under low velocity impact, Composites Science and Technology, Volume 64, 2004, Pages 1021–1027.

123. Luo RK, Green ER, Morrison CJ., Impact damage analysis of composite plates. International Journal of Impact Engineering, Volume 22, 1999, Pages 435–47.

124. Her S.C., Liang Y.C., The finite element analysis of composite laminates and shell structures subjected to low velocity impact, Composite Structures, Volume 66, 2004, Pages 277–285.

125. Meo M., Antonucci E. , Duclaux P. , Giordano M., Finite element simulation of low velocity impact on shape memory alloy composite plates, Composite Structures, Volume 71, 2005, Pages 337–342

126. Meo M., Morris A.J., Vignjevic R., Marengo G., Numerical simulations of low-velocity impact on an aircraft sandwich panel, Composite Structures, Volume 62, 2003, Pages 353–360.

127. Hosseinzadeh R., Shokrieh M.M., Lessard L., Damage behavior of fiber reinforced composite plates subjected to drop weight impacts, Composites Science and Technology Volume 66, 2006, Pages 61–68.

128. Li C.F., Hub N., Yina Y.J., Sekinec H., Fukunaga H., Low-velocity impact-induced damage of continuous fiber-reinforced composite laminates. Part I. An FEM numerical model, Composites Part A, Volume 33, 2002, Pages 1055–1062.

129. Li C.F., Hub N., Chenga J.G., Fukunagac H., Sekinec H., Low-velocity impact-induced damage of continuous fiber-reinforced composite laminates. Part II. Verification and numerical investigation, Composites Part A, Volume 33, 2002, Pages 1063–1072.

130. Pica RDW, Hinton E., Finite element analysis of geometrically nonlinear plate behavior using a Mindlin formulation, Computer Structures, Volume 11, 1980, Pages 203–15.

131. Besant T., Davies G.A.O., Hitchings D., Finite element modeling of low velocity impact of composite sandwich panels, Composites A, Volume 32,2001, Pages 1189-1196.

132. Duan S.H., Ye T.Q., Three dimensional frictional dynamic contact analysis for predicting low-velocity impact damage in composite laminates. Advances in Engineering Software, Volume 33, 2002, Pages 9-15.

133. Elder D.J., Thomson R.S., Nguyen M.Q., Scott M.L., Review of delamination predictive methods for low speed impact of composite laminates, Composite Structures Volume 66,2004, Pages 677–683.

134. Hou J.P., Petrinic N., Ruiz C., A delamination criterion for laminated composites under low-velocity impact, Composites Science and Technology, Volume 61, 2001, Pages 2069–2074.

135. Mikkor K.M., Thomson R.S., Herszberg I, Weller T., Mouritz A.P., Finite element modelling of impact on preloaded composite panels, Composite Structures, Volume 75, 2006, Pages 501–513.

136. Naik N.K., Meduri S., Polymer-matrix composites subjected to low-velocity impact: effect of laminate configuration, Composites Science and Technology, Volume 61, 2001, Pages 1429–1436

137. Palazotto A.N., Herup E.J., Gummadi L.N.B., Finite element analysis of low-velocity impact on composite sandwich plates, Composite Structures, Volume 49,2000, Pages 209-227

138. Tiberkak R., Bachene M., Rechak S., Necib B.,Damage prediction in composite plates subjected to low velocity impact, Composite Structures, In Press, Corrected Proof, Available online 24 March 2007.

140. Naik N. K., Sekher C.Y. and Meduri S., Damage in woven-fabric composites subjected to low-velocity impact, Composites Science and Technology, Volume 60, Issue 5, April 2000, Pages 731-744.

141. Lee Y.S., Kang K.H. and Park O., Response of hybrid laminated composite plates under low-velocity impact, Computers & Structures, Volume 65, Issue 6, December 1997, Pages 965-974.

142. Yang, S. H. and Sun, C. T., Indentation law for composite laminates. ASTM STP, 1982, 786, 425449.

143. Almohandes A. A., AbdeI-Kader M. S. and Eleiche A. M., Experimental investigation of the ballistic resistance of steel-fiberglass reinforced polyester laminated plates Composites Part B, Volume 27B, 1996, Pages 447-458.

144. Gupta N.K., Madhu V., An experimental study of normal and oblique impact of hard-core projectile on single and layered plates, International Journal of impact Engineering, Volume 19, 1997, Nos. 5-6, Pages 395-414.

145. Villanueva G. R., Cantwell W.J., The high velocity impact response of composite and FML-reinforced sandwich structures Composites Science and Technology, Volume 64,2004, Pages 35–54.

146. DeLuca E., Prifti J., Betheney W. and Chou S. C., Ballistic Impact Damage of S 2-Glass-Reinforced plastic structural armor composites science and technology, Volume 58 1998, Pages 1453-1461.

147. Goncalves D.P., Melo F.C.L., Klein A.N., Al-Qureshi H.A., Analysis and investigation of ballistic impact on ceramic/metal composite armour International Journal of Machine Tools & Manufacture, Volume 44, 2004, Pages 307–316.

148. Gupta N.K., Ansari R., Gupta S.K., Normal impact of ogive nosed projectiles on thin plates International Journal of Impact Engineering, Volume 25, 2001, Pages 641-660.

149.Piekutowski A. J., Forrestal M. J., Poormon K. L., and Warren T. L., Perforation of aluminum plates with ogive-nose steel rods at normal and oblique impacts, International Journal of Impact Engineering, Volume 18,1996, Nos 7 8, Pages. 877-887.

150. Karamis M.B., Tasdemirci A., Nair F., Failure and tribological behaviour of the AA5083 and AA6063 composites reinforced by SiC particles under ballistic impact Composites Part A, Volume 34, 2003, Pages 217–226.

151. Tarim N., Findik F., Uzun H., Ballistic impact performance of composite structures Composite Structures, Volume 56, 2002, Pages 13–20.

152. Findik F., Tarim N., Ballistic impact efficiency of polymer composites, Composite Structures, Volume 61, 2003, Pages 187–192.

153. Kim Hyonny, Welch D.A., Kedward K.T., Experimental investigation of high velocity ice impacts on woven carbon/epoxy composite panels Composites Part A, Volume 34, 2003, Pages 25–41.

154. Wu E. and Chang L.C., Woven glass/epoxy laminates subject to projectile impact, International Journal of Impact Engineering, Volume 16, 1995, No. 4, Pages 607-619.

155. Zaretsky E., DeBotton G., M. Perl The response of a glass fibers reinforced epoxy composite to an impact loading, International Journal of Solids and Structures, Volume 41,2004, Pages 569–584.

156. Cork C.R., Foster P.W., The ballistic performance of narrow fabrics, International Journal of Impact Engineering, Volume 34, 2007, Pages 495–508.

157. Cheeseman Bryan A., Bogetti T.A. Ballistic impact into fabric and compliant composite laminates, Composite Structures, Volume 61, 2003, Pages 161–173.

158. Hosur M.V., Vaidya U.K., Myers D. , Jeelani S., Studies on the repair of ballistic impact damaged S2-glass/vinyl ester laminates Composite Structures, Volume 61, 2003, Pages 281–290.

159. Boccaccini A.R. , Atiq S. , Boccaccini D.N. , Dlouhy I. , Kaya C., Fracture behaviour of mullite fibre reinforced–mullite matrix composites under quasi-static and ballistic impact loading Composites Science and Technology, Volume 65, 2005, Pages 325–333.

160. Iremonger M. J. and Went A. C., Ballistic impact of fibre composite armours
by fragment-simulating projectiles Composites Part A, Volume 2lA, 1996, Pages 575-581.

161. Franzen R.R., Orphald.L. and Anderson Jr C.E., The influence of experimental design on depth-of-penetration (dop) test results and derived ballistic efficiencies, International Impact Engineering, Volume 19, 1197, no. 8, Pages 727-737.

162. Horsfall I. and Buckley D. The effect of through-thickness cracks on the ballistic performance of ceramic armour systems Int. J. Impact Engineering, Volume 18, 1196, No. 3, Pages 309-318.

163. Tanoglu M., Seyhan A. T., Investigating the effects of a polyester preforming binder on the mechanical and ballistic performance of E-glass fiber reinforced polyester composites International Journal of Adhesion & Adhesives, Volume 23,2003, Pages 1–8.

164. Tanoglu M., McKnight S.H., Palmese G.R., Gillespie Jr.,J.W., The effects of glass-fiber sizings on the strength and energy absorption of the fiber/matrix interphase under high loading rates, Composites Science and Technology, Volume 61, 2001, Pages 205-220.

165. Starratt D., Sanders T., Cepus E., Poursartip A., Vaziri R., An effcient method for continuous measurement of projectile motion in ballistic impact experiments, International Journal of Impact Engineering, Volume 24, 2000, Pages 155-170

166. Czarnecki G.J., Estimation of the V_{50} using semi-empirical (1-point) procedures Composites Part B, Volume 29B, 1998, Pages 321-329.

167. Naik N.K., Doshi A.V., Ballistic impact behaviour of thick composites: Parametric studies Composite Structures, In Press, Corrected Proof, Available online 30 January 2007.

168. Naik N.K., Shrirao P., Reddy B.C.K., Ballistic impact behaviour of woven fabric composites: Formulation International Journal of Impact Engineering, Volume 32, 2006, Pages 1521–1552.

169. Naik N.K., Shrirao P., Reddy B.C.K., Ballistic impact behaviour of woven fabric Composites. Parametric studies Materials Science and Engineering A, Volume 412 , 2005, Pages 104–116.

170. Ben-Dor G., Dubinsky A., Elperin T., A model for predicting penetration and perforation of FRP laminates by 3-D impactors Composite Structures, Volume 56, 2002, Pages 243–248.

171. Ben-Dor G., Dubinsky A. and Elperin T., New area rules for penetrating impactors, International journal of Impact Engineering, Volume 21, 1998, Nos. 1-2, Pages 51-59.

172. Ben-Dor G., Dubinsky A. and Elperin T, Optimization of two-component composite armor against ballistic impact. Composite Structures, Volume 69, 2005, Pages 89–94.

173. Billon H.H., Robinson D.J., Models for the ballistic impact of fabric armour, International Journal of Impact Engineering, Volume 25, 2001, Pages 411-422.

174. Gu. B., Analytical modeling for the ballistic perforation of planar plain-woven fabric target by projectile Composites Part B, Volume 34, 2003, Pages 361–371.

175. Parga-Landa B. and Hernandez-Olivares F., An analytical model to predict impact behaviour of soft armours, Int. J. Impact Engineering, Volume 16, No. 3, 1995, Pages 455-466.

176. Nadler B, Steigmann D.J., A model for frictional slip in woven fabrics, C. R. Mecanique , Volume 331, 2003, Pages 797–804.

177. Jovicic J., Zavaliangos A., Ko F., Modeling of the ballistic behavior of gradient design composite armors Composites Part A, Volume 31, 2000, Pages 773–784.

178. Potti S. V. and Sun C. T., Prediction of impact induced penetration and delamination in thick composite laminates. International Journal of Impact Engineering , Volume 19, 1997, no. , Pages 31- 48.

179. Sun C. and T Potti S. V., Simple model to predict residual velocities of thick composite laminates subjected to high velocity impact. International Journal of Impact Engineering, Volume 18, 1996, no. 3, Pages 339-353.

180. Puente L. J., Zaera R., Navarro C., An analytical model for high velocity impacts on thin CFRPs woven laminated plates. International Journal of Solids and Structures, Volume 44, 2007, Pages 2837–2851.

181. Wen H.M., Penetration and perforation of thick FRP laminates. Composites Science and Technology, Volume 61, 2001, Pages 1163–1172.

182. Fatt M.S. H., Lin C., Revilock Jr. D.M., Hopkins D.A., Ballistic impact of glare fiber–metal laminates. Composite Structures, Volume 61, 2003, Pages 73–88.

183. Morye S.S., Hine P.J., Duckett R.A., Carr D.J., Ward I.M., Modeling of the energy absorption by polymer composites upon ballistic impact. Composites Science and Technology, Volume 60, 2000, Pages 2631-2642.

184. Fawaz Z., Zheng W., Behdinan K., Numerical simulation of normal and oblique ballistic impact on ceramic composite armours. Composite Structures, Volume 63, 2004, Pages 387–395.

185. Mahfuz H., Zhu Y., Haque A., Abutalib A., Vaidya U., Jeelani S., Gama B., Gillespie J., Fink B., Investigation of high-velocity impact on integral armor using Finite element method. International Journal of Impact Engineering, Volume 24, 2000, Pages 203-217.

186. Riddle R., Lesuer D., Syn C., Gogolewski R., Cunningham B., Application of metal laminates to aircraft structures: Prediction of penetration performance. Finite Elements in Analysis and Design, Volume 23, 1996, Pages 173-192.

187. Zhang G.M., Batra R.C., Zheng J., Effect of frame size, frame type, and clamping pressure on the ballistic performance of soft body armor, Composites Part B, In Press, Corrected Proof, Available online 10 May 2007

188. Borvik T., Hopperstad O.S., Berstad T., Langseth M., Numerical simulation of plugging failure in ballistic penetration, International Journal of Solids and Structures. Volume 38, Issues 34-35, August 2001, Pages 6241-6264

189. Gu B., Xu J., Finite element calculation of 4-step 3-dimensional braided composite under ballistic perforation, Composites Part B, Volume 35, 2004, Pages 291–297.

190. Lim C.T., Shim V.P.W., Ng Y.H., Finite-element modeling of the ballistic impact of fabric armor. International Journal of Impact Engineering, Volume 28, 2003, Pages 13–31.

191. Nandlall D., Williams K. and Vaziri R., Numerical simulation of the ballistic response of grp plates. Composites Science and Technology, Volume 58, 1998, Pages 1463-1469.

192. Espinosa H. Dwivedi D.S., Zavattieri P. D. and Yuan G., A numerical investigation penetration in multilayered material/structure systems. International journal of solid structures, Volume 35, 1995, no. 22, Pages 2975--3001.

193. Katayama M. and Kibe S., Numerical study of the conical shaped charge for space debris impact International Journal of Impact Engineering, Volume 26, 2001, Pages 357-368.

194. Silva M.A.G., Cisma-siu C., Chiorean C.G., Numerical simulation of ballistic impact on composite laminates International Journal of Impact Engineering, Volume 31 2005, Pages 289–306.

195. Arias A., Zaera R., Lopez-Puente J., Navarro C., Numerical modeling of the impact behavior of new particulate-loaded composite materials. Composite Structures, Volume 61, 2003, Pages 151–159.

196. Rabb R. J. and Fahrenthold E.P., Numerical simulation of oblique impact on orbital debris shielding, International Journal of Impact Engineering, Volume 23, 1999, Pages 735-744.

197. Walter, M.E., and Ravichandran G., Experimental simulation of matrix cracking and debonding in a model brittle matrix composite. Exp. Mech., Volume 37(2), 1997,Pages 126–131.

198. Zhang X., Hounslow L., Grassi M. Improvement of low-velocity impact and compression-after-impact performance by z-fibre pinning. Composites Science and Technology, Volume 66, 2006, Pages 2785–2794.

199. Byun J.H., Song S.W., Lee C.H., Um M.K., Hwang B.S., Impact properties of laminated composites with stitching fibers. Composite Structures, Volume 76, 2006, Pages 21–27.

200. Lopresto V., Melito V., Leone C., Caprino G., Effect of stitches on the impact behaviour of graphite/epoxy composites. Composites Science and Technology, Volume 66 2006, Pages 206–214.

201. Aymerich F., Priolo P., Characterization of fracture modes in stitched and unstitched cross-ply laminates subjected to low-velocity impact and compression after

impact loading. International Journal of Impact Engineering. Volume 35, Issue 7, July 2008, Pages 591-608

202. Hosur M.V., Vaidya U.K., Ulven C., Jeelani S., Performance of stitched/unstitched woven carbon/epoxy composites under high velocity impact loading. Composite Structures, Volume 64, 2004, Pages 455–466.

203. Caprino G., Lopresto V., Santoro D., Ballistic impact behaviour of stitched graphite/epoxy laminates. Composites Science and Technology, Volume 67, Issues 3-4, March 2007, Pages 325-335.

204. Mouritz A.P., Ballistic impact and explosive blast resistance of stitched composites. Composite Part B, Volume 32, 2001, Pages 431-439.

205. Larsson Fritz., Damage tolerance of a stitched carbon/epoxy laminate. Composites Part A, Volume 28A, 1997, Pages 923-934.

206. Mines R.A.W., Roach A.M., Jones N., High velocity perforation behaviour of polymer composite laminates. International Journal of Impact Engineering, Volume 22, 1999, Pages 561-588.

207. Dickinson LC, Farley GL, Hinders MK., Translaminar reinforced composites: a review. J Compos Technol. Res, Volume 21, 1999, Pages 3–15.

208. Freitas G, Magee C, Dardzinski P, Fusco T., Fibre insertion process for improved damage tolerance in aircraft laminates. Journal of Advanced Material, Volume 24, 1994, Pages 36–43.

209. Freitas G, Fusco T, Campbell T, Harris J, Rosenberg S., Z-fiber technology and products for enhancing composite design. In: Proceedings of 83rd meeting of AGARD structures and materials panel. 1996.

210. Partridge IK, Cartie´ DDR, Bonnington T., Manufacture and performance of Z-pinned composites. In: Advani S, Shonaike G, editors.Advanced polymeric materials: structure property relationships. CRC Press LLC; 2003 [Chapter 3].

211. Clarke A, Greenhalgh E, Meeks C, Jones C., Enhanced structural damage tolerance of CFRP primary structures by z-pin reinforcement. In: Proceedings of the 44th AIAA/ASME/ASCE/AHS structures, structural dynamics and materials conference, Norfolk, April 2003. AIAA-2003-1679.Compos Mater 1999; 33:1002–29.

212. Sankar B.V., Zhu H., The effect of stitching on the low-velocity impact response of delaminated composite beams, Composites Science and Technology, Volume 60, 2000, Pages 2681-2691.

213. Bibi G, Leicy D, Hogg PJ, Kemp M., High temperature damage tolerance of carbon fibre reinforced plastic. Composites, 199, Pages 414–24.

214. Levin K., Effect of low velocity impact on compression strength of quasi-isotropic laminate. In: Proceedings of American Society for Composites: first technical conference, Technomic, Lancaster, PA;1986. p. 313–25.

215. Kwang-Hee I, Cheon-Seok C, Sun-Kyu K, In-Young Y., Effects of temperature on impacts damages in cfrp composite laminates. Composites Part B, Volume 32, 2001, Pages 669–82.

216. Zimmerman RS, Adams DF., Impact performance of various fiber reinforced composites as a function of temperature. In: Proceeding of 32nd International SAMPE symposium, Anaheim, CA; 1987. P.1461–71.

217. Lo´pez-Puente J, Zaera R, Navarro C., The effect of low temperatures on the intermediate and high velocity impact response of CFRPs. Composites Part B, Volume 33 2002, Pages 559–66.

218. Dutta PK., Low temperature compressive strength of glass fiber reinforced polymer composites. J Offshore Mech Arctic Eng., Volume 116, 1994, Pages 167–172.

219. Hirai Y., Hiroyuki Hand Jang-Kyo K., Impact response of woven glass-fabric composites—II. Effect of temperature. Composites Science and Technology, Volume 58, Issue 1, January 1998, Pages 119-128.

220. Levin K., Effect of low velocity impact on compression strength of quasi-isotropic laminate. In: Proceedings of American society for composites: 1st technical conference. Technomic, Lancaster, PA, 1986. p. 313–25.

221. Khojin A. S., Bashirzadeh R., Mahinfalah M. and Jazar R. N., The role of temperature on impact properties of Kevlar/fiberglass composite laminates Composites Part B: Engineering, Volume 37, Issues 7-8, October-December 2006, Pages 593-602.

222. Gómez-del Río T., Zaera R., Barbero E. and Navarro C., Damage in CFRPs due to low velocity impact at low temperature. Composites Part B: Engineering, Volume 36, Issue 1, January 2005, Pages 41-50.

223. Go´mez-del Rý´o T., Zaera R., Barbero E., Navarro C., Damage in CFRPs due to low velocity impact at low temperature. Composites Part B, Volume 36, 2005, Pages 41–50.

224. Gustin J, Joneson A, Mahinfalah M, Stone J., Low velocity impact of combination Kevlar/fiber carbon sandwich composite. Journal of Composite Strucures, Volume 69(4), 2005, Pages 396–406.

225. Khojin A.S., Mahinfalah M., Bashirzadeh R. and Freeman B., Temperature effects on Kevlar/hybrid and carbon fiber composite sandwiches under impact loading. Composite Structures, Volume 78, Issue 2, April 2007, Pages 197-206

226. Schultz, J. M. and Friedrich, K., Effect of temperature and strain rate on the strength of a PET/glass fiber composite. Journal of Material. Science, Volume 19, 1984, Pages 2246-2258.

227. Belingardi G., Cavatorta M. P. and Paolino D. S., Repeated impact response of hand lay-up and vacuum infusion thick glass reinforced laminates. International Journal of Impact Engineering, In Press, Corrected Proof, Available online 21 March 2007

228. Zhu X., Dou H., Ban Z., Liu Y. and He J., Repeated impact test for characterization of hard coatings. Surface and Coatings Technology, Volume 201, Issues 9-11, 26 February 2007, Pages 5493-5497.

229. Baucom J.N., Zikry M.A. and Rajendran A.M., Low-velocity impact damage accumulation in woven S2-glass composite systems Composites Science and Technology, Volume 66, Issue 10, August 2006, Pages 1229-1238.

230. Morais W.A., Monteiro S.N. and D'Almeida J.R.M., Effect of the laminate thickness on the composite strength to repeated low energy impacts. Composite Structures, Volume 70, Issue 2, September 2005, Pages 223-228.

231. Morais W.A., Monteiro S.N., D'Almeida J.R.M., Evaluation of repeated low energy impact damage in carbon–epoxy composite materials. Composite Structures, Volume 67 2005, Pages 307–315.

232. Baucom J.N. and Zikry M.A., Low-velocity impact damage progression in woven E-glass composite systems. Composites Part A: Applied Science and Manufacturing, Volume 36, Issue 5, May 2005, Pages 658-664.

233. Morais W. A. de, Monteiro S. N. and D'Almeida J. R. M.. Evaluation of repeated low energy impact damage in carbon–epoxy composite materials Composite Structures, Volume 67, Issue 3, March 2005, Pages 307-315.

234. Hosur M. V., Karim M. R. and Jeelani S., Experimental investigations on the response of stitched/unstitched woven S2-glass/SC15 epoxy composites under single and repeated low velocity impact loading. Composite Structures, Volume 61, Issues 1-2, July 2003, Pages 89-102.

235. Mouritz A. P., Gallagher J. and Goodwin A. A., Flexural strength and interlaminar shear strength of stitched GRP laminates following repeated impacts Composites Science and Technology, Volume 57, Issue 5, 1997, Pages 509-522.

236. Impact Dynamics. Krieger Publishing Company, Malabar, Florida, 1992

237. Gupta N.K., Iqbal M.A. and Sekhon G.S., Effect of projectile nose shape, impact velocity and target thickness on deformation behavior of aluminum plates.International Journal of Solids and Structures, Volume 44, Issue 10, 15 May 2007, Pages 3411-3439.

238. Gupta N.K., Iqbal M.A. and Sekhon G.S., Effect of projectile nose shape, impact velocity and target thickness on the deformation behavior of layered plates International Journal of Impact Engineering, In Press, Corrected Proof, Available online 19 January 2007.

239. Gupta N.K., Iqbal M.A. and Sekhon G.S., Experimental and numerical studies on the behavior of thin aluminum plates subjected to impact by blunt- and hemispherical-nosed projectiles. International Journal of Impact Engineering, Volume 32, Issue 12, December 2006, Pages 1921-1944.

240. Ulven C., U. Vaidya K. and Hosur M. V., Effect of projectile shape during ballistic perforation of VARTM carbon/epoxy composite panels. Composite Structures, Volume 61, Issues 1-2, July 2003, Pages 143-150.

241. Cour-Palais B.G., The shape effect of non-spherical projectiles in hypervelocity impacts, International Journal of Impact Engineering, Volume 26, Issues 1-10, December 2001, Pages 129-143.

242. Schäfer F.K., Herrwerth M., Hiermaier S.J. and Schneider E.E., Shape effects in hypervelocity impact on semi-infinite metallic targets. International Journal of Impact Engineering, Volume 26, Issues 1-10, December 2001, Pages 699-711.

243. Christiansen E.L. and Kerr J.H., Projectile shape effects on shielding performance at 7 km/s and 11 km/s International Journal of Impact Engineering, Volume 20, Issues 1-5, 1997, Pages 165-172.

244. Wen H. M., Predicting the penetration and perforation of FRP laminates struck normally by projectiles with different nose shapes. Composite Structures, Volume 49, Issue 3, July 2000, Pages 321-329.

245. Chen J. K. and Medina D. F., The effects of projectile shape on laminated composite perforation. Composites Science and Technology, Volume 58, Issue 10, October 1998, Pages 1629-1639.

246. Turgutlu A., Al-Hassani S. T. S. and Akyurt M., The influence of projectile nose shape on the morphology of interface in impact spot welds, International Journal of Impact Engineering, Volume 18, Issue 6, September 1996, Pages 657-669.

247. Liu D, Malvern LE. Matrix cracking in impacted glass/epoxy plates. Journal of Composite Material, Volume 21, 1987, Pages 594–609.

248. Hosseinzadeh R., Shokrieh M. M., Lessard L., Damage behavior of fiber reinforced composite plates subjected to drop weight impacts. Composite Science and Technology Volume 66, 2006, Pages 61-68.

249. Scarponi C, Briotti G, Barboni R, Marcone A, Iannone M., Impact testing on composites laminates and sandwich panels. Journal of Composite Materials, Volume 30 1996, Pages 1873–911.

250. Liu D. Impact-induced delamination—a view of bending stiffness mismatching. J of Composite Material, Volume 22, 1988, Pages 674–92.

251. Hosur M. V., Murthy C. R. L., Ramamurthy T. S., Shet A., Estimation of impact-induced damage in CFRP laminates through ultrasonic imaging NDT&E International, Vol. 31, 1998, No. 5,Pages. 359-374.

252. Aymerich, F., and Meili, S., "Ultrasonic evaluation of matrix damage in impacted composite laminates." Composites Part B, Volume 31, 2000, Pages 1–6.

253. Gao, S.L., and Kim, J.K., Scanning acoustic microscopy as a tool for quantitative characterization of damage in CFRPs. Composite Science and Technology, Volume 59, 1999, Pages 345-354.

254. Scarponi, C., and Briotti, G., "Ultrasonic technique for the evaluation of delaminations on CFRP, GFRP, KFRP composite materials." Composites Part B, Volume 31, 2000, Pages 237–243.

255. Mouritz, A.P., Townsend, C., and Shah Khan, M.Z., "Non-destructive detection of fatigue damage in thick composites by pulse-echo ultrasonics." Composites Science and Technology, Volume 60, 2000,Pages 23-32.

256. Dong, Y.J., Ye, N., and Bai, Y.L., "On-line observation of interlaminar damage by ultrasonic inspection." Composites Science and Technology, Volume 59, 1999, Pages 957-961.

257. Deluca E., Prifti J., Betheney W. and Chou S.C., Ballistic impact damage of S2-Glass Reinforced plastic structural armor. Composite Science and Technology, Volume 58, 1998, Pages 1453-461.

258. Kinsey A, Saunders DEJ, Soutis C., Post-impact compressive behavior of low temperature curing woven CFRP laminates. Composites, Volume 26, 1995; 661–667.

259. Lagace PA, Wolf E. Impact damage resistance of several laminated material systems. J Am Inst Aeronaut Astronaut, Volume 33, 1995, Pages 1106–1113.

260. Gardiner, D.S., and Pearson, L.H., “Acoustic-emission monitoring of composite damage occurring under static and impact loading.” Experimental Techniques: 22-28 (Nov. 1985).

261. Bolduc, M., and Roy, C., “Evaluation of impact damage in composite materials using acoustic emission.” ASTM STP 1156: 127-138 (1993).

262. Liu, C., Rosakis, A.J., and Stout, M.G., “Dynamic fracture toughness of a unidirectional Graphite/Epoxy composite.” 2001 ASME IMECE/AMD-25400.

263. Lambros, J., and Rosakis, A.J., “Dynamic crack initiation and growth in thick unidirectional graphite/epoxy plates.” Composites Science and Technology, Volume 57, 1997, Pages 55-65.

264. Nunes L.M., Paciornik S., D’Almeida J.R. M., Evaluation of the damaged area of glass-fiber-reinforced epoxy-matrix composite materials submitted to ballistic impacts. Composites Science and Technology, Volume 64, 2004, Pages 945–954.

265. Zhang Z.Y., Richardson M.O.W., Low velocity impact induced damage evaluation and its effect on the residual flexural properties of pultruded GRP composites. Composite Structures, Volume 81, Issue 2, November 2007, Pages 195-201.

266. Takeda S., Minakuch S., Okabe Y., Takeda N., Delamination monitoring of laminated composites subjected to low-velocity impact using small-diameter FBG sensors. Composites Part A, Volume 36, 2005, Pages 903–908.

267. Roh J.H., Kim J.H., Adaptability of hybrid smart composite plate under low velocity impact, Composites Part B, Volume 34, 2003, Pages 117–125.

268. Abrate, S., Impact on Composite Structures, Cambridge University Press, Cambridge, UK, 1998.

269. Reid, S.R., and Zhou, G., Impact Behaviour of Fibre-reinforced Composite materials and Structures. Woodhead Publishing Ltd and CRC Press LLC 2000.

270. Pavier, M.J., and Clarke, M.P., “Experimental techniques for the investigation of the effects of impact damage on carbon-fibre composites.” Composites Science and Technology, Volume 55, 1995, Pages 157-169.

271. Boll, D.J., Bascom, W.D., Weidner, J.C., and Murri, W.J., “A microscopy study of impact damage of epoxy-matrix carbon-fibre composites.” Journal of Materials Science Volume 21,1986, Pages 2667-2677.

272. Liu D., Lillycrop L.S., Malvern L.E., and Sun, C.T., “The evaluation of delamination-an edge replication study.” Experimental Techniques 11(5), 20-25 (1987).

273. Cantwell W.J., Davies P. and Kausch H.H., “Repair of impact-damaged carbon fiber PEEK composites.” SAMPE Journal, Volume 27(6), 1991, Pages 30-35.

274. Cantwell W.J., and Morton J., Comparison of the low and high velocity impact response of CFRP. Composites, Volume 20(6), 1989, Pages 545-55.

275. Cantwell W.J., “The influence of fibre stacking sequence on the high velocity impact response of CFRP.” J. Materials Science Letters 7, 1998, Pages 756-758.

276. Daniel, I.M., and Wooh, S.C., “Deformation and damage of composite laminates under impact loading.” In A.K. Mal, and Y.D.S. Rajapakse (eds.), Impact Response and Elastodynamics of Composites, ASME publication AMD-116: 11-26 (1990).